Controlled Release of Gentamicin from Polyelectrolyte Multilayers to Treat Implant-Related Infection

by

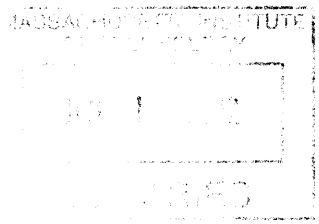

Joshua Seth Moskowitz

B.S. Materials Science and Engineering
Cornell University (2007)

M.S. Chemical Engineering Practice
Massachusetts Institute of Technology (2009)

SUBMITTED TO THE DEPARTMENT OF CHEMICAL ENGINEERING IN PARTIAL FULFILLMENT OF THE REQUIREMENTS FOR THE DEGREE OF

DOCTOR OF PHILOSOPHY IN CHEMICAL ENGINEERING
AT THE
MASSACHUSETTS INSTITUTE OF TECHNOLOGY

JUNE 2012

Signature of Author: _____

Joshua S. Moskowitz
Department of Chemical Engineering
July 30, 2010

Certified by: _____

Paula T. Hammond
Bayer Chair Professor of Chemical Engineering
Thesis Supervisor

Accepted by: _____

Patrick S. Doyle
Professor of Chemical Engineering
Graduate Officer

Controlled Release of Gentamicin from Polyelectrolyte Multilayers to Treat Implant-Related Infection

by

Joshua Seth Moskowitz

Submitted to the Department of Chemical Engineering on July 30, 2010 in Partial Fulfillment of the Requirements for the Degree of
Doctor of Philosophy in Chemical Engineering

Abstract

Polyelectrolyte multilayered (PEM) coatings were fabricated to incorporate and release the small, hydrophilic antibiotic gentamicin from implant surfaces for infection control. The use of a cationic hydrolytically cleavable poly(β-amino ester) rendered these films biodegradable, yielding both diffusion-based and surface-erosion based release of this therapeutic. The Layer-by-Layer (LbL) assembly platform was used to create conformal, micron scale reservoirs with highly tunable drug release. Film release profiles were engineered through film architecture design and post-processing crosslinking techniques. Delivery of gentamicin was sustained for weeks, which is a significant improvement from previous gentamicin-releasing LbL systems. To gain better insight on the mechanisms of release and aid in rational film design, a theoretical treatment of the physical system was performed. These results include an analytical mathematical model describing the release of drug per surface area of film as a function of time as well as a computational model that simulates the time-dependent concentration profiles in these LbL systems.

These erodible, antibiotic coatings were demonstrated to be bactericidal against *Staphylococcus aureus*, an infectious microorganism that is highly relevant to implant-related infections. Film degradation products were generally nontoxic toward MC3T3-E1 osteoprogenitor cells. A reproducible *in vivo* rabbit bone infection model was developed to test the PEM coatings against sterile, uncoated placebos; subsequent *in vivo* experimentation demonstrated the proof-of-principle that an antibiotic-eluting LbL film can efficaciously treat a pre-existing implant-related infection.

One further application was studied which combined the release-based mechanism of these erodible films with a permanent, contact-killing LbL film. This combination has the treatment benefit of an initial burst release of antibiotic, prevents biofilm formation, and reduces the probability of developing antibiotic resistance due to the prolonged presence of sublethal concentrations of gentamicin.

Thesis Supervisor: Paula T. Hammond, Bayer Professor of Chemical Engineering

Thesis Supervisors

Paula T. Hammond, Ph.D

Bayer Professor and Executive Officer of Chemical Engineering

Massachusetts Institute of Technology

Thesis Committee

Myron Spector, Ph.D

Professor of Orthopedic Surgery

Harvard Medical School

Darrell J. Irvine, Ph.D

Professor of Materials Science

Massachusetts Institute of Technology

J. Christopher Love, Ph.D

Professor of Chemical Engineering

Massachusetts Institute of Technology

Acknowledgements

I have been fortunate to work with a truly amazing and talented set of people throughout my graduate experience. The work presented within this thesis has been strongly inspired by these interactions.

My premier appreciation is extended to Professor Paula T. Hammond, who has been my greatest mentor throughout the duration of my graduate experience at MIT. She provided me with an opportunity to work on a challenging, fascinating, cutting-edge research project and offered extensive guidance and intellectual support throughout the duration of my involvement. Her open-mindedness afforded me, on many occasions, to pursue avenues of my greatest interest. Her most unique and defining attribute that had the greatest impact on me was her energetically cheerful, positive attitude that would only enhance my daily motivation.

I would like to thank my thesis committee, Professors Myron Spector, Darrell J. Irvine, and J. Christopher Love, for offering their sincere and constructive advice on how to overcome my greatest research challenges. Their collaboration has significantly impacted the efficiency and quality of my research. It has been academically stimulating and an absolute pleasure for me to work with such a supportive committee.

I thank Professor Robert E. Cohen for his brainchild PhDCEP program and his support of my PhDCEP incoming class of 2007. Were it not for this unique doctoral track, I would have enrolled in the Department of Materials Science and Engineering.

I would like to acknowledge Professors George Malliaras (École Nationale Supérieure des Mines de Saint-Étienne), Shu Yang (University of Pennsylvania), and Ali Yazdani (Princeton University), each for inviting me into their labs and allowing me to pursue independent research. Collectively, they have spurred my decision to continue onto higher education.

Dr. Helen Chuang and her colleague Jeff Easley were integral in helping me get comfortable in the lab, and trained on most of the relevant techniques that enabled me to successfully carry out the responsibilities associated with this thesis. Helen's continued collaboration has not only been helpful for sharing ideas and discussing experiments, but has also provided much personal support. I am sincerely grateful for these altruistic interactions.

Within the Hammond group, Dr. Raymond Samuel's expertise as an orthopedic surgeon has helped me better understand how to develop an *in vivo* infection model. He has additionally contributed an enormous sum to all aspects of my research (and life) by providing his worldly and astute advice at my request. Ray was nothing short of an 'alpha-colleague', and I feel fortunate to have had the opportunity to work so closely with such a talented and selfless person. Furthermore, I hope that one day I will have the same zest for life that I see in Ray.

I owe my appreciation to the LbL subgroup—Mara Lee Macdonald, Renée Smith, Dan Schmidt, Anita Shukla, and Jessie Wong for their insightful discussions. I have had the added

enjoyment of pursuing a team-based project with Jessie Wong, which has since strengthened our friendship.

I wish to thank Michael Blaisse, a brilliant undergraduate chemistry student who will begin his tenure as a Ph.D student at the University of California at Berkeley next year. Mike has given me the opportunity to take the role of a mentor and has worked very diligently under my leadership throughout the duration of my graduate work. He has contributed significantly to both the experimental and theoretical aspects of this thesis, and I consider him my closest teammate within the Hammond Lab. I hope that Mike's experience was as rewarding for him as it was for me.

For the *in vivo* work, I am sincerely grateful for the efforts of Dr. Hu-Ping Hsu, who performed all animal surgeries. Most of what I know about surgical technique has been acquired via my apprenticeship with Dr. Hsu. He has helped me think through the surgical aspects of the animal model and was a vital component to the success of this project. Drs. Jean C. Lee, Mitch Harris, and Scott Martin each contributed substantially to development of the *in vivo* infection model. Dr. Lee's expertise in microbiology essentially shaped the data collection and analysis procedures for the *in vivo* experiment. Dr. Harris and Dr. Martin gave me the opportunity to witness a live orthopedic surgery and generously spent their time meeting with me to discuss the details of the infection model. I thank the entire E25 staff in the MIT-DCM facility, and specifically regard the efforts of Dr. Alison Hayward and Catrina Wong, who were invaluable assets and teachers of animal care and anesthesia. I wish to thank Ellen Buckley and Nikki Lew for microbiological analysis, and Dr. Wayne Schwark (Cornell University) for gentamicin quantification assays.

I appreciate the administrative staff that have allowed for the smooth functioning of my graduate experience—Linda Mousseau, Suzanne Easterly, Katie Lewis, and Christine Preston have been extraordinarily supportive. Christine, in particular, has handled countless issues and requests from me.

I acknowledge Steve Chapin, Byron Masi, Justin Quon, and Adel Ghaderi for their periodic sanity checks. These great friends have contributed to the richness of my MIT experience, and have certainly provided for some excellent memories, which I hope we continue to produce.

Ultimately, my personal, emotional, social, athletic, and academic wellbeing have all relied on those closest to me: my family and friends. This thesis is dedicated to you, as it is you who have made me who I am. To my mom and dad, who have given me endless support, unrestricted love, and a true opportunity to succeed—you believed in me and I have made it. To my sister and brother, who each have mutually pushed me to pursue my goals and strive to give my best—you both will do great things and I will be here for you as you have been there for me. To my grandparents, Gerry, Arnie, Phyllis, and Reuben (a.k.a. Ron), for their continuous love and care throughout my life—you are so special to me and I'm grateful to have all four of

you to see me through this program. To my aunts, uncles, and cousins—we are fortunate to have such a close family. To my closest friends, who have shaped my life and continue give me something to look forward to each week. To Kelsey Ann Handstad, the one who I will share forever with, I love you.

JOSHUA SETH MOSKOWITZ

Massachusetts Institute of Technology,
July 31, 2010

J. S. Moskowitz is thankful for financial support by the National Institutes of Health, National Institute of Aging (5R01AG029601-03). This work made use of the Center for Materials Science and Engineering shared facilities, the animal facilities of MIT's Division of Comparative Medicine, the Institute of Soldier Nanotechnologies (ISN), as well as the Robert Langer Laboratory.

Biography

Joshua Seth Moskowitz was born in Nashua, NH on October 21, 1984. He was raised in this city until his departure for college upon graduation from Bishop Guertin High School. He learned advanced mathematics at a very early age through questions posed by his grandfather Ron, which were rewarded with silver dollars or 50-cent pieces. In high school, he continued to find solace in mathematics and spent a summer teaching himself calculus via an online course provided through Stanford University. This independent effort eventually set the stage for achievement of the BGHS Mathematics Trophy upon graduation.

Josh was an avid soccer player through his adolescent years, representing the state of NH at the USYSL regional championships on four occasions and ultimately captaining his high school team during his senior year. His affinity for the mathematics and sciences, and enduring interest in soccer guided him to Carnegie Mellon University for the 2003-2004 academic year, during which he participated on the varsity soccer team. He made many friends and greatly enjoyed his time in Pittsburgh, but began to realize that competitive soccer would not continue to guide his future. Josh's distaste for quitting something that he started made it difficult to justify staying at Carnegie Mellon and leaving the varsity soccer team. Therefore, he decided that to accept a transfer offer at Cornell University and join his good friend and old high school teammate, Timothy Ulm.

Tim integrated Josh into the Cornell social network, and Josh quickly fell in love with Ithaca, NY. He pursued a degree in Materials Science and Engineering, in part due to the fascinating research prospects. After completing a semester long class taught by Professor George Malliaras, Josh was contacted by George himself about a research position in his lab. Without hesitation, he began his first experience as a researcher under the unparalleled guidance of Jason Slinker (who has recently accepted a professorship at the University of Texas at Dallas). His work was focused on improving the efficiency and lifetime of organic light emitting diodes. The remainder of Josh's fulfilling tenure at Cornell was peppered with research, classes, intramural soccer, and fun. He participated in two National Science Foundation funded research programs, one in Professor Shu Yang's lab at the University of Pennsylvania (2005) working on magnetically functionalized polymer nanopost arrays and the other in Professor Ali Yazdani's lab at Princeton University (2006) working on graphene. Each experience reinforced his decision to pursue graduate work.

Upon graduation, Josh finally moved back "home" to greater Boston to begin work on an advanced degree. Although offered admission to the Sc.D program through the Department of Materials Science and Engineering at MIT, he elected to switch majors and embark on a unique program offered through the Department of Chemical Engineering. This program, the Ph.D in chemical engineering practice (CEP), offered a joint opportunity with the MIT Sloan School of Management, which allows doctorate students to combine their graduate research

with world-class business education. Such an opportunity, in light of his grandfather's history of founding a successful technology-based company and Josh's rapidly growing interest in management, was not to be matched. MIT has since been a wondrous boon for him, constantly presenting intellectual challenges and testing his will to achieve. He has met a truly diverse and talented collection of individuals who have each uniquely contributed to his defining experience. After completing an application-driven, original research project, and earning an education in management, Josh is excited come full circle by integrating his problem solving skills as a researcher with his superior teamwork and leadership experience as a business student to address conventional industrial problems. As of this writing, Josh has accepted a Senior Consultant position at Deloitte (U.S. – Boston) to begin in October 2012.

Table of Contents

Table of Figures

Table of Tables

Chapter 1 Introduction

1.1 *Incidence, Economics, and Drug-Device Combinations*

Most implanted devices are associated with orthopedics as over 800,000 joint replacements are performed in North America each year—reflecting a 200% increase between 1999 and 2002 alone [1, 2]. Primary joint replacements (also known as *arthroplasties*) are typically performed on patients with arthritis or major injury to alleviate pain and restore motion to the joint. These operations add up to an annual expenditure of $1.4 billion in the United States for total hip arthroplasty and $2.59 billion for total knees with 2/3 of these costs being offset by Medicare [3]. As expected, the number of revision surgeries is also on the rise at 17.5% for hips and 8.2% for knees [1]. Since revision surgeries require extended use of hospital resources and surgeon time, subtracting 1% from each of these values would have saved $112.6 million and $100 million for hips and knees respectively [1, 4].

In order to promote implant success, there has been rising interest in the design and implementation of combination devices. According to the United States Food and Drug Administration, a *combination device* is an apparatus that includes two or more regulated components (i.e. drugs, devices, or biologics) that are combined and produced as a single entity [5]. Drug-device combination products have garnered increasing attention from both pharmaceutical and medical device companies as a general strategy to address persisting complications in clinical practice. Coordinated design of such devices has the potential to greatly improve both device performance as well as the associated quality of life for the patient. Since efficacy of a drug-device combination is generally not a linear combination of adding existing technologies together, these products can offer synergistic advantages over administering both the drug and device separately in their conventional forms.

This thesis focuses on the incorporation of the small, hydrophilic antibiotic gentamicin into polyelectrolyted multilayered (PEM) surface coatings for tunable, local, and sustained delivery from implants based on Layer-by-Layer (LbL) assembly. These films are specifically

designed to treat an existing implant-related infection. Among the attractive features of LbL (which are discussed at length in section 1.6), the critical advantage that places LbL on the cutting edge of existing technologies is its potential to release multiple therapeutics, simultaneously or sequentially, and thus allow for smart design of local therapeutic delivery from drug-device combinations for optimized treatment. For the stated case of orthopedic implants, the pertinent set of complications that could be addressed include pain, inflammation, infection, and long term loosening of the implant. The work presented herein was conducted under a financial support parcel whose overarching aim was to develop a thin film solution to address this precise set of complications. Nevertheless, the end goal of a multi-therapeutic product necessitates design and optimization of individual therapeutic systems. The work in this thesis specifically addresses the antibiotic delivery component for the treatment of infection.

1.2 *Outline of Thesis*

Chapter 1 highlights the problem of device-associated infections, introduces the benefits of local drug release, and explains how polyelectrolyte multilayered (PEM) coatings stand out from competing technologies as an approach to addressing these issues. Using orthopedic implants as the model substrate for these combinations, the goal of this research was to develop an antibiotic coating that would be capable of eradicating an existing device-associated infection in a direct exchange arthroplasty. In orthopedics, the conventional method to treat device-associated infection is a two-stage process involving removal of the infected device, radical and extensive debridement of dead or infected tissue, local insertion of a high-concentration antibiotic-eluting spacer, six weeks of intravenous antibiotic therapy, and a follow-up surgery to re-implant a new sterile device. An antibiotic coating that is sufficiently effective against an existing infection would promote a one-stage re-implantation procedure that calls for direct exchange of the infected implant with a new, drug-coated implant without the need for antibiotic therapy or a second surgery. To this end, design of the coating requires burst-release of drug to immediately eradicate existing infection followed by weeks of sustained local delivery as phrophylaxis. Chapter 1 outlines the work that has been done toward this goal, and outlines the specific aims of this thesis.

Chapter 2 articulates the strategies and details of achieving the desired release profile from PEM films using an engineering-driven, application-focused approach. Among the techniques for controlling the loading and release of gentamicin are: liposome encapsulation, complex film architectures, thermal crosslinking, and the 'sponge' effect. The films are shown to load substantial amounts of cargo, retain drug activity upon release, and have some level of biocompatibility with osteoprogenitor cells.

Chapter 3 offers a theoretical view of the release behavior of gentamicin from the PEM systems. A simple mathematical framework is developed and applied to describe the drug release as a function of time. Using the model, predictions are made regarding the tenability of release profiles by changing drug concentration, film thickness, and drug diffusivity.

Chapter 4 presents a reproducible *in vivo* bone infection model using New Zealand White rabbits. The model was designed to simulate a contaminated one stage arthroplasty where the animals were intentionally given implant-related infection using a *Staphylococcus aureus* surface-colonized peg, which was press-fitted into a drilled defect in the rabbit femur. This model set the foundation for an *in vivo* clinical comparison between film-coated implants and sterile, uncoated placebos; results are discussed in detail in Chapter 5.

Chapter 6 builds upon the work in the first five chapters and demonstrates the versatility of LbL systems. This chapter focuses on a side project which combines two independent film architectures that each has unique bactericidal functionality. The combination films are first release-killing, and then become contact-killing upon exhaustion of the therapeutic cargo. Although this dual mechanism concept is demonstrated for releasable gentamicin, it can be extended to other therapeutics offering a powerful, multi-functional design for drug-device combinations.

After thesis summarization in Chapter 7, Chapter 8 is appended as a capstone that integrates the technology described in this thesis with a broader commentary regarding the state U.S. healthcare, and describes a new enabling technology that may help recent medical developments penetrate the market.

1.3 *Advantages to Local Delivery of Drugs*

Local drug delivery offers significant advantages over systemic drug delivery. Among the most important are smaller overall doses, less susceptibility to the development of resistance, and avoidance of systemic drug exposure, which can be toxic [5]. The reduced dosages correlate with reduced costs. Furthermore, therapeutic entities such as genes and proteins cannot be delivered through standard alimentary or parenteral tracts due to harsh conditions in the former and rapid clearance in the latter. With respect to antibiotics in drug-device combinations, there can be the added benefit of direct mitigation of device-associated infections. Local antibiotic delivery systems should be designed to initially provide effective doses of drug straight to the target site to combat elevated post-operative infection risk, and then maintain therapeutic levels of release over prolonged periods of time to undermine any latent infection [6]. The release kinetics are to be uniquely designed for a particular drug, device, implant site, and disease, while ensuring that device performance is not impaired.

1.4 *Implant-related Infection and Biofilms*

Over two million nosocomial infections occur in the United States annually with an average hospital cost around $15,000 [5]. More than half of these are associated with implanted devices [3]. Implant-associated infection can occur due to any implanted medical device such as minimally invasive contact lenses, to temporary urinary catheters and endotracheal tubes, to permanent cardiac valves and orthopedic implants [7]. Specifically for orthopedics, the economic and health related penalties to treat an implant-related infection add up to a total cost of about five to seven times that of the initial surgery, longer hospital residency with limited mobility, and the potential for skeletal defects, limb shortening, renewed disability, and death [8, 9]. Today, with the increased use of medical devices and onset of a major orthopedic implant market due to the aging baby-boomer population, the need to address the common clinical problem of hospital-related infection is paramount.

Pathogens can be introduced to the implant surface by exogenous organisms on the skin, non-sterile surgical tools, the local environment, or even systemically circulating bacteria, which can become spontaneously pathogenic upon attachment to the implant surface. The

latter is particularly concerning since such an event can take place at any time (even years) after implantation. Upon attachment, the bacteria rapidly proliferate and create a protective mucopolysaccharide matrix known as a biofilm [10]. Within the biofilm environment therapeutics have a lower diffusion rate and bacteria have decreased metabolism, each which lends to enhanced antibiotic resistance [11]. The biofilm allows sessile colonies to communicate more effectively, exchange genetic material (thus allowing antibiotic-resistance transfer), and elude host humoral response. Biofilms can propagate infection by giving rise to planktonic satellites that can travel to other, non-colonized surfaces. Due to the fact that mature biofilms generally do not respond to administered therapeutics or host immune responses, their existence generally requires removal of the implant before local and systemic treatment can become effective [12]. The two major drug-device combination strategies that are currently employed to control infection include the use of drugless anti-adhesive materials that prevent bacteria attachment and direct incorporation of drugs into or onto a medical device [13].

1.5 *Orthopedic Implants and Osteomyelitis: Opportunity*

Among the millions of orthopedic implants inserted annually, bone-implant integration is a common clinical problem that leads to bone resorption, loosening, and opportunistic infection. One study demonstrated the presence of bacteria in over 72% of implants extracted for aseptic loosening [14]. Despite the standard pre-operative procedures that include antibiotic prophylaxis, antimicrobial shower, shaving, and application of disinfectants, infection rates on the order of 1% still persist. Therefore recent efforts have been directed at integrating drug delivery with these devices to accelerate bone formation and healing while also treating infection [15].

Osteomyelitis is the inflammatory response and accompanying bone deconstruction caused by an infecting microorganism. It is commonly associated with the existence of a biofilm. *Staphylococcus aureus* is the single largest contributor to osteomyelitis and accounts for two-thirds of operative specimen isolates [16]. Conventional therapies to treat osteomyelitis are often inadequate due to limited blood supply to the skeletal tissue and poor

drug penetration into the infected bone [17]. Simply increasing the systemic dosage can cause toxic side effects and is therefore not a resolution. Thus, local drug delivery from the surface of implants is attractive since it poses a viable alternative to systemic techniques.

The gold standard technique to control orthopedic implant infection is the use of antibiotic loaded bone cement (ALBC). ALBC uses poly(methyl methacrylate) (PMMA) (also known as acrylic) that has been loaded with clinically relevant antibiotics such as gentamicin, vancomycin, or tobramycin [18-21]. One study that surveyed the Scandinavian arthroplasty registers followed up on more than 240,000 total hip replacements, and reported a 50% reduction in the infection rate using these cements [22]. The use of pre-blended bone cement has been widely accepted in Europe for decades, and became approved for use in the United States in 2003. Bone cements typically release their therapeutic cargo in bi-phasic manner. First, there is a burst release of drug that takes place on the order of one day followed by a much longer tail of incomplete release that lasts for weeks. The release behavior of these systems is controlled by the loading ratio of drug to polymer, bulk porosity of the cement, surface area, and roughness [23-25].

There is substantial *in vivo* evidence that these cements perform superior to unloaded cements with respect to infection prevention [5]; however, despite the positive advantages to using ALBC, there are some drawbacks that have been elucidated. Pharmacokinetic studies suggest that elution of gentamicin from PMMA cements is imperfect; less than 50% of the total cargo is released within 4 weeks, after which continuous release was ceased [26-28]. Diffusive elution of drug from cements often has unstable and unpredictable release kinetics [29, 30]. This can lead to large fluctuations in the local drug concentration causing local tissue toxicity, or worse, emergence of drug-resistant pathogens [31]. In the event of infection or failure, revision becomes very difficult, requiring the removal of the cemented nonbiodegradable PMMA before osteogenesis can help fill the defect site. In such a procedure, bone substance is lost, and residual PMMA debris can cause fibrous encapsulation and foreign body response [32]. Also, the polymerization reaction is highly exothermic [33], which limits the types of therapeutics that can be delivered from bone cement (e.g. growth factors would be denatured). This heat, along with any residual methacrylate monomer poses toxicity issues for healthy bone cells [34].

For ALBC specifically, drug release leads to the formation of pores within the cement matrix, which provides a highly favorable environment to harbor any remaining bacteria [31]. Finally, ALBC is well-mixed, thus negating the opportunity for smart design of complex or sequential release profiles of individual therapeutics. As of 2007, only five ALBC composites were approved for clinical use by the United States' Food and Drug Administration, and their use is restricted to prophylaxis rather than treatment of existing infection [16]. If the traditional 11% usage rate of ALBC in primary arthroplasties were increased to 50%, the economic effect of replacing plain cement with ALBC—requiring an average increase of $300 per packet—was estimated to increase the overall health care costs in the United States by $117 million [35]. This would be offset by the savings salvaged from a supposed lower overall infection rate. Given the current prevalence of total joint replacements, the infection rate would need to be reduced from 1.5% to 0.3% (i.e. 80% reduction in incidence rate).

These drawbacks leave open a window of opportunity for the development of a next-generation therapeutic coating. Currently, there is no approved coating for the treatment of existing infection. Recent alternative materials for use as drug releasing surface coatings include hydroxyapatites [36], biodegradable poly(L-lactic acid) [37], poly(lactic-co-glycolic acid) [38], sol-gels [39, 40], biodegradable polyhydroxyalkanoates [41], and others. Release rates from materials that depend on rate of surface degradation can be accurately tuned by changing the coating composition. Overall, there is need for an implant coating with tunable, release-based infection control that does not present host toxicity issues or inhibit incorporation of other delicate therapeutics such as anti-inflammatory agents and growth factors while imparting a permanent biofilm-resistant functionality. To date, no such combination film meets all of these specifications.

1.6 *Layer-by-Layer Films for Drug Delivery: Solution*

The true birth of LbL assembly took place in 1966 with a publication authored by Ralph Iler who studied the buildup of charged inorganic colloidal multilayers at DuPont [42]. After a couple relatively latent decades, the 'modern age' of this technology began as it was thrust into the limelight during the '90s [43], in part by Gero Decher's publication in Science [44]. Decher

pioneered the general use of polyelectrolytes for multilayered systems [45, 46] and helped publish the first textbook on this subject in 2003 [47]. LbL assembly of alternately charged polyelectrolytes has now become a well-established method for 'bottom up' engineering of surface coatings [48]. PEM films have the potential to make an important impact in the medical world as a drug delivery vehicle. They produce conformal coatings on most surfaces [49-51] with nanometer thickness precision [52] and highly tunable drug loading [53]. Functional components are incorporated into the film at the exact layer of interest [44-47, 54] so that these films can be engineered to deliver multiple different drugs with complex release profiles [48, 55]. The LbL fabrication process is simple, economical, and gentle. One of the major advantages to this technique is the all-aqueous fabrication condition, which allows for the integration of biologically active materials such as proteins [56], DNA [57], peptides [58, 59], and enzymes [60] without denaturing or loss of function. Additionally, as with any local drug delivery system, lower doses are required, less systemic drug exposure is endured, and for antibiotics, resistance is mitigated [5].

As a result of the rising interest in drug-device combinations, coatings for orthopedic implants are an excellent application for localized drug delivery and prevention of infection [40, 61]. This provides an opportunity for PEMs to be incorporated onto the surfaces of these prostheses, and make an unparalleled impact since PEMs can be built with painkillers [62, 63], antibiotics [53], and growth factors [64-66] to sequentially deliver the exact treatment necessary for optimal recovery. PEMs will release their therapeutic components upon degradation, and can be designed to do this in specific settings such as in the presence of enzymes [67-69], small molecules [70-72], reducing agents [73], electrochemical potential [74, 75], and most importantly for the proposed application, aqueous physiological environment [76].

To address the latter mechanism of degradation, Professor David Lynn and colleagues have designed a class of hydrolytically degradable synthetic polycations, which can serve as both a structural component in a PEM film and a transient element that is cleaved by water, hence facilitating disassembly [48, 77, 78]. By adjusting the hydrophobicity of these polycations, the degradation rates and corresponding release rates can be tuned [79]. As a

result, the use of these polycations for drug delivery applications has been the topic of several recent publications [63, 80-83]. Degradable PEM films are currently the only thin film drug coating technology that enables large payload, tunabilty, sustainable release, *and* the potential for delivery of multiple therapeutic agents with co- or sequential release profiles.

1.7 *Specific Aims of Thesis*

The work presented in this thesis describes the engineering of a thin film that erodes in top-down fashion when subjected to physiological condition via the use of a hydrolytically degradable poly(β-amino ester). This allows the antibiotics payload to be released locally with precise dosage and timing. Films are designed to be highly conformal, functionalizable, biocompatible, easy to process, and economical. The specific drug of interest for this work is the small hydrophilic molecule gentamicin, which previously faced the problem of premature diffusion out of PEM films [53]. The application of interest is the treatment and prevention of orthopedic implant-related osteomyelitis, which generally develops as a result of *S. Aureus*. This research involves the design, construction, and characterization of films that can be applied to orthopedic implants such that they effectively kill *S. Aureus* when placed in physiological condition. To advance this technology, the proposed research is broken down into three specific aims:

1. Demonstrate control over dosage and release rates of gentamicin from polyelectrolyte multilayers with the particular objective of attaining release duration on the order of weeks
2. Establish reproducible bone infection model *in vivo*
3. Demonstrate *in vivo* efficacy of gentamicin-releasing, PEM coated prostheses

Chapter 2 Engineering PEM Coatings for the Prolonged Release of Antibiotics

2.1 *Designing the Antimicrobial Film Using Electrostatic Layer-by-Layer Self-Assembly*

With respect to film components, the design of layer-by-layer systems for the release of antibiotics in physiological environment has three basic functional requirements that must be addressed: (1) incorporation of a therapeutic, (2) a mechanism of release, and (3) any other materials necessary to permit stable layer-by-layer film growth without compromising biocompatibility. Gentamicin sulfate is a small, water-soluble aminoglycoside antibiotic with five amine groups that are protonated at low pH to a maximum charge of +5.0 (Figure 2-1, left), and thus easily incorporated into thin film systems that rely on electrostatic interactions [53]. Gentamicin has a minimum inhibitory concentration below 0.156 μg/mL against *S. aureus* UAMS-1 (Figure 2-1, right) which is consistent with literature values for other strains of *S. aureus* [84]. Because gentamicin is nephrotoxic and ototoxic at elevated systemic levels, the low concentration necessary for local delivery via LbL systems is advantageous.

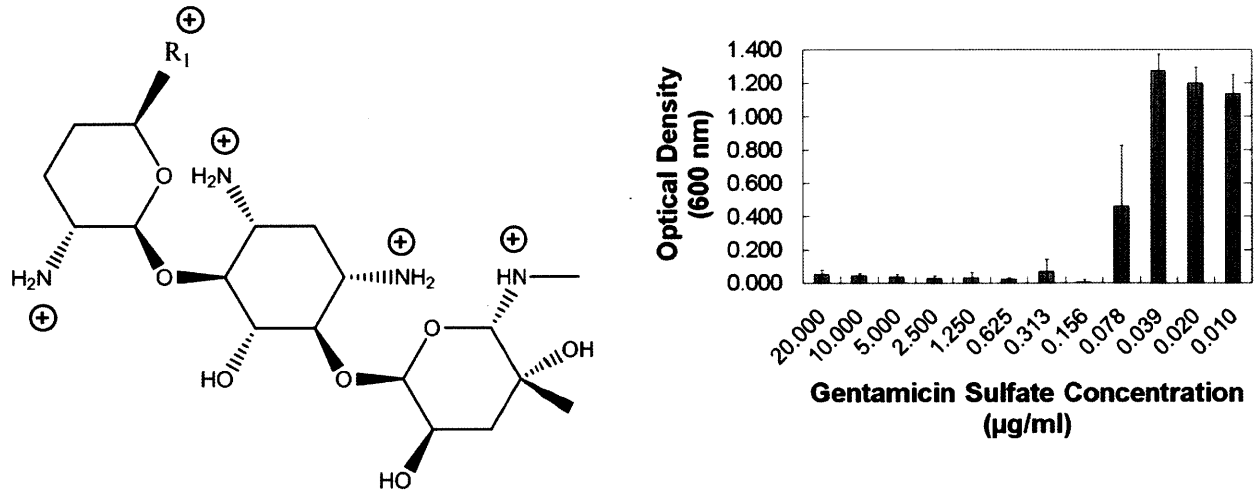

Figure 2-1. (Left) Structure of gentamicin. Sites protonated in fully charged state are indicated. Information on R_1 groups and their relative content percentages can be obtained from Mediatech, Inc. (Lot #: 61098046).

(Right) In vitro efficacy of gentamicin sulfate against S. aureus (ATCC 49230) in CMHB over a 16 h incubation period at 37 °C. Data represent the mean ± standard deviation of triplicate samples.

To enable hydrolytic breakdown in physiological environment (37 °C, pH 7.4), a class of polycations known as poly(β-amino esters), which are easily synthesized by stepwise conjugation of bis amine monomers to diacrylate esters was used [78]. These polymers undergo hydrolytic cleavage of their ester bonds to eventually yield their original biocompatible monomeric units, and have been successfully incorporated into multilayer films for controlled release [76, 85]. The specific choice of the polymer species shown in Figure 2-2, which is defined in this thesis as Poly 1, is due to its relatively slow degradation rate, biocompatibility, and high charge density [76]. The amines present along the backbone of Poly 1 are protonated at neutral to low pH, yielding the positive charge necessary for the buildup of electrostatic LbL systems. Neither Poly 1 nor its small molecule degradation products were found to be cytotoxic toward fibroblastic NIH3T3 cells [78], monkey kidney Cos-7 cells [80], or even murine pre-osteoblast MC3T3 cells [53].

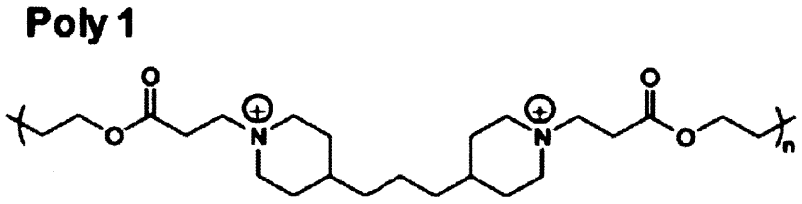

Figure 2-2. Structure of Poly 1.

Both of the functional components—gentamicin and Poly 1—are positively charged under standard deposition conditions (pH 5.0). Therefore, an anionic component is required to allow for the stable growth of the LbL film. The biopolymer hyaluronic acid (HA) had previously been employed for this purpose [53]; however, films built with HA result in highly diffusive systems that rapidly lose their payload before complete film degradation occurs. The standard therapeutic regimen for antibiotics requires prolonged presence at high concentrations. Relevant timeframes for treatment tend to be on the order of weeks. To this end, two major efforts were set forth in this thesis: (1) encapsulation of gentamicin inside of large, charged liposomes to limit its diffusivity within the PEM matrix and prolong its release, and (2) examination of alternative film architectures.

2.1.1 Liposomes

Liposomes initially gained popularity as a drug delivery vehicle to protect and control the release of its cargo [86]. There has been specific interest in the direct coating of implants with liposome-encapsulated therapeutics to enhance the duration of their local drug release [87]. Gentamicin has been studied as one particular candidate for liposomal drug delivery [88]. A major advantage to the use of liposomal gentamicin is the fact that its biodistrubution *in vivo* can be controlled via the use of liposome surface charge [89]. A second advantage is that liposomes can assist the intracellular delivery of gentamicin, whose hydrophilic nature generally inhibits its flux across the lipid bilayer of cell membranes [90-92]. This is important in light of the fact that *Staphylococcus aureus*, the pathogen responsible for approximately 80% of all human osteomyelitis cases, has been shown to thrive intracellularly and subsequently develop antibiotic resistance [93]. When these osteoblasts die, the viable bacteria are released and can re-infect new cells [94]. Finally, *In vivo* treatment of osteomyelitis via the use of liposomal gentamicin has recently shown some success [95].

It was hypothesized that the encapsulation of gentamicin in a large enough biodegradable and biocompatible material could prevent easy diffusion of the small molecule within LbL film architectures and hence prolong its release. The use of liposomal carriers in PEM films has been a relatively recent development in controlled release technology [96-98]. Although liposomes are favorable for delivery of hydrophilic drugs, micelles can be used as an extension to this technology for hydrophobic cargoes [81, 99]. Unless working with crosslinkable lipids [100], liposomes are typically stabilized with a polyelectrolyte shell in order to prevent rupture and self-assembly of the lipid bilayer in a flat conformation on the surface of the growing LbL film [101]. The choice of polyelectrolyte and relative charge density of the liposome surface are also important in achieving effective deposition of liposomes onto the surface of growing LbL films. Specifically, depending on the relative strength of polyelectrolyte-polyelectrolyte interactions compared to those of the polyelectrolyte-liposome interactions, stripping of the polyelectrolyte stabilizer may occur in place of liposome deposition [102]. With proper system design, successful incorporation of intact liposomes into polyelectrolyte multilayers with unique cargoes has been reported [103, 104].

2.1.1.1 Experimental

2.1.1.1.1 Materials

Poly 1, a poly(β-amino ester), was synthesized as previously described [78]. Silicon wafers (test grade n-type) were purchased from Silicon Quest (Santa Clara, CA). Linear poly(ethyleneimine) (LPEI, 23966-2, M_n = 25 kDa) was purchased from Polysciences, Inc. Nonradiolabeled gentamicin sulfate (GS) purchased in powder form were from Mediatech, Inc. (Herndon, VA). Sodium hyaluronate (or hyaluronic acid (HA), M_n = 1.7 MDa) was purchased from Lifecore Biomedical, Inc. (Chaska, MN). Dioleoylphosphatidylethanolamine (DOPE), N-succinyl-DOPE, N-glutaryl-DOPE, polyethylene glycol (PEG)-C_{16}-ceramide, and extrusion materials were purchased from Avanti Polar Lipids (Alabaster, AL). Poly (sodium 4-styrenesulfonate) (PSS, M_w = 1 MDa), 3 M concentrated sodium acetate buffer (pH 5.2), poly (L-lysine) (28 kDa), and cation-adjusted Mueller Hinton Broth (cMHB) were purchased from Sigma-Aldrich (St. Louis, MO). ^{3}H-GS (250 μCi total, 1 mCi/mL in ethanol, 200 μCi/mg) and ^{14}C-cholesteryl hexadecyl ether (CHE, 250 μCi total, 0.1 mCi/mL in toluene, 55 mCi/mmol) were obtained from American Radiolabeled Chemicals, Inc. *Staphylococcus aureus* (*S. aureus*) was acquired from ATCC (25923, Manassas, VA). Dialysis membranes were purchased from SpectraPor (Rancho Dominguez, CA). Fetal bovine serum (FBS) was purchased from Invitrogen (Carlsbad, CA). Modified simulated body fluid (m-SBF) was prepared as described previously [105]. All materials and solvents were used as received without further purification.

2.1.1.1.2 Encapsulation of Gentamicin in Liposomes

Relevant liposome compositions include DOPE—N-succinyl-DOPE—PEG-C_{16}-ceramide (69:30:1 molar ratio) and DOPE—N-glutaryl-DOPE—PEG-C_{16}-ceramide (69.5:30:0.5 molar ratio). Encapsulation of drug was performed according to a previously reported method [90, 92]. Briefly, lipids were mixed in chloroform and the solvent pulled off by rotary evaporation. Dried lipid films (representing 25 mg of total lipid) were rehydrated by the addition of 1.0 mL of 50 mg/mL GS in 100 mM sodium acetate buffer, pH 5.0. For liposome characterization experiments in the absence of GS, rehydration was performed without drug. After extensive vortexing, the mixture was subjected to five freeze-thaw cycles and eleven extrusions through a

0.1 μm pore size filter using the mini extruder. The repetitive freeze-thaw cycles were used to achieve drug distribution equilibrium by physical disruption of the phospholipid bilayers. The extrusion was used to produce uniform liposome sizes (Figure 2-3). The final product was diluted and non-encapsulated drug was dialyzed out using a cellulose membrane with 8 kDa cutoff.

2.1.1.1.3 Stabilization of Liposomes with PLL

Liposome solutions (1 mL) containing 0.2 mg/mL lipid were slowly dropped into an equal volume of agitated PLL solution (10^{-4}— 0.2 mg/mL) at room temperature. Dynamic light scattering and zeta potential measurements were performed on samples at various times after fabrication using a Zeta-PALS (Brookhaven Instruments Corp.) at room temperature. Samples were stored at 4, 25, or 37 °C.

2.1.1.1.4 Imaging

Atomic force microscopy (AFM) was performed with a Veeco Nanoscope V with Dimension 3100 and accompanying software. Scanning electron microscopy (SEM) was conducted with a JEOL JSM-6060 and accompanying software.

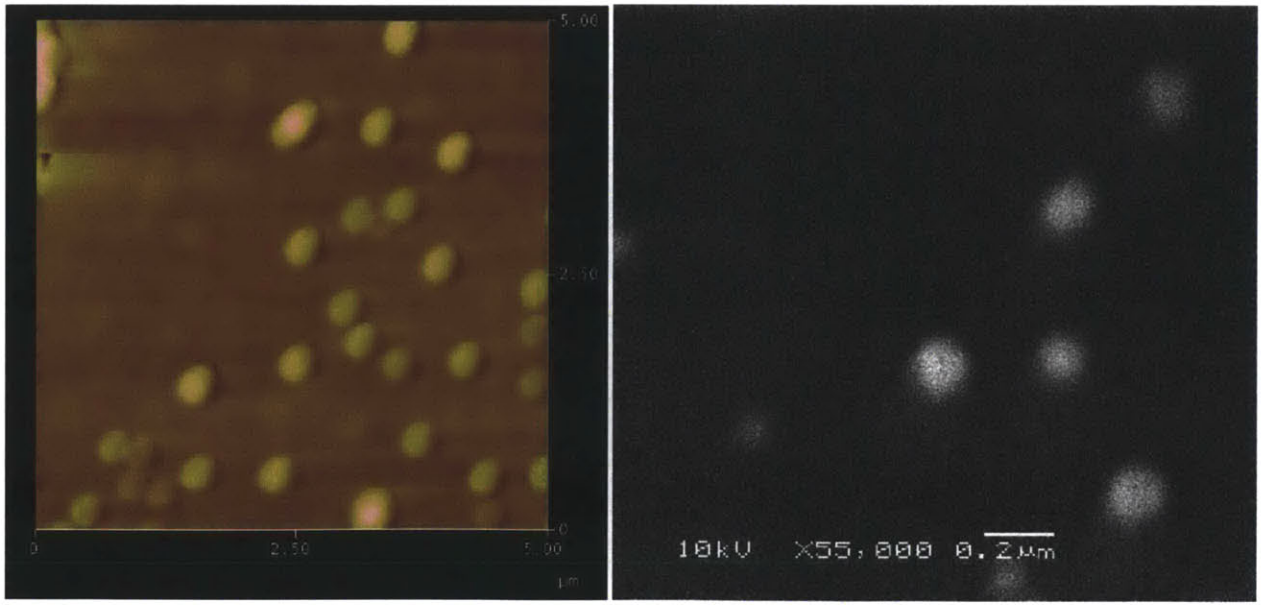

Figure 2-3. (Left) AFM and (right) SEM images of liposomes on a silicon surface.

2.1.1.1.5 Preparation of Electrolyte Solutions

Dipping solutions containing Poly 1 and HA were prepared at 2 mg/mL in 100 mM sodium acetate buffer and pH-adjusted to 5.0 with 1.0 N sodium hydroxide. Free GS was prepared at 10 mg/mL in 100 mM sodium acetate and pH-adjusted to 5.0. Stabilized, liposome encapsulated gentamicin (PLL-Lipo-GS) was prepared at 0.4 mg/mL with respect to lipid content as described in sections 2.1.1.1.2 and 2.1.1.1.3. LPEI and PSS dipping solutions were prepared at 2 mg/mL in ultra pure water and pH adjusted to 4.25 and 4.75 respectively. All solutions were prepared with water from a Milli-Q Plus (Bedford, MA) at 18.2 MΩ.

2.1.1.1.6 LbL Deposition

All films were constructed on silicon as follows according to the alternate dipping method [44]. Substrates were rinsed with methanol and ultra pure water, dried under nitrogen, and plasma etched in oxygen using a Harrick PDC-32G plasma cleaner at high RF power for 75 seconds. Layer-by-layer thin film deposition was performed either by hand or using a Carl Zeiss HMS Series Programmable Slide Stainer. A nondegradable bilayer of LPEI/PSS was deposited first by immersion of the plasma treated substrates in LPEI for 30 minutes followed by a single ultra-pure water rinse, and finally in PSS for 30 minutes followed by a single ultra-pure water rinse. The degradable films were deposited on top of this PSS-terminated surface. The tetralayer architecture of $[\text{Poly 1/HA/GS/HA}]_n$ was constructed by alternate dipping in Poly 1 or GS for 9 minutes followed by a cascade rinse of three 100 mM sodium acetate baths for 10, 20, and 30 seconds, and then into HA for 9 minutes followed by a similar rinse cycle. When dipping PLL-Lipo-GS, a 35 min dip cycle and a single 30-second rinse bath were used. The process was repeated *n* times depending on the desired experiment. All polymer solutions and gentamicin solutions were completely replaced every 25 and 50 tetralayers, respectively.

For films used in drug release experiments, the GS solution was spiked with 25 μL ^{3}H-GS per 50 mL dipping solution yielding a 0.5 μCi/mL product. No other part of the LbL deposition process was changed.

2.1.1.1.7 Sample Sizes and Data

Sample sizes are indicated in figure captions. Data are presented as mean ± standard deviation unless otherwise specified.

2.1.1.2 Results and Discussion

2.1.1.2.1 Stabilization of Liposomes with PLL

Initial efforts were dedicated toward liposome fabrication and stabilization, followed by determination of drug loading, efficacy against *S. aureus*, and finally deposition of liposomes into erodible LbL films. To determine the optimum mixing ratio of liposomes to PLL, it was necessary to determine how much PLL was required to fully reverse the surface charge on the liposomes without yielding excess polymer. N-succinyl-DOPE and N-glutaryl-DOPE are negatively charged lipids and PEG-C_{16}-ceramide was used as a surfactant to prevent aggregation of native liposomes. Increasing the concentration of the cationic PLL led to the behavior seen in Figure 2-4 (left), where the average particle diameter was small at low and high mass ratios of PLL to lipid, but rapidly became very large near a mass ratio of 0.1. This suggests that at a mass ratio near 0.1, there was significant aggregation of neighboring vesicles due to bridging via the PLL polymer chains. It has been shown that larger PLL chains allow for greater charge overcompensation on the vesicle surface (which arises due to their loopier conformation upon adsorbance), and therefore reduces this effect of aggregation [106]. The zeta potential data are consistent (Figure 2-4, right) as this mass ratio corresponds to the charge transition regime, which precludes the aggregation as the charge neutrality allows the liposomes to come into closer proximity with each other.

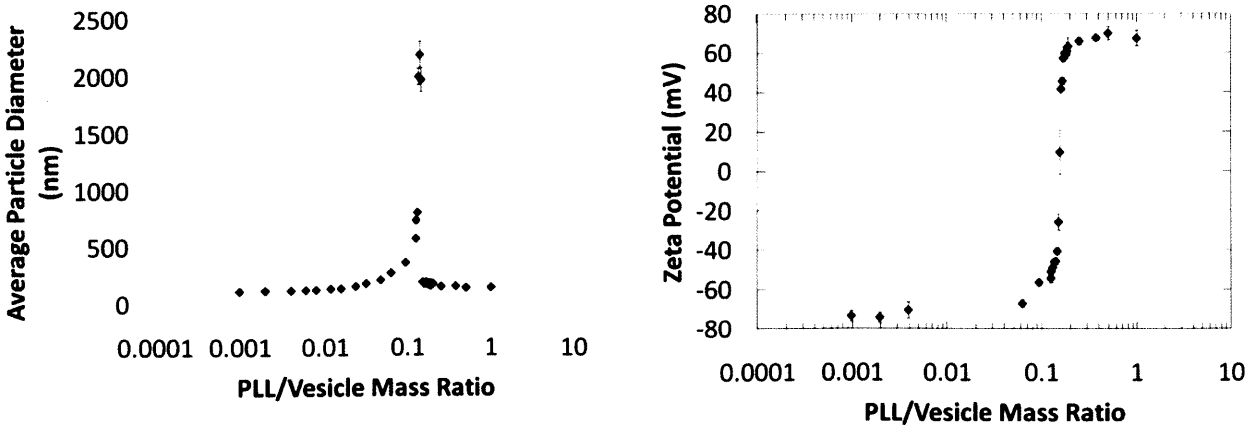

Figure 2-4. (Left) Average diameter of liposome-PLL complexes formed using PLL with molecular weight of 28 kDa as a function of mass ratio. (Right) Zeta-potential measurements of the same samples. Data represent the mean ± standard deviation of multiple measurements performed on a single prepared sample for each point.

A similar experiment was conducted for gentamicin-loaded liposomes, and it was found that this transition occurs earlier, which was likely due to the presence of the positively charged gentamicin on the outer shell of the liposome surface thus requiring less polymer for complete surface charge reversal.

2.1.1.2.2 Shelf Life of Liposomes

Using the proper mass ratio of PLL to lipid to stabilize the liposomes as suggested by the zeta potential information, the shelf life of these carriers was studied. Determination of shelf life was important to ensure that performance of liposomes fabricated from the same batch could be accurately compared after different durations of storage. It was important to ensure that the integrity of the liposomes would not be rapidly compromised when placed into physiological condition. Liposomes stored at 4 °C maintained their size and surface charge for over two months after fabrication (Figure 2-5, top). Liposomes stored at room temperature or 37 °C maintained their size and surface charge for the full two weeks studied (Figure 2-5, middle). The polyelectrolyte shell adds about 30 nm to the diameter of the native liposomes, and completely reverses the surface charge. A repeat of the shelf life experiment at 4 °C was conducted in the presence of FBS (Figure 2-5, bottom). The FBS contains proteins, which can be isoelectric in nature and therefore provide a favorable environment for individual lipids to form complexes, hence degrading the vesicle carriers. The loss of material from each liposome causes a reduction in the average measured particle size. The zeta potential for the unstabilized liposomes was reduced to about -20 mV.

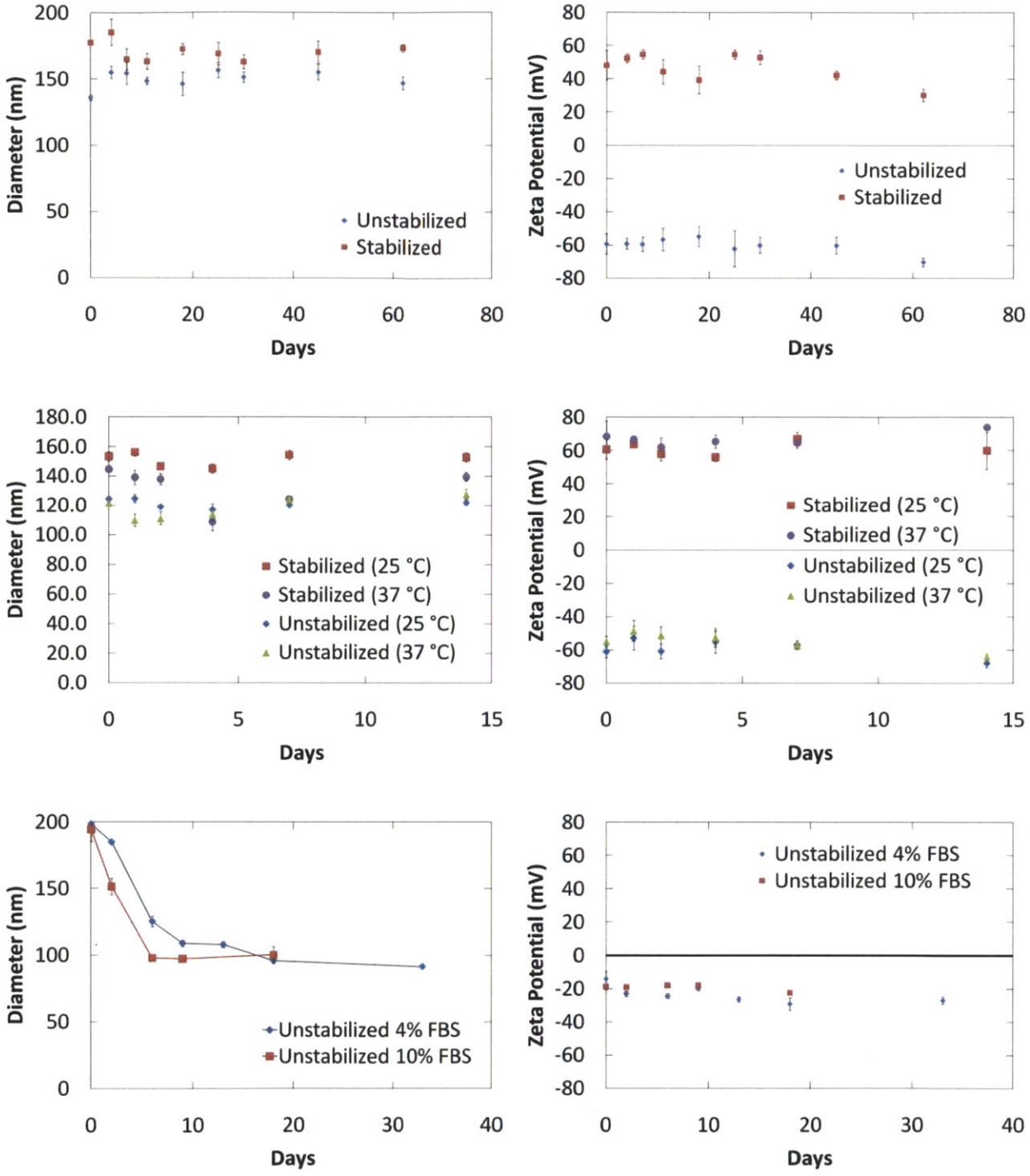

Figure 2-5. Diameter and zeta potential of liposomes stored at 4 °C without serum (top), 25 and 37 °C without serum (middle), and 4 °C with serum (bottom) as a function of time. Data represent the mean ± standard deviation of multiple measurements performed on a single prepared sample for each point.

2.1.1.2.3 Activity of Gentamicin-Loaded Liposomes

By measuring radioactivity of the ^{14}C-CHE and ^{3}H-GS both before and after dialysis, it was determined that the initial loading of drug was approximately 0.07 mg-GS/mg-liposome. This compares to about 0.22 mg/mg for the model formulation that served as the basis of this work [92]. Unstabilized liposomes charged with gentamicin slowly released their cargo over time. The rate of release was highly dependent on the storage temperature (Figure 2-6). When stored in the refrigerator, the liposomal formulations lost about half of the initially loaded gentamicin over the course of four months, or less than 0.5% of the initial value per day. At room temperature, the liposomes lost over 4% per day. Although PLL-stabilized liposomes may provide for longer drug retention, the LbL deposition process generally requires days, which corresponds to measurable drug loss and subsequent incorporation of free gentamicin into the growing LbL films.

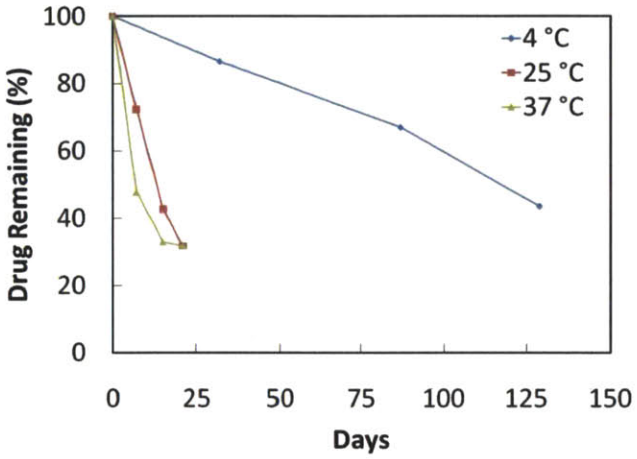

Figure 2-6. Gentamicin loss as a function of time for unstabilized liposomes stored at various temperatures in 100 mM NaOAc, pH 5.0. One sample was prepared and re-measured throughout the experiment for each temperature.

A microdilution assay was used to determine the minimum inhibitory concentration (MIC) of unstabilized GS-loaded liposomes (GS-Lipo) against *S. aureus*. As shown eariler with the FBS, the liposomes also rapidly degraded in the presence of the nutrient-rich cation-adjusted Mueller Hinton Broth. Therefore, the GS-Lipo were separately prepared in 100 mM NaOAc before being assayed and compared to an assay control of pristine NaOAc buffer without GS-Lipo (Figure 2-7, top). The exact liposome concentration was unknown since it was determined that during dialysis of gentamicin, about 2% of the total liposome content was also

discarded; hence, the values in Figure 2-7 represent a slight over-estimate of the MIC. The sodium acetate buffer was nontoxic towards *S. aureus* at all concentrations investigated in this experiment. The drug-loaded liposomes yielded an upper bound of the MIC at 78.13 μg/mL (with respect to lipid mass). This corresponds to about 5.5 μg/mL of drug content, which is an order of magnitude higher than the MIC for free gentamicin. Possibilities for the discrepancy include: variability in the determined gentamicin content of liposomes (leading to an overestimate), overestimate in the liposome concentration used in the microdilution assay, and the fact that some of the positively charged gentamicin is complexed with the negatively charged lipids thus rendering it less active.

When PLL-stabilized liposomes were used for a similar assay, the MIC was reduced to about half the value of unstabilized case (Figure 2-7, bottom). The antibiotic nature of polycations has previously been documented [107, 108], and the PLL control (containing free polyelectrolyte without liposomes) yielded efficacious results alone at high enough concentration (i.e. 0.625 mg/mL).

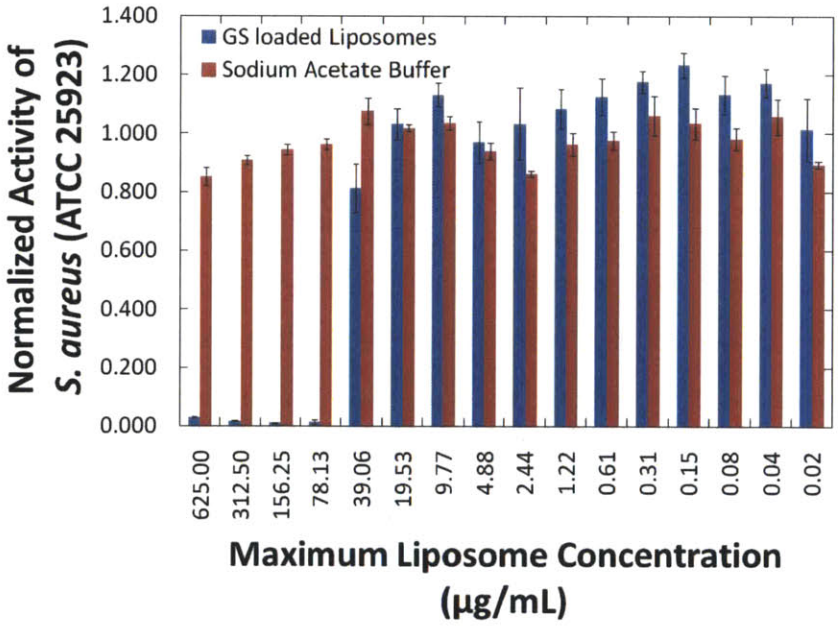

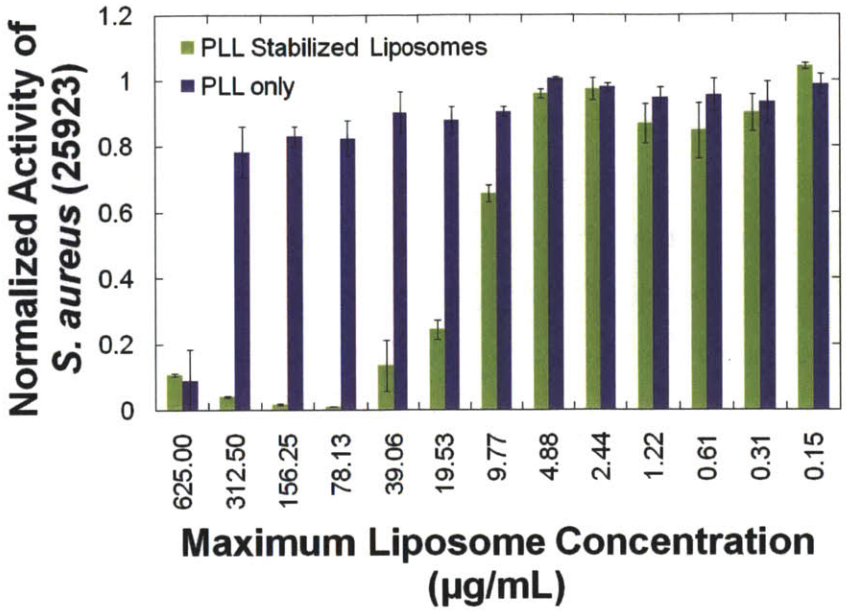

Figure 2-7. Determination of the MIC of GS-Lipo (top) and PLL-GS-Lipo (bottom) against *S. aureus*. Data represent the mean ± standard deviation of triplicate samples.

2.1.1.2.4 Performance of Liposome-LbL Films

After determining that the stable, GS-loaded liposomes could be synthesized while maintaining activity against *S. aureus*, it was necessary to begin incorporating the liposomes into polyelectrolyte multilayered films. To this end, initial efforts were aimed at comparing the performance of the PLL-Lipo-GS to free gentamicin using identical film architectures. Specifically, 50 tetralayer films were built with either [Poly 1/HA/GS/HA] or [Poly 1/HA/PLL-Lipo-GS/HA]. Two major metrics were considered: release kinetics and total drug loading. Looking at the release curves depicted in Figure 2-8,[1] the release rate was distinctly slower for liposomal gentamicin (i.e. duration was increased almost twofold from the case of free drug); however, the total drug load of the liposomal films was substantially reduced (more than 25x) from the case of free gentamicin. Although this comparison was conducted using only one particular LbL system, the general findings are expected to apply to most systems. Liposomal carriers are much bigger than the small-molecule gentamicin, and according to the Einstein diffusivity relation, their diffusivities should scale with the inverse of the particle size, which

[1] Neither film architecture continued to release drug beyond the final data point shown.

leads to slower release kinetics. The reduction in total drug load was initially thought to correlate to sub-optimal packing of the liposomes on the film surface. To test for this, liposomal films with two tetralayers were constructed and imaged with the AFM (Figure 2-9). It was found that the liposomes did not form a close-packed network on the surface; however, the packing density was significant and likely would not allow for more than a 3-4x increase. Assuming that the total drug loading of a liposomal LbL film scales linearly with the total liposome loading, then the liposomal films would still contain about 7-8x less drug than the case of free gentamicin. Therefore, the discrepancy can be explained by the fact that the large size of the liposomes required a substantial film volume that could otherwise be occupied by free drug. Furthermore, the more diffusive nature of gentamicin is actually beneficial in achieving large drug loadings since more drug can be driven into the film throughout the deposition process.

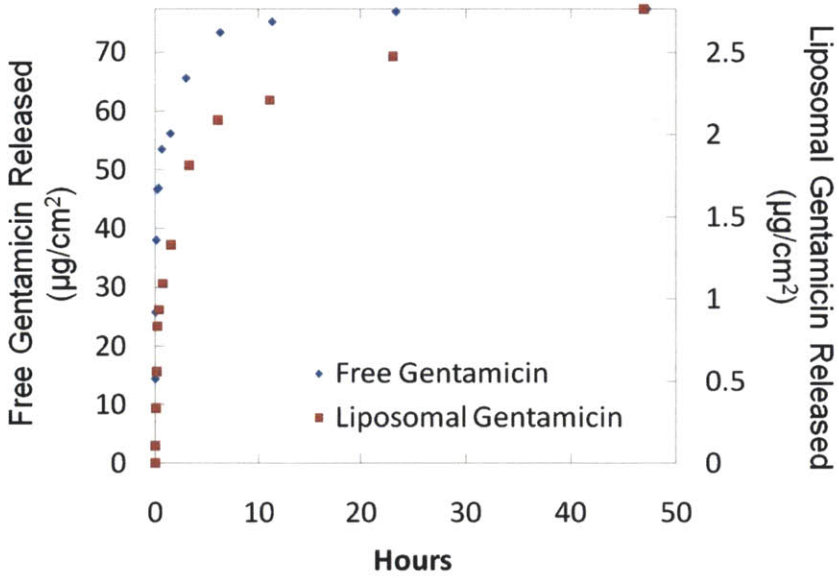

Figure 2-8. Cumulative gentamicin release for [Poly 1/HA/GS/HA]$_{50}$ plotted on the left ordinate and [Poly 1/HA/PLL-Lipo-GS/HA]$_{50}$ plotted on the right ordinate. Data sets represent values from one sample each.

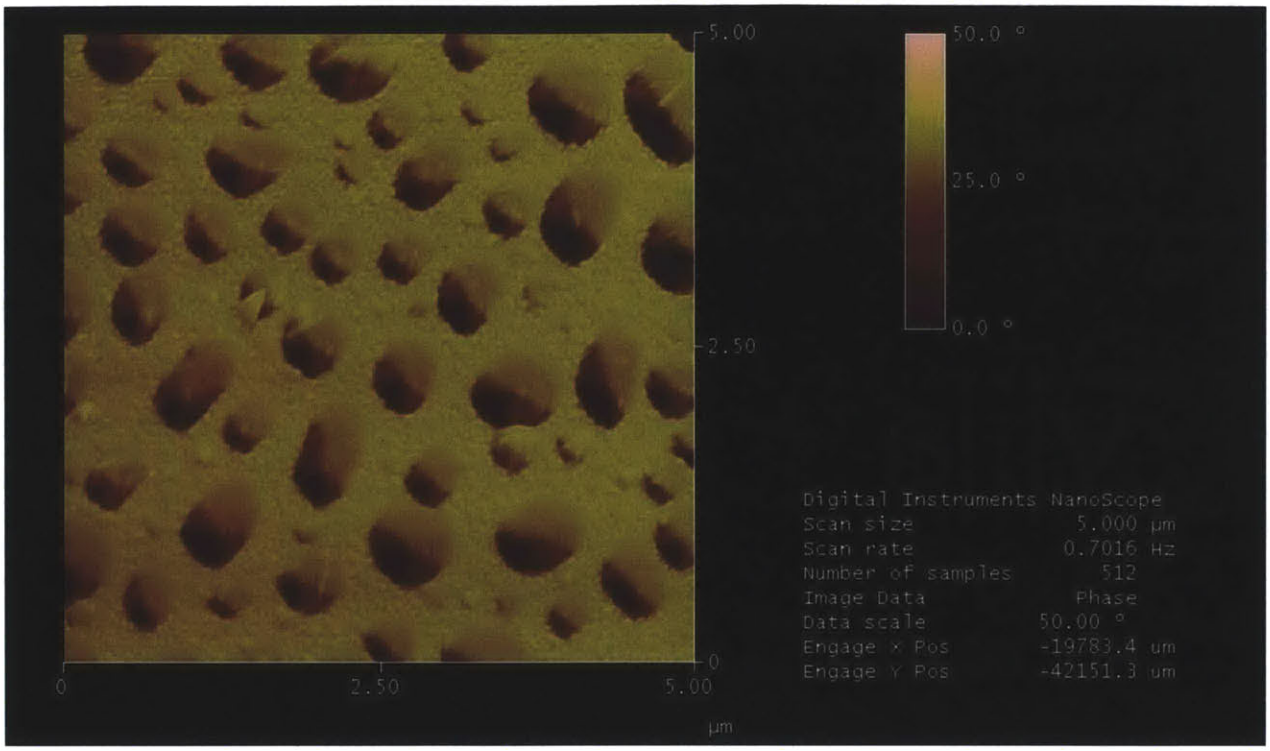

Figure 2-9. AFM phase image of [Poly 1/HA/PLL-Lipo-GS/HA]$_2$.

With respect to the application of existing implant-related infections, the necessity of large drug loading trumps that of the enhanced release kinetics. Without being able to virtually eradicate the existing infection with a bolus of drug, there is no need for prolonged presence of antibiotics since the bacteria will continue to thrive. It has been shown that a 2x increase in release duration comes at the cost of total drug payload. As a result, the liposomal LbL delivery of gentamicin, although possible, may not be the best route of antibiotic administration for the current application.

2.1.1.3 Conclusions

The use of liposomes in LbL films is promising for controlled release as a general platform, but is most appropriate for therapeutics that do not require significant mass loading while requiring significant control on release characteristics. For the case of antibiotics, large quantities of drug are both necessary and more important than prolonged release duration. Therefore, the liposomal LbL system studied here fell short. Although liposomes are capable of enhancing the release duration of gentamicin, their substantial mass compromises a significant amount of film

volume that could otherwise contain free drug. The use of liposome-mediated delivery of gentamicin is an attractive route for intracellular delivery of drug and therefore is still relevant, but this mechanism of gentamicin delivery from LbL films for the treatment of existing implant-related infection is not endorsed based on the data presented here.

2.1.2 Alternative Film Architectures

Given that the liposomes decreased the total loading of gentamicin in polyelectrolyte multilayered films, an effort was put forth to screen for the best performing film architecture with respect to loading and release duration. To remain consistent with the specifications for antibiotic implant coating design, films must be able to deliver their cargo at a rate that is capable of eradicating existing infection, control any latent infection in the surrounding tissues, prevent future colonization of the implant surface, and meet biocompatibility requirements. Consequently, the materials and architectures considered within the following section were chosen due to their biocompatibility and prevalence in LbL systems. The following screening experiments uncover the importance of some of the chemical considerations (with respect to material choice and film architecture) that form a basis for rational film design.

2.1.2.1 Experimental

2.1.2.1.1 Materials

Poly 1 and Poly 2 were synthesized as previously described [78]. Poly 2 contains two additional methylene units within the repeat unit when compared to Poly 1. Silicon wafers (test grade n-type) were purchased from Silicon Quest (Santa Clara, CA). Linear poly(ethyleneimine) (LPEI, M_n = 25 kDa) was purchased from Polysciences, Inc. Phosphate buffered saline (PBS) and nonradiolabeled gentamicin sulfate (GS) purchased in powder form were from Mediatech, Inc. (Herndon, VA). Sodium hyaluronate (or hyaluronic acid (HA), M_n = 1.7 MDa) was purchased from Lifecore Biomedical, Inc. (Chaska, MN). Poly (sodium 4-styrenesulfonate) (SPS, M_w = 1 MDa), poly(acrylic acid) (PAA, M_w = 1.25 MDa), PAA (25% in water, M_w = 50 kDa), dopamine hydrochloride, chitosan (CHI, medium molecular weight), and 3 M concentrated sodium acetate buffer (pH 5.2) were purchased from Sigma-Aldrich (St. Louis, MO). 1-ethyl-3-[3-

dimethylaminopropyl]carbodiimide hydrochloride (EDC) was purchased from Thermo Fisher Scientific (Waltham, MA). ^{3}H-GS (250 μCi total, 1 mCi/mL in ethanol, 200 μCi/mg) and ^{14}C-cholesteryl hexadecyl ether (CHE, 250 μCi total, 0.1 mCi/mL in toluene, 55 mCi/mmol) were obtained from American Radiolabeled Chemicals, Inc. Dialysis membranes were purchased from SpectraPor (Rancho Dominguez, CA). Modified simulated body fluid (m-SBF) was prepared as described previously [105]. All materials and solvents were used as received without further purification.

2.1.2.1.2 Synthesis of PAA-DOPA

Functionalization of the carboxylic acids on the PAA backbone required the use of the EDC zero-length crosslinker. The reaction ratio was set to achieve 50% dopamine functionalization. Four grams of PAA solution (25% in water) was added to 1.077 g of EDC and 1.318 g of dopamine in 45 mL of PBS (10 mM, pH 5.5). The pH of the reaction mixture was re-adjusted to 5.5 and the reactants were allowed to mix for at least one hour at room temperature. After reaction, the mixture was dialyzed extensively through a 12-14 kDa cutoff membrane and lyophilized. Overall functionalization was determined to be 30% by nuclear magnetic resonance (NMR). Reaction and characterization were kindly performed by Dr. Byeong-Su Kim.

2.1.2.1.3 Preparation of Polyelectrolyte Solutions

All solutions were prepared at 2 mg/mL in 0.1 M NaOAc and pH adjusted to 5.0. The GS solution was spiked with 5 μL ^{3}H-GS per 50 mL dipping solution yielding a 0.1 μCi/mL product without significantly changing the concentration of the GS dip bath. LPEI and PSS dipping solutions were prepared at 2 mg/mL in water and pH adjusted to 4.25 and 4.75 respectively with 1 M sodium hydroxide and 1 M hydrochloric acid. All solutions were prepared with water from a Milli-Q Plus (Bedford, MA) at 18.2 MΩ.

2.1.2.1.4 Polyelectrolyte Deposition

All polyelectrolyte LBL thin films were constructed as follows according to the alternate dipping method [44]. Substrates were rinsed with methanol and ultra pure water, dried under nitrogen, and plasma etched in oxygen using a Harrick PDC-32G plasma cleaner at high RF

power for 75 seconds. Layer-by-layer thin film deposition was performed using a Carl Zeiss HMS Series Programmable Slide Stainer. A nondegradable bilayer of LPEI/PSS was deposited first by immersion of the plasma treated substrates in LPEI for 30 minutes followed by a single ultra-pure water rinse, and finally in PSS for 30 minutes followed by a single ultra-pure water rinse. The degradable films were deposited on top of this PSS-terminated surface by alternate dipping in a cationic species (i.e. Poly 1, CHI, or GS) for 9 minutes followed by a cascade rinse of three 100 mM sodium acetate baths for 10, 20, and 30 seconds, and then into the anionic species (i.e. PAA, PAA-DOPA or HA) for 9 minutes followed by a similar rinse cycle. All polymer solutions and gentamicin solutions were completely replaced every 25 and 50 tetralayers, respectively.

2.1.2.1.5 Release of Gentamicin

Films were immersed into 3 mL of modified simulated body fluid (m-SBF) [105] in a tightly capped Falcon tube maintained at 37 °C. Degradation environments were kept sealed from the ambient to minimize evaporative loss. A 1 mL sample was extracted from the Falcon tube at predetermined time points and replaced with 1 mL prewarmed m-SBF in a manner so as not to mechanically disturb the hydrated film. The time points were selected with a greater frequency at early times to reflect the kinetics of release. Each extracted sample was mixed with 5 mL ScintiSafe Plus 50% (Fisher Scientific, Atlanta, GA) prior to GS quantification. The resulting mixtures were analyzed using a Tricarb Model 2810 TR liquid scintillation counter (Perkin Elmer, Waltham, MA). The raw data in disintegrations per minute (DPM) was converted directly to μg of drug using the DPM value for the dipping solution (10 mg/mL). Total release from the film at the *i*th timepoint was calculated by the following equation:

$$m_i = (C_i \times 3\ \text{mL}) + (1\ \text{mL}) \sum_{j=1}^{i-1} C_j$$

where m_i (μg) is the the total cumulative mass of GS released from the film at the time of measurement *i*, C_i (μg/mL) is the concentration of sample *i* (which is multiplied by a total of 3 mL in the Falcon tube), and the summation term adds up the total extensive quantity of gentamicin removed in each of the *i*-1 former aliquots.

2.1.2.2 Results and Discussion

2.1.2.2.1 Enhancing the Loading and Release of Gentamicin

The choice to cease troubleshooting of the liposomal LbL systems and redirect research efforts of this thesis toward alternative architectures was, in part, driven by the results of an experiment inspired by the work of Salomäki and Kankare [109]. Their study showed that $(CHI/HA)_n$ films built up exponentially in the absence of PAA, but that by periodically inserting a layer of PAA into this growing film, the growth characteristics were shifted toward linear growth. Specifically, $(CHI/PAA)_n$ and $(CHI/HA/CHI/PAA)_n$ yielded strictly linearly growing films, while insertion of PAA every 16^{th} layer allowed the film to grow exponentially between PAA deposition steps, but reset the buildup rate to almost zero after each PAA step. They concluded that PAA likely acted as a diffusion barrier in this system. Therefore, this concept was applied to the (Poly 1/HA/GS/HA)$_n$ system with the goal of controlling the diffusion of the small, hydrophilic gentamicin and consequently enhance release duration. (CHI/PAA) was alternated with (Poly 1/HA) every other tetralayer leading to the overall film architecture (Poly 1/HA/GS/HA)$(CHI/PAA/GS/PAA)_n$. Comparing films with equal total number of layers (i.e. 100 tetralayers to 50 octolayers), the (CHI/PAA) barrier yielded films with an order of magnitude increase in total loading and release duration (Figure 2-10, left) from the traditional tetralayer architecture of (Poly 1/HA/GS/HA) [53].

Films with the octolayer architecture (Poly 1/HA/GS/HA)(CHI/PAA/GS/PAA) were then compared to counterparts with dopamine-functionalized PAA (Figure 2-10, right). It was hypothesized that the addition of bulky side groups to PAA would further enhance its functionality as a diffusion barrier. Over the timescales studied, the dopamine-functionalized samples led to significantly reduced total loading compared to the pristine PAA, and negligible release rates were achieved after about 24 hours. It is possible that the more hydrophobic nature of the dopamine side groups compared to that of the former carboxylate groups provided a less favorable environment for gentamicin to enter the film. Regardless, these initial concept experiments elicited the necessity of a more thorough architecture screening to optimize the choice and order of film components.

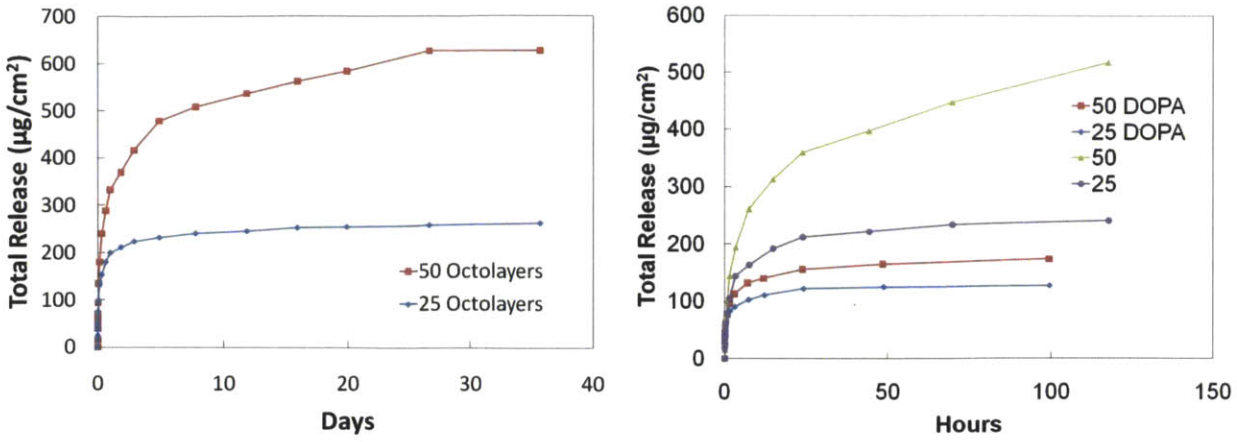

Figure 2-10. (Left) Release profile of (Poly 1/HA/GS/HA)(CHI/PAA/GS/HA)$_n$ with n = 25 and n = 50. (Right) Comparison in total drug release between (Poly 1/HA/GS/HA)(CHI/PAA/GS/HA)$_n$ and (Poly 1/HA/GS/HA)(CHI/PAA-DOPA/GS/HA)$_n$ at n = 25 and 50 octolayers. Data sets represent values from one sample each.

2.1.2.2.2 Screening for a Best-Performer

Experiments were designed to achieve strong reproducibility so as to confidently uncover the best-performing film architecture. Each experiment involved the batch fabrication and characterization of one sample set. A sample set is defined as one sample from each type of film architecture. Release quantities from each sample set were normalized to the maximum release value of the best performing film architecture in that particular set. For each comparison, three separate repeat experiments, each normalized to their own best-performer, were conducted completely independently.

In the first comparison (Figure 2-11, left), the total release decreased according to (Poly 1/PAA/GS/HA)$_{50}$ > (CHI/PAA/GS/HA)$_{50}$ > (CHI/HA/GS/HA)$_{50}$. Analyzing the latter two architectures first, the substitution of PAA for HA yielded substantially greater release. This result was already observed for films incorporating Poly 1 instead of CHI (Figure 2-8 compared to Figure 2-10, left). The charge density along the backbone of PAA is greater than that of HA, which leaves significantly more accessible charges for gentamicin to interact with during its deposition step. Substituting in Poly 1 for CHI further enhanced the release. Poly 1 is a hydrolytically degradable polycation while CHI is stable in water. Consequently, the CHI-based films are non-erodible in aqueous buffer and release their drug in diffusive manner. The Poly 1

films, however, are able to erode completely and additionally release strongly bound drug. Although it is difficult to draw firm conclusions concerning release kinetics when comparing these 50 tetralayer architectures, it is expected that at larger tetralayer numbers, the erosion-based release of films incorporating Poly 1 will become more apparent at later times relative to the diffusion based release.

In the second comparison (Figure 2-11, right), the total release decreased with (Poly 1/PAA/GS/PAA)$_{50}$ > (Poly 2/PAA/GS/HA)$_{50}$ > (Poly 1/HA/GS/PAA)$_{50}$. It was hypothesized that the position of PAA within the repeat structure of the multilayered stack would play a role in attaining higher loads. While placement of PAA directly before a drug deposition step would allow gentamicin to access a larger number of carboxylates than HA and therefore load gentamicin more densely into the growing film, placement of PAA directly after a drug deposition step was expected to limit the amount of previously loaded gentamicin from diffusing out of the film. Separately, it was hypothesized that the use of Poly 2 in place of Poly 1 would enhance release duration due to the presence of the additional ethylene group in the repeat unit making the backbone more hydrophobic and hence resistant to hydrolytic degradation; however, it was also expected that the same hydrophobic nature of Poly 2 might limit the total loading of the hydrophilic drug. It was found that despite the increased hydrophobicity of Poly 2 compared to Poly 1, the placement of PAA within the repeat structure of the multilayered stack dominated the drug loading characteristics. Comparing (Poly 1/PAA/GS/PAA)$_{50}$ and (Poly 2/PAA/GS/HA)$_{50}$, the former had better total drug load and similar (if not more prolonged) release duration. In addition to the repelling effect of the Poly 2 hydrophobicity on gentamicin loading compared to Poly 1, the HA may have allowed more drug to diffuse out of the film throughout the LbL buildup process than PAA. Furthermore, the comparable release kinetics of these architectures despite the use of Poly 1 in the former alludes to the stabilizing behavior of PAA over HA in these systems.

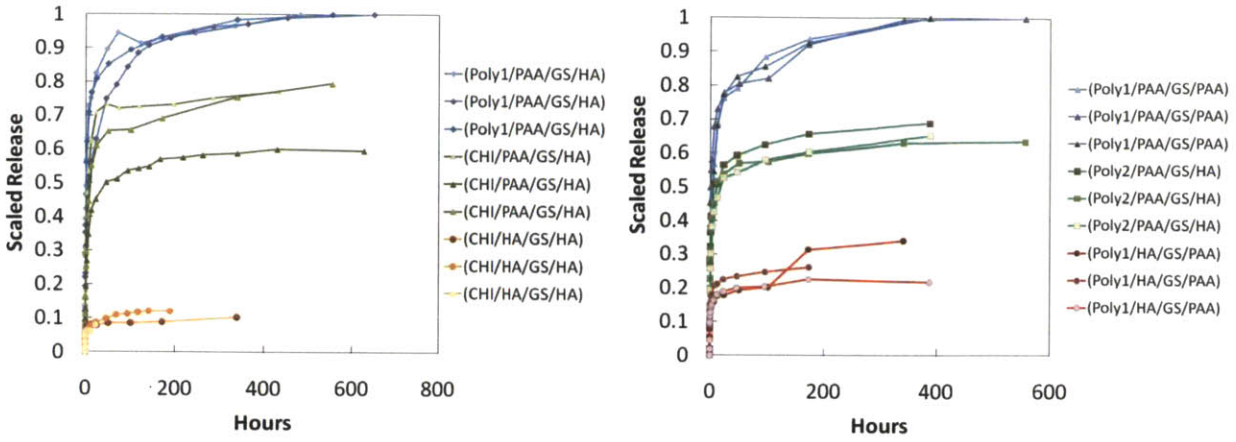

Figure 2-11. (Left) Comparison in total drug release between (Poly 1/PAA/GS/HA)$_{50}$, (CHI/PAA/GS/HA)$_{50}$, and (CHI/HA/GS/HA)$_{50}$. (Right) Comparison in total drug release between (Poly 1/PAA/GS/PAA)$_{50}$, (Poly 2/PAA/GS/HA)$_{50}$, and (Poly 1/HA/GS/PAA)$_{50}$. Each data set contains information from one sample. Data sets were generated in batches of three—one of each film architecture—and normalized to the maximum release value for that particular batch. Thus, each graph contains three independent repeat experiments. Data sets represent values from one sample each.

Extending upon the results shown in Figure 2-10 and Figure 2-11, a final screen for a best-performing architecture was conducted (Figure 2-12). There are two major takeaways from this experiment. First is that increasing the HA content of the multilayer film relative to the PAA content decreases its ability to load and retain gentamicin. Second is that the CHI substitution for Poly 1 doesn't add any noticeable benefit to the total release. Therefore, the definitive architecture for use as an antibiotic implant coating as a result of these screening efforts was (Poly 1/PAA/GS/PAA)$_n$.

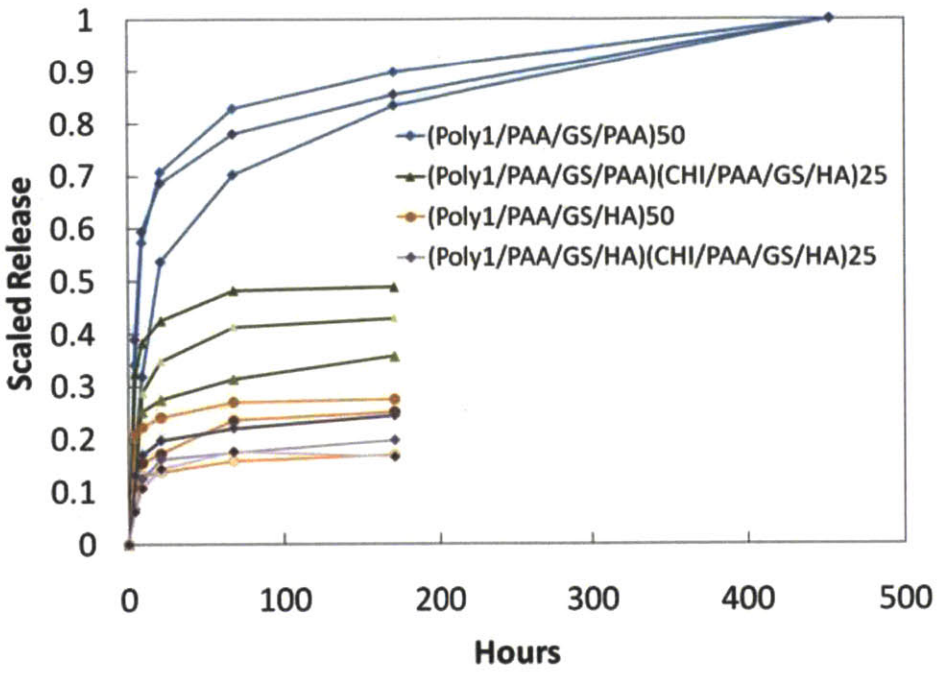

Figure 2-12. Comparison in total drug release between (Poly 1/PAA/GS/PAA)$_{50}$, (Poly 1/PAA/GS/PAA)(CHI/PAA/GS/HA)$_{25}$, (Poly 1/PAA/GS/HA)$_{50}$, and (Poly 1/PAA/GS/HA)(CHI/PAA/GS/HA)$_{25}$. Data sets were produced in a similar manner to those presented in Figure 2-11 and contain values from one sample each.

2.1.2.3 Conclusions

Beyond the obvious biocompatibility issue, the single most important issue to address when designing antibiotic coatings for implantable medical devices is the ability to eradicate an infection. Second to this is the prolonged presence of antibiotics near the implant surface to prevent any possibility of biofilm formation. Therefore, with respect to total release of gentamicin from polyelectrolyte multilayers, the best performing system studied here was (Poly 1/PAA/GS/PAA)$_n$. This architecture significantly enhanced the ability of the LbL films to load drug over previously published systems [53]. PAA provides a higher density of carboxylates per length of polymer than HA, thus presenting a greater number of ionic sites to bind gentamicin. Poly 1 imparted erodible functionality (compared to CHI) which allowed near-100% release of the loaded drug. Comparisons in release kinetics were less conclusive since films with limited numbers of tetralayers were used in these studies. In theory, prolonged durations should be

attainable by increasing the total number of layers in the film and rates can be tuned by choice of the erodible polycation [79].

2.2 *Characterization of the Performance of [Poly1/PAA/GS/PAA]$_n$*

The work presented in this section has been reproduced from the published manuscript entitled "The effectiveness of the controlled release of gentamicin from polyelectrolyte multilayers in the treatment of Staphylococcus aureus infection in a rabbit bone model" by Joshua S. Moskowitz, Michael R. Blaisse, Raymond E. Samuel, Hu-Ping Hsu, Mitchel B. Harris, Scott D. Martin, Jean C. Lee, Myron Spector, and Paula T. Hammond (*Biomaterials*, vol. 23, pp. 6019-30, 2010) with permission from Elsevier.

PAA has been used in its bulk form as both a gentamicin delivery vehicle in an *in vivo* osteomyelitis model [110] and an orthopedic implant coating to enhance the biocompatibility of titanium-based surfaces [111]. Unlike HA, PAA can act as a diffusion barrier within multilayer films [109], and has a much larger glass transition temperature (T_g) (106 °C compared to about 14 °C), thereby resulting in mechanically more rigid films that release the relatively diffusive gentamicin over a longer timescale. A set of GS release experiments directly compared PAA to HA using the architecture [Poly1 / Anion / GS / Anion]$_{50}$; the polyanions are compared in Figure 2-13. The 1.25 MDa PAA films (n = 4) incorporated about 7.5 times more GS than the 1.7 MDa HA films (n = 8). This could be partly due to the difference in charge density along each respective polymer backbone (i.e. difference in total charges per mass of repeat unit for each polymer). Given identical polymer concentrations by mass in the fully charged state, the PAA would have approximately 5.26 times more charge than the HA. This results in comparatively less interaction and bonding of HA with GS in the multilayer films.

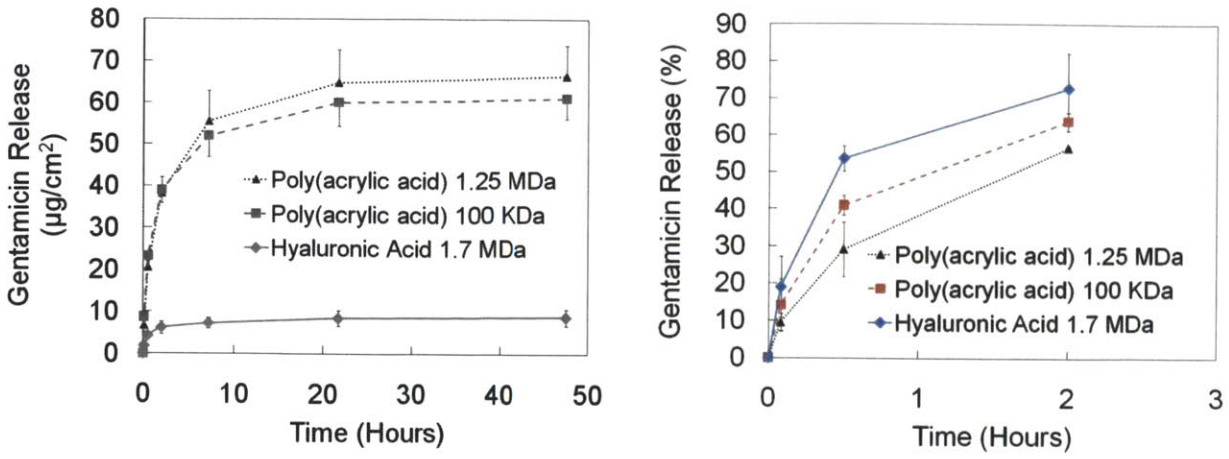

Figure 2-13. (Left) Cumulative amount of gentamicin released from [Poly 1 / Anion / GS / Anion]$_{50}$ films. (Right) Normalized plot shows differences in release kinetics. Data sets represent the mean ± standard deviation of n = 4 samples for 1.25 MDa PAA, n = 6 for 100 kDa PAA, and n = 8 for HA.

The screening experiments also sought to determine the benefit of using 1.25 MDa PAA over 100 kDa PAA. It was found that the high molecular weight PAA (n = 4) did indeed incorporate greater amounts of drug than the low MW counterpart (n = 6), but not by a significant margin. Subsequent experiments utilized the 1.25 MDa PAA.

2.2.1 Growth, Erosion, and Release of [Poly 1/PAA/GS/PAA]$_n$.

One of the major advantages to LbL systems is that the thickness of the films can be tuned according to the total number of layers deposited. Since drug is cyclically incorporated throughout the growth process as one of the structural components, the total drug loading scales with thickness and is therefore also tunable (but not independently). The [Poly 1/PAA/GS/PAA]$_n$ architecture resulted in stable and reproducible film growth up to 200 tetralayers (Figure 2-14).

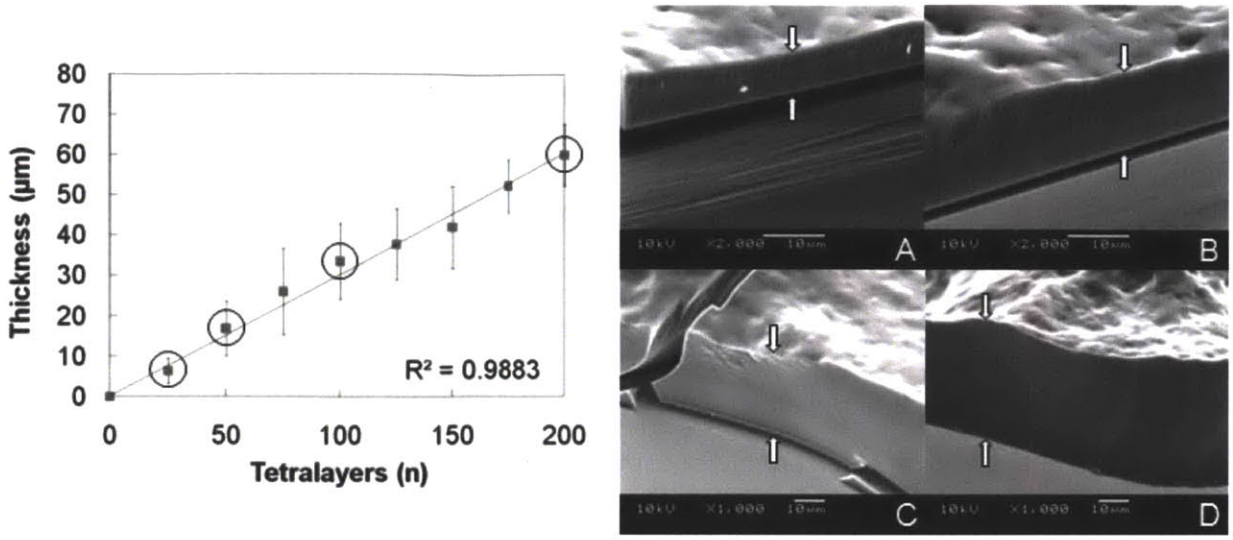

Figure 2-14. (Left) Growth curve for [Poly 1/PAA/GS/PAA]$_n$. SEM images are provided for the circled data points. Thicknesses were measured by profilometry at four predetermined points on each substrate and averaged over three replications. The error bars represent the average root mean squared roughness from triplicate samples and quadruplicate measurements per sample. (Right) SEM images of the growing film on a silicon surface at (A) n = 25, (B) n = 50, (C) n = 100, and (D) n = 200 layers. White arrows mark the film edge. Nota bene: the scale changes between (B) and (C).

Several studies have sought to explain differences in observed growth behavior of LbL systems [112-117]. The simplest systems grow solely in linear fashion as polyelectrolytes in solution interact only with the oppositely charged outermost layer of the growing film. Bilayer thicknesses during basic linear growth range from the nanometer scale to tens of nanometers. Exponential growth is generally observed when there is at least one diffusive component that absorbs into the bulk of the growing multilayer film, and each subsequent deposition cycle leads to increased increments of material absorbed. Based on the data, for which the average bilayer thickness is on the order of 150 nm, it is hypothesized that the films begin building in the exponential regime due to the diffusive nature of gentamicin (477 Da). After the film is grown beyond a threshold thickness—which takes place before the 25 tetralayer data point—there is a transition from the exponential regime to a secondary linear regime. This occurs when the film becomes so thick that the time provided for diffusion (i.e. 9 minute dip cycles) is less than the time necessary for the gentamicin to access the entire thickness of the film via diffusion. As a result, this diffusion-limited growth curve appears despite the presence of a

diffusive component, but exhibits much larger bilayer thicknesses. Details of this transition and how to control its onset are described elsewhere [115, 116]. One implication of this behavior is that it is expected that the concentration of gentamicin is greatest in the diffusion zone of the film (i.e. the outermost region), which therefore contributes to an initial burst-release behavior of drug.

The surface roughness increases with the total number of deposited tetralayers until about n = 50, after which it remains relatively constant (8.6 ± 1.6 μm) as observed both with profilometry and scanning electron microscopy (data not shown). The unusually high values of roughness in the current system are likely a result of significant interdiffusion of PAA, which is a weak polyanion with a solution dissociation constant (pKa ≈ 6.5) [118] that lies above the deposition condition (pH = 5.0), and the small positively charged molecule gentamicin. The combination of this interdiffusion and some small amount of film dissolution during the assembly period is a likely cause of some diffusive loss of material from the film, which introduces roughness during the deposition process.

2.2.2 *In Vitro* Activity against *Staphylococcus Aureus*

One of the deliverables of this study was to confirm the killing efficacy of these LbL constructs against *S. aureus* in an *in vitro* assay and further ensure that the ethylene oxide (EtO) sterilization procedure does not change release kinetics, since sterilization is required for all implantable medical devices. Kirby-Bauer disk diffusion assays provide both qualitative information and a quantitative estimate of the amount of gentamicin that has diffused through agar by measuring the zone of inhibition (ZOI). In Kirby-Bauer disk diffusion assays, agar plates were inoculated with exponentially growing *S. aureus* in cation-adjusted Mueller Hinton Broth (CMHB) at 10^8 CFU/mL, and incubated with the sample at 37 °C for 16-18 hours. The diameter of the inhibition zone was measured in millimeters. $[\text{Poly 1/PAA/GS/PAA}]_{200}$ + $[\text{Poly 1/PAA/GS}]_1$ films were grown on identical titanium rods with dimensions similar to those used in the *in vivo* experiment (Chapter 5). One of the rods was subjected to EtO sterilization while the other was left unsterilized. Each rod was pressed into a separate agar plate and BD Sensi-Disc standards with 10 μg of gentamicin were used to ensure that the ZOIs could be accurately compared. The

ZOI was virtually unchanged by the 12 hour EtO cycle, which supports the fact that EtO is an effective way to sterilize the LbL system without altering film loading or release kinetics. Furthermore, the Kirby-Bauer diameter, which is the diameter of the ZOI minus the linear dimension of the eluting agent (e.g. the rod), was approximately 22.8 mm in comparison to the 18.1 mm generated by the Sensi-Disc standard (Figure 2-15); *in vitro* diameters that exceed 15 mm are generally regarded as a good predictor of effective treatment against *S. aureus* [119].

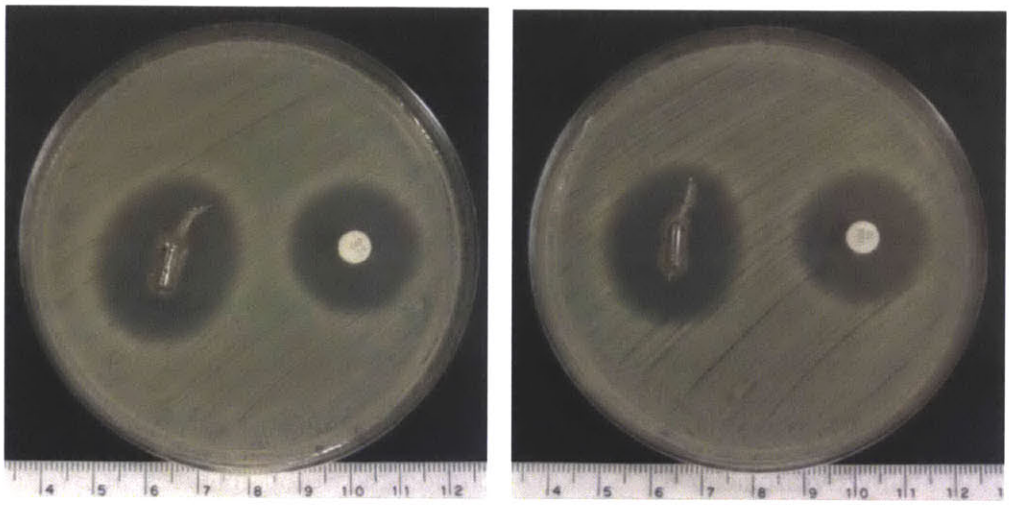

Figure 2-15. Untreated (left) and EtO treated (right) titanium rods coated with [Poly 1/PAA/GS/PAA]$_{200}$ + [Poly 1/PAA/GS]$_1$ produced a baseline zone of inhibition of 25.6 mm (measured perpendicular to the long axis of the rod) against S. aureus after overnight incubation at 37 °C. As a control, the sample is referenced to a commercially available BD Sensi-Disc. The lighter color at the rod surface is a result of the ruptured agar and not the presence of bacteria. The scale bar is in centimeters.

2.2.3 Cytotoxicity toward MC3T3-E1 Cells.

2.2.3.1 MTT Assay Details

The MTT stock solution was prepared in minimum essential medium alpha (α-MEM) without the phenol red pH indicator at a concentration of 5 mg/ml and stored at -20 °C. The working MTT solution (0.5 mg/ml) was prepared immediately before use by dilution of the stock MTT solution in α-MEM growth medium without phenol red. The MC3T3-E1 culture medium was replaced by the appropriate volume of the MTT working solution and incubated at 37 °C and 5% CO2 in humidified air for exactly 4 hours. The MTT culture medium was gently aspirated at the

completion of the 4-hour incubation period. The formazan metabolic precipitate produced within the MC3T3-E1 cells was dissolved with the addition of dimethyl sulfoxide to the cultures and shaking of the plates. The homogenous purple solution was distributed into clear 96-well plates (100 µL/well) in 4 to 6 replicates. The absorbance reading of the MTT solutions were performed at 570nm with 630nm reference wavelength using a BioTek PowerWave XS Microplate spectrophotometer which reports data as the difference in absorbance between the test and reference wavelengths. Control well (containing 100 µl of DMSO) and blank wells were always included on each 96-well plate and this absorbance reading (typically measuring 0.045) was subtracted from all MTT absorbance readings.

2.2.3.2 Live/Dead® Viability/Cytotoxicity Details

The recommend working solution of 2 µM calcein and 4 µM ethidium homodimer-1 was prepared in PBS and supplemented with 0.2 mg/ml Hoechst 33342. In brief, MC3T3-E1 cultures were rinsed with warm PBS and then incubated with an appropriate volume of the modified Live/Dead® Viability/Cytotoxicity Kit working solution for 30-60 minutes at 37 °C. The dye solution was gently aspirated from cultures, rinsed with PBS, and the cultures were fixed with 10% formalin at room temperature for 15 minutes in the dark.

2.2.3.3 Results

MTT assays were run to determine the cytotoxic effect of these films against MC3T3-E1 murine cells, subclone 4 with high osteoblast differentiation and mineralization activity. The experiment was designed to mimic an overcompensated situation where films were eluted at 37°C for one week (≈70% of cargo, Chapter 5) into a small buffer reservoir forming a more concentrated test sample relative to what would be experienced *in vivo*. The experiment was repeated in triplicate for films of 100 and 200 tetralayers, and results compared to a negative control of untainted minimum essential medium (alpha) buffer. Since the *in vivo* environment is both a larger reservoir and an open system, the concentrations of degraded material achieved in this *in vitro* experiment should exceed those that would be experienced by the same films *in vivo* barring any local gradients at the film surface that would exist in any antibiotic film-eluting system.

There was no statistical difference in metabolic activity of the cells between the control and 100 tetralayer elution buffers in this assay (single tailed student's t-test assuming equal variances, Figure 2-16A). However, the 200 tetralayer elution buffers did cause a significant reduction in the metabolic activity of the cells. Upon further investigation via the Live/Dead® assay and direct imaging with fluorescence microscopy, it was confirmed that the 100 tetralayer films were benign towards the MC3T3-E1 cell line and present no apparent biocompatibility issues (Figure 2-16B). In contrast, the 200 tetralayer elution buffer (Figure 2-16C) caused a clear reduction in cell viability as a result of the increased concentration of eluted material. Dead cell percentages were calculated for each test group from cell counts of the fluorescent images (Figure 2-16D). The discrepancy between the reduced metabolic activity (~70% reduction) and the cell viability (~25% reduction) suggests that the metabolic activity per cell is also reduced. These cytotoxic effects must be a result of either Poly 1 (or degradation products), GS, PAA, or complexes. Past studies have determined the biocompatibility of Poly 1 towards a variety of cell lines [53, 78, 80], and PAA is an FDA-approved, biocompatible material that has been studied for use as a surface coating to enhance the biocompatibility of titanium implants [111]. It is well-known that GS is nephrotoxic and ototoxic at elevated systemic concentrations, which reinforces one of the main benefits of localized drug delivery systems. A 200 tetralayer film contains roughly 600 $\mu g/cm^2$ of GS (Chapter 5), which after one week would have eluted about 450 $\mu g/cm^2$ of drug (i.e. 70%) into the 4.5 mL/cm^2 of buffer, yielding a 100 µg/mL solution of GS. Isefuku *et al.* determined that GS concentrations above 100 µg/mL caused reduction in osteoblast alkaline phosphatase activity which is necessary for proper enzyme function [120]. At higher concentrations of GS, osteoblast cell proliferation was affected. Likely the GS—whether complexed or not—is likely the culprit for the onset of the observed cytotoxic effects of the 200 tetralayer elution buffers.

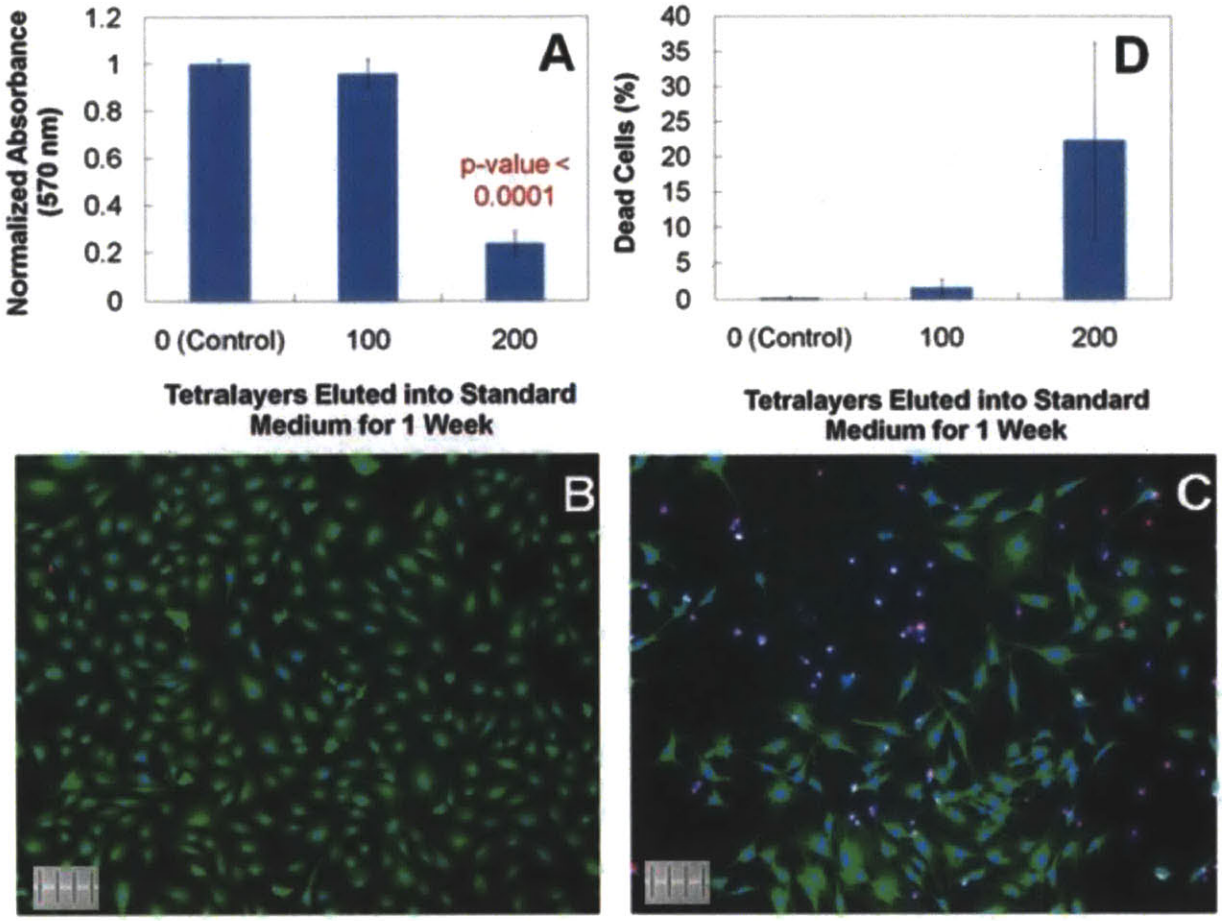

Figure 2-16. (A) MTT metabolic activity of MC3T3 cells after 16-18 hr treatment in elution buffer normalized to negative control (i.e. cells incubated in standard medium). The p-value was computed using a single-tailed student's t-test assuming equal variances, and data represent the mean ± standard deviation for three different samples. Images of MC3T3 cells subjected to 16-18 hr treatment in (B) 100 and (C) 200 tetralayer elution buffer. Live cells are represented by a blue nucleus surrounded by green cytoplasm. Dead cells are represented by a red nucleus. (D) Percentage (and standard deviation) of dead cells calculated from triplicate images. Scale bar hash marks are spaced 100 μm apart.

2.3 *Post-Processing Techniques for Controlled Release*

2.3.1 Crosslinking

It was hypothesized that by creating a lightly crosslinked network throughout the degradable films, the diffusion pathways for gentamicin would become much more tortuous and hence prolong its release kinetics. Both thermal and ultraviolet radiation techniques were initially

considered as candidates for achievement of crosslinking. For thermal crosslinking, films were placed into a Shel Lab vacuum oven. For ultraviolet crosslinking, films were treated in a Spectroline UV Crosslinker Select Series. Release profiles for films with varying treatments are shown in Figure 2-17. Ultraviolet crosslinking treatment of 1 hour under intensity greater than 4 mW/cm^2 did not noticeably alter the release kinetics from the as-made samples (Figure 2-17, right). The thickness and roughness of these samples—about 15 μm and 3 μm, respectively—likely scattered the UV light such that only the outermost surface received any significant crosslinking. Hence, the effects of UV radiation were not studied further.

As for thermal crosslinking, both time and temperature proved to be important parameters with respect to tuning the final film behavior. Films baked for 30 minutes at 130 °C or less had little effect on release behavior; however, increasing the temperature to 140 °C and 160 °C respectively led to an incremental increases in the release duration of gentamicin. Films baked at 130 °C for 2 hours had a similar effect. These effects are clear indications that physical (i.e. dehydration) or chemical (i.e. amide or anhydride formation) changes have taken place within the bulk of the film.

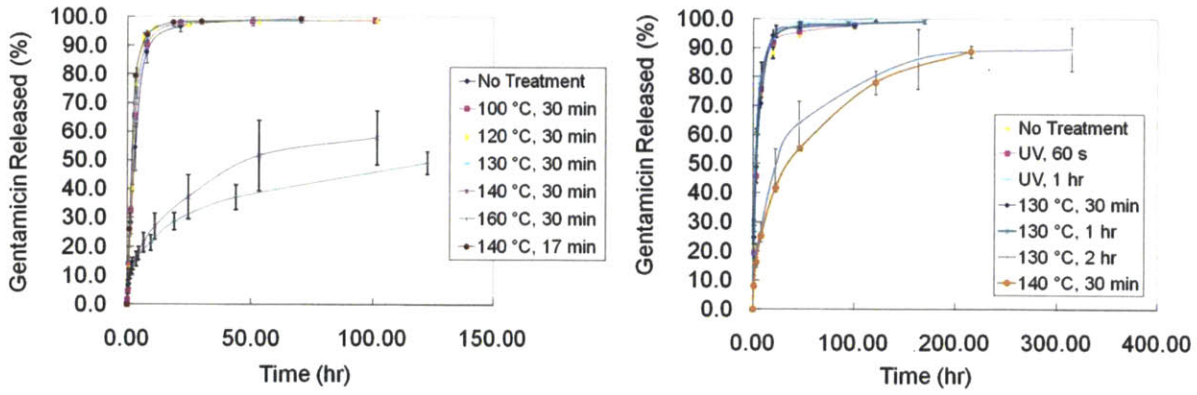

Figure 2-17. Release profiles of [LPEI/SPS]$_{10}$+[Poly1/PAA/GS/PAA]$_{50}$ treated with various crosslinking conditions in PBS at 37 °C. Data sets represent the mean ± standard deviation of triplicate samples.

To test for the existence of covalent bonding between gentamicin and PAA (i.e. amide formation), the bioactivity of drug released from untreated, 140 °C (30 minutes), and 170 °C (30 minutes) films was tested against *S. aureus* 25923 (Figure 2-18). 50 tetralayer samples were released into cation-adjusted Mueller Hinton Broth, measured for gentamicin content using

liquid scintillation counting, and then applied directly to bacteria cells at different dilutions. All experiments were performed in triplicate. The untreated samples yielded a minimum inhibitory concentration (MIC) of about 0.1 $\mu g/cm^3$ (Figure 2-18, A) which was consistent with literature values [53, 82, 84]. The 140 °C samples yielded an MIC that appeared to be slightly lower than this value (Figure 2-18, B) indicating that full bioactivity is retained after 140 °C heat treatment for 30 minutes. The slight decrease could potentially be a result of complexing phenomena that allow the drug to more effectively permeate the bacterial cell membranes. The 170 °C samples had no observed MIC within the concentration range studied (Figure 2-18, C), indicating that the MIC has been shifted higher by more than an order of magnitude. This shift is consistent with the fact that the gentamicin was covalently binding with another component of the film—likely through amide formation between the primary amines on gentamicin and the free carboxylic acids on PAA—thus rendering it inactive.

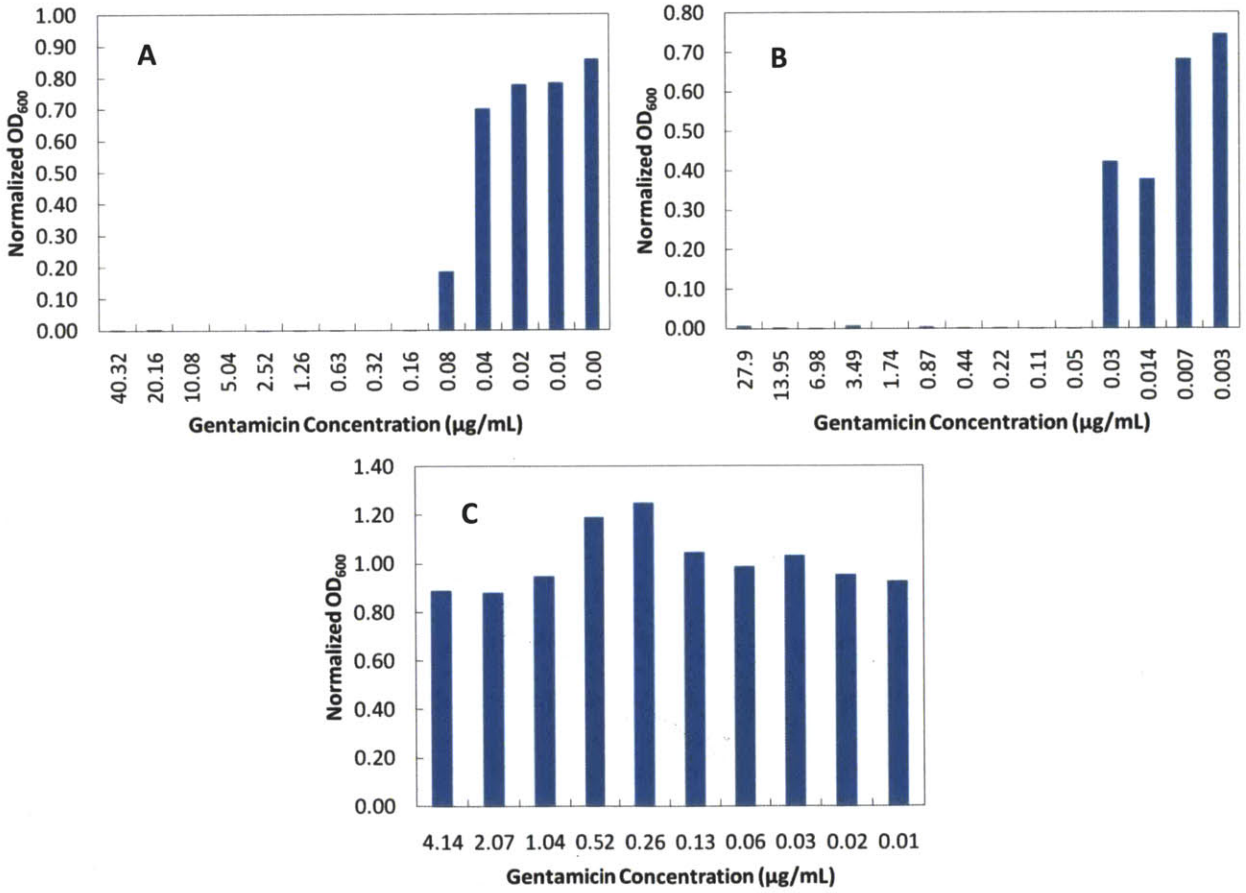

Figure 2-18. Microdilution assays determining the minimum inhibitory concentration of drug eluted from A) untreated films, B) films heated at 140 °C for 30 minutes, and C) films heated at 170 °C for 30 minutes. All graphs are normalized to the negative control. All data represent the average values of three separate measurements from a single sample. Similar results were observed for two additional repeat experiments each using a separate sample (data not shown).

The erosion characteristics of the films was studied by immersing the films into PBS at 37 °C and three unique behaviors were observed between untreated films and heat treated films at 140 °C (30 minutes) and 170 °C (30 minutes). The untreated films were found to anneal such that the films transitioned from being macroscopically rough (i.e rms roughness of 3 μm) to macroscopically smooth (i.e. rms roughness < 1 μm). This suggested that bulk rearrangement of the film components was possible, which is reminiscent of a lack of a crosslinked network. The initial erosion rate proceeded at about 10%/2 hours (data not shown). Unlike the untreated samples, there was no observed change in the roughness of the 140 °C samples when placed into the erosion medium, which pointed to the existence of some degree of crosslinking. These samples did, however, undergo initial erosion rates that were similar to the untreated samples. Therefore, the crosslinking was likely of the hydrolytically reversible anhydride type between carboxylic acids along the PAA chains. The similar initial erosion rates yet different release rates between untreated samples and 140 °C samples suggest that the effective diffusivity of gentamicin in the polymer matrix has been enhanced in the case of the latter. Samples baked at 170 °C did not exhibit any significant erosion behavior even when placed in 60 °C release medium or exposed to 1M sodium hydroxide. Further, these films tended to float off the silicon substrate and remain intact in solution. Such mechanical durability can be attributed to the formation of amide bonds. Release from these films was, consequently, diffusion based.

Samples of $[LPEI/SPS]_{10}$+$[Poly1/PAA/GS/PAA]_{25}$ were built on infrared transparent silicon for analysis via a Nexus Fourier Transform Infrared spectrophotometer (Figure 2-20). The formation of anhydrides (red dashed lines at about 1800, 1750, and 1030 cm^{-1}, Figure 2-20, left) became quite apparent after high 170 °C temperature treatment, which was consistent with previous observations in the heat treatment of PAA [121, 122]. Additionally, a significantly more pronounced amide peak corresponding to the carbonyl stretching in CONH was observed

near 1650 cm^{-1} (blue dashed line, Figure 2-20, left) [123, 124]. Peaks at about 1715 (carbonyl stretching of COOH), 1550 (asymmetric stretching of COO^-), and 1400 (both COOH and COO^-) cm^{-1} (green dashed lines, Figure 2-20, left) were correspondingly diminished, as expected. While the existence of noticeable crosslinking peaks helped to confirm the observed physical behavior of samples treated at high temperature, there was less conclusive FTIR evidence for these conclusions at 140 °C. Although it was possible that crosslinking could have taken place to a less detectable extent, one significant observation was that the signal from hydroxyl stretching (broad peak centered near 3300-3400 cm^{-1}, Figure 2-20, right) was considerably reduced in the case of the 140 °C samples when compared to the untreated samples. This could be attributed to thermal dehydration of the films, which could potentially restrict the ability of water to quickly access the bulk of the film when placed into aqueous medium, thus slowing the diffusion-based drug release process as well as limiting the ability of the film to undergo the same rapid annealing rearrangements that were observed in untreated films.

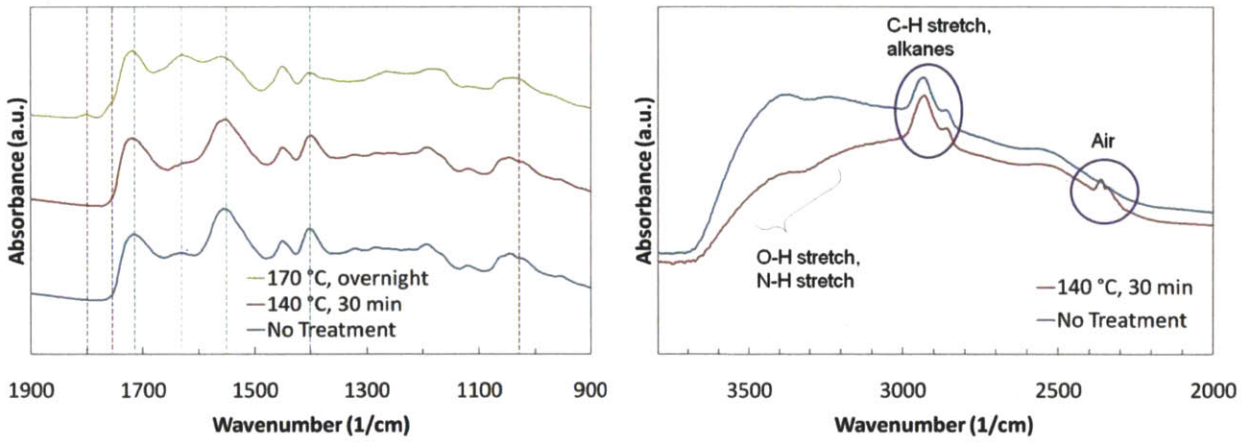

Figure 2-19. FTIR spectra of one sample first untreated, then baked at 140 °C for 30 minutes, and finally baked again overnight at 170 °C. (Left) Spectra between wavenumbers 900 and 1900, and (right) spectra between wavenumbers 2000 and 3800. Data were selected as characteristic examples amongst six repeat experiments. All data sets were reported used a minimum of 32 scans.

2.3.2 Sponge Effect

Using the model system (Poly 1/PAA/GS/PAA)$_{50}$, the effect of increasing concentration of the gentamicin dip bath was studied. It was found that beyond the initial burst release phase, the kinetics of release were not substantially altered by the concentration of the gentamicin dip bath (Figure 2-20). Beyond the first day, the rates of release were found to be approximately zero order and relatively similar regardless of the gentamicin concentration. There are several inferences that can be made. With each drug deposition step, a fraction of the drug entering the film will interact with the existing free ionic sites and form electrostatic bonds. The number of molecules forming electrostatic bonds with the growing multilayer film is independent of the concentration of the gentamicin dip bath. The remainder of the drug is driven into the multilayered stack due to the chemical potential of the dip bath and remains nonspecifically bound within the film. This quantity increases with increasing concentration of the dip bath until the point where the film becomes completely saturated with drug. Upon rinsing, much of this nonspecifically bound drug diffuses out of the film; however since both the diffusion and the rinse cycle are time-dependent processes, the diffusion process may not be complete on the timescale of the rinse cycle. As a result, the bolus release of drug that is observed during a release experiment is highly correlated with the concentration of nonspecifically bound gentamicin and therefore highly correlated with the concentration of the gentamicin dip bath (and duration of the dip time). The linear release phase is correlated with the electrostatically bound drug, which is relatively constant per area when comparing samples with an equal number of deposition steps.

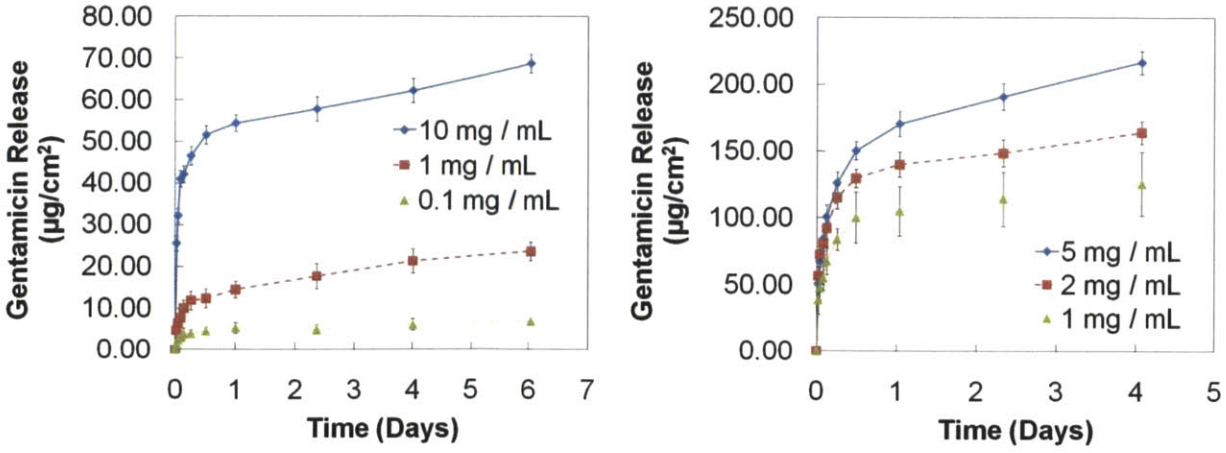

Figure 2-20. Effect of increasing the concentration of the gentamicin dip bath on release kinetics in (left) ultra pure water and (right) modified simulated body fluid. The differences in total release quantities were a result of the pH of the release medium as discussed in more detail in Chapter 3. Data sets represent the mean ± standard deviation of triplicate samples.

To further investigate the diffusive release that takes place throughout the timescale of a rinse cycle, the release of three separate films with the (Poly 1/PAA/GS/PAA)$_n$ architecture were compared to counterparts that contained an additional three layers—(Poly 1/PAA/GS)$_1$—without a final rinse cycle (Figure 2-21). It was found that this technique predominantly affected the burst release phase, and yielded a total increase in drug loading on the order of 20%. As described earlier, by simply changing the concentration of gentamicin in this final deposition step, this "sponge" technique could potentially be used to tune the burst release phase without significantly changing release kinetics.

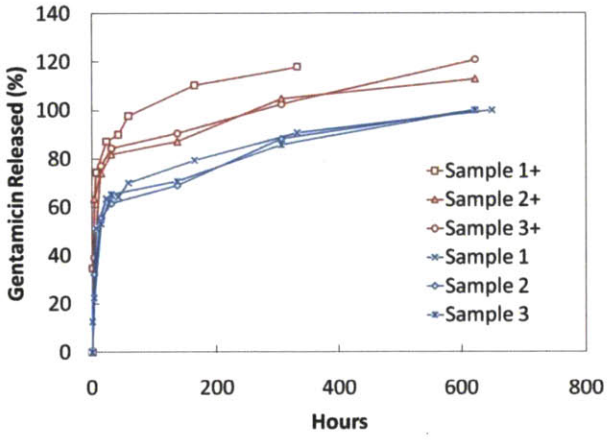

Figure 2-21. Effect of ending on a drug deposition step without a final rinse. Each of the three samples shown here are compared against their '+' counterpart which contains an additional (Poly 1/PAA/GS)$_1$ without a final rinse cycle. Data sets represent individual samples.

Chapter 3 Theoretical Treatment of Drug Release from PEM Coatings

3.1 *Introduction*

The goal of this theoretical treatment is to derive an analytical function to describe mass of drug released per area of film (Q) as a function of time, which is based on physically relevant processes. The approach is to first solve a highly simplified abstraction from the true physical system, and then incorporate any necessary complexities later. Although previous work has described the drug release from surface and bulk eroding polymer matrices, emphasis was placed on development of an immediately useful model for erodible thin films that does not require the use of finite element analysis [125, 126] or many parameters [127]. After development of this initial theoretical treatment, a numerical description of the drug-releasing system based on finite differences is coded in MATLAB for comparison to the analytical derivation.

3.2 *The Mathematical Framework*

To begin, the assumption is made that the film components are homogeneously distributed throughout the bulk of the film and that each mechanism of release works completely independently:

(3-1) $$Q(t) = Q(t)_{\text{erosion}} + Q(t)_{\text{diffusion}} + Q(t)_{\text{ejection}} + Q(t)_{\text{other}}$$

Here, *Q(t)* is the drug released per area of film. The release mechanisms of erosion, diffusion, and ejection are the only significant phenomena described in literature that are relevant to most drug releasing LbL systems. Film erosion and drug diffusion-based release are the most widely studied release mechanisms. Ejection is the pH-induced release of film components when subjected to media that are of a different pH than the film deposition conditions causing charge mismatch and subsequent equilibrium-seeking behavior [128]. To simplify the current problem, it is assumed that $Q(t)_{other}$ is small, and that release experiments are conducted at the deposition conditions hence negating the mechanism of ejection:

(3-2) $$Q(t) = Q(t)_{\text{erosion}} + Q(t)_{\text{diffusion}}.$$

To effectively parse out the contributions from each release mechanism and help validate the model, release experiments should be conducted at the most stable conditions possible to promote surface-based erosion over bulk degradation. Therefore, to determine these conditions, a set of [Poly 1/PAA/GS/PAA]$_{50}$ were built with growth characteristics shown in Figure 3-1.

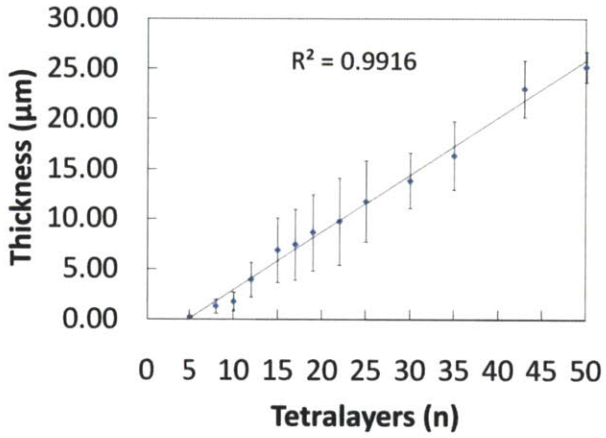

Figure 3-1. Growth curve of [Poly 1/PAA/GS/PAA]$_n$ used for model validation. Measurements were made on triplicate samples and error bars indicate the rms roughness values (note: use of standard deviation of thickness would have yielded much tighter error bars). For the thickness measurements, all coefficients of variation were less than 0.5.

When determining the effects of ionic strength and pH on degradation behavior, these drug releasing tetralayer samples were compared to all-polyelectrolyte samples of [Poly 1/PAA]$_{100}$. It was found that ionic strength does not significantly impact degradation behavior of the erodible films until sufficiently high concentrations of salt were added (>300 mM, Figure 3-2, left). Ionic strength does not play a role in hydrolysis of Poly 1, but does impact the rate at which ionic bonds can be broken, which is an important step in the erosion process. Within a factor of three from the 100 mM deposition conditions, film stability was virtually independent of ionic strength. According to Figure 3-2, right, film degradation is most stable in the pH range of 4.0 to 5.5, which was expected as this represented the vicinity of the deposition conditions; however, upon further investigation of the relative thickness/roughness (which is a metric of film smoothness), it was found that pH 5.0 uniquely allows the bilayer films to erode in the

most stable manner (Figure 3-3, left). Again, this was expected as it corresponds to the exact deposition condition and minimizes the effect of material ejection from the film surface, which can induce roughness. The inconclusive results and large coefficients of variation for the tetralayer films (Figure 3-3, right) were caused by the limited number of samples studied for each data point (i.e. n = 3). The coefficients of variation for the pH 5.0 and 5.5 samples were 0.64 and 0.50 respectively. Based on these results, it is reasonable to hypothesize that the deposition condition is the most stable for studying film degradation and drug release.

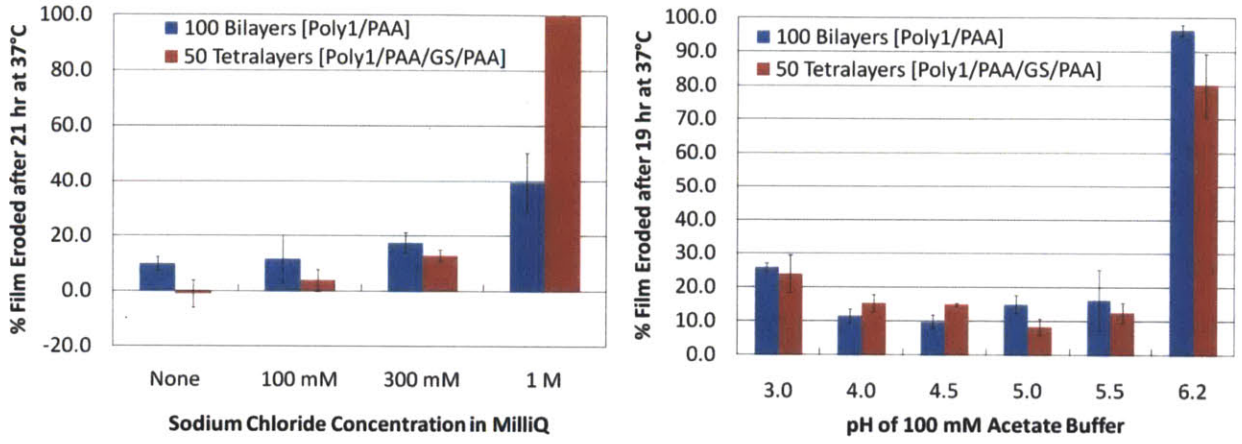

Figure 3-2. Effect of ionic strength (left) and pH (right) on erosion of $[Poly\ 1/PAA]_{100}$ and $[Poly\ 1/PAA/GS/PAA]_{50}$. Measurements represent the mean ± standard deviation of triplicate samples.

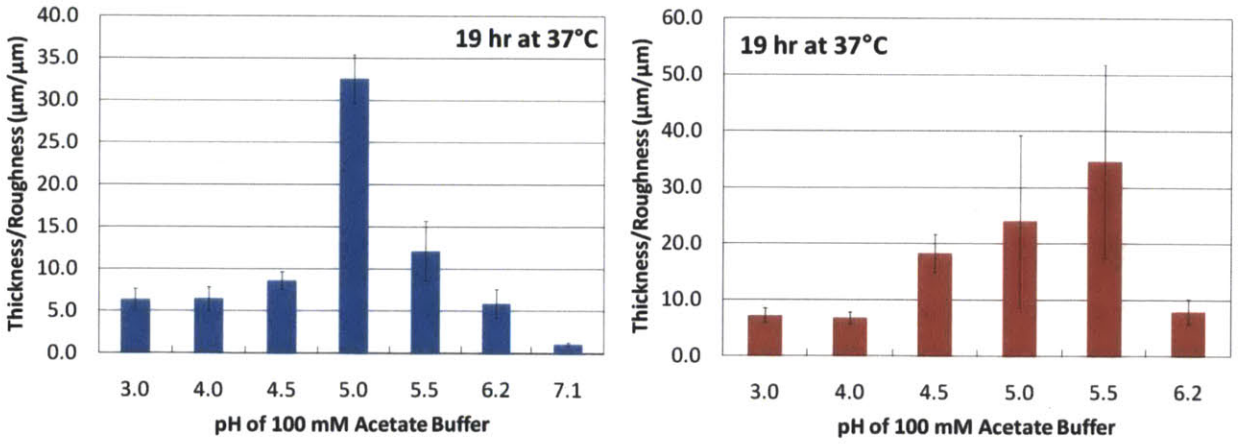

Figure 3-3. Effect of pH on the relative thickness/roughness (i.e. smoothness index) of $[Poly\ 1/PAA]_{100}$ (left) and $[Poly\ 1/PAA/GS/PAA]_{50}$ (right) after erosion in 100 mM NaOAc for 19 hr at 37 °C. Measurements represent the mean ± standard deviation of triplicate samples.

3.2.1 Defining Erosion-Based Release

The fundamental scaling analysis that can be conducted for hydrolytically erodible drug release systems is a comparison between the relevant timescales of water diffusion through the sample matrix versus the rate of hydrolytic degradation. This determines if the sample matrix is bulk-eroding or surface-eroding. For this, a dimensionless Deborah number ε is used and is defined as:

(3-3) $$\varepsilon = \frac{\langle x \rangle^2 \lambda \pi}{4 D_{\text{eff}} \ln\left[\langle x \rangle\right] - \ln\left[\sqrt[3]{M_n / N_A (N-1)\rho}\right]}$$

where the numerator relates to the timescale for water diffusion and the denominator relates to the timescale for hydrolytic degradation [129]. Large values of ε suggest that water takes a long time to diffuse relative to the reaction, leaving water excluded from the bulk of the matrix, thus suggesting that the matrix is surface-eroding. Small values suggest that the diffusion time is relatively short and that the reaction takes place everywhere throughout the matrix, suggesting that the matrix is bulk-eroding. For an example system, $\langle x \rangle$ represents the film thickness (20 μm), D_{eff} represents the diffusivity of drug in water (10^{-8} cm^2/s), M_n is the number average molecular weight of the erodible polymer (6 KDa), N is the degree of polymerization (32), ρ is the polymer density (1 g/cm^3), and λ is the first-order rate constant of polymer degradation (1.925×10^{-5} s^{-1}) [78]. Using these arguments, ε takes a value on the order of 10^{-4} suggesting bulk-erosion. However, this analysis is likely an oversimplification for systems studied in this thesis.

Drug that is released as a result of erosion is considered to be strongly bound drug (i.e. drug that is electrostatically bound to the bulk of the film and not free to diffuse out of the film without accompanied erosion). It is not released until the film itself dissociates. Many processes govern the rate of film erosion. A simplified version is shown in Figure 3-4 where water diffuses to the ester bonds, hydrolysis begins, ionic bonds break and re-form, and dissociation of unbound material leaves the film surface. Film erosion is thus affected by pH, ionic strength, and temperature of the erosion medium as well as the material properties of the structural components making up the LbL film. Tentatively, it is assumed that mean field theory

applies for erosion-based release. Specifically, whichever mechanisms govern erosion should take place uniformly across the surface of the film and the overall effective erosion rate can be estimated to be a constant. This is somewhat supported by the kinetic erosion data shown for [Poly 1/PAA/GS/PAA]$_{50}$ in 100 mM NaOAc buffer (pH 5.0, Figure 3-5A), although a true representation of the erosion rate should consider the total mass lost as opposed to thickness reduction. Since only three samples were used to determine each data point, it is not conclusive whether erosion is truly linear or higher order. Using a simplified one-parameter model for erosion-based release, the rate constant (which is a function of the erosion conditions and film characteristics) can be measured experimentally. For linear erosion, the film thickness (h) is reduced at a constant rate (R_{eff}) according to

(3-4) $$\frac{dh}{dt} = -R_{eff}$$

(3-5) $$h(t) = h_0 - R_{eff}t$$

where h_0 is the intial film thickness. For first-order erosion, h would be reduced according to

(3-6) $$\frac{dh}{dt} = -R_{eff}h$$

(3-7) $$h(t) = h_0 e^{-R_{eff}t}.$$

Whether zero-order or first-order, R_{eff} holds an Arrhenius relationship with temperature (Figure 3-5C and Figure 3-5D). In the real multilayered system, it is possible that the erosion characteristics may change with time due to the development of inhomogeneities. Therefore, Arrhenius plots showing the interpolated data from Figure 3-5A are conducted for the first day (Figure 3-5C) as well as for the entire erosion timeframes studied (Figure 3-5D)

Assuming for now that the erosion behavior is adequately represented by the linear, zero-order approximation, the total release per area as a function of time becomes

(3-8) $$Q(t) = r_{eff}t + Q(t)_{\text{diffusion}}$$

(3-9) $$r_{eff} = C_{GS}R_{eff}$$

where r_{eff} is an effective rate of release of drug per area per time and C_{GS} is the concentration of strongly bound gentamicin, which is assumed to be homogeneous throughout the film. r_{eff}

contains all necessary rate-limiting information behind the true mechanism of erosion as it governs the overall process of erosion shown in Figure 3-4.

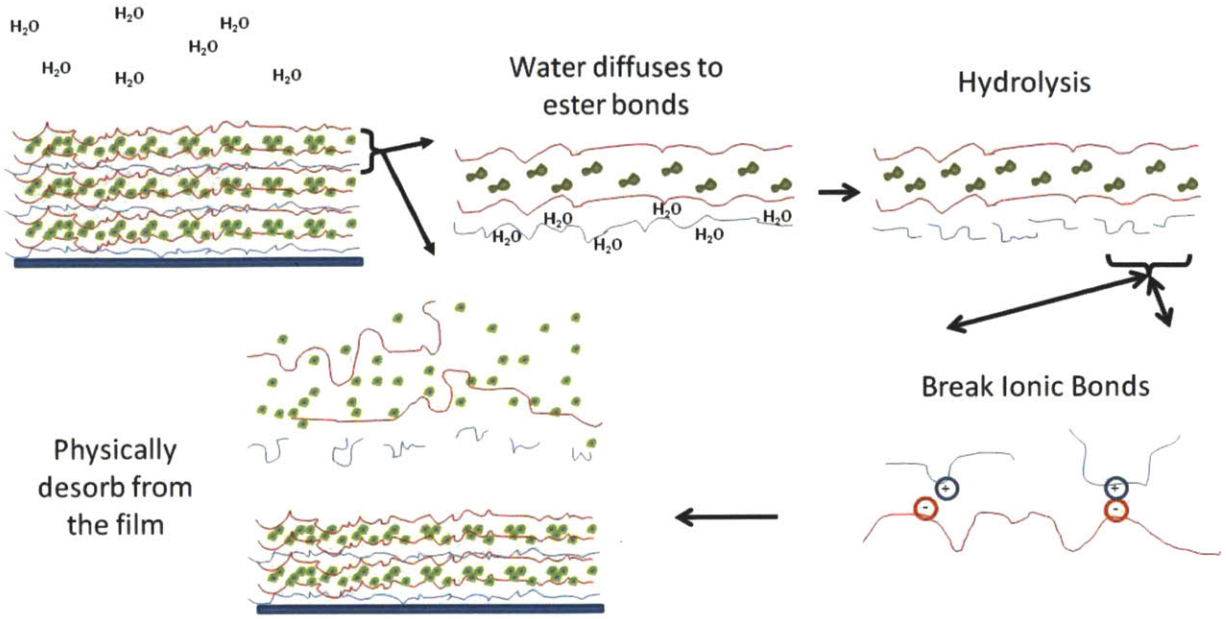

Figure 3-4. (Clockwise from top left) Initial state with the LbL film immersed in aqueous environment; water diffuses into the film as predicted by scaling arguments; hydrolysis takes place at rates that are dictated by local pH and temperature; simultaneously, ionic bonds continue to break and re-form at rates that are controlled, in part, by the concentration of salts (collision theory); after sufficient hydrolysis, it becomes kinetically possible for all remaining ionic bonds to break such that material can dissociate from the film surface.

The assumption of independent release mechanisms is valid if the timeframe for diffusive release is sufficiently shorter than the timeframe for erosion-based release. This would allow the mathematical treatment of the diffusion process to assume constant thickness and the erosion process to assume homogeneous distribution of material. Diffusion would dictate *Q(t)* at short times and erosion would dominate *Q(t)* at longer times. Figure 3-5B shows the corresponding release profiles for samples that were eroded at 4 and 37 °C. At 4 °C, the drug release effectively ceased after 100 hours, whereas at 37 °C, the release continued linearly. These match the behavior of their corresponding samples in Figure 3-5A. Furthermore, the diffusive burst of drug at 37 °C appears to subside very quickly relative to the prolonged linear erosion-based release phase.

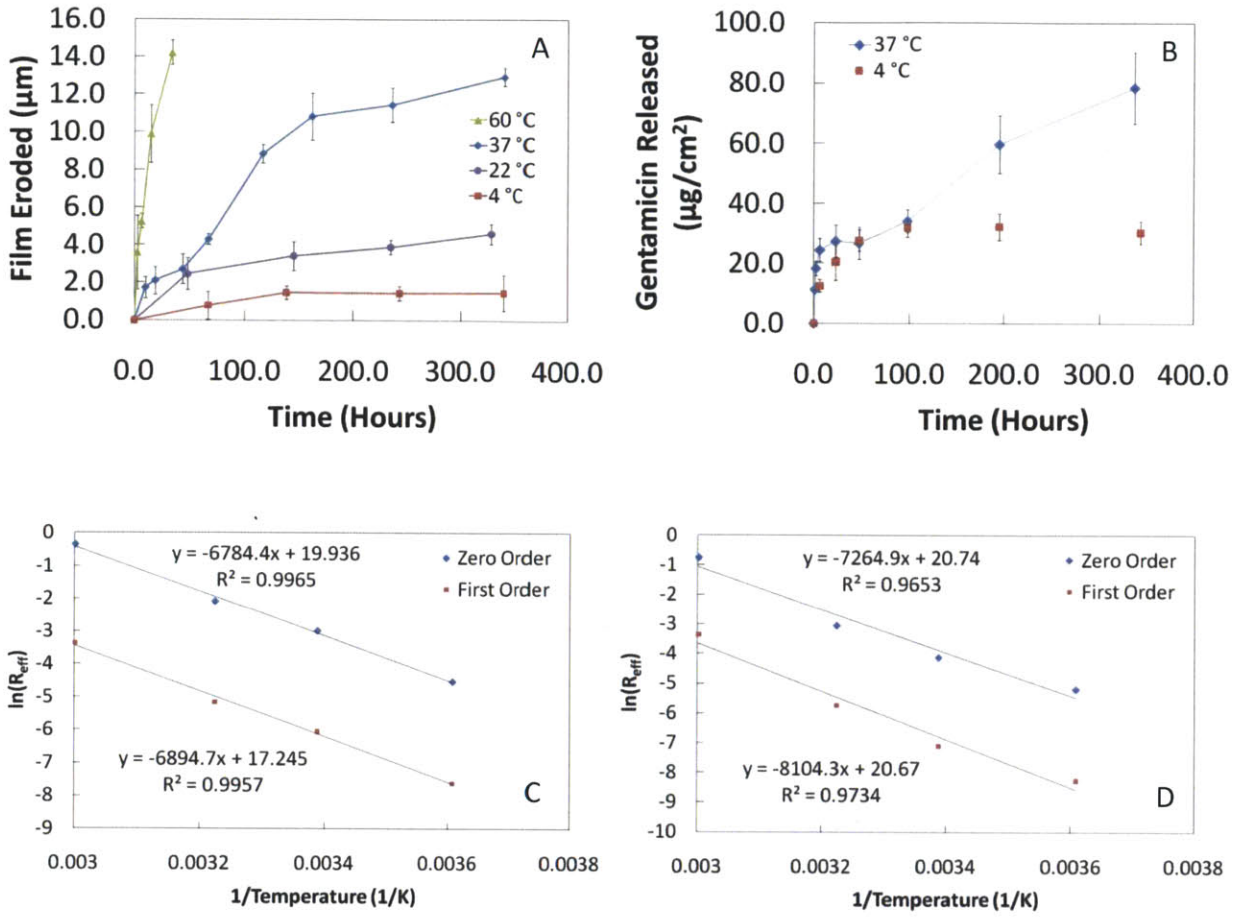

Figure 3-5. Top: (A) Kinetic erosion profiles of [Poly 1/PAA/GS/PAA]$_{50}$ in 100 mM NaOAc pH 5.0 at different temperatures, and (B) corresponding release profiles. All measurements represent the mean ± standard deviation of triplicate samples. Bottom: Arrhenius relationships for the erosion rate constant (R_{eff}) using zero-order (linear) or first-order (exponential) interpolated representations of the data sets in (A). (C) The Arrhenius relationship for the first day of erosion or (D) the full duration studied.

3.2.2 Defining Diffusion-Based Release

Mathematical treatment of diffusion assumes that the drug is well mixed throughout the film, the film is homogeneous and inert, and there is no film erosion. The physical problem is described in Figure 3-6. Drug that is released as a result of diffusion is considered to be weakly bound drug (i.e. drug that is not ionically bound within the bulk of the film and thus able to diffuse freely throughout the film). The film initially contains a concentration of weakly bound drug, C_0, while the infinite medium outside of the film initially contains no drug. As drug is released, the concentration within film is assumed to quickly equilibrate and therefore remain

homogeneous with a value of C_a.[2] C_a is a function of time as it is depleted throughout the release process. Far away from the film surface, the drug concentration remains at zero.

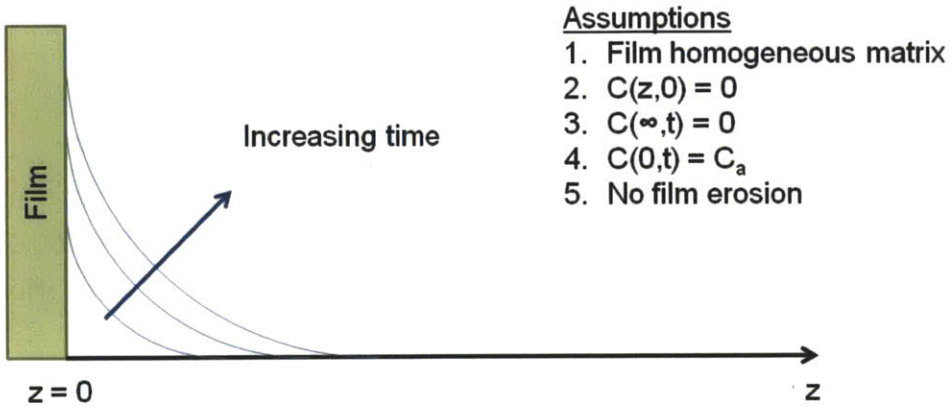

Figure 3-6. Physical diffusion problem describing drug release from film into infinite medium.

The Fickian diffusion governing equation is:

(3-10) $$\frac{\partial C}{\partial t} = D\frac{\partial^2 C}{\partial z^2}$$

where C is the concentration of a chemical species, t is a time coordinate, z is a spacial coordinate, and D is the effective diffusivity of drug. The initial and boundary conditions are shown in Figure 3-6. The particular value of interest in determining $Q(t)_{diffusion}$ is the flux across the film-solution interface (N). To determine an analytical form for flux, it is first necessary to determine the order-of-magnitude penetration depth of drug into the surrounding medium. This scaling analysis is analogous to that done by William M. Deen in his textbook [130]:

(3-11) $$\frac{\partial KC_a}{\partial t} \sim \frac{KC_a}{t}$$

(3-12) $$\frac{\partial^2 KC_a}{\partial z^2} \sim \frac{KC_a}{\delta^2}$$

where K is a partition coefficient and C_a is the average drug concentration remaining in the film. The concentration of drug in the LbL film depletes over time as drug is released diffusively and

[2] Assuming a diffusivity on the order of 10^{-6} cm^2/s and a film thickness on the order of 20 μm, the estimated time for drug to diffuse completely across the full film thickness would be about 1 s.

is therefore not a constant (Figure 3-7). A simple mass balance suggests that the concentration of remaining drug in the film at any given time (C_a) is equal to the total initial concentration C_0 minus the amount that has been released $Q(t)_{\text{diffusion}}/h$, where h is the total film thickness:

(3-13) $$C_a = K\left(C_0 - \frac{Q_{\text{diffusion}}}{h}\right).$$

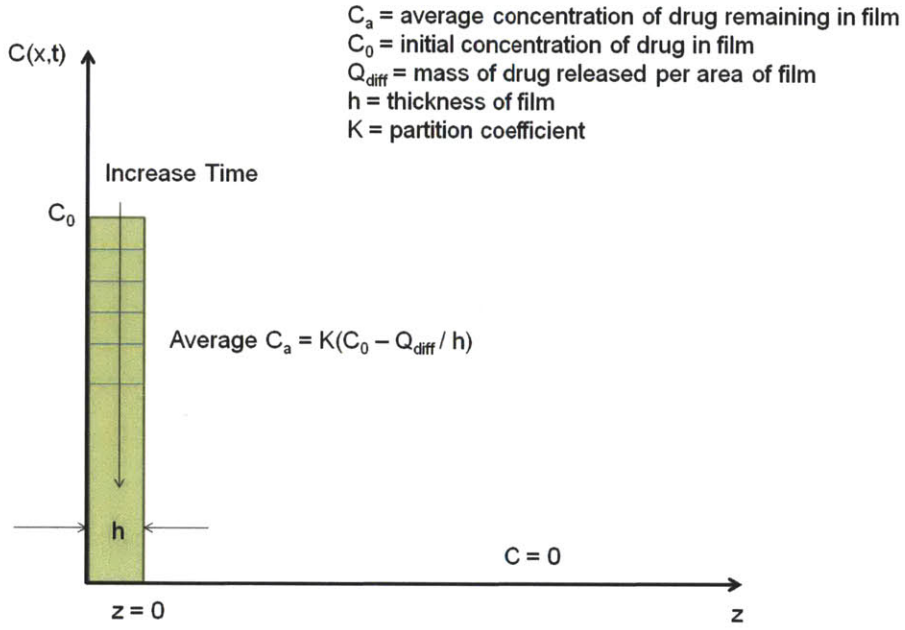

Figure 3-7. The average concentration of drug remaining in the film depletes with time as drug mass is released. The partition coefficient accounts for the preference of drug to remain in the film versus the infinite medium at equilibrium.

Substituting these scaling estimates into equation (3-10) and solving for δ yields $\delta \sim (Dt)^{1/2}$. The diffusion length over which the concentration drops from KC_a to zero is δ. Flux is defined as mass of drug released per area per time. Therefore, the flux of drug out of the film can be approximated to scale proportionally to the concentration drop that takes place over diffusion distance δ. Using the standard $\delta = 2(Dt)^{1/2}$ for the one-dimensional diffusion length,

(3-14) $$N_z\big|_{z=0} = -D\left.\frac{\partial C}{\partial z}\right|_{z=0} \approx -D\left(\frac{\Delta C}{\Delta z}\right) = -D\left(\frac{0 - KC_a}{\delta - 0}\right) = D\left(\frac{KC_a}{\delta}\right) = D\left(\frac{KC_a}{2\sqrt{Dt}}\right).$$

(3-15) $$\frac{dQ_{\text{diffusion}}}{dt} = N_z\big|_{z=0} = D\frac{KC_a}{2\sqrt{Dt}} = \left(\frac{D}{t}\right)^{1/2}\frac{KC_a}{2}.$$

Plugging equation (3-13) into (3-15) yields a simple ordinary differential equation. The initial condition is no drug release. The system to be solved is:

(3-16) $$\frac{dQ_{\text{diffusion}}}{dt} = \left(\frac{D}{t}\right)^{1/2} \frac{K}{2}\left(C_0 - \frac{Q_{\text{diffusion}}}{h}\right)$$

(3-17) $$Q_{\text{diffusion}}(0) = 0.$$

This can be done by hand by separation of variables, integration, and rearrangement:

(3-18) $$\frac{dQ_{\text{diffusion}}}{C_0 - \frac{Q_{\text{diffusion}}}{h}} = \frac{K}{2}\left(\frac{D}{t}\right)^{1/2} dt$$

(3-19) $$-h\ln\left(C_0 - \frac{Q_{\text{diffusion}}}{h}\right) = K\ Dt^{\ 1/2} + C'$$

(3-20) $$\left(C_0 - \frac{Q_{\text{diffusion}}}{h}\right) = C' \exp\left(-\frac{K}{h}\ Dt^{\ 1/2}\right)$$

where C' is an arbitrary constant. Using the initial condition, $C' = C_0$. Thus, the overall solution to this diffusion problem becomes

(3-21) $$Q_{\text{diffusion}} = hC_0\left[1 - \exp\left(-\frac{K}{h}\ Dt^{\ 1/2}\right)\right]$$

which yields the final form

(3-22) $$Q_{\text{diffusion}} = A\left[1 - \exp\ -Bt^{1/2}\ \right].$$

This solution contains physical information about the system, and is a more accurate representation of the diffusion contribution at longer times than the theoretical treatment by Higuchi [131] who derived the famous square root relationship with time:

(3-23) $$Q = \sqrt{\frac{D\varepsilon}{\tau}(2A - \varepsilon C_s)C_s t}\ .$$

The square root relationship can be recovered from equation (3-22 by using a Taylor series expansion. After plugging the diffusion solution back into the total release equation (3-2), and simplifying with arbitrary constants *A*, *B*, and *C*,

(3-24) $$Q(t) = r_{\text{eff}} t + hC_0 \left[1 - \exp\left(-\frac{K}{h} \, Dt^{1/2} \right) \right]$$

(3-25) $$Q(t) = Ct + A\left[1 - \exp\ -Bt^{1/2} \ \right]$$

(3-26) $$A = hC_0$$

(3-27) $$B = \frac{KD^{1/2}}{h}$$

(3-28) $$C = r_{\text{eff}}$$

This resulting three-parameter analytical equation fits most available poly(β-amino ester) erodible system data sets fairly well (see section 3.4).

3.3 *Model Predictions*

A total of ten different analytical equations were ultimately considered in this thesis as candidates to fit the release data from hydrolytically degradable LbL films. Of these, the model developed above was the only non-phenomenological equation that addressed both major mechanisms of release, and it generally yielded the best fit amongst the other phenomenological equations. The resulting functional form contained three parameters. Parameter C (3-28) contains information on the erosion rate, while parameters A and B (3-26) and (3-27) respectively) contain information on the magnitude and rate of diffusion. In the simple treatment presented here, it was assumed that these parameters did not change with time and that the overall equation was valid until the film completely eroded. Figure 3-8 top, left shows one particular least-squares regression of this model applied to (Poly 1/PAA/GS/PAA)$_{200}$ + (Poly 1/PAA/GS)$_1$, the architecture used in the *in vivo* study described in Chapter 5. The model fit the data relatively well with R^2 = 0.9968. Figure 3-8A, B, and C show the effect of increasing each of the parameter values while holding the others constant. Looking at B and C, it becomes clear that the early stage and late stage kinetics are dominated by diffusion and erosion, respectively.

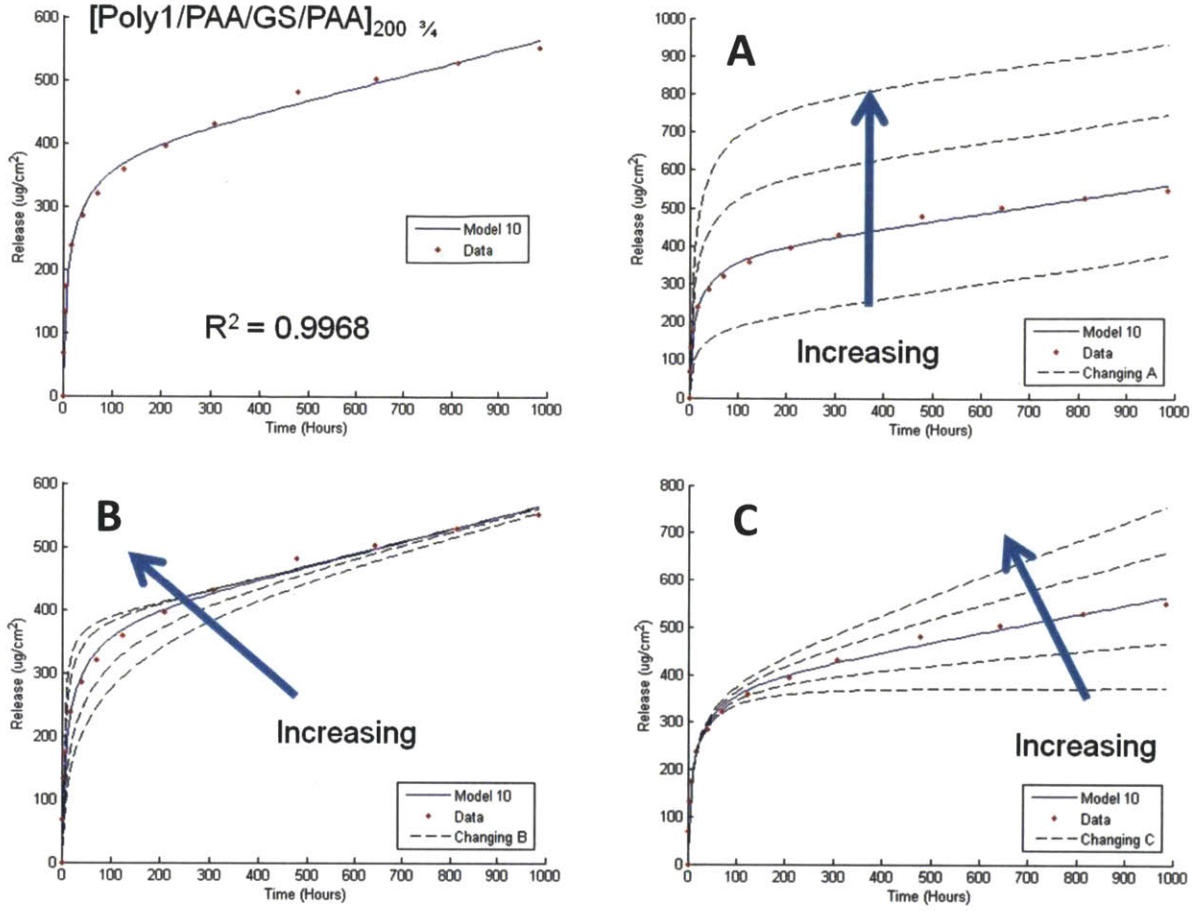

Figure 3-8. (Top, left) Model (3-25 fit to the release data from the (Poly 1/PAA/GS/PAA)$_{200}$ + (Poly 1/PAA/GS)$_1$ architecture described in Chapter 5 via a least squares regression. (A) Effect of increasing parameter A, (B) effect of increasing parameter B, and (C) effect of increasing parameter C.

Although the assumption of constant film thickness for the diffusion problem was inherently false, it may still be applicable to systems whose diffusion mechanism takes place on a much shorter timescale than erosion. This way, the contribution of diffusive release becomes quite small relative to erosion before parameters A and B can change significantly, and the contribution of erosion-based release remains small while the film is rapidly changing composition due to diffusion. In the case of linear erosion (equation (3-5)), the time to 5% reduction in film thickness ($t_{5\%}$) is

(3-29) $$t_{5\%} = \frac{0.05h_0}{R_{eff}} = \frac{0.05C_{GS}h_0}{r_{eff}} = \frac{0.05C_{GS}h_0}{C}.$$

Before this time is reached, it is assumed that $h \approx h_0$. To determine if the contribution of diffusive release has become small enough, there are two relevant methods. First, is to compare the diffusion rate to the erosion rate and calculate the time to which the rate of diffusive release becomes approximately 5% of the rate of erosion-based release (t_{small}):

(3-30) $$\frac{dQ_{diffusion}}{dt} = \frac{AB}{2\sqrt{t}}\exp(-Bt^{1/2})$$

(3-31) $$\frac{dQ_{erosion}}{dt} = C$$

(3-32) $$\frac{AB}{2\sqrt{t_{small}}}\exp(-Bt_{small}^{1/2}) = 0.05C.$$

If t_{small} is $\leq t_{5\%}$, then the assumption of independent mechanisms can hold since with 95% of the film thickness still present, the contribution of diffusive release has already become small compared to the erosion-based release. Second, is to calculate the time to which the rate of diffusive release reaches 95% of its final value ($t_{95\%release}$)

(3-33) $$Q_{diffusion} = A\left[1-\exp(-Bt^{1/2})\right]$$

(3-34) $$0.95A = A\left[1-\exp(-Bt^{1/2})\right]$$

(3-35) $$t_{95\%release} = \left(\frac{-\ln(0.05)}{B}\right)^2.$$

If $t_{95\%release}$ is smaller than $t_{5\%}$, then diffusion has nearly reached completion before any significant erosion has taken place. Of course these analyses can be improved by using time dependent parameters (A(t), B(t), and C(t)), but regressed parameters can give an estimate on the validity of these assumptions.

Overall five different physical constants are represented in A, B and C. The concentration of diffusive drug, C_0, only affects the magnitude of diffusion-based release (Figure 3-9). C_0 can be tuned by changing the concentration of the drug deposition bath during the final deposition step (see chapter 2.3.2 Sponge Effect). This enables control on the magnitude of total loading without otherwise affecting the release kinetics. The partition

coefficient, K, and effective diffusivity of drug, D, appear only in parameter B and therefore only affect the diffusion rate. K depends on the chemical nature of the drug as well as the interface between the film and the release medium (and is thus determined experimentally). It is expected that the $K \approx 1$ for films that become well hydrated in aqueous environment (equation (3-3). The effect of D on the drug release profile is shown in Figure 3-10. Highly diffusive drug particles have a more pronounced burst release as the film quickly reaches its erosion-based release phase. Less diffusive drug particles get released over a much longer timescale. In theory, diffusivity can be controlled by either encapsulating the drug in larger carriers, or careful selection of the other polyelectrolyte components in the LbL system. The thickness of the multilayered film, h, plays a dual role (Figure 3-11). When holding drug concentration constant, the total drug release quantity scales linearly with the total film thickness. Separately, the diffusive release rate increases with decreasing film thickness. This is reminiscent of the Fickian diffusion length where thicker films will require longer timescales for the drug to diffuse across, and hence longer times before said drug can contribute to cumulative release.

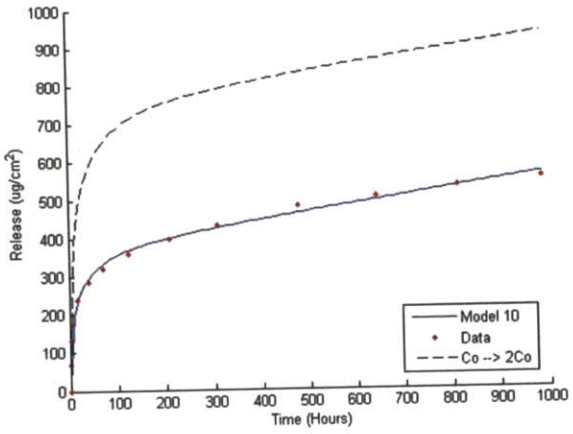

Figure 3-9. Model prediction of release profile after increasing the concentration of diffusive drug by a factor of 2 while keeping all other values constant. Model 10 is the non-phenomenological model described in this chapter.

The erosion-based release rate, r_{eff}, is an experimental constant that determines the slope of the linear release phase. As an improvement to the model, a more detailed mathematical treatment of the rate limiting steps governing erosion-based release should be incorporated

into r_{eff}. Likely these parameters will include the ionic strength, temperature, and pH of the erosion medium, as well as the chemical nature of the hydrolytically degradable polymers in the system.

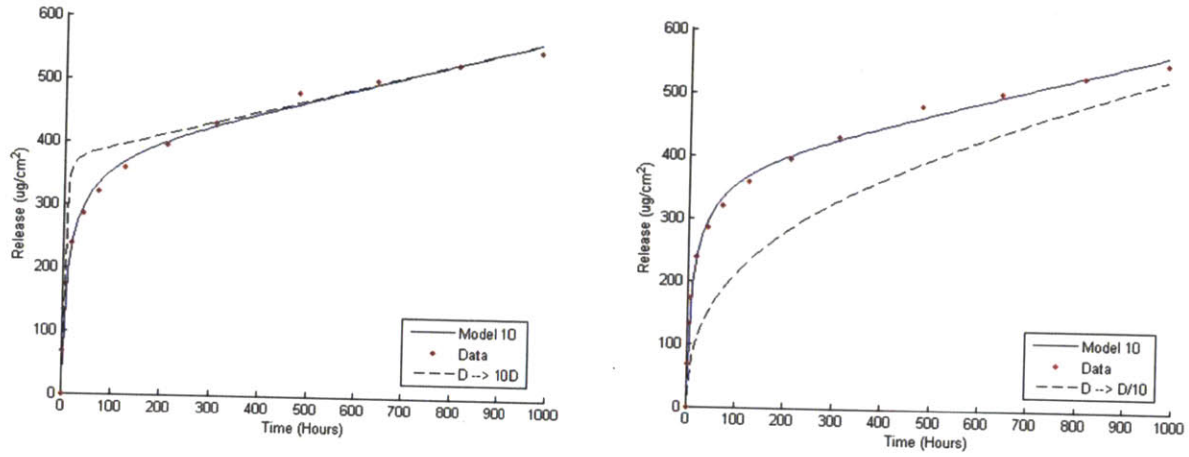

Figure 3-10. Model prediction of release profile after increasing (left) and decreasing (right) the diffusivity of the drug by a factor of 10 while keeping all other values constant.

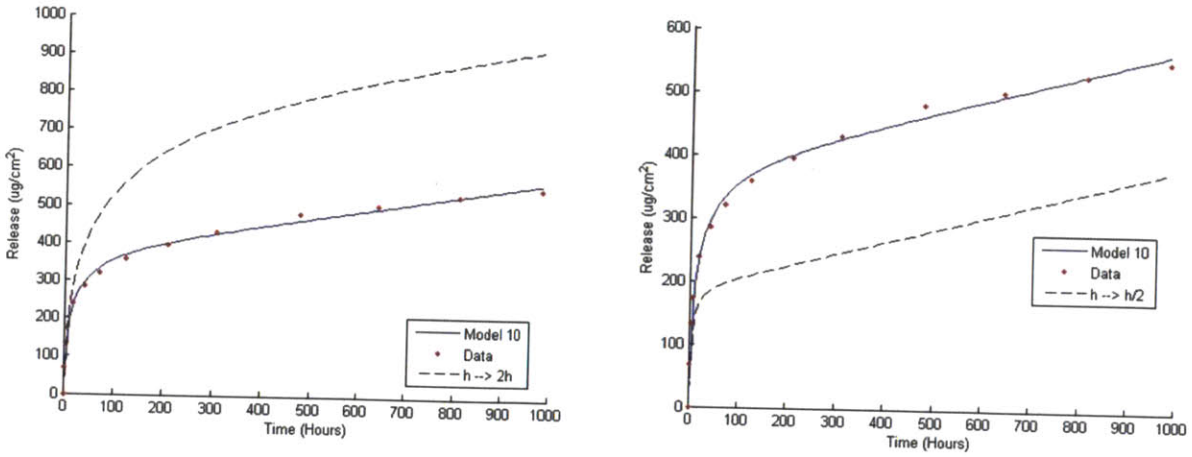

Figure 3-11. Model prediction of release profile after increasing (left) and decreasing (right) the thickness of the LbL film by a factor of 2 while keeping all other values constant.

3.4 *Validating the Analytical Model for Existing Systems*

Although the ultimate test of model validation would be its ability to accurately predict release profiles for new systems, the initial metric of validation here was to A) ensure satisfactory fit to currently available data sets and B) determine if the outputted parameters and trends for these

existing systems make sense. To this end, the model was first tested against a set of poly(β-amino ester)s (AB1, A2, A3, and A4 from Figure 3 of Smith *et al.* [79]). These polycations differed by the number of methylene groups per repeat unit of the polymer backbone (i.e. 3, 4, 6, and 9 respectively). The polycations were alternately layered with ^{14}C-dextran sulfate and allowed to elute into a phosphate buffered solution at room temperature. In all four cases, the fit to the data was very good with $R^2 > 0.99$ (Figure 3-12). These polymers were chosen based on their increasing hydrophobicity, which correlated with slower degradation and slower release rates as would be expected in an aqueous environment. The sole exception was A4 (Figure 3-12, bottom right), which bulk destabilized and fell apart on a much shorter timescale.

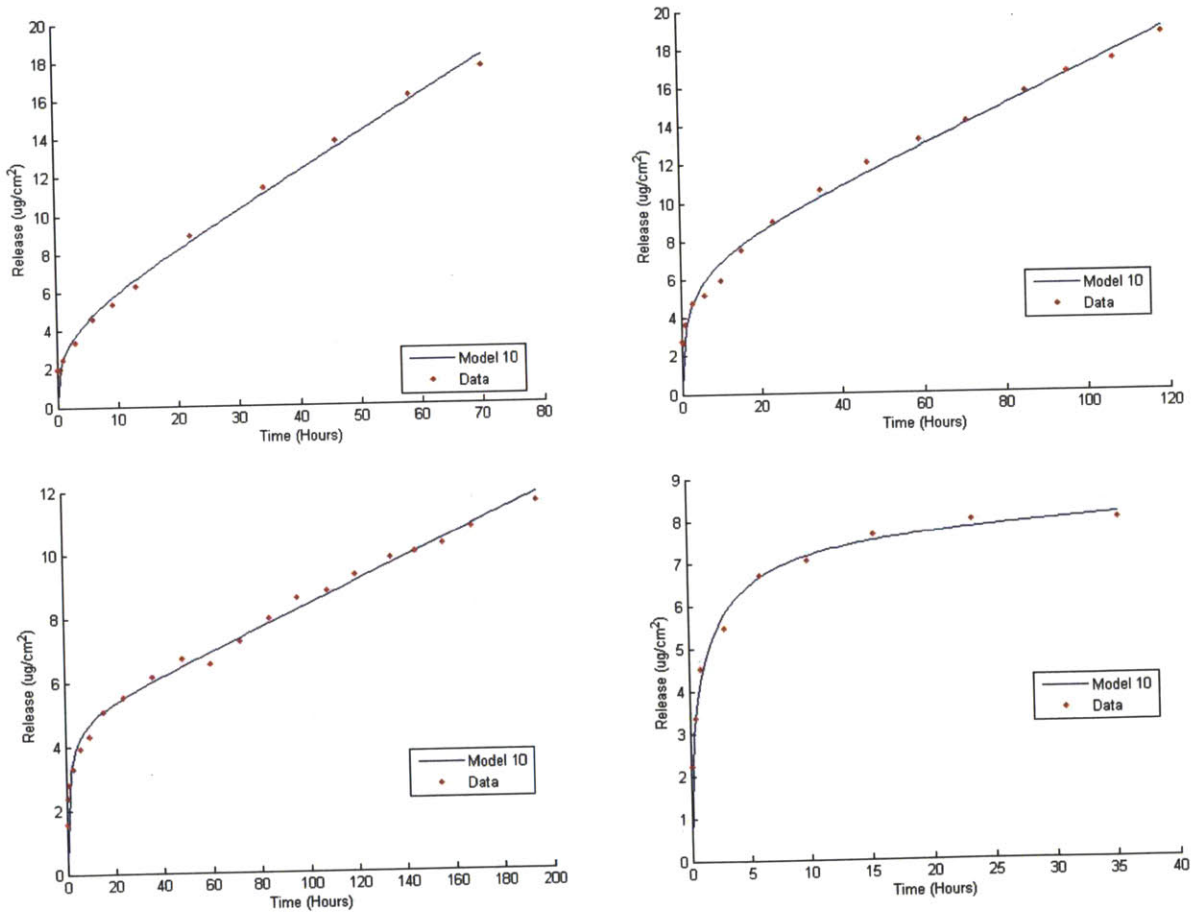

Figure 3-12. Clockwise from top left: Release of dextran sulfate (DS) from erodible films made with $(AB1/DS)_{20}$, $(A2/DS)_{20}$, $(A3/DS)_{20}$, and $(A4/DS)_{20}$.

These plots were normalized to their final release quantities and re-regressed with the model. The trend in erosion-based release rates outputted by the model followed the trend in

hydrophobicity, as expected: $r_{eff,AB1}$ = 10.7 x 10^{-3}, $r_{eff,A2}$ = 5.5 x 10^{-3}, and $r_{eff,A3}$ = 2.7 x 10^{-3} 1/cm^2-s. Furthermore, the model also predicted a significantly higher fraction of diffusive release for A4 than for the other polycations; parameter A_{A4} = 0.70, which was more than two times the parameter A value for the other polycations. This is suggestive of the bulk destabilization that was observed experimentally.

The strongest validation efforts conducted thus far have been directed at two systems for which there was enough information to back out diffusivity values based on the output parameters (Figure 3-13). Assuming $K \approx 1$, the predicted diffusivity could be calculated from the outputted B parameter given the initial thickness measurement, h. Using this method, the model predicted $D_{gentamicin}$ = 1.5 x 10^{-6} cm^2/s (Figure 3-13, left) and $D_{vancomycin}$ = 5.0 x 10^{-8} cm^2/s (Figure 3-13, right). These values agreed well with the literature values of 2.3 x 10^{-6} cm^2/s for gentamicin in 2% agar [132] and 4.7 x 10^{-8} cm^2/s for vancomycin in 25% w/w Poloxamer 407 in water [133].

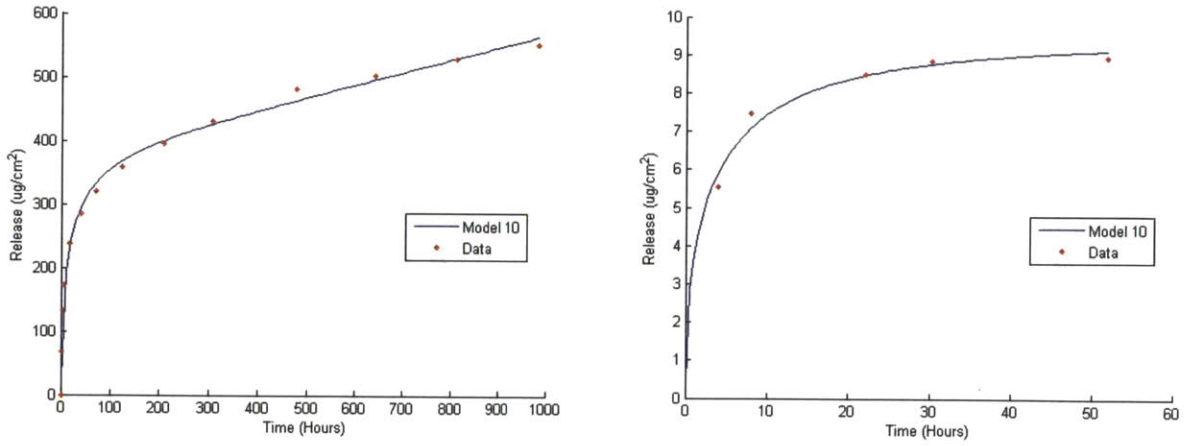

Figure 3-13. (Left) (Poly 1/PAA/GS/PAA)$_{200}$ + (Poly 1/PAA/GS)$_1$ with R2 = 0.997 and (right) (Poly 1/Chondroitin/ Vancomycin/Chondroitin)$_{60}$ with R^2 = 0.994.

3.5 *Possible Extensions to the Analytical Model*

The most immediate extension to the current mathematical model would be to incorporate the changing film thickness h into the diffusion treatment. Although intuitively simple, this yields a much more complex mathematical integration of:

(3-36) $$\frac{dQ_{\text{diffusion}}}{dt} = \left(\frac{D}{t}\right)^{1/2} \frac{K}{2}\left(C_0 - \frac{Q_{\text{diffusion}}}{r_{eff}t}\right)$$

(3-37) $$Q_{\text{diffusion}}(0) = 0.$$

Using MAPLE, this system was solved to be

(3-38) $$Q_{\text{diffusion}} = C_0 K \ Dt^{1/2} - \frac{DC_0K^2}{\pi r_{eff}} \exp\left(\frac{K}{r_{eff}}\left[\frac{D}{t}\right]^{1/2}\right) Ei\left(\frac{K}{r_{eff}}\left[\frac{D}{t}\right]^{1/2}\right)$$

where *Ei(x)* is the exponential integral. In modeling, there is a general tradeoff between accuracy and usefulness. Although less simple to work with, equation (3-38) only requires one additional parameter to solve when performing a least squares regression and should marginally increase the quality of the fit. Since the second term of this solution is small as *t* approaches zero, the form of the overall solution still upholds Higuchi's square root relationship of release versus time at early times. Moreover, in a non-erodible system where $r_{eff} = 0$, the system again recovers this relationship. Finally, if the drug is non-diffusive, if the concentration of diffusive drug is zero, or if the drug partitions perfectly into the film (i.e. $K = 0$), then $Q_{\text{diffusion}}$ does not contribute to the overall release.

The next extension would be to correct for the effective diffusivity *D* of drug in the polymer matrix. Since the chemical nature of the matrix changes with time as the hydrolytically degradable polymer is cleaved, the effective diffusivity is also expected to change. One way to do this is to allow:

(3-39) $$D = D_{aq} \frac{\varepsilon}{\tau} \exp(k_s t)$$

where D_{aq} is the drug diffusivity in free water, ε is the porosity of the polymer matrix, τ is the tortuosity of the polymer matrix, and k_s is the polymer chain scission rate constant [134, 135].

The effective erosion rate, r_{eff}, although used as an independent parameter in the present theoretical treatment, is not a physical parameter of the system. Therefore, a quantitative representation of r_{eff} would yield a more universal analytical solution. Specifically, it would be beneficial to write r_{eff} as a function of erosion medium characteristics (i.e. ionic

strength, pH, temperature, and concentrations of other components, etc.) and film chemistry (i.e. degradation characteristics of the poly(β-amino ester) [136],[3] charge density of the polyelectrolytes, ionic bond strengths, etc.).

Finally, all of the theoretical work described in this chapter was aimed at expressing drug release per area of film as a function of time. Once an adequate analytical equation has been developed, the next logical step would be to develop a Lotka-Volterra model [136] of antibiotic predation on bacteria (e.g. *S. aureus*) in a site of infection. Such a model would need to combine the results from this chapter with the predicted transient pharmacokinetics that describe uptake by the body, uptake by cells, and general clearance, and apply them against the inherent growth rate of bacteria [137] as well as the potential buildup of antibiotic resistance [138]. Development of an accurate predator-prey model would be a powerful predictor as to whether a particular coating could treat a particular infection, and would lay the framework for intelligent film design.

3.6 *Numerical Treatment of Diffusion-Based Release*

To numerically code the diffusion-based release, the system was divided into an array of finite elements. 10% of these elements were used to spacially describe the concentrations within the film, and 90% of these elements were used to spacially describe the concentrations in the medium. Element size for the film (z_{film}) was chosen based on the total film thickness and total number of desired elements to describe the film. More elements give greater accuracy and resolution, but require greater computational time. The initial condition was set up such that all of the film elements had a uniform concentration of drug while all of the medium elements had zero drug. Inputs for the system were C_0, D, h, (each as defined earlier) and "ratio" which designates the ratio of aqueous diffusivity (D) to that of the drug in the polymeric matrix of the film (D_{film}). The partition coefficient was assumed to be 1. At each time step, the entire concentration vector was updated via an iterative process using the formula:

[3] Antheunis *et al.* summarize the existing degradation models for hydrolytic degradation of aliphatic polyesters, and propose a new autocatalytic equation.

(3-40) $$C_{t+\Delta t} = C_t + (\Delta t) DC''$$

where the size of the time step (Δt) is determined by

(3-41) $$\Delta t = \left(\frac{1}{D}\right)\left(\frac{z_{\text{medium}}}{2}\right)^2 = \left(\frac{1}{D_{\text{film}}}\right)\left(\frac{z_{\text{film}}}{2}\right)^2.$$

Thus the medium element size (z_{film}) is inherently set by the time step, D, and "ratio". C'' was calculated using second-order accurate finite difference formulae. Central differences were used for values of C'' away from the system boundaries and film-solution interface. Forward difference and backward difference formulae were used for the boundaries, and uniquely derived central differences were used for the film-solution interface taking into account the non-uniform grid spacing for simulations that utilize "ratio" values not equal to 1. In each iteration the total mass in the system is summed up and compared to the initial mass in the system so that discrepancies (i.e. introduced error) can be corrected by rescaling the entire system to its initial value. No flux boundary conditions were enforced by averaging the values of the two elements next to each boundary, and redistributing the mass evenly before the next iteration. Finally, the total released drug (i.e. the drug residing in the medium elements) was summed up and stored in a $Q_{\text{diffusion}}$ vector while the total simulation time was stored in a parallel time vector. All masses were outputted at the end of the simulation for bookkeeping. MATLAB code is available in the Appendix: MATLAB Code for Numerical Treatment of Drug Release.

The trends predicted by this numerical model as a result of changing each of the three parameters C_0, D, and h followed the expected outcome. Figure 3-14 (left) shows the effect of increasing initial drug concentration and Figure 3-14 (right) shows the effect of decreasing aqueous diffusivity. In both cases, the plots have been curtailed in time for easier comparison. The sole effect of increasing initial concentration is to increase the total amount of drug released without changing release kinetics (i.e. normalized plots align exactly). The effect of decreasing the aqueous drug diffusivity is to decrease the kinetic rate at which the system approaches 100% release. Figure 3-15 shows the effect of increasing the total film thickness for two different cases: one where the mass in the system does not change (left), and the other

where the total mass in the system scales with the film thickness (right). When holding the mass in the system constant, the thickness parameter acts similar to aqueous drug diffusivity and only affects the rate at which the system approaches 100% release. Thinner films achieve this value faster than thicker films. When allowing the mass in the system to scale with the film thickness, the result becomes identical to Figure 3-11 where thicker films release more drug, but at a slower rate.

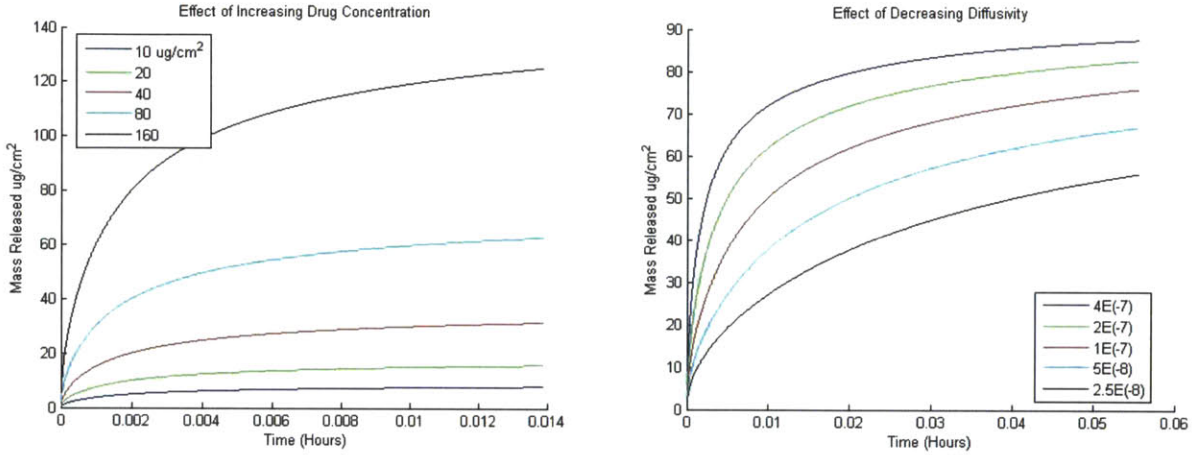

Figure 3-14. (Left) Effect of increasing initial drug concentration in the film (C_0) while holding all other parameters constant. (Right) Effect of decreasing the aqueous drug diffusivity (D) while holding all other parameters constant.

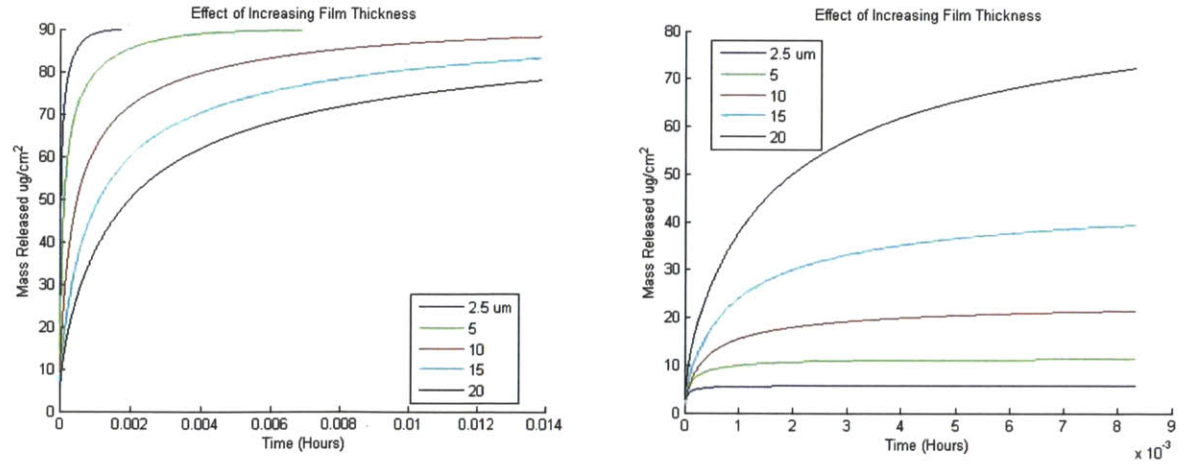

Figure 3-15. (Left) Effect of increasing the total film thickness (h) while holding all other parameters constant. (Right) Effect of increasing total film thickness (h) while allowing the total mass of drug in the system to scale with film thickess.

Figure 3-16 shows the space-time development of the drug concentration profile for an example system. This simulation was ran for a 20 micron film with 50,000 $\mu g/cm^3$ of drug (i.e. a total loaded mass of 100 $\mu g/cm^2$) and an aqueous drug diffusivity of 4×10^{-10} cm^2/s. Six profiles are shown between times 00:00:00 (hh:mm:ss) and 13:53:20, which correspond to total release quantities of 0, 6, 13, 28, 52, and 76 $\mu g/cm^2$ of the original 100.

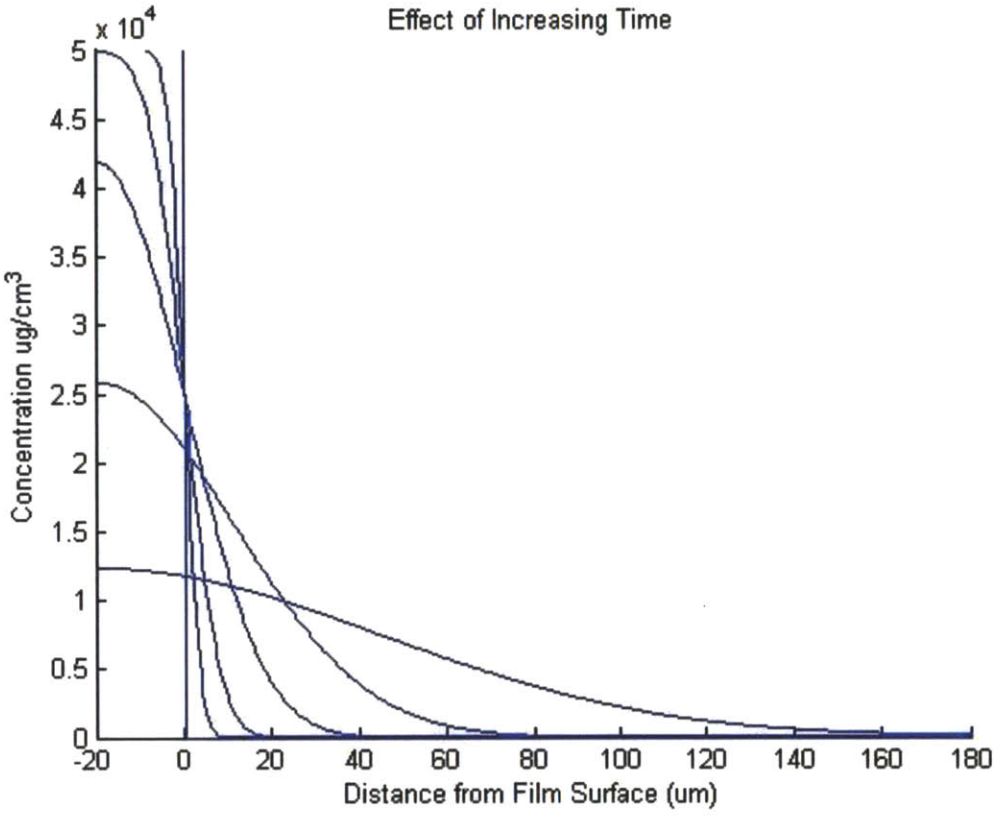

Figure 3-16. Space-time concentration profile of drug. Initially all drug is loaded into the first 20 microns of the system. The six plots shown here range from t = 0 to t ≈ 14 hours.

To compare the numerical and analytical models, outputs from numerical simulations were fitted with were fitted with a least squares regression using the analytical model from section 3.2.2. An example fit is example fit is shown in Figure 3-17, however visual evidence alone does not confirm that the physical parameter inputs to the simulation accurately correspond with the physical meaning of the analytical solution parameter outputs. Therefore the simulation was run seven different times by varying the input parameters, and regressed with the analytical model each time. The expected values of analytical parameters A and B were computed from the simulation inputs and compared to the analytical parameter fitted outputs from each regression. These data are shown in Table 3-1. Comparison between Simulation Inputs and Analytical Fit Outputs.

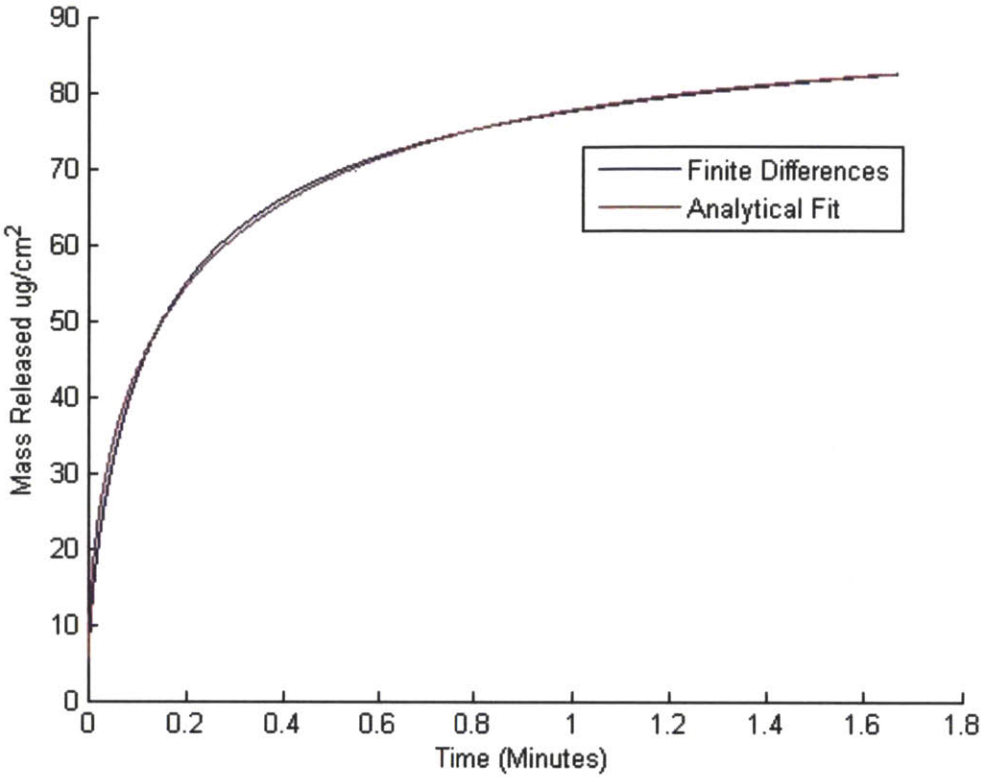

Figure 3-17. Example analytical fit of the simulated first 1.8 minutes of release from a 20 micron film eluting drug with an aqueous diffusivity of 4.0 x 10^{-7} cm^2/s and an initial film concentration of 50,000 $\mu g/cm^3$.

In all cases, the fitted parameter A was within 2 $\mu g/cm^2$ of its expected value and the fitted parameter B was within a factor of 1.3 of its expected value while the coefficients of determination were all near 1.0. This indicates that the physical meaning of parameters A and B and mathematical functional form derived via the analytical treatment must hold some degree of accuracy (i.e. A must be proportional to C_0 and h and B must be proportional to $D^{1/2}$ and h^{-1}). Additionally, it was found that the fitted parameter B consistently underestimates the expected value. This could be due to error during the scaling analysis, which assumed that the diffusion length δ was equal to $2(Dt)^{1/2}$. The prefactor 2 was arbitrarily selected due to its occurrence in other analytical solutions [130], but may not have been entirely accurate. Regardless, both models agree well with each other and fit release profiles relatively accurately.

Table 3-1. Comparison between Simulation Inputs and Analytical Fit Outputs.

MATLAB Simulation					Analytical Fit		
C_0 (μg/cm^3)	D (cm^2/s)	h (μm)	Expected A*	Expected B	Fitted A	Fitted B	R^2
50000	4.00E-08	20	90	0.100	90.6	0.083	0.997
25000	4.00E-08	20	45	0.100	45.3	0.083	0.997
100000	4.00E-08	20	180	0.100	181.1	0.083	0.997
50000	4.00E-07	20	90	0.316	88.1	0.278	0.998
50000	4.00E-09	20	90	0.032	90.6	0.026	0.997
100000	4.00E-08	10	90	0.200	88.8	0.170	0.998
25000	4.00E-08	40	90	0.050	88.2	0.044	0.998

*** Equilibrium values are expected to be 90% of the total initial mass since only 90% of the total elements in the simulation are defined as the elution buffer.**

Chapter 4 Design of a Reproducible *In Vivo* Bone Infection Model

The work presented in this chapter has been reproduced from the published manuscript entitled "The effectiveness of the controlled release of gentamicin from polyelectrolyte multilayers in the treatment of Staphylococcus aureus infection in a rabbit bone model" by Joshua S. Moskowitz, Michael R. Blaisse, Raymond E. Samuel, Hu-Ping Hsu, Mitchel B. Harris, Scott D. Martin, Jean C. Lee, Myron Spector, and Paula T. Hammond (*Biomaterials*, vol. 23, pp. 6019-30, 2010) with permission from Elsevier.

4.1 *Introduction*

Osteomyelitis, or the inflammatory response to an infecting microorganism that causes bone damage, is a disease that can occur on any bone at any age. Acute osteomyelitis occurs on the order of days to weeks and involves the formation of sequestra, or separations of dead bone from the surrounding live bone. As the body tries to repair the sequestra, new bone is formed such that the sequestra are enveloped. The new bone is called involucrum and makes the delivery of systemic antibiotics extremely difficult. Chronic osteomyelitis is a robust infection lasting months to years, and is characterized by prolonged existence of pathogens, inflammation, sequestra, and fistulous tracts. Relapses and clinical signs lasting for longer than 10 days are clear signs of chronic osteomyelitis [9, 139]. One of the major introductory routes of these microorganisms into the human body is postoperative sepsis after orthopedic surgery. In 2001, over 100,000 fracture-fixation devices resulted in infection within the United States alone [140]. Additionally, it has been estimated that the 500,000 joint replacements conducted annually in the United States have had infection rates on the order of 1% despite the utilization of sterile medical practice and systemic antibiotics [16, 141]. The economic and health-related penalties for enduring such an infection are enormous.

The current gold standard treatment in the United States is a two-stage re-implantation process. Specifically, the patient will endure two additional surgeries requiring debridement of dead and dying tissues, removal of the infected implant, insertion of a high-concentration

antibiotic spacer, 6 weeks of intravenous antibiotic therapy, and re-implantation of the missing device. This directly results in longer hospital residency, prolonged pedestrian immobility, the possibility of skeletal defects and limb shortening, and a total cost estimate that can exceed five times that of the initial surgery [8]. Although relatively effective at eradicating infection, such a two-stage process is a tremendous burden on any patient who has to endure it. Therefore the development of a drug-delivery coating that could introduce a confident one-stage re-implantation procedure would be a paradigm shift that would significantly impact the lives of patients who need revision arthroplasty.

Staphylococcus aureus is the infecting pathogen responsible for about two thirds of chronic osteomyelitis clinical isolates [16]. *S. aureus* is a Gram-positive coccus that has developed more resilient strains which are resistant to antibiotics such as methicillin (MRSA) [142], and more recently vancomycin (VRSA) [143]. Among the list of antibiotics that are efficacious against *S. Aureus* [144], gentamicin has been selected as the drug of interest in this study, in part due to its broad bactericidal spectrum. Its mechanism of bactericidal activity is its ability to disrupt protein synthesis by binding to the 30S subunit of the bacterial ribosome [145]. It has a low minimal inhibitory concentration (MIC) against not only *S. aureus* (0.25 μg/mL for ATCC 25923) but also other osteomyelitis-relevant classes of bacteria such as *Pseudomonas* (1 μg/mL for ATCC 27853) and *Enterobacteriaceae* (0.5 μg/mL for ATCC 25922) [84]. Furthermore, gentamicin has already been shown to be successful in inhibiting the viability of *S. Aureus* both *in vitro* [146] and *in vivo* [147]. The standard systemic dose of gentamicin is about 3 mg per kg of bodyweight per day [148]. Since increased doses could lead to unnecessary toxicity and antibiotic resistance, local delivery systems become tremendously attractive.

Before studies can be conducted to find new ways to treat osteomyelitis, one must be able to establish a reproducible bone infection *in vivo*. To this end, animal models using mice [149], rats [150, 151], guinea pigs [152], chickens [153], rabbits [154], dogs [155], pigs [156], and goats [157] have all been reported and include *S. Aureus* as the pathogenic agent. Rabbits are by far the most widely used animal model since they are more prone to infection than other animals, relatively inexpensive, and generally preferred to rats due to the larger nature of their

skeleton, which is necessary for fixation devices [158]. Goats are an excellent model for testing human sized implants, but pilot scale studies should first be conducted on a smaller animal model. *S. Aureus* can be introduced via inoculum or a colonized foreign body. This study uses the latter approach as it is more directly relevant to the application of a contaminated implant during primary arthroplasty, and it provides an implant surface onto which bacteria may form a biofilm. Eradication of sessile bacteria colonized under a robust biofilm requires orders of magnitude higher concentration of antibiotics than planktonic bacteria in the same medium [159, 160].

4.2 *Experimental*

4.2.1 Materials

Cation-adjusted Mueller Hinton Broth II (CMHB, 90922) was purchased from Sigma-Aldrich (St. Louis, MO). Sterile, deionized water was obtained from Mediatech, Inc. (Herndon, VA). Bacto agar and Brucella broth with 20% glycerol were purchased from BD (Franklin Lakes, NJ). All materials were used as received without further purification. *S. aureus* UAMS-1 (ATCC 49230) is a human clinical isolate from a chronic osteomyelitis case [161]. All anesthesia and sampling tools including needles, Vacutainers, SurgiLube, bandages, sutures, sterile cups, lactated Ringer's solution, isoflurane gas, pentobarbital, and medications including ketamine, xylazine, buprenorphine, and meloxicam were supplied by the E25 animal facility. Surgical tools including drill, saw, scalpels, scissors, forceps, and clips were supplied by Dr. Hu-Ping Hsu. Rabbits were purchased from Covance (Princeton, NJ).

4.2.2 Colonization of Implants.

Poly(methyl methacrylate) (PMMA) cylinders were fabricated by the MIT Central Machine Shop to be 8.0 mm long and 2.8 mm in diameter. The cap of each peg, defined here to be the top 1.0 mm of the shaft, had a 3.0 mm diameter. A 1.0 mm diameter hole was drilled perpendicular to the axis of the rod just under the cap. These rods were suspended from the lid of a glass jar using stainless steel 3-0 gage wire threaded through the 1.0 mm hole and subjected to EtO gas for sterilization. Under sterile condition 150 mL CMHB was added to this jar, which completely

immersed all suspended rods. *S. aureus* was grown overnight in CMHB (via toothpick inoculation) and added to the jar at a dilution ratio of 1:1000 (150 µL). The bacteria were then allowed to surface colonize the acrylic pegs overnight.

The following day, the suspended pegs were subjected to three consecutive 150 mL sterile water baths, each rinse lasting 60 seconds without agitation. After air drying, the suspended pegs were stored at -80 °C. All surface colonized pegs were prepared less than one week prior to use.

4.2.3 Approval of *In Vivo* Procedures.

The Committee on Animal Care (CAC) at MIT approved all experiments and animal care procedures. All experiments involving animals were conducted under in a sterile field at a facility certified by the Association for Assessment and Accreditation of Laboratory Animal Care. Sample-size estimation was done using GPower with a significance level of 5% and a minimum power of 80% [162]. These parameters suggested that at least six rabbits should be used to determine the reproducibility of infection. Six male New Zealand White rabbits were enrolled for the development of the bone infection model with weight range of 2.64 to 3.13 kg (mean and standard deviation, 2.85 ± 0.19).

All rabbits were allowed to acclimate to the facility for a minimum of one week prior to their first operation. They were housed in separate cages in a climate-controlled facility with free access to antibiotic-free food including commercial pellets, hay, and water. Each rabbit was examined by a veterinarian prior to each operation.

4.2.4 Experimental Bone Infection Model.

Anesthesia was induced by intramuscular doses of ketamine (35 mg/kg) and xylazine (5 mg/kg). The rabbits were additionally administered a subcutaneous (SQ) dose of buprenorphine (0.03 mg/kg) and meloxicam (0.2 mg/kg). The left hind leg of each rabbit was shaved from the ankle to the hip and prepared with alternating Betadine scrub and 70% isopropyl alcohol (IPA). Anesthesia was maintained throughout the operation using 2% isoflurane gas with oxygen at 1–1.5 L/min via an endotracheal tube. Lactated Ringer's solution was administered through a

catheter inserted into the cephalic vein, at an initial rate of 10 mL/kg-hr and then tapered according to observed hemodynamic parameters. A straight medial side incision approximately 3.5-4.0 cm was centered on the knee joint line. The skin and soft tissue were dissected to the deep investing fascia. A small longitudinal incision was made at the front portion of the superior attachment of the medial collateral ligament (approximately 10 mm above a branch of popliteal artery) to release the periosteum and expose the medial femoral condylar surface. Using a sterile drill bit, a defect about 8.5 mm in length was drilled parallel to the axis connecting the medial and lateral condyles (Figure 4-1A, B, and C). Irrigation was maintained throughout drilling to remove particulate matter. Blood loss was monitored, and animals received three times the estimated loss in Lactated Ringers solution throughout the procedure. After saline joint lavage and hemostasis, one *S. aureus* colonized peg was press-fit into the defect (Figure 4-1D). The exposed face of the peg and surgical wire were then cleaned thoroughly with alcohol wipes with the aim of preventing infection unrelated to the bone. The surgical site was closed in layers using 3-0 interrupted sutures for the investing fascia, 3-0 sutures for the superficial fascia and subcutaneous tissue, followed by reapproximation of the skin with a subcuticular stitch using an uninterrupted 4-0 suture (Figure 4-1E, F, and G). A subcutaneous dose of Lidocaine (2 mg/kg) was delivered at the surgical site while closing. Each animal was monitored closely until full recovery from anesthesia was observed. Postoperative analgesia was achieved with three subcutaneous doses of buprenorphine (one every 8-10 hours) and two doses of meloxicam (one every 24 hours). Animals were monitored daily for food intake, stool and urine output, and behavior. The residence time allowed for the development of bone infection was four days.

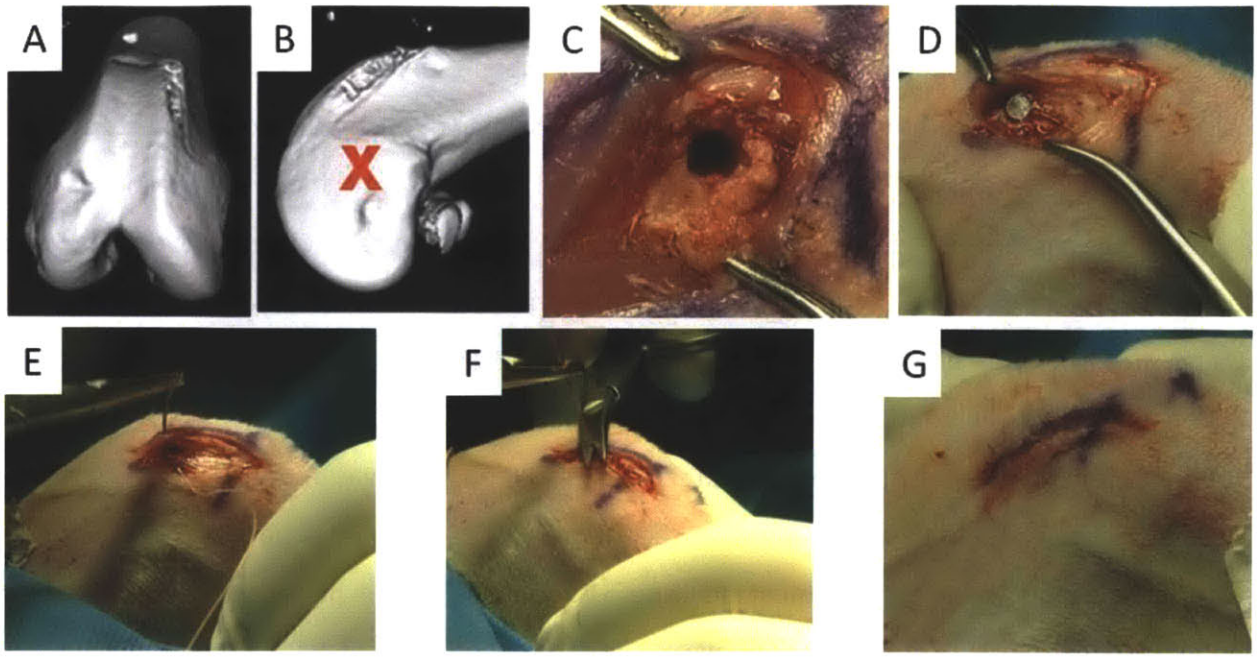

Figure 4-1. (A and B) MicroCT images of the rabbit femur. The drill site is marked with the red 'X'. (C) Drilled defect in the medial femoral condyle of the left hind limb. (D) Defect site with implant set in place. (E and F) Closing of the surgical site. (G) Closed wound.

4.2.5 Analysis of Infection.

Rabbits were given preanesthesia via intramuscular doses of ketamine (35 mg/kg) and xylazine (5 mg/kg). Blood was then drawn from the heart and stored in Vacutainer tubes with anticoagulant (ethylenediaminetetraacetic acid (EDTA) for complete blood counts or heparin for blood cultures) or serum separator elements (for blood chemistry, C-reactive protein, and gentamicin assays). This was followed by euthanasia using an intravenous dose of pentobarbital (120 mg/kg) injected into the marginal ear vein. Each left knee joint was prepared with Betadine solution, the implant extracted, and stored in a sterile vial. The infected region of each femur was then extracted aseptically by cutting perpendicular to the distal metaphysis axis at about 5.0 mm from the proximal edge of the drilled defect. All soft tissue was debrided from its surface, and the entire outside surface of the bone was sterilized using 70% (v/v in water) isopropyl alcohol wipes without disturbing the defect. The bone was then weighed, snap-frozen in liquid nitrogen, and homogenized using a BioPulverizer (BioSpec, Bartlesville, OK). The well-mixed powder was then added to 5 mL of Brucella broth and stored

at -80 °C before analysis. Quantitative culturing was initiated after 1 to 4 days of storage. As a control, contralateral femurs of placebo subjects (n = 5) were prepared in a similar manner.

Complete blood counts, blood cultures, and microbiology were performed at the microbiology lab within MIT's Division of Comparative Medicine. Blood chemistry was determined by Idexx Laboratories, Inc. (North Grafton, MA), and gentamicin assays were conducted at the Veterinary Medical Center of Cornell University (Ithaca, NY). All explants were rolled and streaked on trypticase soy agar plates with 5% sheep blood (VWR International), and incubated overnight to determine the qualitative extent of surface colonization. The bone homogenates were thawed, vortexed vigorously for 30 seconds, serially diluted, and plated to determine the concentration of bacteria in the homogenate (colony forming units (CFU)/mL). Plates with the largest countable number of bacteria were used in the statistical analyses, and subsequent dilutions with greater than 20 CFU were averaged in with this value. Since the sensitivity of this assay is 10 CFU/mL (corresponding to 1 CFU on the undiluted plate), a blank undiluted plate was assigned half the value of the experimental uncertainty (i.e. 5 CFU/mL).

4.2.6 Statistical Analysis

Raw data of bacterial populations were not normally distributed and therefore required nonparametric statistical methods. Log-transformed CFU data were analyzed with parametric statistical tests. All statistical analyses were conducted using a Type I error rate of 0.05, single-tailed testing. Power analyses were performed with the use of G-Power. The Mann-Whitney U-test (nonparametric) was performed in StatView (SAS Institute Inc.). F-tests for variances and subsequent t-tests for means were computed using the Analysis Toolpack in Microsoft Excel. Statistical power greater than 0.80 and p-values smaller than 0.05 were considered to be significant. Sample sizes are indicated in figure captions. Data are presented as mean ± standard deviation unless otherwise specified.

4.3 *Results and Discussion*

4.3.1 Reproducibility of the Bone Infection Model

The bone infection model was designed to reproducibly simulate a primary surgery that introduces implant-related osteomyelitis. Although less frequent than the use of bacteria inoculum, foreign bodies have been used in past *in vivo* studies to help increase the rate of infection due to facilitation of biofilm formation on the implant surface and greater resilience of bacteria within [158, 163]. In this study, PMMA rods were intentionally surface colonized via submersion into *S. aureus* culture. These rods were then introduced to their subjects by press-fitting into a drilled defect in the medial femoral condyle of the left hind limb. Since soft tissue infection was not relevant to this study, an attempt was made to sterilize the exposed cap of each rod with alcohol wipes after press-fitting. The incubation time for propagation of infection within the local bone was set to four days.

Infection of *S. aureus* was successfully contained near the defect site. As a result, blood cultures from all rabbits were negative. Five contra-lateral femurs were extracted and homogenized. Plating of these suspensions also yielded negative cultures. After the pretreatment period, the surgical sites were re-opened and PMMA rods extracted to determine surface colonization. Results of these cultures indicated the presence of *S. aureus* exclusively as the infecting agent. The plates provide a qualitative metric on the extent of surface colonization of the explanted rods (Figure 4-2), and suggest the existence of infection within the defect site.

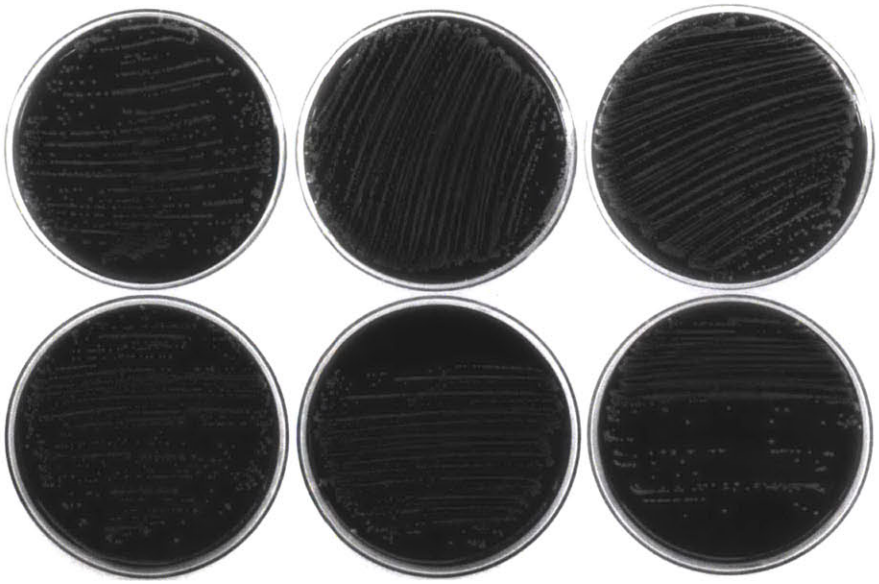

Figure 4-2. Blood agar plates of explanted PMMA rods that were rolled down the center of the plate and streaked for qualitative analysis of device surface colonization. Each plate corresponds to one rabbit. Each white dot corresponds to a single CFU.

As a result of the inflammatory-infectious response, body weight decreased significantly. Including the animals used for the *in vivo* experiment described in Chapter 5, the rabbits lost an average of 9.1 ± 3.3% of their bodyweight (with a maximum of 15.4% and minimum of 3.0%, n = 33) throughout the bone infection period. The correlation of this trend with the existence of infection has been documented in other studies [164, 165]. Although all thirty-three rabbits underwent the pretreatment infection model, only six rabbits were euthanized without re-implantation for quantitative analysis of bone cultures and blood chemistry of the bone infection model. These six rabbits had their infected femurs prepared into a homogenate for determination odf CFU/mL by serial dilution. The total CFU present within the extracted bone was back-calculated using the bone concentration in the homogenate (g/mL) and total bone extracted from the rabbit (g). The mean number of $\log_{10}$(CFU) per defect site for these six rabbits was 6.36 ± 0.94, which confirms a reproducible and highly infected defect site.[4]

[4] The standard deviation is reminiscent of general exponential growth behavior in bacteria, and is relatively narrow considering the highly variable nature of *in vivo* experiments.

Complete blood counts (n = 9) and blood chemistry (n = 6) data were generated for healthy rabbits prior healthy rabbits prior to the pretreatment period. These values were compared to those of the infected animals infected animals after the pretreatment period (n = 6 for both CBC and blood chemistry). Twelve metrics proved Twelve metrics proved to be statistically significant in differentiating these two groups (i.e. they resulted in a resulted in a post hoc power greater than 80% given a maximum allowable α error rate of 5%, (Table 4-1. Bone Infection Model: Significant Blood Changes

). These changes must either be a result of surgical trauma, or infectious complications. Since the aim of this model was to solely create an infected bed of bone for use in testing the film-coated implants, only parameters that convincingly related to a bacterial infection were of interest. The strongest data in support of this were the total CFU counts, weight loss, the positive explant cultures, and leukocyte counts. The increased leukocyte concentration (p-value < 0.01) is directly related to the presence of infecting microorganisms. Additionally, there was an increase in the proportion of neutrophilic leukocytes in the infected rabbits (50% vs. 30% in healthy rabbits), which is highly reminiscent of acute bacterial infection. Despite the fact that the statistical power associated with this increase was less than 80%, an F-test for variances and subsequent t-test for means assuming equal variances yielded a p-value less than 0.03.

Table 4-1. Bone Infection Model: Significant Blood Changes

		Healthy Rabbits		Infected Rabbits				
Metric	Units	Average	Standard Deviation	Average	Standard Deviation	Pooled Deviation	Effect Size	**Power (α = 0.05)**
Leukocytes	10^3/mm3	5.79	0.96	7.84	1.80	1.35	1.51	**0.86**
Hematocrit	%	42.82	5.09	35.73	3.62	4.58	1.55	**0.87**
Erythrocyte Mean Cell Volume	fl	66.10	3.86	58.63	1.67	3.20	2.34	**0.99**
Alkaline Phosphatase	IU/L	102.67	24.03	41.00	5.55	17.44	3.54	**1.00**
Aspartate Transaminase	IU/L	12.50	2.17	35.33	17.41	12.40	1.84	**0.91**
Creatine Kinase	IU/L	814.17	318.64	3762.50	1057.02	780.65	3.78	**1.00**
Albumin	g/dL	3.93	0.20	3.38	0.22	0.21	2.62	**0.99**
Globulin	g/dL	1.55	0.08	1.93	0.15	0.12	3.15	**1.00**
Calcium	mg/dL	14.05	0.64	12.75	0.48	0.56	2.31	**0.98**
TCO_2 (Bicarbonate)	mEq/L	32.00	1.67	29.17	1.47	1.58	1.80	**0.89**
Albumin/Globulin Ratio		2.57	0.22	1.73	0.15	0.19	4.48	**1.00**
Lipase	IU/L	421.17	78.79	287.00	63.02	71.34	1.88	**0.92**

4.3.2 Limitations to the Model

In this investigation, the greatest weight was placed on developing a bone infection model that can be used to generate proof-of-principle efficacy data from antibiotic LbL films in an *in vivo* environment. Additionally, it was important to maintain relevance to the application of conducting a one-stage direct exchange procedure to replace an infected prosthesis. There are two major limitations to this model. First, the infection procedure is non-quantitative. The PMMA rods were allowed to incubate overnight in *S. aureus* broth with the aim of growing a biofilm throughout the surface of the implant. As a result, the number of CFU in the bacteria challenge to the defect is unknown. Although inoculation models generally inject a known quantity of bacteria, the decision to use the colonized implant was made since it more accurately simulates the specific clinical case that the antibiotic coatings are designed to treat. Moreover, not only is the resulting challenge at the end of the bone infection period more important than strict control over the initial inoculation quantity, but also propagation of bacteria in an *in vivo* environment will differ from subject to subject regardless of the introductory method and exact quantity. The second limitation to this model is that subcutaneous infection local to the defect site is very difficult to control. Subcutaneous infection was not relevant nor treated in this study and caused unnecessary burden on the animals, ultimately resulting in weight losses that sometimes required sacrifice before later time points could be studied (i.e. greater than one week). Since the implants were press-fitted into place, their colonized cap remained exposed to the subcutaneous environment. Despite vigorous attempts to sterilize the exposed surface with alcohol wipes, infection of the local soft tissues remained a great challenge. The presence of infection external to the site of interest unfortunately made comparison of between the blood data of placebo and treatment groups very difficult since treatment was restricted to the bone defect site. Soft tissues were meticulously cleaned and removed from the bone prior to homogenization and did not significantly affect the bone cultures, which were the primary metric of efficacy in this proof-of-principle study. Future work may consider sealing off the implants using bone wax [166], and perhaps additionally deliver systemic antibiotics to better control soft tissue infection. There

was an intentional omission of systemic antibiotics in this study in order to clearly attribute noticeable reductions in CFU counts to that of the antibiotic LbL films.

4.4 *Conclusions*

The *in vivo* bone infection model described in this chapter, which involved four days of bone incubation with a *S. aureus* surface-colonized PMMA peg, was successfully reproduced over six animals. It thus provided an interface through which the antibiotic films could be evaluated. This infection model is an example of acute osteomyelitis due to the short incubation time; development of a local soft tissue abscess, sepsis, and morbidity make longer incubation times challenging and hence development of a chronic osteomyelitis extension to this model requires further consideration. Regardless, the primary deliverable sought from this study was achieved.

Chapter 5 *In Vivo* Evaluation of Antibiotic Polyelectrolyte Multilayer Coatings

The work presented in this chapter has been reproduced from the published manuscript entitled "The effectiveness of the controlled release of gentamicin from polyelectrolyte multilayers in the treatment of Staphylococcus aureus infection in a rabbit bone model" by Joshua S. Moskowitz, Michael R. Blaisse, Raymond E. Samuel, Hu-Ping Hsu, Mitchel B. Harris, Scott D. Martin, Jean C. Lee, Myron Spector, and Paula T. Hammond (*Biomaterials*, vol. 23, pp. 6019-30, 2010) with permission from Elsevier.

5.1 *Introduction*

Past clinically relevant treatment techniques that have released gentamicin locally *in vivo* include bone cement [18, 167], bioactive sol-gel glass [39], injectable polymers [168], polymer coatings [150, 151], and poly(methyl methacrylate) (PMMA) beads [31, 142, 169, 170]. For the specific application of orthopedic implant surfaces, the relevant technology platform is a surface coating with the most widely studied material for this use being antibiotic loaded bone cement (ALBC). ALBC is accepted in the United States for prophylactic use only; however, internationally, ALBC has been used in one-stage revision procedures where the infected implant is directly exchanged with a sterile, ALBC coated implant in a single operation. A review by Jackson and Schmalzried condensed data from twelve different reports totaling 1,299 infected hips that were revised using a one-stage process (almost 99% of which included ALBC) [171]. The overall success rate determined from these revisions was about 83%. The main drawbacks from using antibiotic loaded bone cement are: 1) the PMMA reaction is highly exothermic which causes local tissue damage, 2) un-reacted methyl methacrylate is toxic [34], 3) cemented revisions make future removal much more tedious and difficult to prevent bone damage, and 4) current levels of antibiotic delivery from these cements are insufficient for FDA approval of the direct exchange process, while increased loading malevolently affects the mechanical integrity of the cement [172]. Furthermore, bone cements are not able to incorporate multiple therapeutic agents with individualized release rates, and the heat of the polymerization reaction prohibits the incorporation and release of fragile therapeutic agents

such as growth factors due to denaturation. As a result, the two-stage process requiring six weeks of intravenous antibiotic therapy and local antibiotic-eluting PMMA beads remains the accepted therapy in the United States to fight *S. Aureus* infection arising from implant-related osteomyelitis [16]. One study utilized these beads to heal osteomyelitis in 92 out of 100 patients [170] while a second reported a 90.4% success rate in 405 patients [173].

The goal of this thesis was to develop a drug delivery coating that could help enable the one-stage re-implantation procedure to the United States. Broadly, the coating would need to first provide both analgesics and sufficient levels of antibiotics to eradicate an existing bone infection, then facilitate new bone formation to ensure intimate contact between the bone and implant surface, and finally prevent biofilm formation. The approach was to develop a biocompatible and biodegradable implant coating constructed from polyelectrolyte multilayers. PEM films could potentially directly address the major downfalls of ALBC since they can be designed with biocompatible components to biodegrade without exothermic concerns. Since long term mechanical integrity of the film is unnecessary for an erodible system (as it is for ALBC), gentamicin loading and release specifications can be met without mechanical tradeoff concerns. Furthermore, the chief advantage for the use of PEM films in the present application is that they can incorporate multiple functional components at very specific regions within the layered film architecture, which can enable complex and individualized release rates for each type of cargo [55]. Therefore, there is an opportunity for PEM films to be incorporated onto the surfaces of prostheses to make an unparalleled impact since painkillers [62], antibiotics[53], and growth factors [64, 66] can be incorporated into the film. Upon surface erosion, this coating would be able to deliver each therapeutic agent with individually optimized release profiles to synergistically provide optimal recovery.

The objective of this chapter is to evaluate the antibiotic component of this conceptual multi-drug film, *in vivo*. Although the onset of research efforts directed at development of PEM coatings for titanium implants has begun [174, 175], this is the premier study that demonstrates proof-of-principle that an LbL coated implant can locally deliver small hydrophilic antibiotics to efficaciously treat a *S. aureus*-related bone infection *in vivo*. The LbL architecture used in the following *in vivo* experiment is the first such architecture capable of long-term

release of gentamicin (i.e. greater than 30 days), which not only improves upon sustained durations reported in other small-molecule LbL systems [53, 62, 103], but also makes these films competitive with existing technologies [39, 168, 176].

5.2 *Experimental*

5.2.1 Materials

Poly 1, a poly(β-amino ester) depicted in Fig. 1, was synthesized as previously described [78]. Silicon wafers (test grade n-type) were purchased from Silicon Quest (Santa Clara, CA). Medical grade titanium dowels were received from Titanium Industries (Rockaway, NJ). Linear poly(ethyleneimine) (LPEI, 23966-2, M_n = 25 kDa) was purchased from Polysciences, Inc. Poly (sodium 4-styrenesulfonate) (PSS, 434574, M_w = 1 MDa), Poly(acrylic acid) (PAA, 306215, M_v = 1.25 MDa), 3 M concentrated sodium acetate buffer (S7899, pH 5.2) were purchased from Sigma-Aldrich (St. Louis, MO). Sterile, deionized water and nonradiolabeled gentamicin sulfate (GS) purchased in powder form were from Mediatech, Inc. (Herndon, VA). ^{3}H-GS (250 μCi total, 1 mCi/mL in ethanol, 200 μCi/mg) was obtained from American Radiolabeled Chemicals, Inc. Bacto agar and Brucella broth with 20% glycerol were purchased from BD (Franklin Lakes, NJ). Concentrated castile soap and 70% v/v isopropyl alcohol pads were kindly donated by Triad Medical (Hartland, WI). All materials and solvents were used as received without further purification.

5.2.2 Preparation of Polyelectrolyte Solutions

Dipping solutions containing Poly 1 and PAA were prepared at 2 mg/mL in 100 mM sodium acetate buffer and pH-adjusted to 5.0 with 1.0 N sodium hydroxide. GS was prepared at 10 mg/mL in 100 mM sodium acetate and pH-adjusted to 5.0. LPEI and PSS dipping solutions were prepared in ultra pure water and pH adjusted to 4.25 and 4.75 respectively. All solutions were prepared with water from a Milli-Q Plus (Bedford, MA) at 18.2 MΩ.

5.2.3 Polyelectrolyte Deposition.

In vitro experiments utilized silicon substrates. Films for *in vivo* use were built on titanium pegs. All polyelectrolyte LBL thin films were constructed as follows according to the alternate dipping method [44]. Substrates were rinsed with methanol and ultra pure water, dried under nitrogen, and plasma etched in oxygen using a Harrick PDC-32G plasma cleaner at high RF power for 75 seconds. Layer-by-layer thin film deposition was performed using a Carl Zeiss HMS Series Programmable Slide Stainer. A nondegradable bilayer of LPEI/PSS was deposited first by immersion of the plasma treated substrates in LPEI for 30 minutes followed by a single ultra-pure water rinse, and finally in PSS for 30 minutes followed by a single ultra-pure water rinse. The degradable films were deposited on top of this PSS-terminated surface. The tetralayer architecture of $[\text{Poly 1/Anion/GS/Anion}]_n$ was constructed by alternate dipping in a cationic species (i.e. Poly 1 or GS) for 9 minutes followed by a cascade rinse of three 100 mM sodium acetate baths for 10, 20, and 30 seconds, and then into the anionic species (i.e. PAA or HA) for 9 minutes followed by a similar rinse cycle. The process was repeated *n* times depending on the desired experiment. All polymer solutions and gentamicin solutions were completely replaced every 25 and 50 tetralayers, respectively.

For films used in drug release experiments, the GS solution was spiked with 25 µL ^{3}H-GS per 50 mL dipping solution yielding a 0.5 µCi/mL product without significantly changing the concentration of the GS dip bath. No other part of the LbL deposition process was changed.

Films prepared on titanium pegs for the *in vivo* work were grown to $[\text{Poly1/PAA/GS/PAA}]_{200}$ + $[\text{Poly1/PAA/GS}]_1$ and allowed to air dry without a final rinse. Additionally, these implants were subjected to a 12-hour cycle of ethylene oxide (EtO) gas for sterilization in an Anprolene AN74*i* cabinet (Andersen Sterilizers, Inc., Haw River, NC).

5.2.4 *In Vitro* Characterization of Drug Release and Film Erosion

Films used for drug release experiments were stored at 4 °C until use. Films with ^{3}H-GS were immersed into 3 mL of modified simulated body fluid (m-SBF) [105] in a tightly capped Falcon tube maintained at 37 °C. Degradation environments were kept sealed from the ambient to minimize evaporative loss. A 1 mL sample was extracted from the Falcon tube at

predetermined time points and replaced with 1 mL prewarmed m-SBF in a manner so as not to mechanically disturb the hydrated film. The time points were selected with a greater frequency at early times to reflect the kinetics of release. Each extracted sample was mixed with 5 mL ScintiSafe Plus 50% (Fisher Scientific, Atlanta, GA) prior to GS quantification. The resulting mixtures were analyzed using a Tricarb Model 2810 TR liquid scintillation counter (Perkin Elmer, Waltham, MA). The raw data in disintegrations per minute (DPM) was converted directly to μg of drug using the DPM value for the dipping solution (10 mg/mL). Total release from the film at the *i*th timepoint was calculated by the following equation:

$$m_i = (C_i \times 3\ \text{mL}) + (1\ \text{mL}) \sum_{j=1}^{i-1} C_j$$

where m_i (μg) is the the total cumulative mass of GS released from the film at the time of measurement *i*, C_i (μg/mL) is the concentration of sample *i* (which is multiplied by a total of 3 mL in the Falcon tube), and the summation term adds up the total extensive quantity of gentamicin removed in each of the *i*-1 former aliquots.

Films used for erosion experiments were constructed with the architecture [Poly 1 / PAA / GS / PAA]$_{200}$. As in the release experiments, these films were immersed into 3 mL of m-SBF in a tightly capped Falcon tube maintained at 37 °C. At each predetermined time point, a minimum of three films were removed from the m-SBF and allowed to air dry. The dry state thicknesses were scratched with a razor blade and their thickness measured by profilometry at four predetermined locations using a KLA-Tencor P-16 Profilometer. Triplicate measurements were made on each film.

5.2.5 Approval of *In Vivo* Procedures

The Committee on Animal Care (CAC) at MIT approved all experiments and animal care procedures. All experiments involving animals were conducted under in a sterile field at a facility certified by the Association for Assessment and Accreditation of Laboratory Animal Care. Sample-size estimation was done using GPower with a significance level of 5% and a minimum power of 80% assuming one-sided alternate hypothesis (i.e. antibiotic films should decrease infection when compared to the placebo group) [162]. These parameters suggested that at

least six rabbits should be used per test group per time point. Twenty-seven male New Zealand White rabbits were ultimately enrolled in the present study with weight range of 2.50 to 3.78 kg (mean and standard deviation, 3.07 ± 0.34) and were randomized into four test groups: (1) four day placebo (n = 6), (2) four day treatment (n = 6), (3) seven day placebo (n = 7), and (4) seven day treatment (n = 8).

All rabbits were allowed to acclimate to the facility for a minimum of one week prior to their first operation. They were housed in separate cages in a climate-controlled facility with free access to antibiotic-free food including commercial pellets, hay, and water. Each rabbit was examined by a veterinarian prior to each operation.

5.2.6 Removal of Colonized Rod and Insertion of a Test Implant.

Four days after their initial surgery, 27 rabbits were anesthetized and prepared for a second surgery as described previously (Chapter 4). After thorough debridement of the subcutaneous and soft tissue abscess, each acrylic peg was removed (Figure 5-1A and Figure 5-1B) and placed into a sterile vial for microbiological analysis (see 5.2.7 Sampling Schedule and Analysis of Infection).

The 27 rabbits were divided into four test groups: four day sterile implants (n = 6), four day LbL coated implants (n = 6), seven day sterile implants (n = 7), and seven day LbL coated implants (n = 8). Each test implant was carefully press-fitted into the bone defect (Figure 5-1C and Figure 5-1D). Implants with antibiotic films were dipped in sterile water for less than one second in order to hydrate prior to insertion. Castile soap solution was prepared by adding one 0.3 oz. packet to 1.0 L of sterile water [177]. The subcutaneous and soft tissue areas were thoroughly irrigated using this solution without disturbing the implant or defect. All animals were sutured, dosed with postoperative analgesia, and monitored daily as described above.

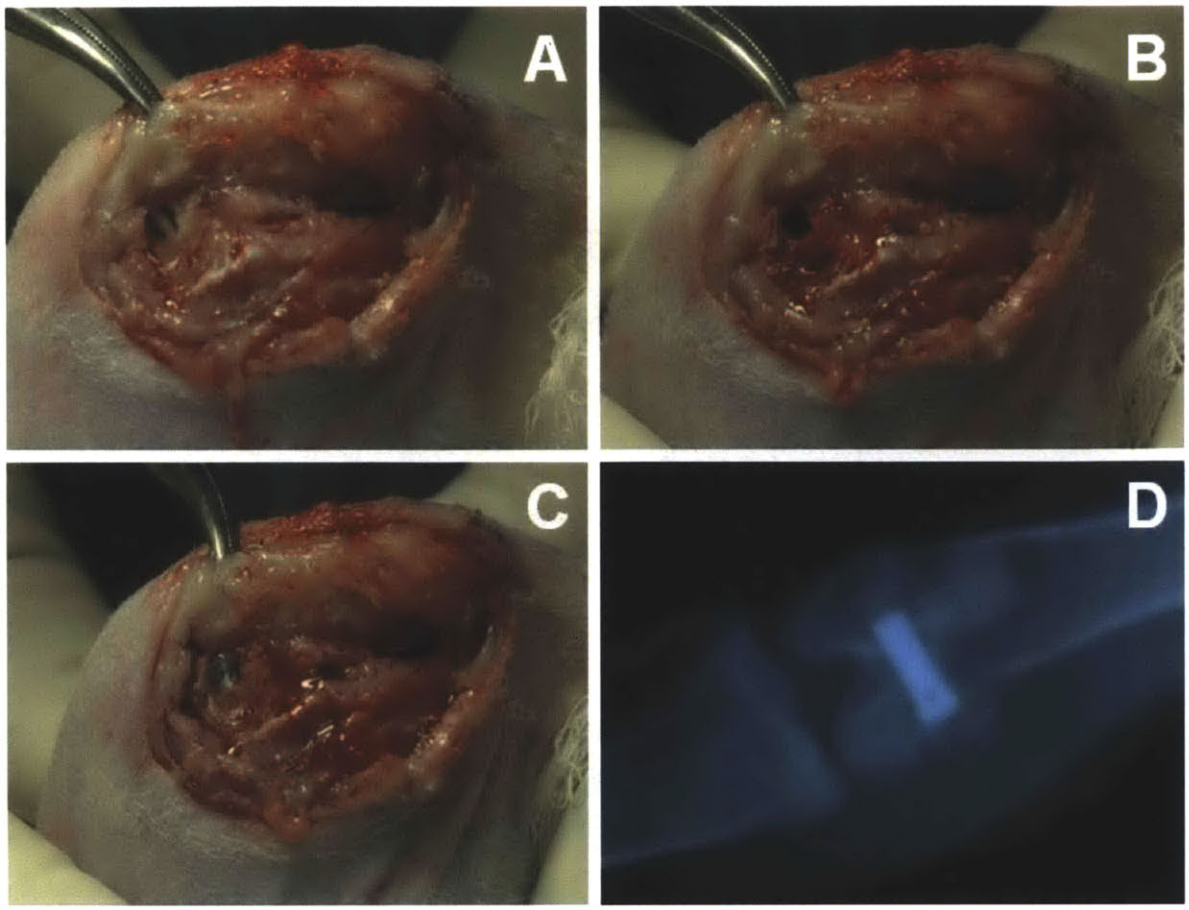

Figure 5-1. (A) Opened defect site with infected PMMA implant exposed. (B) The PMMA implant has been extracted leaving a void. (C) Without washing the defect site, a titanium sample implant is press-fit into the void. (D) Anterior-posterior radiograph showing the placement of the titanium peg in the medial femoral condyle of the left hind limb.

5.2.7 Sampling Schedule and Analysis of Infection.

Sampling schedule and expected propagation of bacteria in the defect site are depicted in Figure 5-2. The bone infection model described in Chapter 4 comprises the first four days of the study for each rabbit, after which a second surgery is performed which directly exchanges the infected acrylic implant for either a coated (treatment) or uncoated (placebo) titanium implant. Animals are euthanized at either 4 or 7 days after re-implantation. Details of infection analysis are described in Chapter 4.

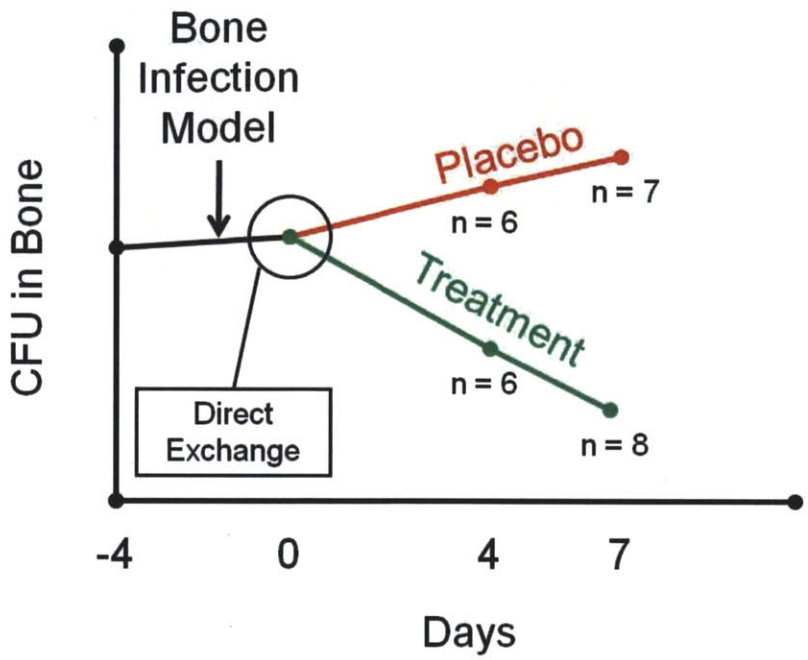

Figure 5-2. Schematic of the hypothesized magnitude of infection in the defect site as a function of time. The initial surgery described in Chapter 4 is conducted at day -4. The direct exchange described in this chapter is conducted at day 0. All n-values correspond to the total number of animals euthanized in that particular test group.

5.2.8 Statistical Analysis.

Raw data of bacterial populations were not normally distributed and therefore required nonparametric statistical methods. Log-transformed CFU data were analyzed with parametric statistical tests. All statistical analyses were conducted using a Type I error rate of 0.05, single-tailed testing. Power analyses were performed with the use of G-Power software. The Mann-Whitney U-test (nonparametric) was performed in StatView (SAS Institute Inc.). F-tests for variances and subsequent t-tests for means were computed using the Analysis Toolpack in Microsoft Excel. Statistical power greater than 0.80 and p-values smaller than 0.05 were considered to be significant. Sample sizes are indicated in figure captions. Data are presented as mean ± standard deviation unless otherwise specified.

5.3 *Results and Discussion*

The primary aim of this thesis was to design films that could treat an existing bone infection. Accordingly, the desired release profile contains an initial burst release of drug over the first few days to sterilize the infected implant site, followed by a prolonged zero-order release that prevents surviving bacteria from multiplying and re-colonizing the surface of the implant. The extended release should last weeks to allow the patient's immune system enough time to resolve any latent infection. Therefore, films were built with [Poly 1/PAA/GS/PAA]$_{200}$ + [Poly 1/PAA/GS]$_1$ for a total of 803 individually deposited layers (on top of the nondegradable baselayers). The 200 tetralayers were used to achieve long-term release. The final adsorption step of gentamicin allowed excess GS to permeate and load into the film without a final rinse. This provided a means of incorporating excess unbound drug available for immediate diffusive release upon immersion into a physiological environment (approximately 20% increase in total drug load from the 200 tetralayer films), which would be followed by gradual surface-erosion based release of the remaining drug-containing film.

5.3.1 Release and Erosion Characteristics of Treatment Samples

The films (n = 3) released approximately two thirds of their total load within the first three days in m-SBF maintained at 37 °C (Figure 5-3). This aqueous buffer closely models the conditions of human blood plasma without the biological components [105]. Likely, there are three major factors contributing to this burst release: 1) excess unbound drug diffuses out of the film, 2) m-SBF has a pH of 7.4 which causes some de-protonation of the amines on GS molecules that were originally loaded into the film at pH 5.0, thereby reducing the charge state of GS to approximately +3.5 [178] and facilitating the release of loosely interacting molecules, and 3) the salts present in the m-SBF diffuse into the film and compete for the same ionic sites as the GS, which further enhances drug release. Since the films exhibit super-linear growth behavior with gentamicin as one of the key diffusing species, it is anticipated there is a GS-rich diffusion zone at the film-solution interface [115, 116]. It is likely that the rapid loss of GS from this region of the film may trigger subsequent film instability and deconstruction, leading to faster release than would be expected from hydrolysis of Poly 1 alone. This is, in part, supported by

assessment of film erosion data (Figure 5-3A). Films were grown to 200 tetralayers and immersed in m-SBF. They were removed at pre-determined time points and their dry state thicknesses determined by profilometry on at least triplicate samples with triplicate measurements per sample. Film thickness decreased rapidly during the burst release phase of drug elution, followed by relatively linear erosion behavior consistent with zero-order release. The effects of the three putative mechanisms noted above are expected to play an important role primarily during burst release phase, as the zero-order release phase pertains to strongly bound drug and the stabilized film, which erodes due to hydrolytic degradation of the polycation.

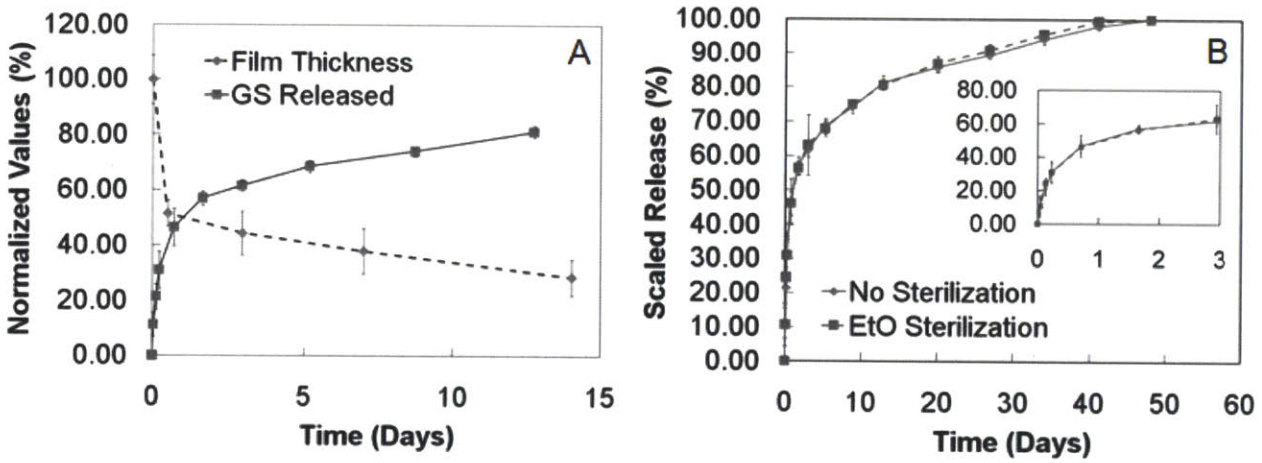

Figure 5-3. (A) Normalized film erosion from [Poly 1 / PAA / GS / PAA]$_{200}$ films and normalized GS release from [Poly 1 / PAA / GS / PAA]$_{200}$ + [Poly 1 / PAA / GS]$_1$ films. Erosion values are normalized to initial film thickness with the error bars representing the normalized rms roughness averaged over triplicate samples. Release values are normalized to the final release quantity (582 μg/cm^2) with error bars representing standard deviation of triplicate samples. Release data have truncated for convenience of comparison. (B) Cumulative antibiotic release from [Poly 1/PAA/GS/PAA]$_{200}$ + [Poly 1/PAA/GS]$_1$ films in m-SBF at 37 °C before (replotted from (A)) and after an effective dose of ethylene oxide gas. Inset contains data from the first three days. All values are reported as mean ± standard deviation of triplicate samples.

Beyond day three, the films continue to release drug in a relatively linear fashion until their expiration at 5.5 weeks (Figure 5-3B). The average total loading of these films exceeded 550 μg/cm^2. This compares favorably against the rapid release architectures based on hyaluronic acid [53]. From days 3 to 13, the films released over 11 μg/cm^2/day, and during the subsequent four weeks, the films released over 4 μg/cm^2/day. The diffusivity of gentamicin in

different environments including collagen, agar, and mucus, has been reported to be on the order of 10^{-6} cm^2/s [132, 179], which would translate to a local linear velocity that is less than 1 cm/hr. If this is consistent with the drug behavior in the local joint, then the concentration of drug would exceed the MIC of gentamicin against *S. aureus* for over five straight weeks from the initial implant date. The linear release phase observed in the films is indicative of a controlled, surface-erosion based release that is consistent with the observed zero-order erosion behavior in Figure 5-3A. Theoretically, if the drug concentration throughout the film thickness is constant, and no gradients develop within the film during release, then the normalized film thickness and released drug amounts should total to 100%; as shown in Figure 5-3A, these data are consistent with the model of linear scaled release.

Any implant or medical device inserted into the body of a human or animal must be sterilized in order to prevent the possibility of subsequent infection. The three most popular sterilization techniques used clinically include autoclave, gamma irradiation, and ethylene oxide (EtO) gas. The autoclave creates a moist heat environment that rapidly destructs the hydrolytically degradable films. Gamma irradiation was not investigated since it is not generally applicable to LbL systems due to potential crosslinking or scission issues which could change release kinetics [180-183]. Ethylene oxide (EtO) gas treatment is a room temperature process that subjects the film to a highly effective killing agent without chemically changing the film components, and therefore film performance is preserved. The films were subjected to a 12 hour EtO cycle and subsequently stored for at least 24 hours to allow any residual gas to dissipate from the film. After comparing sterile and non-sterile films in triplicate, EtO gas appeared to have virtually no effect on release kinetics, and did not significantly alter the total loading of gentamicin in the LbL films ($p = 0.48$) (Figure 5-3B).

In order to prevent any possibility of shrouding the effect of the antibiotic films in treating existing bone infection, two major relevant clinical procedures that would otherwise be used in a real operation were intentionally omitted: the use of systemic antibiotics and debridement of the bone defect. After the four day pretreatment period described in the previous chapter, twenty-seven rabbits underwent a direct exchange operation in which either an uncoated titanium implant (placebo, n = 13), or film-coated titanium implant (treatment, n =

14, Figure 5-4A and Figure 5-4C) replaced the incumbent, *S. aureus*-colonized PMMA rod. There was no other tampering of the defect site. Soft tissue complications were considered irrelevant to the primary goal of treating the local infected bone. Consequently, to reduce unnecessary burden on the animals, all abscesses were drained of pus, and both infected and necrotic soft tissues external to the defect site were thoroughly extracted before a final wash using castile soap solution. These procedures were conducted with an implant in place and care was taken to ensure that the implant site was not disturbed. All blood cultures (detectability limit, 10 CFU/mL) performed in this study were sterile indicating that none of the animals were septic.

5.3.2 Local Infection Quantifiaction

Six animals from each of the placebo and treatment test groups were euthanized four days after direct after direct exchange. Films were not completely eroded at this time point (Figure 5-4B and Figure 5-4D). Total Figure 5-4D). Total colonization of devices in the treatment group was substantially lower than that of the that of the placebo group (Figure 5-5A). Five of six animals (83%) in the placebo group had >200 CFU of *S. aureus* on their explanted titanium device compared to zero of six animals in the treatment group (maximum of 22 CFU). Total CFU counts in the bone homogenates confirmed gross infection in six of six animals from the placebo test group, whereas three of six animals in the treatment group yielded sterile bone cultures (Figure 5-5C and Table 5-1. Raw CFU Data from Bone Homogenates.*

). A Mann-Whitney U-test comparing the underlying distributions of raw CFU data at the four day time point indicated that the reduction in CFU counts due to the antimicrobial LbL films was statistically significant ($p < 0.004$) when compared to those of the placebo test group. This was further verified by analyzing the log-transformed data via an F-test for variances ($p > 0.15$) and subsequent t-test assuming equal variances ($p < 1 \times 10^{-8}$). At four days after direct exchange, the antibiotic films decreased the average bacteria burden by an average of almost five orders of magnitude.

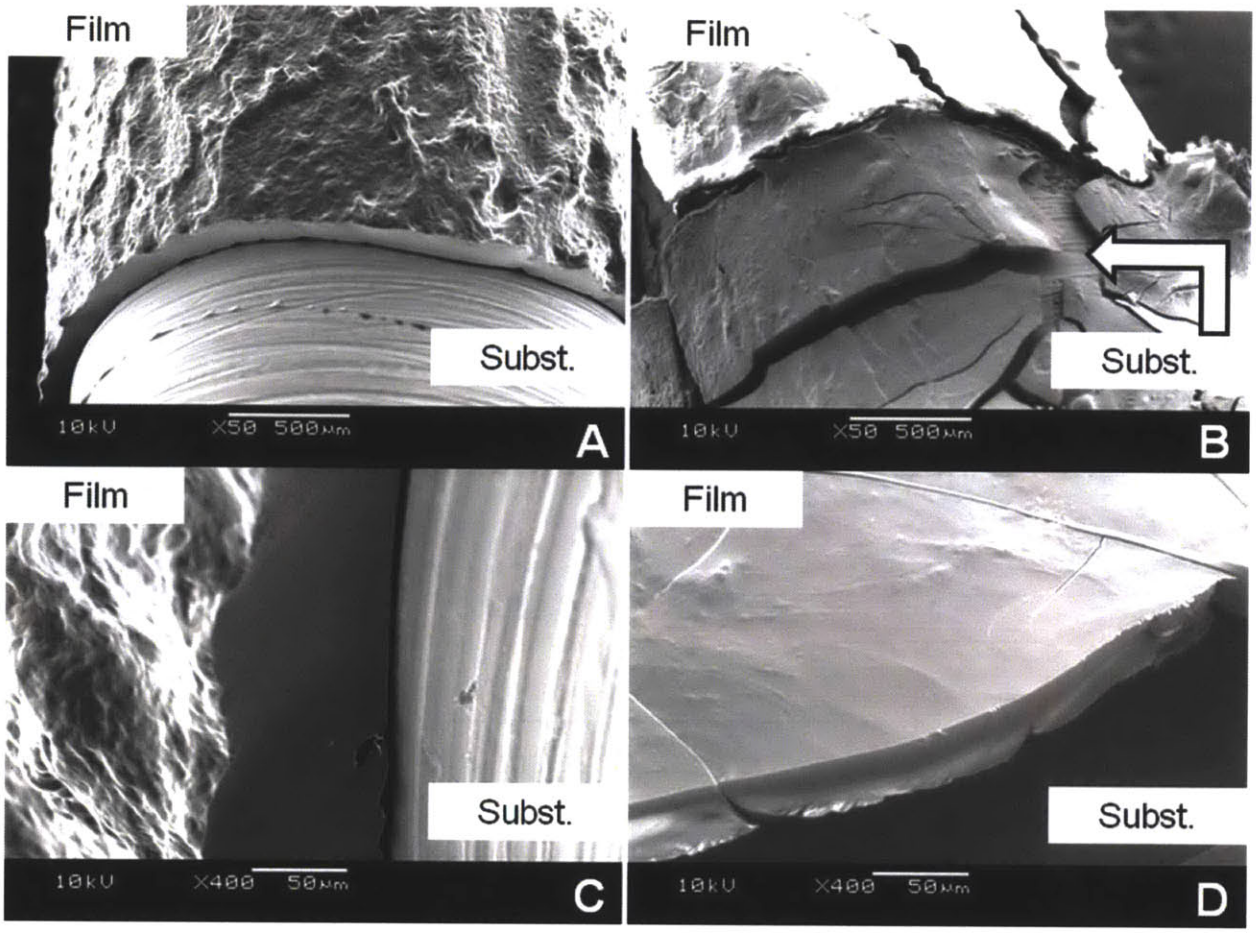

Figure 5-4. SEM images of the PEM film on a titanium implant (i.e. substrate) before implantation (A and C), and after 4 days incubation in the defect site (B and D).

One week after direct implant exchange, the remaining fifteen animals were euthanized (placebo n = 7 and (placebo n = 7 and treatment n = 8). Films were still not completely eroded at this time point (data not shown). (data not shown). A qualitative assessment of the total surface colonization of the explanted devices on day devices on day seven indicated that the LbL coatings continued to prevent re-colonization of the implant surface the implant surface when compared to the placebo films (Figure 5-5B). Five out of seven animals (71%) in the placebo group had *S. aureus* colonization that exceeded 200 CFU on their explanted devices compared to zero out of eight animals in the treatment group (maximum was 190 CFU). This result is favorable since infectious complications become much more robust and hostile if biofilm formation occurs on the implant surface. While all animals in the placebo test group had sizeable CFU counts, two of eight animals (25%) in the treatment group did not have detectable quantities of bacteria. The Mann-Whitney U-test ($p < 0.03$), F-test ($p < 0.05$), and subsequent t-test assuming unequal variances ($p < 0.02$) confirmed that the two order of magnitude reduction in CFU counts was statistically significant (Figure 5-5C and Table 5-1. Raw CFU Data from Bone Homogenates.*

). There was no significant decrease in CFU count from day four to day seven within the placebo group. In this case, the staphylococcal infection is only controlled by the host immune system since no antimicrobial agents were introduced during the direct exchange procedure.

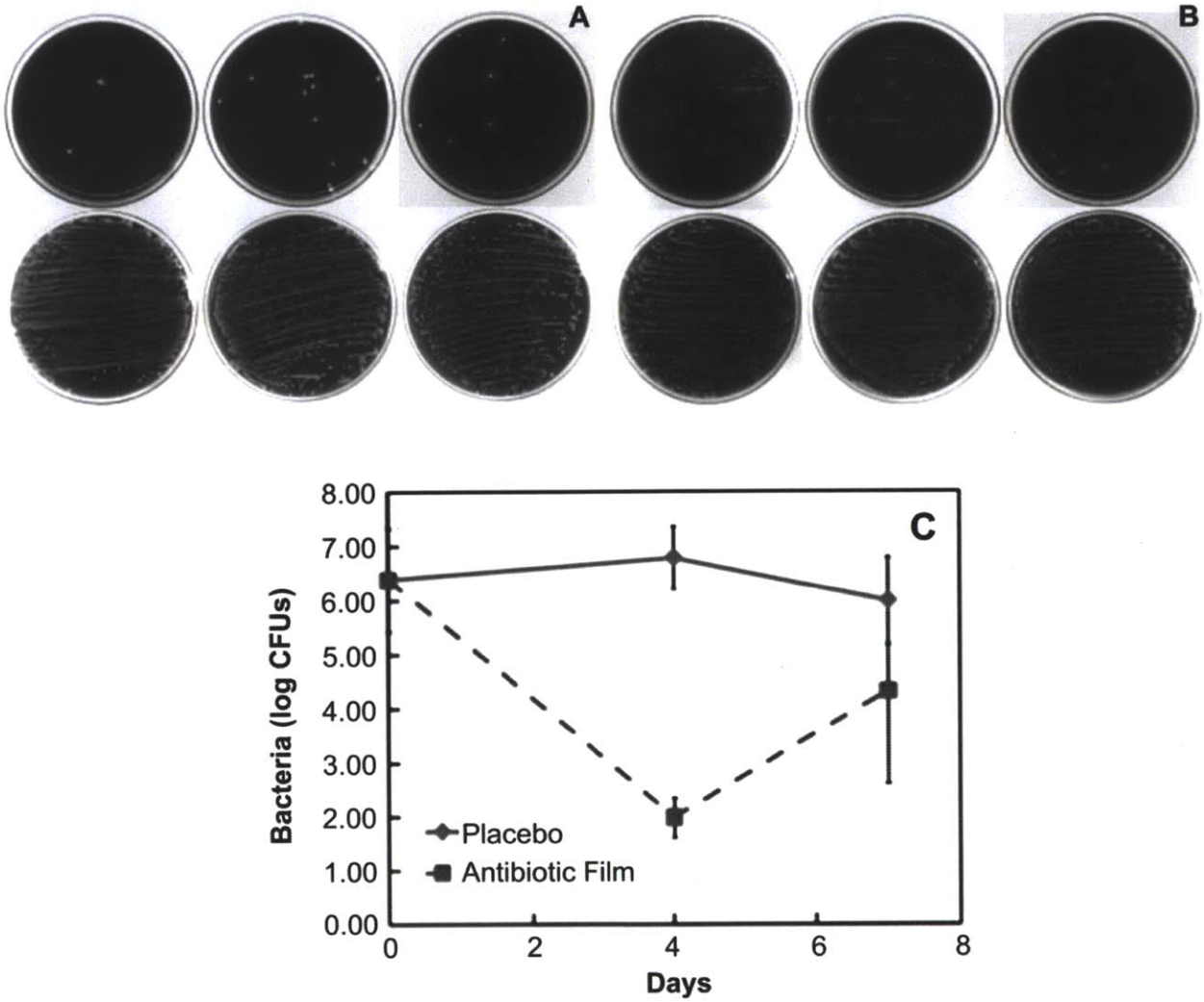

Figure 5-5. (A) Blood agar plates of explanted titanium rods that were rolled down the center of the plate and streaked for qualitative analysis of device surface colonization. Each plate corresponds to one rabbit. Each white dot corresponds to a single CFU. Explants from the four day treatment group (top row) are compared to explants from the four day placebo group (bottom row). None of the sterile plates are depicted. (B) Explants from the seven day treatment group (top row) are compared to explants from the seven day placebo group (bottom row). (C) Final counts (Mean ± SD) of log-transformed Staphylococcus aureus CFU data in femoral condyles at day zero and after direct exchange. Raw data are available in Table 5-1. Raw CFU Data from Bone Homogenates.*

Table 5-1. Raw CFU Data from Bone Homogenates.*

Day 0	Day 4		Day 7	
-	Placebo	Treatment	Placebo	Treatment
(n = 6)	(n = 6)	(n = 6)	(n = 7)	(n = 8)
69316	965890	<100	37974	<100
619909	1640307	<100	351712	<100
2726860	5968565	<100	395446	48782
4357991	13320000	107	1883778	51988
18073728	17418853	246	2305662	51994
22406365	24410566	285	5714794	153463
-	-	-	6722259	351552
-	-	-	-	1899258

* **Each value corresponds to total femoral colonization of one animal. The randomized data are reorganized in increasing value. The values were determined by dividing the CFU/mL of the serial diluted homogenates by the bone concentration (g/mL) and then multiplying by the total bone mass (g). Undetectable CFU values were assumed to be half the detection limit (i.e. 5 CFU/mL) and are labeled here as <100.**

The increase in variance and magnitude of infection for the treatment group between days four and seven, however, was significant (F-test, $p < 0.005$ and t-test, $p < 0.01$). The increase in variance can be attributed to the fact that unsaturated bacteria populations tend to have non-steady state behavior. Specifically, they will either continue to propagate until all available resources are utilized, or be killed off in the presence of bactericidal agents until the population is eradicated. This behavior is evident in MIC assays since the wells of the microtiter culture plate are either turbid or clear, depending on the antibiotic concentration used in each well. In the case of the rabbits, six of the eight subjects in the treatment group were not completely eradicated of bacteria at day seven. If the rate of bacteria propagation exceeds the rate of drug treatment, then the animal would not be cured and eventually endure bacterial infection similar to those of the placebo group. Since the *in vitro* elution profile of these LbL films yields a monotonically decreasing drug release rate, and since the bolus release phase has already passed by day four, it is unclear whether the release rate of the remaining drug in the uneroded film would be sufficient to clear these six animals of infection at later time points. Regardless, the final CFU counts at equilibrium would be either near zero or on the order of 10^6 (according to the infection model), which is the reason for the observed difference in variances. The

increase in magnitude of infection at day seven could have further been a result of a potential re-seeding issue due to the growing subcutaneous infection adjacent to the defect site. Antibiotic resistance of the bacteria from the seven day treatment group has been ruled out after testing their susceptibility to gentamicin (Figure 5-6).

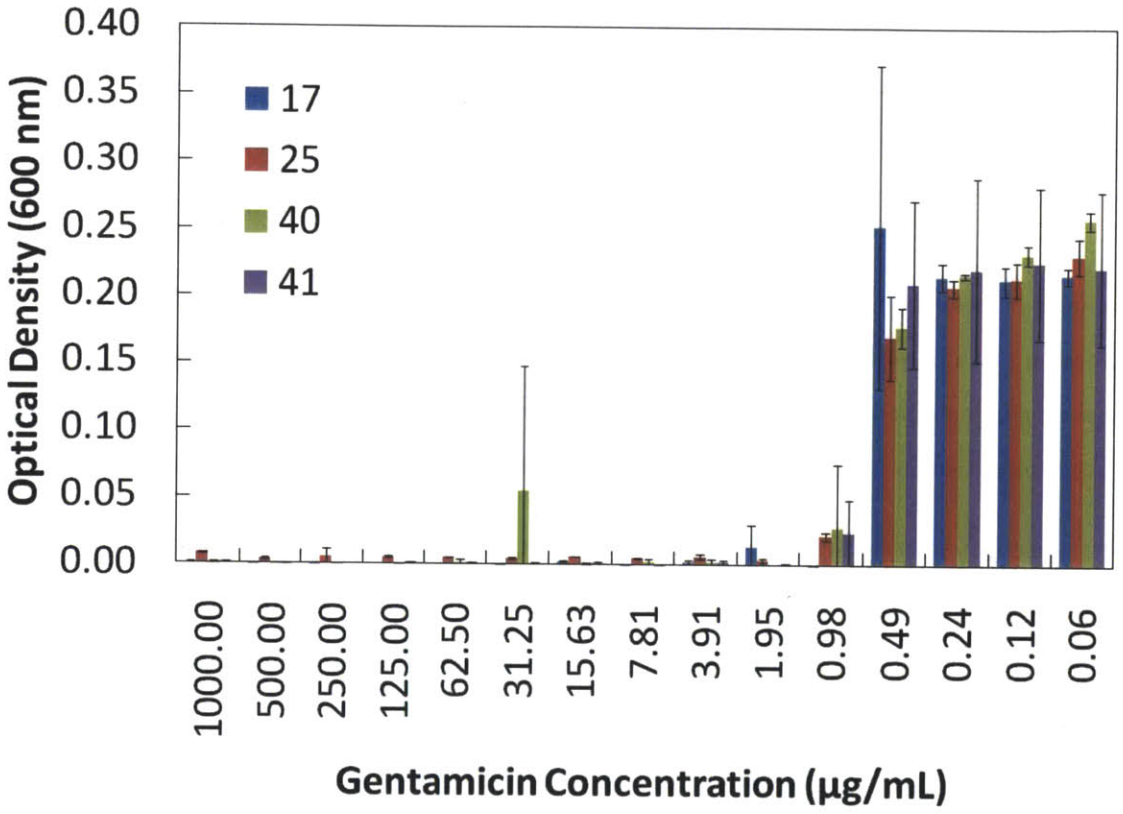

Figure 5-6. Antibiotic susceptibility of bacteria recovered from four of the six infected rabbits in the seven day treatment group. Each number (17, 25, 40, 41) corresponds to one animal. Data represent mean ± standard deviation of triplicate measurements per sample.

5.3.3 Local Gentamicin Quantification

Both serum and the supernatants of centrifuged bone homogenates were sent to Cornell University's College of Veterinary Medicine for gentamicin quantification by fluorescence polarization immunoassay (FPIA). As expected, there was no detectable amount of gentamicin in any serum or placebo homogenate sample that was analyzed in this study (detection limit = 0.27 µg/mL). The four day treatment group had 60.5 ± 34.9 µg GS (maximum 83.2 µg, minimum 18.4 µg, n = 6) remaining in the condylar region of the femur after removal of the

coated device. The seven day treatment group had one animal with significantly higher GS quantity than the other seven animals (i.e. 259.1 μg), which was likely due to residual film that detached from the titanium implant surface upon extraction and therefore remained in the defect site after implant removal. After omitting this outlier data point from further analysis, the seven day treatment group had 23.4 ± 15.8 μg GS (maximum 57.9 μg, minimum 12.1 μg, n = 7). Since it was not clear whether the GS would be efficiently flushed away from the surgical site on the timescale of one week, a two-tailed t-test was conducted to compare the means of the four- and seven-day treatment groups. The significant decrease ($p < 0.05$) in GS quantity at seven days in comparison to four days implies that the rate of uptake of drug by the body exceeded the rate of elution by the LbL coatings over these three days. This result is important in light of the *in vitro* cytotoxicity assays, which determined that without sufficiently fast pharmacokinetics, gentamicin concentrations could potentially reach locally toxic levels. As expected, this was not the case for the *in vivo* study; however, the homogenized GS quantities at both four and seven days after implantation do continue to exceed the MIC of GS against *S. aureus* (i.e. 0.1 μg/mL) (assuming that the condylar region of a single rabbit femur has a volume on the order of milliliters).

Following the results of the *in vitro* release profile, it was expected that the initial differences in CFU counts between each test group at day four since this corresponds to the conclusion of the burst release phase. Under the condition of complete eradication, the day seven comparison should have expanded these differences. However, under the condition of incomplete eradication (as is the case in some of the animals in this study), the bacteria were able to re-propagate under the diminishing antibiotic release rate of the LbL films and re-establish gross infection. The bone infection model was designed to present a major bacteria challenge with a 100% infection rate [158], and address this infection solely with the use of the antibiotic films. In a real revision operation of an infected implant site, the role of systemic antibiotics and defect management are tremendously important. The current standard of care for patients undergoing orthopedic surgery requires receipt of a preoperative systemic dose of a cephalosporin antibiotic, which is capable of diffusing out of capillary beds to assist with infection control [184]. Additionally it is well known that adequate surgical debridement and

cleaning of a previously infected defect site before insertion of a new implant are the single most important practices in infection control [21, 185]. In practice, the irrigation procedure generally involves a high pressure rinse of soap or antibiotic solution [177, 186] to help forcibly remove any sessile infectious microorganisms. Although the current bone infection model omits the use of these practices, investigation of follow-up times greater than one week may benefit from co-delivery of systemic cefazolin [184], and cleaning of the defect site (e.g. with hydrogen-peroxide and povidone-iodine solutions) [164] while being careful to account for proper controls. Under this revised procedure, the bacterial burden placed on the LbL films would be reduced and the seven day treatment group may have yielded a greater rate of eradication.

5.3.4 Limitations to the Study

The results presented here have achieved the primary aim of this study, which was to generate proof-of-principle data that support a reasonable measure of efficacy of an antibiotic eluting LbL system *in vivo*. There are a few key limitations to the present study. Histological and micro-computer tomographical analyses, which would yield additional information on bone healing and local host responses to the bacterial infection and antibiotic coatings, were not conducted, and dose response was not examined in this study. Although they were deemed beyond the scope of this study, these experiments will be necessary when assessing long-term viability of this approach. As noted above, the bacterial challenge was high and the one-stage re-implantation did not involve any systemic antibiotics or cleaning of the infected bone defect as would be done in an actual clinical case. Nonetheless, it was demonstrated that remediation of bone infection takes place over the course of days. Future work that addresses multi-component release or aims to treat an existing infection in a larger animal model with human sized implants can use an infection model that employs a smaller inoculum challenge or supplements the treatment with systemic antibiotics and proper debridement, to better represent a more realistic clinical situation.

The most immediate issue witih the [Poly 1/PAA/GS/PAA]$_n$ LbL architecture that should be addressed is its mechanical integrity. PAA is a polymer with a T_g well above room

temperature rendering it brittle in the dry state. Therefore these films are relatively fragile and must be handled with care in order to avoid shattering; however, brief hydration via a rapid dip cycle in sterile water (i.e. less than 1 second) allows the films to hydrate and become more hydrogel-like, which permits easy insertion into the defect site. The implications of this problem are that scale-up, transportation, and handling could present unnecessary difficulties. This opens an avenue of future work directed at gathering mechanical data as a result of substituting various ratios of PAA for a more pliable biocompatible polyanion.

5.4 *Conclusions*

The sequence of developing a technology, determining its *in vitro* performance, developing an *in vivo* model, and demonstrating *in vivo* efficacy is an iterative process. Specifically, this study describes the performance of only one film architecture in one experimental model, and now given this information, it is possible to re-design both the films and the model. The results described here are favorable and have achieved the aim of the study. The erodible LbL film did indeed release enough active antibiotic into the locally infected site to yield statistically significant treatment when compared to the placebo. However, It is also clear from the study that improvements can be made to both the film architecture and the model. Although the data at four days were quite favorable, there appeared to be a rebound in the infection at seven days. The film architecture design of 803 layers was a best-guess for the first past at this experiment, and the choice to omit systemic antibiotics and significant debridement and lavage of the defect site was due to the concern of achieving sterility that could not be attributed to the antibiotic films with certainty. The burst release phase of the drug is most important at eradicating infection, and the prolonged release is primarily used for prevention. The burst release can be enhanced by increasing the concentration of drug and dip time for the final deposition step. In a 2.0 version of the study, it would be advantageous to increase the quantity of nonspecifically bound drug in the coating during the final deposition step, especially if no changes are made to the animal model. Furthermore, the use of an *in vivo* model requiring intravenous antibiotics and greater maintenance of the defect site would provide a cleaner interface to test the films, hence allowing observation at much later time points. In

hindsight, incorporation of these ideas into the experimental plan would minimize the possibility of infection rebound.

Chapter 6 Dual Functional Bactericidal Coatings

Work done in this chapter was done jointly with Jessie Wong. A corresponding manuscript entitled "Dual Functional Polyelectrolyte Multilayer Coatings for Implants: Permanent Microbicidal Base with Controlled Release of Therapeutic Agents" by Sze Yinn Wong, Joshua S. Moskowitz, Jovana Veselinovica, Ryan A. Rosario, Ksenia Timachova, Michael R. Blaisse, Renée C. Smith, Alexander M. Klibanov, Paula T. Hammond has been reproduced in part with permission from *JACS*, vol. 132, pp. 17840-8, 2010. Copyright 2010 American Chemical Society.

6.1 *Introduction*

Recently, there has been great interest in developing drug-device combinations to address various medical applications [5, 187]. Examples include cardiovascular prostheses [5, 188], orthopedic implants [82, 150], stents [189], biosensors [190], and electrical leads [191]. The two primary causes of implant failures are adverse foreign body response and implant-related infection, each which could benefit from such combination therapies. Focusing on the latter, implant failure due to device-associated infection adds up to approximately 1 million cases annually [192]. Of these, catheter-associated urinary tract infection represents the most prevalent example accounting for about 40% of all nosocomial infections [193], and orthopedic implant-related infections including both joint prostheses and fracture fixation devices represent the most costly example ringing up close to $2 billion (USA) in annual treatment expenditures despite their lower infection rate [192]. Regardless of the implant type, the basic pathogenic mechanism for infection is that of bacterial colonization of the device surface, which can lead to the development of a biofilm. A biofilm is a matrix of sessile bacteria consisting of about 15% bacterial cells by mass and 85% hydrophobic exopolysaccharide fiber matrix [194]. Biofilms can damage surrounding tissues and give rise to planktonic bacteria cells that spread infection. The biofilm environment prevents the bacteria from being easily targeted by normal therapeutic levels of antibiotics [159, 160]. Current engineering approaches to biofilm control include the use of drug-device combinations that elute high concentrations of antibiotics locally in an effort to eradicate planktonic bacteria before biofilm formation, and the use of ultrasonic energy [195] or weak DC field [196] to disrupt an existing biofilm hence

making it more susceptible to standard treatment. As the persisting search for biofilm-resistant materials continues, the release of local antibiotics from implant surfaces remains the most common strategy for prevention; however, the standard release kinetics of many antibiotic-releasing systems is problematic. Generally, the initial burst-release phase is efficacious in achieving eradication; however, this is often followed by a monotonically decreasing rate of elution that eventually exposes any existing bacteria to sub-lethal concentrations of antibiotic, hence allowing the development of resistant strains. In theory, having a permanent microbicidal surface coating that does not lose its functionality would prevent bacterial attachment thus preventing biofilm formation.

Polyelectrolyte multilayer films have been studied extensively for applications in drug delivery since the assembly process can be conducted at pH and temperature conditions that are gentle to biological molecules such as antibiotics, growth factors, and painkillers [53, 63, 65]. PEM films can be easily incorporated onto the surfaces of implants to provide controlled and localized drug delivery of these therapeutic agents. In this work, films are constructed using the layer-by-layer deposition technique [44], in which oppositely charged species (polymers, molecules, nanoparticles, etc.) are adsorbed sequentially onto an initially charged substrate. PEM films are additionally attractive because of their simple and economical fabrication process. They can be built on most geometries with nanometer scale control over thickness and surface properties [52, 112]. Consequently, the amount of material loaded is highly tunable, which is a very attractive characteristic for drug delivery because many treatment regimens overload the body with drug in hope that a small amount of drug will actually be delivered to a specific area of the body. Owing to its versatility, LbL technology has been already been applied to a broad range of fields including drug delivery [53, 63, 65, 81, 83, 197], membranes and electrodes for energy applications [198, 199], and electro- or magneto-responsive surfaces [200, 201], and remains an attractive candidate for implant coatings.

In this chapter, a bifunctional platform made of a permanent microbicidal PEM thin film combined with a hydrolytically degradable PEM film that releases an antibiotic is presented. This dual-functional combination film would maintain the benefits of conventional drug-releasing systems while adding the significant advantage of long-term biofilm prevention. The

proposed construct in this work could find a promising future as next-generation surface coating for implants.

6.2 *Experimental*

6.2.1 Materials

Poly(2-ethyl-2-oxazoline) (Mw of 500 kDa), 1-bromododecane, iodomethane, tert-amyl alcohol, poly(acrylic acid) (PAA; Mn = 239 kDa), poly(sodium 4-styrenesulfonate) (SPS; Mw = 70 kDa), 3 M concentrated sodium acetate buffer (NaOAc; pH 5.2), 1,4-butanediol diacrylate, and other solvents and common buffers were purchased from Sigma-Aldrich (St. Louis, MO). PAA (Mw = 50 kDa) and linear poly(ethylenimine) (LPEI; Mn = 25 kDa) were purchased from Polysciences (Warrington, PA). 4,4-trimethylenedipiperidine was acquired from Alfa Aesar (Ward Hill, MA). Gentamicin sulfate (GS) and phosphate-buffered saline (PBS; pH 7.4, 137 mM NaCl, 2.7 mM KCl, 10 mM Na2HPO4) were purchased from Mediatech, Inc. (Herndon, VA). Tritium-labeled gentamicin (^{3}H-GS; 250 μCi total, 1 mCi/mL in ethanol, 200 μCi/mg) was obtained from American Radiolabeled Chemicals, Inc. Silicon wafers (test grade n-type) were procured from Silicon Quest (Santa Clara, CA). Cation-adjusted Mueller Hinton Broth II (CMHB) and BactoAgar were obtained from Difco BD (Franklin Lakes, NJ). Alpha minimum essential medium (α-MEM), fetal bovine serum (FBS), penicillin/streptomycin solution, fluorescein conjugated albumin from bovine serum (BSA) , MTT (tetrazolium [3-(4,5-dimethylthiazol-2-yl)-2,5-diphenyltetrazolium bromide) assay kit, and Live/Dead Viability/Cytotoxicity kit for mammalian cells were all purchased from Invitrogen (Carlsbad, CA). All reagents were used without further purification.

MC3T3-E1 murine preosteoblasts, *Staphylococcus aureus* 25923, and *Staphylococcus aureus* 33592 with gentamicin resistance were all retrieved from ATCC (Manassas, VA).

6.2.2 Synthesis of Polymers

Poly(β-amino ester) Poly 1 was synthesized as previously described [78]. Briefly, a solution of 4,4-trimethylenedipiperidine (34.1 mmol) in 50 mL anhydrous tetrahydrofuran (THF) was added to the diacrylate monomer (34.1 mmol) dissolved in an equal volume of anhydrous THF. The reaction mixture was purged with nitrogen and stirred for 48 hours at 50°C. Afterwards, the

reaction mixture was cooled to room temperature and precipitated into cold hexanes. Polymers were collected via filtration.

Linear N,N-dodecyl-methyl-LPEI (DMLPEI; Figure 6-1) was synhesized as previously described [202]. In short, LPEI (Mw of 217 kDa) was produced in house by deacylation of 500 kDa poly(2-ethyl-2-oxazoline) [203]; the product was dissolved in water, precipitated with aqueous potassium hydroxide, filtered, and washed repeatedly with water. The resulting deprotonated LPEI was alkylated first with 1-bromododecane (96 h at 95 °C) and then with iodomethane (24 h at 60 °C) to produce the end product DMLPEI. Polymers were collected and dried under vacuum prior to NMR.

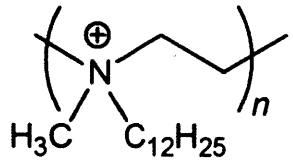

Figure 6-1. Structure of DMLPEI (compliments of Jessie Wong).

6.2.3 Preparation of Polyelectrolyte Solutions

Solutions of Poly1, GS, and PAA were prepared at 2 mg/mL in 0.1 M NaOAc. Dipping solution of DMLPEI was prepared at 1 mg/mL in 1-butanol. Poly1, GS, and PAA solutions were pH adjusted to 5.0. For films used in GS release experiments, the GS solution was spiked with 5 µL ^{3}H-GS per 50 mL dipping solution yielding a 0.1 µCi/mL product without significantly changing the concentration of the GS dip bath. LPEI and PSS dipping solutions were prepared at 2 mg/mL in water and pH adjusted to 4.25 and 4.75 respectively with 1 M sodium hydroxide and 1 M hydrochloric acid. All solutions were prepared with water from a Milli-Q Plus (Bedford, MA) at 18.2 MΩ.

6.2.4 LbL Film Assembly

Films were assembled as previously described [108]; briefly, LbL films were assembled on silicon substrates using a programmable Carl Zeiss HMS slide stainer. Substrates were cleaned with methanol and ultra pure water, dried under nitrogen, and plasma-etched in oxygen using a Harrick PDC-32 G plasma cleaner on high radiofrequency for 1 min and then immediately

immersed into the first polycation solution (i.e. DMLPEI or LPEI depending on the experiment) for at least 10 min. Samples were either prepared with nondegradable bilayers of the bactericidal DMLPEI/PAA or the non-bactericidal LPEI/PSS. For the former, a cascade rinse cycle of three 1-butanol rinse baths (1 min, 30 s, 30s) followed by three water baths (1 min, 30 s, 30 s) was used after deposition of DMLPEI, and the reverse cycle of water then 1-butanol after PAA. For the latter, a cascade rinse cycle of three water baths (10 s, 20 s, and 30 s) was used after each polyelectrolyte dipping.

For the combination films, (Poly 1/PAA)$_5$ was first deposited onto (DMLPEI/PAA)$_{10}$ in order to facilitate uniform buildup of subsequent GS-containing films. Then deposition of the tetralayer architecture (Poly1/PAA/GS/PAA)$_n$ was performed as previously described [197]. Films with (DMLPEI/PAA)$_{10}$(Poly1/PAA)$_5$(Poly1/PAA/GS/PAA)$_{20}$ were used for drug release and film degradation studies. Characterization of the growth of (Poly1/PAA/GS/PAA)$_n$ films on top of (DMLPEI/PAA)$_{10}$(Poly1/PAA)$_5$ films, was done with n = 5, 10, 15, 20 and 30 (Figure 6-2). As a control in the efficacy studies comparing films with the bactericidal base layer functionality (i.e. (DMLPEI/PAA)$_{10}$) to those without bactericidal functionality, the architecture (LPEI/PSS)$_{10}$(Poly1/PAA/GS/PAA)$_{20}$ was used.

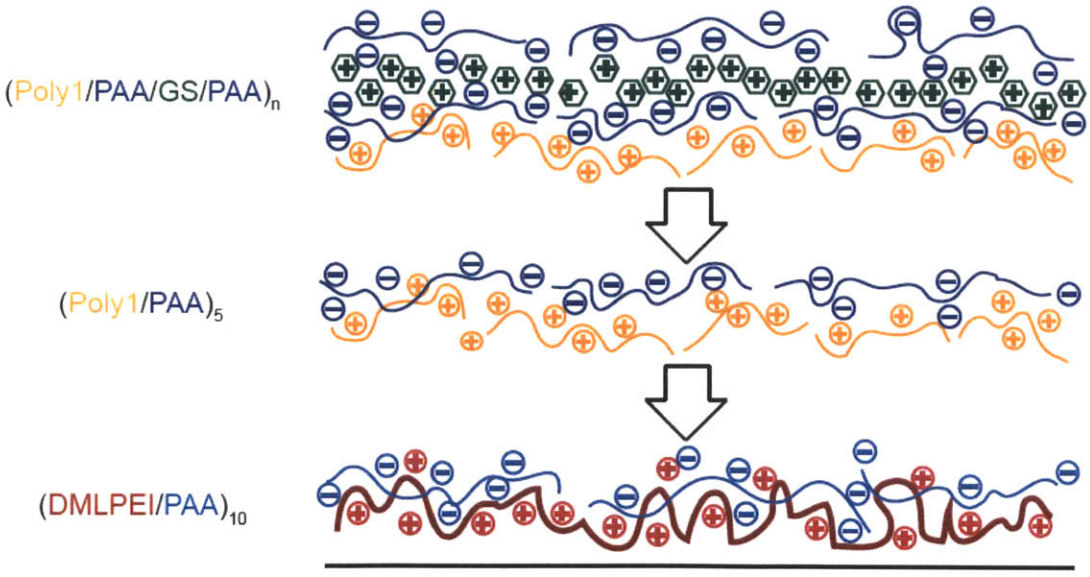

Figure 6-2. Schematic of the combination film with the permanent bactericidal base film deposited first, the erodible adhesion film deposited second, and the erodible GS-eluting film deposited on top (courtesy of Ksenia Timachova).

6.2.5 Characterization of Film Growth, Erosion, and Release

After film deposition, all films were allowed to air dry. For film growth, thicknesses of the $(DMLPEI/PAA)_{10}$ films were measured using a spectroscopic ellipsometer (Woollam M-2000D). All thickness measurements were made at five different points on each film and averaged over three separate films. Roughness measurements of films were generated using a surface profilometer (KLA Tencor P-16). Thickness measurements of films were verified using the surface profilometer. In the case of $(DMLPEI/PAA)_{10}(Poly1/PAA)_5(Poly1/PAA/GS/PAA)_n$ combination films, both thickness and roughness measurements were performed by profilometry at four predetermined locations per film using a Veeco Dektak 150 surface profiler and averaged over three separate films.

For degradation studies, samples were immersed into 10 mL of PBS in a tightly capped Falcon tube maintained at 37°C. At each time point, films were removed from the PBS, allowed to air-dry and measured. All dry state thicknesses were determined via profilometry at four locations and averaged over at least three films.

For GS release experiments, samples were immersed into 20 mL of PBS in a tightly capped Falcon tube maintained at 37°C. Degradation environments were kept sealed from the ambient to minimize evaporative loss. A 1 mL sample was extracted from the Falcon tube at each predetermined time point and mixed with 5 mL ScintiSafe Plus 50% (Fisher Scientific, Atlanta, GA) prior to GS quantification. The resulting mixtures were analyzed using a Tricarb Model 2810 TR liquid scintillation counter (Perkin Elmer, Waltham, MA). The raw data in disintegrations per minute (DPM) was converted directly to μg of drug using the DPM value for the dipping solution (2 mg/mL). Total release from the film at the *i*th timepoint was calculated by the following equation:

(6-1) $$m_i = (C_i V_i) + (1\ \text{mL}) \sum_{j=1}^{i-1} C_j$$

where m_i (μg) is the the total cumulative mass of GS released from the film at the time of measurement i, C_i (μg/mL) is the concentration of sample i (which is multiplied by the total volume V_i remaining in the Falcon tube as of the ith measurement), and the summation term adds up the total extensive quantity of gentamicin removed in each of the i-1 former aliquots.

6.2.6 Bactericidal Activity of Films

Two assays were used in these studies, a mediaborne assay and a Kirby Bauer assay, each as previously described [53, 108]. All experiments were conducted in triplicate. Briefly, for the mediaborne assay, *S. aureus* 25923 with no gentamicin resistance was grown up overnight at 37°C in CMHB. The culture was then centrifuged at 2,700 rpm for 10 min, washed, re-suspended in fresh CMHB media, and diluted to 10^6 cells/mL. Film-coated substrates were compared to blank Si controls by incubating with the bacterial broth at room temperature for various durations: 15 min, 30 min, 1 h and 2 h promoting bacteria adhesion onto the surface. A separate two-week experiment was done where every three days, the solution in each Petri dish was refilled with 2 mL of fresh CMHB media to replace fluid loss due to evaporation in the incubator, and to provide fresh nutrient for the bacteria to thrive. After the two weeks, each sample was removed and rinsed three times with fresh medium to remove any nonspecifically bound bacteria from the surface. Each sample was then incubated overnight at 37°C under a slab of agar imaged the following day.

To determine if protein adsorption would compromise the microbicidal activity of $(DMLPEI/PAA)_{10}$ films, films and blank silicon substrates were incubated in 100 □g/mL fluorescein conjugated albumin solution at 37°C for 1 h. Films were then removed, rinsed thrice in fresh PBS, and imaged via fluorescent microscopy. These samples were further tested with the mediaborne assay using the 2 h incubation time.

For the Kirby-Bauer assay, *S. aureus* was grown overnight at 37°C in CMHB and re-inoculated the following day; agar plates were streaked with the exponentially growing *S. aureus* at 10^8 cells/mL. Tests compared blank silicon, contact killing $(DMLPEI/PAA)_{10}$, release-killing $(LPEI/PSS)_{10}(Poly1/PAA/GS/PAA)_{20}$, and dual functional $(DMLPEI/PAA)_{10}(Poly1/PAA)_5$ $(Poly1/PAA/GS/PAA)_{20}$ after increasing degradation times of $(Poly1/PAA/GS/PAA)_{20}$. Zones of

inhibition (ZOI) were imaged. To further distinguish the unique functionality of the nondegradable, contact-killing $(DMLPEI/PAA)_{10}$ surface, a GS-resistant strain of *S. aureus* (33592) was used to perform a separate Kirby-Bauer assay.

6.2.7 In Vitro Cytotoxicity: Adhesion and Proliferation of Cells

Films were tested with murine pre-osteoblast cells (MC3T3-E1) which were seeded on $(DMLPEI/PAA)_{10}$ and compared to uncoated glass slides. Cells were grown in α-MEM supplemented with 10% FBS and 1% penicillin/streptomycin at 37°C with 5% CO_2. Substrates were placed in the bottom of 6-well plates and each well seeded with 150,000 cells and 3 mL of media. To investigate cell adhesion to the surface of the films, two sets of experiments were performed in parallel: cells in media with FBS and without FBS. Cells were cultured for 6 h on substrates and cell adhesion investigated by examining morphology (via light microscopy); for metabolic activity (via MTT assay), cells were cultured on samples for 3 h in normal growth media, and 3 h in growth media containing 10% MTT. Substrates were transferred to new 6-well plates to quantify only those cells which were adherent to the substrate. 1 mL of dimethyl sulfoxide was added to solubilize the resulting purple formazan crystals. 100 μL aliquots from each sample were placed into a 96-well microtiter plate and absorbance measured at 570 nm with a 690 nm correction. All samples were measure in triplicate. Cell metabolic activity was calculated relative to the negative control (uncoated glass slide). Proliferation experiments requiring the same experimental procedure were conducted on the same set of films at days 1, 3, and 7 in FBS-enriched media.

6.2.8 Sample Sizes and Data

Sample sizes are indicated in figure captions. Data are presented as mean ± standard deviation unless otherwise specified.

6.3 *Results and Discussion*

6.3.1 Design of Combination Films with Dual Functionality

The primary aim of this study was to design a combination film that could exhibit adaptable dual functionality with a permanent microbicidal base film, $(DMLPEI/PAA)_{10}$, and a hydrolytically degradable top film made with cationic poly(β-amino ester) Poly1 that is capable of incorporating and releasing drugs. In this work, this concept was demonstrated using a model system with the small, hydrophilic antibiotic gentamicin as the example therapeutic to eradicate infection at an implant site before unveiling a biofilm-resistant surface. The permanent microbicidal base film was built up via electrostatic interaction between a positively charged, hydrophobic polymer DMLPEI (a quaternary ammonium salt), and PAA as the polyanion. Previous work has shown that the microbicidal property of DMLPEI can be maximized in a nanometer-scale LbL film by the choice of polyanion, assembly conditions, and post-processing techniques [108].

Poly(β-amino ester)s are a class of polycations that have different hydrolytic degradation rates at physiological condition (37°C, pH 7.4) depending on the particular polymer used [78, 79]. As a result of hydrolytic cleavage of the ester bonds, these polymers have been successfully incorporated into PEM films as an erodible component for controlled release [53, 63, 65, 79, 83, 108, 197]. In this work, the use of Poly 1 is advantageous as it allows tunability of the bolus release of gentamicin and thus can help eradicate an existing infection. The need for long term release of gentamicin is reduced due to the presence of the underlying microbicidal permanent film.

6.3.2 Characterization of Combination Films: Growth, Erosion, and Release

The thickness and roughness of the microbicidal base film $(DMLPEI/PAA)_{10}$—26.4 ± 4.5 nm and 6.8 ± 3.9 nm, respectively—were measured before buildup of the erodible $(Poly1/PAA)5(Poly1/PAA/GS/PAA)_n$ films. Ten bilayers was used in the base film to achieve 100% microbicidal activity and provide a uniform platform for buildup of the subsequent drug releasing layers. $(DMLPEI/PAA)_n$ films had previously been shown to exhibit an initial lag

growth phase where only beyond 4.5 bilayers did the film start growing linearly with complete surface coverage [108]. The thickness and roughness of the combination film $(DMLPEI/PAA)_{10}(Poly1/PAA)_5(Poly1/PAA/GS/PAA)_n$ was then measured and the growth curve depicted in Figure 6-3. The $(Poly1/PAA)_5$ adhesion layer was deposited after the microbicidal base film to help initiate and facilitate uniform deposition of the $(Poly1/PAA/GS/PAA)_n$ film. The $(Poly1/PAA)_5$ adhesion layers increased the total thickness and roughness of the growing film to 75 ± 18 nm and 30 ± 13 nm, respectively. Without the intermediary layers of $(Poly1/PAA)_5$, there was no film growth of $(Poly1/PAA/GS/PAA)_n$ directly on top of $(DMLPEI/PAA)_{10}$. We hypothesized that the hydrophobic nature of the highly interpenetrated $(DMLPEI/PAA)_{10}$ film surface (water contact angle of 85° ± 2°) reduced the ability of the hydrophilic GS molecules to wet and adsorb onto the surface. Adding the buffer layers provided a more hydrophilic surface and reservoir (water contact angle of 67° ± 3°) for the small, diffusive GS molecules to establish themselves within the film. The GS-film exhibited linear growth with micron-scale thickness (average of 0.50 ± 0.05 μm per tetralayer). The large roughness of the $(DMLPEI/PAA)_{10}(Poly1/PAA)_5(Poly1/PAA/GS/PAA)_n$ was a likely result of significant interdiffusion within the film architecture, as well as both film dissolution and diffusive losses that occur during the deposition process. The film thickness increased faster than the surface roughness during film growth leading to increasingly smoother films (relative to the total thickness) at greater tetralayer numbers.

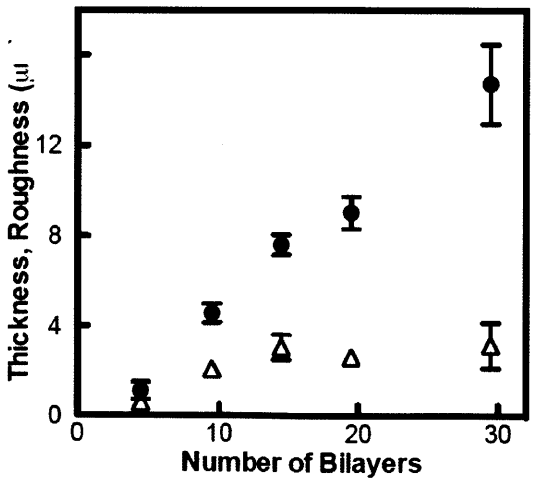

Figure 6-3. Growth curve and roughness of $(Poly\ 1/PAA/GS/PAA)_n$ on top of $(DMLPEI/PAA)_{10}(Poly\ 1/PAA)_5$. Data represent the mean ± standard deviation of triplicate samples.

Degradation of GS-releasing films was linear and complete erosion of films occurred on the order of hours (Figure 6-4, left). Release studies were performed with the same film architectures that were used in the degradation experiments. One of the major advantages of LbL systems is that the quantity of drug incorporated into each film can be tuned according to the total number of deposited layers thus making the LbL technology platform a versatile way to address different applications and drug delivery specifications. The 20 tetralayer GS-releasing films incorporated about 70 $\mu g/cm^2$ of the antibiotic and released over period of 6 hours, with approximately 90% delivery during the first 2.5 hours (Figure 6-4, right); this burst release of antibiotic is critical to control an existing gross infection at an implant site, and hopefully prevent re-propagation. It should be noted that the underlying $(DMLPEI/PAA)_{10}(Poly1/PAA)_5$ film, without the topmost $(Poly1/PAA/GS/PAA)_{20}$ film, can load 6.3 ± 0.8 $\mu g/cm^2$ of gentamicin suggesting that these molecules are able to diffuse through the underlying layers of permanent film. As for the biofilm issue, it is important to minimize the prolonged release of sub-lethal concentrations of GS as this can lead to increased likelihood of the bacteria developing antibiotic resistance, which can make future treatment significantly more problematic; hence, the bactericidal base film provides an attractive alternative to sustained delivery.

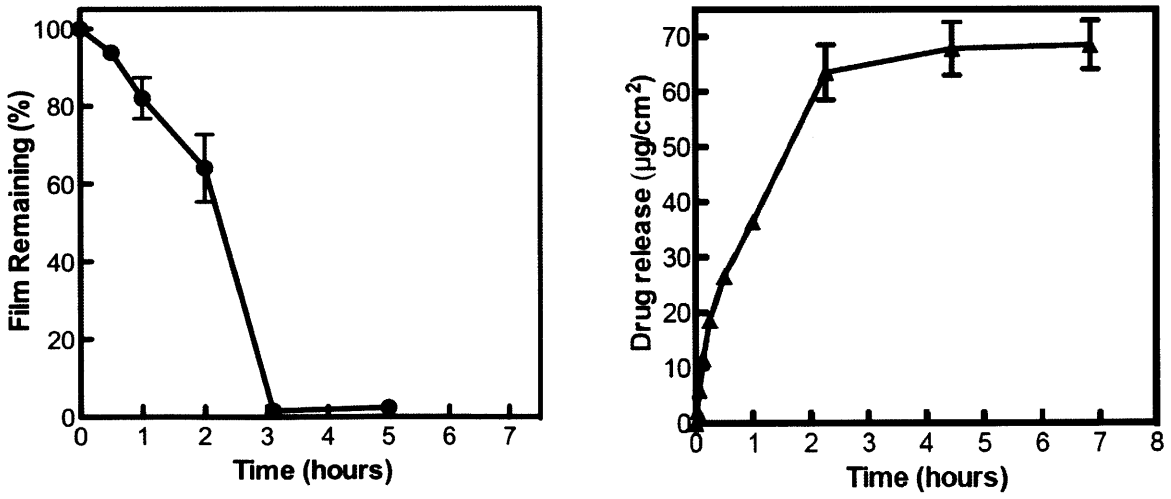

Figure 6-4. Degradation profile (left) and GS-release profile (right) of combination films. Data represent the mean ± standard deviation of triplicate samples.

6.3.3 Bactericidal Activity

Activity of GS released from $(DMLPEI/PAA)_{10}(Poly1/PAA)_5(Poly1/PAA/GS/PAA)_{20}$ combination films was tested via Kirby-Bauer assays and compared to a control of $(LPEI/PSS)_{10}(Poly1/PAA/GS/PAA)_{20}$ (Figure 6-5). Zones of inhibition (ZOIs) developed around 0 min, 15 min and 2 day samples. Each time corresponds to the duration for which the sample was immersed in phosphate buffered saline (PBS) at 37°C. Since the microbicidal base film only kills bacteria directly in contact with it, the ZOIs around the erodible GS films directly indicated that the GS was indeed released from the films and confirmed that it was still active. The smaller ZOIs associated with the 2 day sample in comparison to the 0 min and 15 min samples are reminiscent of a depleting source. Furthermore, the comparatively thicker base of $(DMLPEI/PAA)_{10}(Poly\ 1/PAA)_5$ yields a sample with slightly larger ZOI than its $(LPEI/SPS)_{10}$ counterpart after 2 days of erosion. In the case of the former, the larger reservoir for gentamicin sulfate (harboring 6.3 ± 0.8 μg/cm^2) likely contributes to this effect.

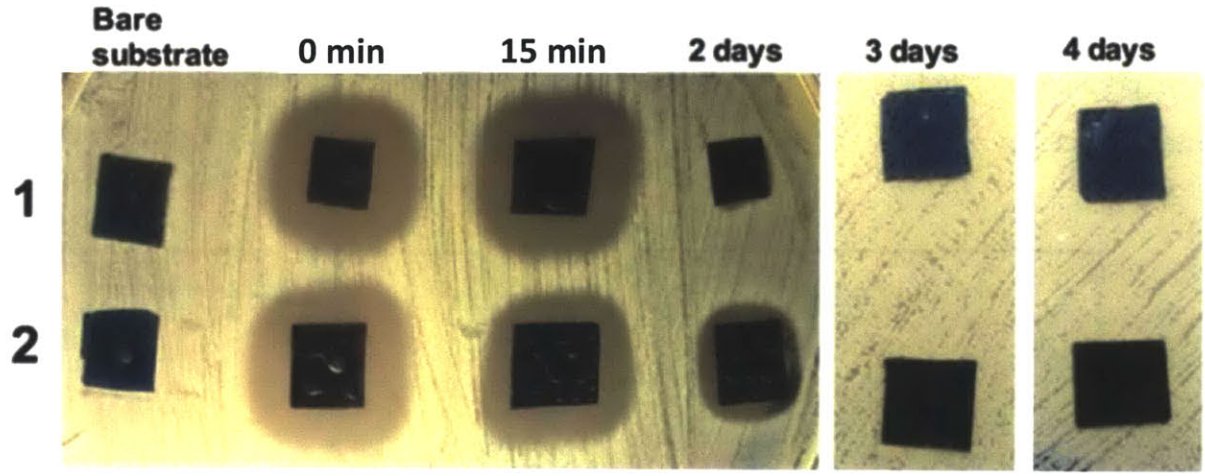

Figure 6-5. Kirby Bauer assays of GS-releasing films eroded for increasing amounts of time in PBS at 37°C. Row 1 shows $(LPEI/SPS)_{10}(Poly\ 1/PAA/GS/PAA)_{20}$ and row 2 shows $(DMLPEI/PAA)_{10}(Poly\ 1/PAA)_5(Poly\ 1/PAA/GS/PAA)_{20}$. All samples were tested with GS-susceptible *S. aureus* except for the 4-day samples. This figure was reproducible over three replications (data not shown) and was produced in collaboration with Jessie Wong.

After the hydrolytically degradable top films had completely eroded, it was important to demonstrate that the newly exposed microbicidal $(DMLPEI/PAA)_{10}$ base films were still efficacious against *S. aureus*. Figure 6-5 reveals that the 3 day samples with the microbicidal

base film show 100% direct contact killing of *S. aureus* whereas films with the standard base film of $(LPEI/SPS)_{10}$ did not show any measurable efficacy relative to the uncoated silicon substrates. To further distinguish the unique functionality of the microbicidal base film and ensure that the observed efficacy was not caused by any remaining ionically bound gentamicin, a GS-resistant strain of *S. aureus* was used to determine the efficacy of a completely eroded $(DMLPEI/PAA)_{10}(Poly1/PAA)_5(Poly1/PAA/GS/PAA)_{20}$ film after immersion in PBS at 37 °C for four days (Figure 6-5, far right). The underlying bactericidal base film again yielded 100% contact killing.

As mentioned earlier, biofilm formation on the surface of an implant is one of the biggest causes of implant failure. Therefore, it is advantageous to prevent the formation of biofilms on the surface of medical implants in the first place. Here, the use of the microbicidal base film $(DMLPEI/PAA)_{10}$ is proposed as a long term surface coating for medical implants to prevent bacterial attachment, with the added versatility of tunable release of therapeutic agents via a degradable LbL film on top to provide additional medical functionality, when required. To this end, $(DMLPEI/PAA)_{10}$ films with completely eroded top films were tested against mediaborne *S. aureus* and found to be effective in preventing bacterial attachment relative to blank silicon substrates for up to two weeks. The blank silicon substrates were shown to be significantly colonized by bacteria after just 15 min incubation in bacteria solution (Figure 6-6).

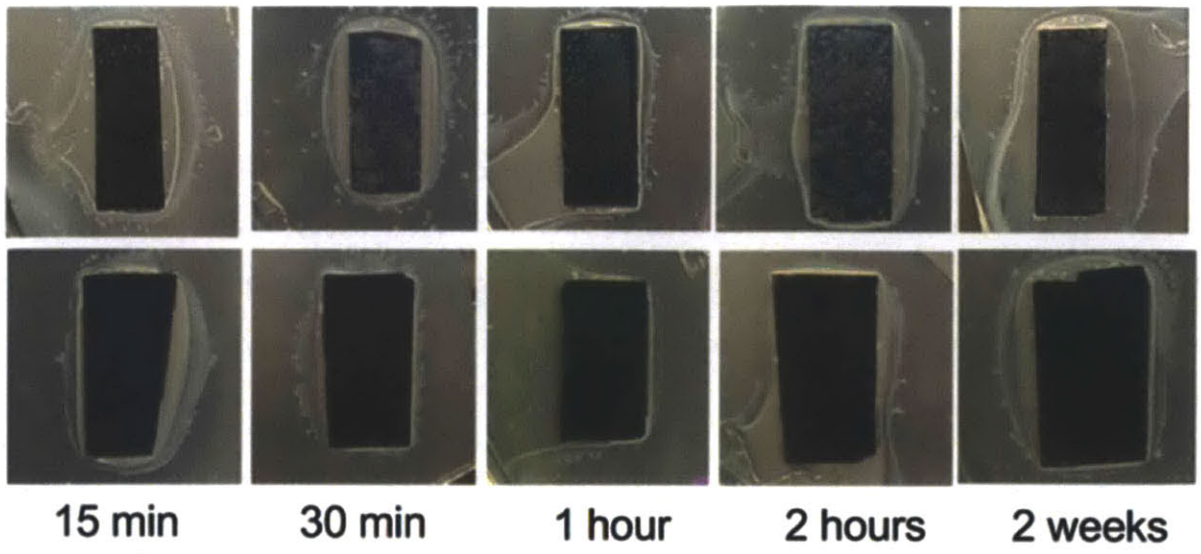

Figure 6-6. Mediaborne assay with increasing time of incubation in *S. aureus* broth; top row shows bare silicon substrates; bottom row shows $(DMLPEI/PAA)_{10}$ films with degradable top films completely eroded (courtesy of Jessie Wong). This figure was reproducible over three replications (data not shown).

Another major issue with implants is protein adsorption from blood plasma onto these foreign surfaces, which changes their chemistry. Therefore, cells at the surface of biomaterials are not necessarily in direct contact with the material itself. To show that the microbicidal functionality of the base film would not be compromised by protein adsorption to the surface, $(DMLPEI/PAA)_{10}$ coated substrates and blank glass slides were incubated in solutions of fluorescently tagged albumin for one hour (Figure 6-7, top). The coated films contained noticeably less protein than the uncoated controls. Then, the albumin treated samples and uncoated silicon controls were tested with the mediaborne assay (1 hour incubation time); film coated substrates were still 100% effective in preventing bacterial attachment, while the blank substrates were heavily colonized (Figure 6-7, bottom). This demonstrated that the permanent microbicidal base film functionality was not compromised even after being subjected to the presence of protein and thus would still prevent formation of biofilms, which further lends to the fact that this film could potentially serve as a long term implant coating.

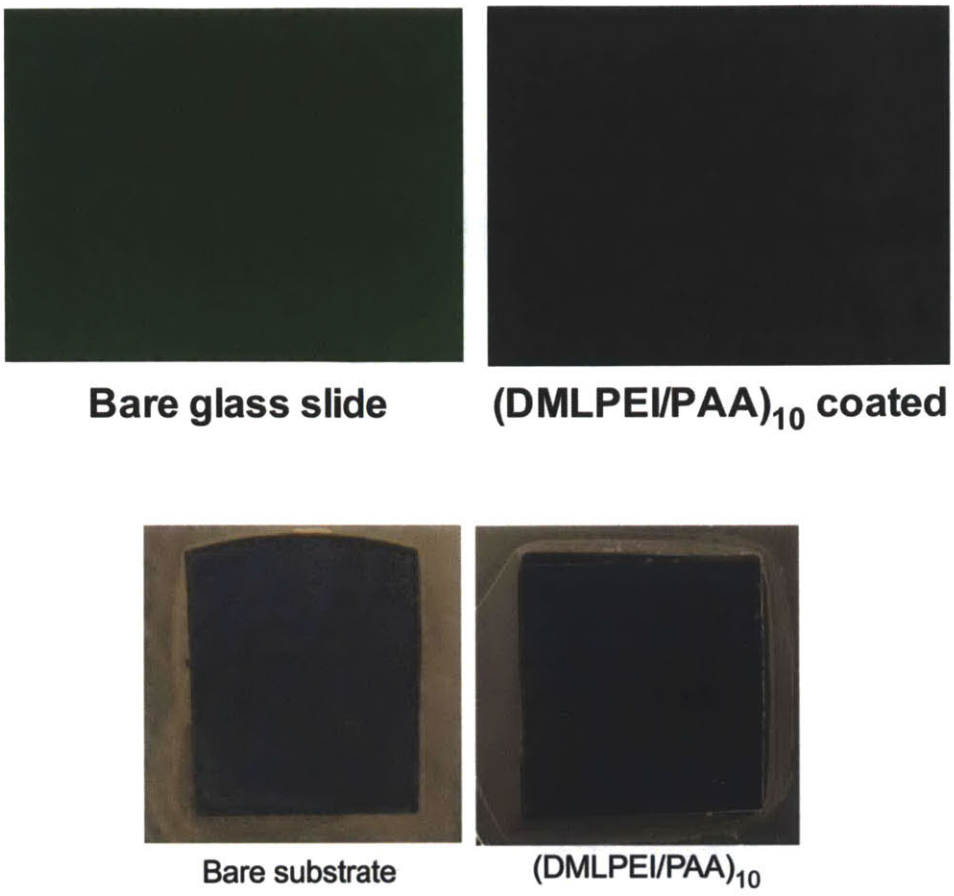

Figure 6-7. (Top) Samples incubated with fluorescently tagged albumin for 1 hour at 37°C. The intensity of green color correlates with the concentration of albumin. (Bottom) Samples incubated with albumin solution and then subjected to the mediaborne assay. This figure was reproducible over three replications (data not shown) and was prepared by Jessie Wong.

6.3.4 Cytotoxicity: Adhesion and Proliferation of Cells on Films

To investigate the cytotoxicity and interaction of cells with these films, murine pre-osteoblast cells (MC3T3-E1) were seeded onto glass coated with $(DMLPEI/PAA)_{10}$ and compared to uncoated controls. There was no measurable difference in adherence of cells to film-coated substrates relative to uncoated glass slides, regardless of the presence of serum in the media. As mentioned before, protein has been shown to adsorb to surfaces; hence, the use of serum-free media ensured that cells were exposed to the surface of the films and not a protein coated surface. An MTT assay, which measures metabolic activity of cells, was compared to

morphology data and found to be consistent. Cell proliferation was investigated via seeding and culturing cells directly on $(DMLPEI/PAA)_{10}$ films for 1 day, 3 days, and 7 days. Both microscopy (Figure 6-8) and MTT data (Figure 6-9) show little difference in proliferation on $(DMLPEI/PAA)_{10}$ compared to blank glass substrates. Therefore, while bacteria cells are not able to colonize surfaces coated with these films even after two weeks incubation in concentrated *S. aureus* broth, cells were able to attach and divide normally on the microbicidal $(DMLPEI/PAA)_{10}$ films, indicating no apparent cytotoxicity associated with these films.

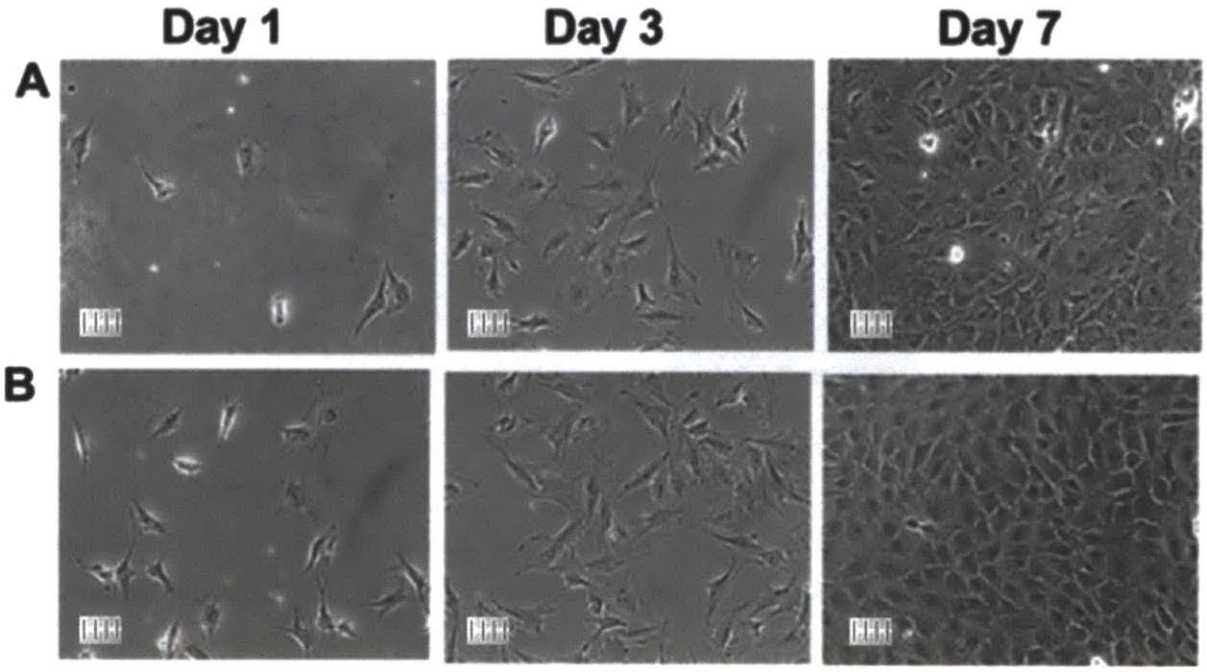

Figure 6-8. Microscope images of MC3T3-E1 cells seeded on (A) blank glass substrates or (B) $(DMLPEI/PAA)_{10}$. Images are representative images selected from triplicate samples and at least triplicate images per sample. Scale bar hash marks represent 100 μm.

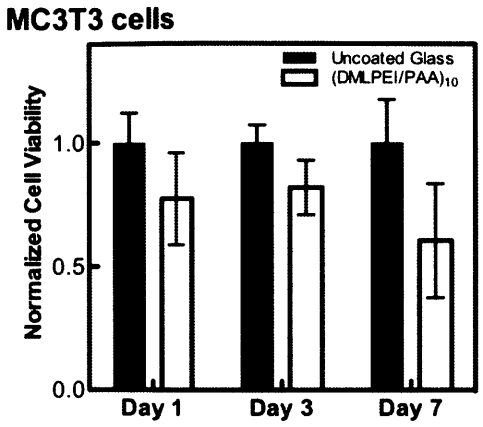

Figure 6-9. MTT data showing metabolic activity of cells seeded on $(DMLPEI/PAA)_{10}$ films compared to an uncoated control. There is no statistical difference between any data pair. Data represent mean ± standard deviation of triplicate samples.

6.4 *Conclusions*

The versatile film architecture presented in this chapter could potentially be used to impart long term microbicidal functionality to a surface while remaining capable of supporting release-based, erodible LbL systems for further therapeutic benefit, depending on the application of interest. It is therefore an alluring, complementary architecture that naturally extends upon the aims of this thesis. Specifically, it is now possible to combine the ability to eradicate an existing infection and maintain prolonged bactericidal functionality without risking the possibility of imparting antibiotic resistance. This is demonstrated in this chapter via the release of gentamicin as a specific example of controlled release of a therapeutic from a hydrolytically degradable film built on top of the permanent microbicidal base film. The films were shown to be non-cytotoxic to MC3T3-E1 murine osteoprogenitor cells as cell adhesion and proliferation were not significantly affected compared to negative controls. The most important observation from this study was that bacteria cells were unable to colonize the surface of the microbicidal $(DMLPEI/PAA)_{10}$ film despite the film surface allowing adhesion and proliferation of mammalian cells, thus showing that this microbicidal base film could find a promising future as surface coating for various implants to help reduce the likelihood of biofilm formation.

Chapter 7 Outlook

7.1 *Summary*

The work in this thesis has advanced the state of antibiotic releasing, hydrolytically erodible PEM systems (which in 2008 was in its infancy [53]). These systems can now deliver therapeutically relevant drug quantities over clinically relevant durations. After screening through an array of biocompatible film architectures (Chapter 2), it was determined that PEM films constructed with the biodegradable poly(β-amino ester) Poly 1 and the synthetic polyanion PAA in the particular order [Poly 1/PAA/GS/PAA]$_n$ were able to incorporate more drug and sustain release over a longer duration than any other architecture studied in this thesis. Films based on this best-performing architecture were shown to be generally benign toward murine pre-osteoblast cells, and release active drug capable of killing *S. aureus in vitro*. The use of liposome-encapsulated gentamicin was found to significantly inhibit drug loading relative to direct loading of native gentamicin. Drug release profiles were highly tunable using the crosslinking and "sponge" techniques. The former, which was studied via the use of heat and ultraviolet radiation, tended to demote the burst release phase in favor of slower release rate and greater overall release duration. The latter directly contributed to the magnitude of the burst release phase until a point of saturation.

In Chapter 3, a simple theoretical treatment to describe drug release from multilayered films was developed with the goal of predicting expected profile trends due to changes in drug concentration, film thickness, drug diffusivity, and film erosion rates. An analytical model was derived from simple scaling arguments and regressed against existing data sets, capitulating results that were in most cases consistent with expectations and literature. As an addition, an equally simple numerical treatment was coded in MATLAB using finite differences to describe the diffusive release of drug from a thin film. These models were developed using a set of simplified assumptions and are thus significant abstractions from true physical experimental conditions. Despite this, they hold value in their ease of use while fitting most data sets quite well. Furthermore, these efforts set a foundation for further theoretical advancement.

Two of the major successes of the work presented herein were the development of a reproducible bone infection model through which antibiotic PEM coatings could be tested (Chapter 4), and subsequent *in vivo* determination of efficacy of the specific PEM constructs of interest (Chapter 5). The infection model was designed to mimic a primary joint arthroplasty with the goal of a 100% contamination rate using the osteomyelitis-pertinent pathogen *S. aureus*. This infection model was used to perform the *in vivo* experiment, which was designed to resolve any observable statistical difference between an antibiotic-releasing, PEM-coated implant and an uncoated, sterile placebo. Although the experiment omitted the use of perioperative intravenous antibiotic therapy and thorough debridement of the infection site, the PEM coatings significantly reduced the bacterial challenge in the bone and on the implant surface at both day four and day seven after direct exchange. As this was only the first iteration of *in vivo* experimentation utilizing antibiotic-eluting PEM films, these results suggest a promising future for these systems.

Chapter 6 exhibits the versatility of LbL technology. Individual PEM systems, whose unique functionalities were combined by simple layering, yielded a dual-functional bactericidal film with both transient release-kill and permanent contact-kill capabilities. This concept expands upon the work presented in the previous chapters and alludes to the possibility of an orthopedic implant coating that can not only treat an existing infection, but also prevent systemically circulating bacteria from ever colonizing the surface of the implant, even years after implantation.

In summary, this thesis expounds upon the use of different strategies to tune the release of gentamicin from LbL films and demonstrates the feasibility of using these films as antibiotic coatings for orthopedic implants. Consequently, three avenues of investigation that would immediately benefit these PEM systems for the application of orthopedic implants are outlined below.

7.2 *Future Work*

7.2.1 Delivery of Multiple Agents

First and foremost, the overarching advantage of the LbL platform over competing technologies is the possibility of using its inherent nano-scale architecture to deliver multiple therapeutic agents with complex release profiles (e.g. pulsatile or sequential release). By layering in each component of the film sequentially, one can theoretically design these PEM films in bottom-up fashion such that upon top-down degradation, each therapeutic agent would be released according to its own loading profile. By careful choice of materials and growth parameters, this would enable a hypothetical film that combines analgesics, antibiotics [197], anti-inflammatory agents [63], and growth factors [65], each with unique timescales of release into the same device coating. Such control would then make co-delivery of multiple therapeutic agents relevant since analgesics and anti-inflammatory agents can be delivered immediately upon implant placement to mitigate pain and foreign body response, while antibiotics are delivered over the course of weeks to manage infection, and growth factors on much longer timescales to promote osteogenesis and integration of tissue with the implant surface.

When combining individually optimized film architectures into a single coating, the primary challenge to overcome will be prevention of interlayer diffusion whereby film components move through the bulk of the hydrated film as a result of local concentration gradients. Such mass transport could destroy the desired layered structure and defeat the objective of attaining sequential, pulsatile, or other complex release profile. To this end, work has begun to control this phenomenon using crosslinked polyelectrolyte barrier layers [55], but interdiffusion remains a significant challenge and presents opportunity for future research.

7.2.2 Revamping the *In Vivo* Model

Given the success of the *in vivo* experiment in this thesis, there are now multiple avenues of future work worth exploring, all of which require a revamped infection model. The model used in this study intentionally deviated from the standard clinical practice of providing systemic antibiotic therapy and thorough debridement of the defect site in order to inarguably prove

that the reduction in bacterial challenge was effected by the PEM constructs. Further development of these systems for eventual use in humans will require consideration of follow-up times beyond one week to ensure that infection has indeed been eradicated and that bone can integrate with the implant. In the next iteration of this study, it is recommended that the model include intravenous antibiotics and/or thorough debridement of the infection site similar to the work done by Alvarez *et al.* [164]. They were able to reproducibly decrease the infectious burden by using a three step wash consisting of saline, hydrogen peroxide, and povidone-iodine and hence were able to follow up on their treatment group out to 12 weeks without any need to perform premature euthanasia due to morbidity. It is expected that by incorporating such clinical control measures into the current model, a higher treatment success rate could be achieved. Pending favorable results from this revamped model, the immediate necessary experiment would be the co- or sequential delivery of gentamicin with bone morphogenic protein 2 (BMP-2, which is being studied concurrently in the Hammond Lab) for both infection treatment and implant integration. BMP-2 is a growth factor that would spur the healthy ingrowth of bone against the implant [204]. Finally, scale-up considerations are ever-present when studying orthopedics in small animal models, and therefore there is need to conduct similar experiments in greater-weight bearing environments (e.g. a goat model).

7.2.3 Biodegradable Polyanions

Both of the functional components used in the best-performing film architecture explored as a part of this thesis were cationic (i.e. Poly 1 and gentamicin). Consequently, a substantial amount of film mass was dedicated to polyanionic "filler" that had limited role other than to act as a biocompatible electrostatic glue to hold the film together. Although a vast library of biodegradable poly(β-amino esters) has already been developed [77], the existence of anionic counterparts [203] is much less prevalent. By layering gentamicin directly with a degradable polyanion, it may be possible to attain even higher loadings than what has been exhibited here. Moreover, co-utilization of multiple erodible components would further enhance the ability to tune the release of these systems. These benefits alone motivate an attempt to synthesize new classes of biodegradable polyelectrolytes with a focus on anionic species.

7.3 *Conclusions*

This thesis has shown that the small, hydrophilic antibiotic gentamicin can be delivered in appropriate concentrations from PEM implant coatings over prolonged periods of time and effectively treat a gross *Staphylococcus aureus* infection *in vivo*. This work can be extended to small, hydrophilic molecules in general, and sets the stage for the development of more advanced LbL systems that will soon incorporate multiple therapeutic agents that can be delivered with individually designed release profiles. While some significant and potentially unforeseen challenges still remain, LbL holds much promise as a drug delivery platform for drug-device combinations and may soon boost the success rates of orthopedic prostheses as well as implantable medical devices at large.

Chapter 8 Capstone

8.1 *Introduction*

The thesis herein describes the design, development, synthesis, and effectiveness of polyelectrolyte multilayered implant coatings for the controlled release of antibiotics in a local physiological environment. It presents a biomedical materials perspective toward understanding, analyzing, and overcoming the technical challenges of this technology. The thesis technology is motivated primarily for use in orthopedic revision surgeries involving total knee or total hip arthroplasties to enable an effective one-stage process where the patient will have a defective or infected implant replaced in a single surgery. Currently, such procedures require patients to undergo a two-stage process. The two-stage process is presented as non-ideal from the *perspective of the patient*, citing a list of undesirable attributes including:

- Two highly invasive surgeries within a six-week period
- Longer hospital residency with limited mobility
- A total economic cost of about five to seven times that of the initial surgery
- Potential for skeletal defects, limb shortening, renewed disability, and death

Revision surgeries require extended use of hospital resources and surgeon time. While implementation of the thesis technology is aimed at addressing these issues, wide-scale market adoption of a new medical technology presents a unique set of challenges (e.g. cost considerations, resource management issues, information dissemination, incentive compensation management, effectiveness of competing technologies) that may inhibit efficient market penetration. This capstone takes a much broader perspective to A) better understand the challenges behind adoption of a new medical technology, B) discuss the role of the current macroeconomic healthcare landscape, C) present an enabling technology as a potential solution to simulating human behavior change and adoption of the new medical technology, and D) discuss the enabling technology's promise and challenges.

8.2 *Payers, Providers, and Patients—Adoption of a New Medical Technology*

The healthcare arena consists of three camps, each which has its own set of interests and each which has the power to block the acceptance of a new medical technology: payers, providers, and patients. Payers may choose not to cover a particular pharmaceutical or technology, which would generally make it unaffordable for patients. Such a decision is primarily dependent on the cost and effectiveness of the new treatment regimen in comparison to competing treatments. Providers may choose not to adopt a new form of treatment due to their individual financial incentives, resource preferences, or beliefs about the new technology. As long as the physician practices medicine in a previously acceptable way, it may be difficult to enforce change. Patients ultimately have some choice with respect to their delivery of care: to the extent that illness or injury allows, the patient can sometimes choose which medical center, physician, and treatment (or no treatment) to receive. This is influenced by out-of-pocket costs and access to information on alternatives.

Any change to existing protocols in healthcare will need to satisfy the needs of each of these camps, separately. Payers want to control spending and limit their costs. Providers have a moral obligation to provide proper treatment to patients in need. They aim to avoid malpractice, and can leverage their expertise to influence the coverage of payers who will ultimately compensate them for their work. Patients want to limit physical and financial burden and may exercise control over their treatment regimen to achieve this end.

As new medical technologies or pharmaceuticals are developed with strong supporting data suggesting improvements to cost or safety, it may seem intuitive that patients opt for the newest treatment regimen, payers start covering it in their insurance policies, and providers adopt it as a new standard in their practice. However, wide-scale roll-out may not be as simple. First, if given the option, patients may be hesitant to elect the newest procedure if the incumbent technology is more well-known or well-accepted. Competing technologies are marketed to patients differently and may influence their decisions. In the specific case of the thesis technology, the prospect of significantly reduced physical burden (i.e. one surgery rather than two) suggests that patients will not present a strong barrier to adoption. Second, payers

may be reluctant to cover a new medical technology in their insurance policies. Even if clinical trials appear to be highly successful, the results of the original study may not extrapolate nationally to other patients and physicians. New treatments that do not lead to overall better outcomes can cause repeat procedures, which drive up medical costs. As an example, Johnson and Johnson's DePuy hip implants were recalled in 2010 as a result of their high failure rate [205]. Upon favorable comparison with incumbent technologies such as antibiotic-loaded bone cement, payers will likely not inhibit adoption of the thesis technology since the one-stage reimplantation has already gained strong traction internationally. Third, physicians who have been performing their procedures repetitively in a specific way for many years may not be willing to change without strong incentive. Additionally, the prospect of potential malpractice that can accompany implementation of new surgical procedures may act as a further disincentive to adoption. The thesis technology may help facilitate cultural acceptance of the one-stage reimplantation in the United States, but adoption by surgeons would still require behavior change, which may slow its market penetration.

To gain widespread adoption, a new medical technology will be first used by a core set of early-adopting physicians who are the most open-minded and willing to consider such cutting-edge procedures. Given that only one third of patients who receive critical care in the United States actually receive it from a physician who is board-certified to perform critical care [206], the supply of early-adopting physicians trained in critical care is even more extremely limited. It is critical to increase the patient reach and mentorship of these physicians as much as possible to drive market penetration of any new technology. This issue highlights the crux of a macroeconomic medical care imbalance that is rapidly gripping the United States: the demand for critical care medicine is on pace to severely outweigh the supply.

A new enabling technology in the field of telemedicine has been developed to directly address this problem. The tele-intensive care unit (also known as tele-ICU or eICU) enhances the reach of physicians trained in critical care medicine. It aims to make healthcare services more effective and efficient and can play a key role in achieving rapid market penetration of a new medical technology.

8.3 *Growing Supply and Demand Imbalance in Healthcare*

Nationally, ICUs treat 6M of the oldest and sickest patients each year. They are associated with the highest mortality rates and costs in healthcare ($107B or 4.1% of the $2.6T annual US healthcare bill) [207]. More than half of ICU patients are over 50 years old, with the likelihood of needing ICU treatment increasing significantly with age [208]. Compounding this issue, about one in five Medicare patients were re-admitted to a hospital within 30 days of discharge, accounting for $18B in 2007 [209]. Given the aging baby boomer population with increasing life expectancy, ICU demand is projected to dramatically increase between now and 2030 to about 54M ICU case-days per year—a tripling from 2006, which corresponds to 4.2% compound average growth rate (CAGR) in demand. This significantly outpaces the growth in ICU bed supply, which is currently experiencing 2% CAGR. These ICU beds cost on the order of $1M each, and most hospitals are unable to afford new beds.

Intensivists are medical professionals who are board-certified to practice critical care medicine (such as pulmonologists, anesthesiologists, surgeons, etc.). They are in extremely limited supply and most clinicians who work in ICUs are not certified in critical care medicine. A critical illness or injury is one that affects vital organ systems in a way that significantly increases the probability of rapid and life-threatening deterioration in a patient's condition [210]. As of 2010, less than 15% of all ICUs were able to provide intensivist care [206], and intensivists currently only see about one third of all patients requiring critical care (with the balance being seen by other medical professionals) [208]. It has been estimated full-time intensivist staffing in metropolitan areas alone could conservatively save over 54,000 lives each year [211]. Intensivists are able to find issues faster and treat them more thoroughly than their non-certified counterparts.

The severity of the supply-demand imbalance of intensivists is expected to worsen over time (Figure 8-1) [208]. The baseline analysis assumes that intensivists continue to provide care to only about one third of all ICU patients, as was the case in 1997. In an ideal world, intensivists provide care to 100% of all ICU patients.

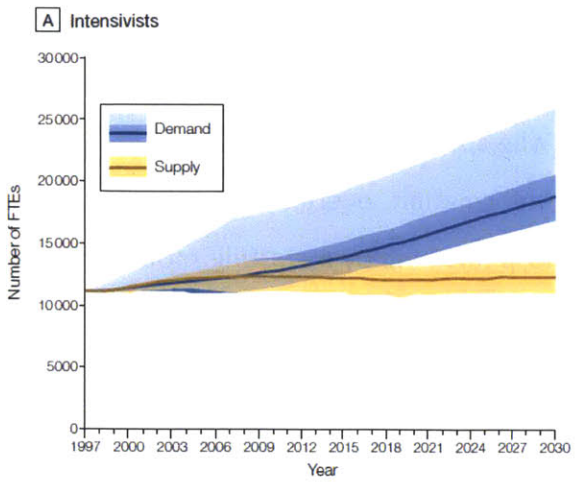

Figure 8-1. [This figure was extracted from reference [208]]. The lines indicate the base model (i.e. expected) scenario. The darker shaded areas represent the upper and lower bounds of the sensitivity analysis. For demand, ICU use was varied by ± 10%. For supply, the number of hours worked by intensivists was varied by ± 10%. The lighter shaded area corresponds to an increase in coverage from one third of all ICU patients to two thirds of all ICU patients. FTE ≡ full time equivalent.

This imbalance and its consequent adverse effects have been formally recognized by the Leapfrog Group. The Leapfrog Group is the leading national association of health care purchasers and advisory board to mostly Fortune 500 organizations with purchasing power of $59B—they mobilize this resource toward making 'giant leaps' in health care quality, safety, and value [212]. Leapfrog recently added a quality standard requiring that ICUs be covered by intensivists who are dedicated to the ICU, seven days per week during daytime hours. These intensivists must return notes >95% of the time within five minutes of being contacted when off site, and must make arrangements for the patient to be visited within five minutes by a certified professional [213]. In 2010, a survey indicated that only 34.5% of hospitals fully meet this standard.

Increasing the supply of intensivists is nontrivial. There are a limited number of physician resident and fellowship positions. As a result, medical schools cannot simply increase enrollment. Additionally, the high cost of medical school combined with cuts to graduate medical education funds has incentivized many potential physicians to opt for other career paths or end up pursuing only the highest paying physician specialties [210].

Increasing the local bed-to-intensivist ratio is also not a nationally viable option to expand intensivist coverage. One study of 2,492 patients demonstrated how leading ICU quality metrics (i.e. mortality and ICU length of stay (LOS)) are affected by increasing the number of beds covered per intensivist from 7.5 to 15 [214]. Although the study found that there was no significant difference in patient mortality, ICU LOS was significantly longer for

patients being treated by intensivists in the 15:1 ratio. The insignificant mortality outcome was caused by the fact that ICUs are staffed with residents and fellows 24 hours per day and seven days per week. The significant ICU LOS outcome was speculated as a potential effect from larger bed to intensivist ratio—specifically, that information overload can lead to more confusion and error. Despite this limitation, most hospitals employ a staffing model that uses on-site intensivist teams to provide critical care (Figure 8-2).

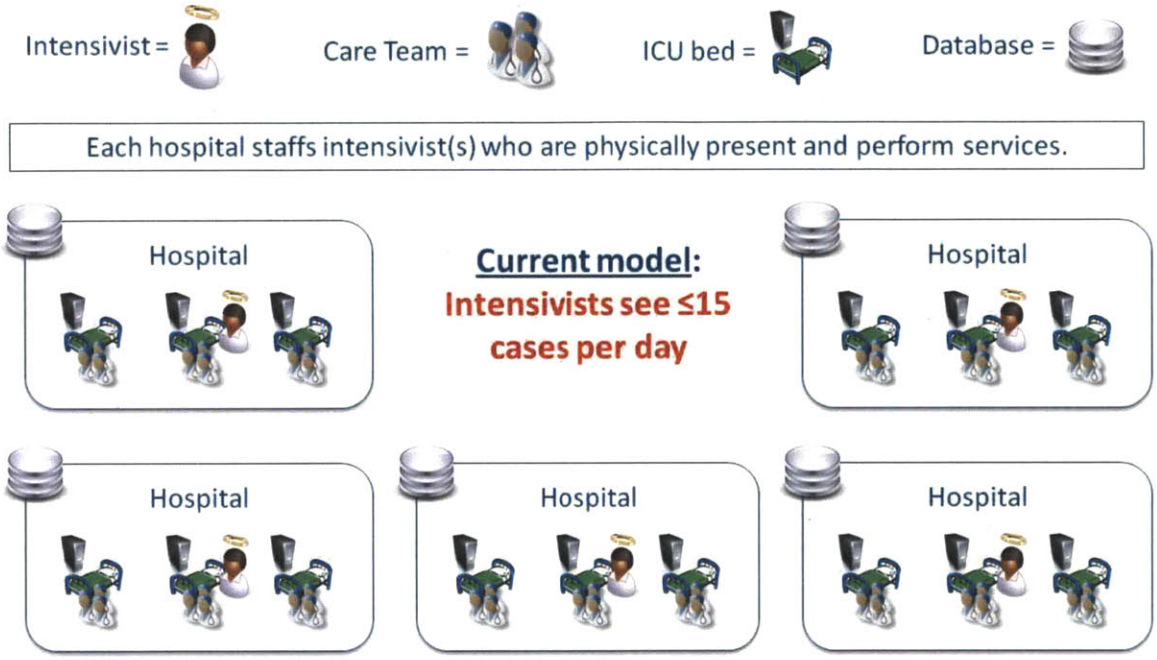

Figure 8-2. Most hospitals aim to staff their own local intensivist teams to provide critical care. According to the study by Dara *et al.*, these hospitals should staff more than one intensivist per 15 ICU beds. Clipart was used with permission from Arcadia Solutions (Burlington, MA).

8.4 *Enabling Intensivists to Reach more Patients*

To address the lack of patient exposure to intensivists, one near-term solution is to improve the efficiency of existing resources. Tele-ICU is an enabling technology platform that can expand the reach of intensivists by allowing them to act as remote-advisors for bedside clinicians. Consequently, the tele-ICU can also play a strong role in driving market acceptance of new medical technologies.

8.5 *The Tele-ICU Platform*

"Tele-ICU can be defined as the provision of care to critically ill patients by remotely located health care professionals using audio, video and electronic links to leverage technical, informational and clinical resources."

Craig M. Lilly, MD, Director, eICU Support Center, UMMMC [207]

Tele-ICU is an enabling technology that extends the reach and effectiveness of intensivists. Local clinician teams balance their time between several different patients. These teams are exposed to distractions, alarms, and their immediate task of providing critical care to a particular patient while simultaneously monitoring status changes to other patients within the same ICU. Some status changes require *immediate* attention as rapid deterioration in a patient's health can happen on the order of minutes. Early detection of critical status changes and patient prioritization are an important challenge for the great majority of clinician teams that do not roster a board-certified intensivist.

The tele-ICU improves the ability of local bedside teams to adequately care for their patients primarily through collaboration with highly-skilled and respected remote intensivists. This is especially important for the two thirds of ICU patients who currently do not receive their care from clinicians with critical care certification, and provides an easy entry point for early-adopting intensivists to confer expertise on new medical technologies to local bedside teams. While local clinicians monitor bedside alarms of patients located physically in different rooms, the tele-ICU technology provides the support of a remotely located intensivist with access to all medical information, laboratory results, cutting-edge decision-making software, and intelligent alerts on physiological trends for all patients at one work station [215]. Tele-ICU physicians have access to electronic detection of non-adherence to daily goal sheets and can conduct audits as necessary to ensure that best practices are carried out. This technology platform provides an ever-present source of critical care expertise and an additional level of clinical surveillance that allows local clinicians to effectively manage their priorities and provide the highest quality care to their patients.

The tele-ICU uses an interconnected set of audio and video technologies. The central command center (or 'support center') is a remote, physical location where intensivists are given virtual access to ICU information from several hospitals. Each local ICU bed is connected to the support center to enable real-time two-way audio and video correspondence. The support center computers collect live vital signs, electronic medical records, current treatment statistics, recent lab test and imaging results, notes, and other physiological status updates from each patient currently occupying a connected ICU bed. This information is presented on a set of monitors with built-in computer-managed decision support algorithms, alerts, and suggested treatment patterns. The tele-intensivist is given access to all possible information needed to help local care teams make decisions and deliver high-quality care (Figure 8-3).

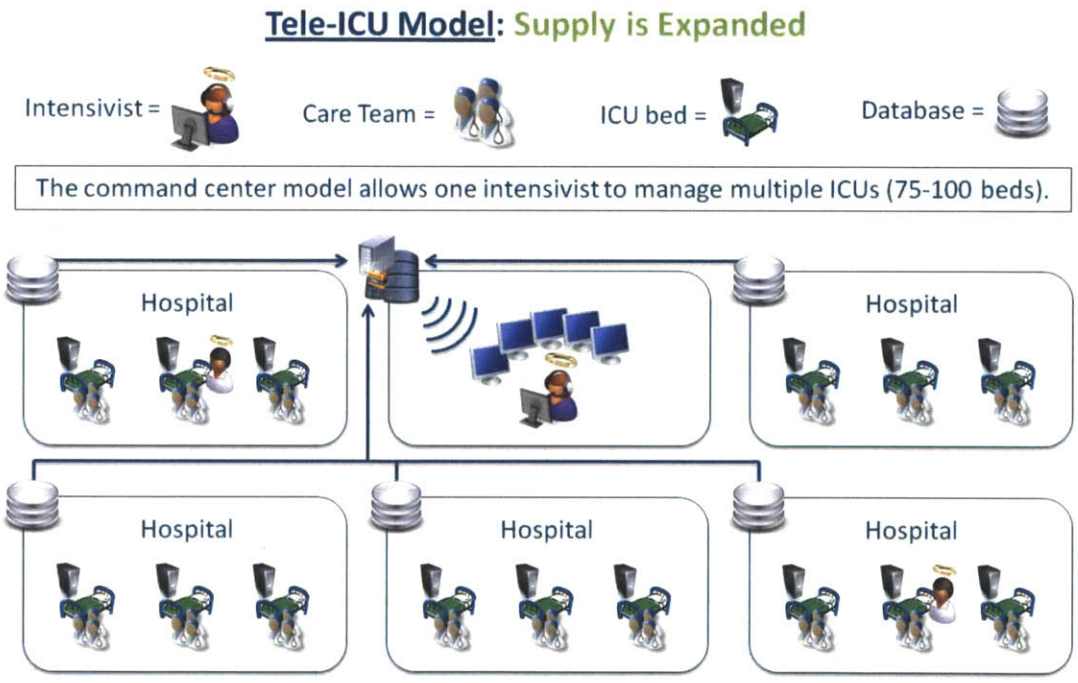

Figure 8-3. The tele-ICU model allows intensivists in a centralized command center to access all patient information from connected ICU beds to help assess patients and make decisions on critical care. The tele-ICU does not replace local bedside care teams. It enhances them with additional coverage and support of an off-site intensivist. This is particularly important for healthcare systems that do not currently employ local intensivists. Clipart was used with permission from Arcadia Solutions (Burlington, MA).

8.5.1 Market Penetration of Tele-ICU Technology

As of 2010, there were 41 active command centers. Command centers can be licensed to monitor up to 500 beds [207] translating to a maximum of 20,500 beds that can covered by existing command centers, or 24% of all ICU beds in the United States. These 41 command centers cover an average of 141 beds each, or 5,800 beds (6.8% of total) across 249 hospitals (7.6% of total). The locations of the command centers are presented in Figure 8-4.

Since 2000, five command centers have been deactivated. While the exact reasons for deactivation are not matters of public record, common barriers to successful tele-ICU implementation are discussed below in section 8.8 Implementation and Barriers.

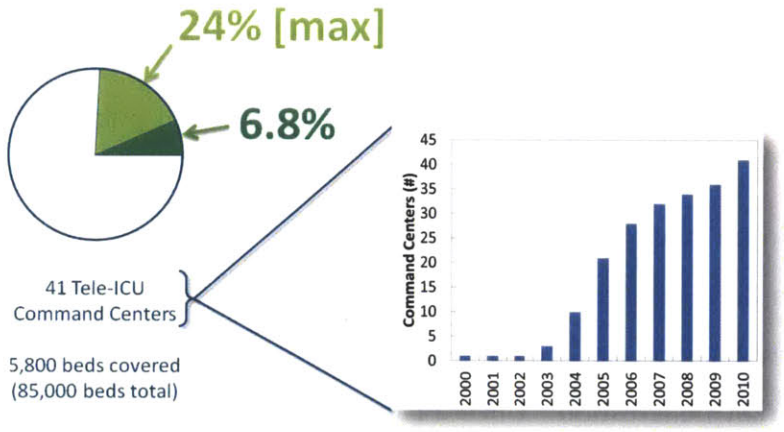

Figure 8-4. Market penetration and location of the 41 active command centers in 2010. Data were extracted from [207].

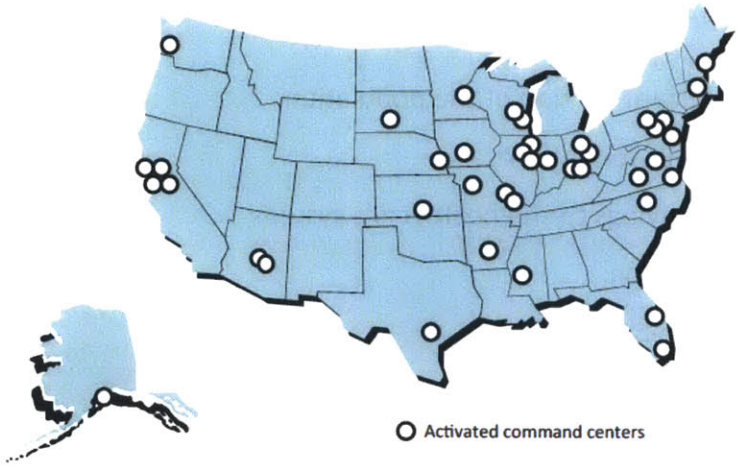

Source: NEHI, 2010

8.5.2 Vendor Alternatives for Tele-ICU Technology

The first player in the tele-ICU market was Philips VISICU. VISICU currently holds the most dominant position with about 85% market share [216]. Cerner and iMDSoft are the two other prominent vendors of tele-ICU-related equipment in the United States. Advanced ICU Care is an outsourcing alternative for healthcare systems that want tele-ICU coverage, but are unable to finance their own command center. Advanced ICU Care is currently the largest independent provider of tele-ICU services in the United States.

8.6 *Driving adoption of the Tele-ICU Platform*

Tele-ICU gained significant traction with the controlled study conducted at the University of Massachusetts Memorial Medical Center (UMMMC) in collaboration with the Massachusetts Technology Collaborative (MTC) and the New England Healthcare Institute (NEHI) published in 2011 [215].

MTC and NEHI became interested in tele-ICU in 2003 as a potential candidate technology for their FAST initiative (i.e. Fast Adoption of Significant Technologies). The FAST initiative focuses on identifying new technologies that improve healthcare quality and reduce cost, but currently exhibit low market penetration. Once a candidate is identified, MTC and NEHI focus their resources on driving widespread acceptance. To qualify, a new technology must meet the following criteria:

1. Address a significant portion of the population.
2. Improve outcomes for patients.
3. Generate a net savings to the health care system.
4. Have low penetration.
5. Offer addressable barriers.
6. Have more than one manufacturer.

Four of these criteria were already satisfied by the tele-ICU platform. First, ICUs address 6M critically ill patients each year. Second, FAST surveys conducted in 2006 indicated that only about 6% of all ICU beds were covered by tele-ICU technology. Third, barriers associated with

successful tele-ICU implementation are seemingly addressable—several tele-ICU systems had already been successfully installed throughout the United States. Finally, there were at least four major players in the tele-ICU market. Two criteria were not yet satisfied: although intensivist coverage of ICUs leads to improved outcomes and cost savings, it was still to be determined if tele-intensivist staffing could achieve similar results.

As UMMMC made the investment to install the first tele-ICU command center in Massachusetts, MTC and NEHI recognized this as an opportunity to investigate tele-ICU's ability to meet criteria 2 and 3. A timeline of events is provided in Figure 8-5.

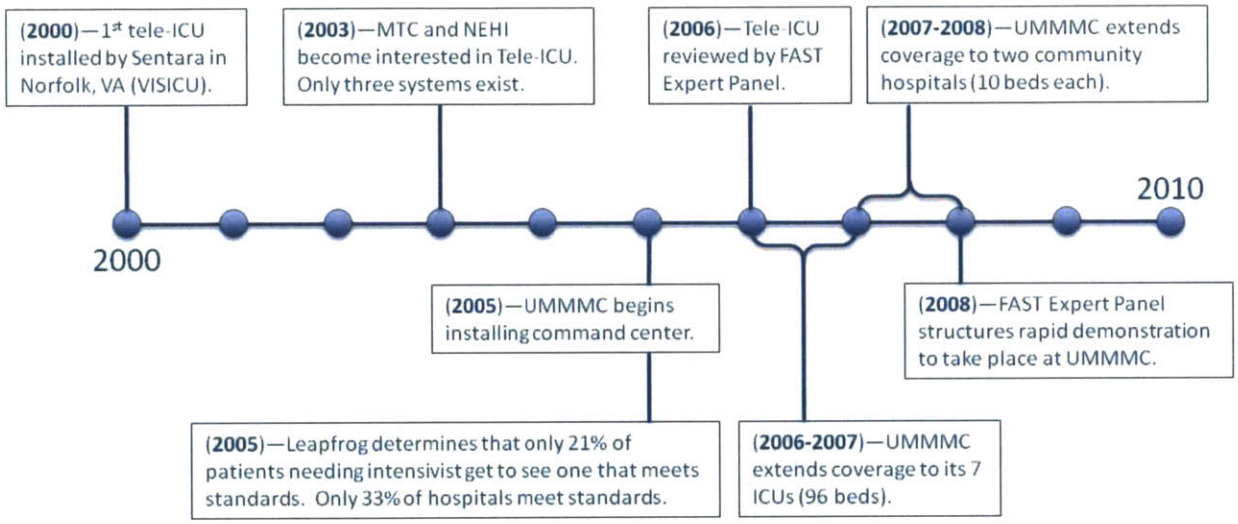

Figure 8-5. Timeline of events leading up to and through the UMMMC study by Lilly *et al.*

8.7 *Disseminating Best Practices with Tele-ICU*

UMMMC's experiment studied two primary outcome metrics: patient mortality and hospital length of stay (LOS). The goal of the study was to determine if tele-ICU would enable the local ICUs to better adhere to best practice protocols and improve their quality of care. MTC and NEHI set benchmarks for successful improvement of patient outcomes. Their mortality target was a 10% reduction in severity adjusted mortality with no increase in hospital mortality rates of discharged patients. Their LOS target was a 12 hour reduction from the initial average LOS (i.e. without tele-ICU support).

Data were collected from both UMMMC's seven ICUs and two separate community hospitals totaling 116 beds. These data were collected for about 6 months prior to tele-ICU installation and 6 months post tele-ICU installation.

The purpose of studying two separate types of medical settings was intentional due to fundamental differences in their ICUs. The academic medical center averaged over 13 beds per ICU (96 total beds) and had special allocation for medical, surgical, trauma, transplant, and cardiac use. For the thesis technology, the academic medical center is the more relevant environment. The community hospitals averaged 10 beds per ICU and were mainly used for patients admitted from the emergency department (i.e. surgical practices were not routinely performed procedures). UMMMC was a referral center for patients with high risk of death when local hospitals do not have the resources to treat such extremely complicated patients. The community hospitals referred their most severely ill or injured patients to UMMMC.
The primary similarity between UMMMC and the community hospitals was that both had excess capacity—UMMMC had occupancy rates in the 80-90% range while the community hospitals had occupancy rates in the 40-50% range—and neither had full intensivist staffing.

The UMMMC study concluded that effective tele-ICU implementation throughout the state of Massachusetts could *conservatively* save 350 lives and $122M for payers on an annual basis. Tele-ICU coverage enabled local bedside teams to treat a much sicker patient mix. The

mean APACHE** score at UMMMC increased by about 30%, post-implementation, while each of the two community hospitals increased by 14% and 18% respectively. Despite the increased severity in patient mix, UMMMC experienced a 20% decline in observed ICU mortality rate and 13% decline in observed hospital mortality rate. ICU observed LOS decreased from 6.4 days to 4.5 days, a 30% decline. In the community hospitals, the severity-adjusted LOS dropped 40% and 16%, respectively. Adherence to best clinical practices significantly increased at all three sites for measures taken against stress ulcers and deep vein thrombosis (Table 8-1). Additionally, measures taken toward cardiovascular protection increased from 80% adherence to 99%, and prevention of ventilator-associated pneumonia increased from 33% to 52%. These numbers were achieved despite the fact that both community hospitals experienced significantly higher occupancy and patient volume due to their ability to address more complex cases with the tele-ICU support.

Table 8-1. Increase in adherence to best clinical practices at UMMMC and each community hospital (this page) [215], and Sutter Health (next page).

		Pre	Post	Change
Stress Ulcer Prevention	UMMMC	83%	96%	16%
	Hospital 1	70%	87%	24%
	Hospital 2	93%	97%	4%

		Pre	Post	Change
Deep Vein Thrombosis	UMMMC	83%	96%	16%
	Hospital 1	70%	85%	21%
	Hospital 2	91%	99%	9%

** Severity adjustment is done using acute physiological and chronic health evaluation (APACHE) scores, which is now in its fourth iteration (APACHE IV). Each patient admitted to an ICU is evaluated based on their diagnosis, heart rate, body temperature, blood pressure, etc. and given an APACHE score, which ranges from 0 to 71 reflecting an immediate risk of mortality from <5% to >85%. Higher APACHE scores correspond to higher risk patients and consequently higher *predicted* mortality rates, so comparing raw mortality rates (i.e. without severity adjustment) before and after tele-ICU implementation may not be an apples-to-apples comparison in the event that there is a significant change in the average health of patients being admitted. Therefore, when comparing pre- and post-tele-ICU *observed* mortality rates, it is important to express these numbers relative to the *predicted* mortality rates. As an example, if the *observed* mortality rate remains constant through the installation of a tele-ICU and the patient population being treated becomes twice as sick, then although the *observed* mortality rate has not changed, the severity-adjusted mortality rate will have clearly improved.

Best Clinical Practice for Patients Diagnosed with Sepsis:	Pre-Tele-ICU	Post-Tele-ICU
Antibiotic administration within 2h	51%	79%
Lactate measurement	49%	55%
Baseline lab blood draw	78%	84%
Blood culture before antibiotic administration	63%	74%

The results at UMMMC provide two significant implications for the thesis technology. First, their study is an example of effective knowledge sharing with two differing healthcare environments. In most cases, the antibiotic coating technology studied in this thesis will be applied to the surface of orthopedic implants that are used in pre-scheduled arthroplasties, which are often conducted at academic medical centers. Academic medical centers are not excluded from the reach of the tele-ICU platform. Second, with the support of remote-intensivists, community hospitals are able to admit a more severe patient mix. To the extent that the tele-ICU platform enables community hospitals to undertake more trauma-related cases, it is conceivable that tele-ICU can facilitate deployment of the thesis technology on the surface of implants used in open reduction internal fixation procedures.

The improvements resulting from tele-ICU implementation at UMMMC are consistent with the findings of peer tele-ICU-adopting health care systems including:

- Reduced severity-adjusted mortality rates
- Reduced ICU LOS
- Reduced Hospital LOS
- Improvement in best practice compliance
- Increased mean APACHE scores
- Higher patient throughput
- Higher patient occupancy
- Risk management and cost avoidance
- Significant savings to payers
- Payback within one year

The major theme behind the tele-ICU platform is dissemination of knowledge and expertise on evidence based medicine, including new medical technologies, to a variety of care settings. Among health care systems with installed command centers, Ministry Saint Clare in Wisconsin significantly outperformed the APACHE predictive outcomes in ICU mortality (33% improvement), hospital mortality (26% improvement), ventilator days (40% improvement), ICU LOS (37% improvement), and hospital LOS (41% improvement) [217]. It achieved near perfect compliance in best-practice protocols involving ventilator-associated pneumonias, central line catheter infections, gastric stress ulcers, and life threatening blood clots. Sentara and Maine Medical Center reduced observed mortality rates by 27% and 20%, respectively. Avera Health decreased severity-adjusted mortality by 29%. Memorial Hermann Health System reduced mortality in all five of its ICUs despite a worsened case mix. Sutter Health improved a variety of best clinical practices (Table 8-1), and demonstrated saving 56 lives in a 30-month period at one facility due to increased adherence to screening for sepsis on admission. Advocate HealthCare cut preventable incidence of ventilator-associated pneumonia by 85% by improving compliance with best-practice protocols [206]. Citing the ability of its tele-ICU system to transmit data at high speeds and generate intelligent alerts, Indiana Health saved 655 additional lives between 2005 and 2010 [218]. The University of Pennsylvania Health System studied the effects of its tele-ICU on 2,811 patients over three years and found statistically significant decreases in ICU mortality (8.4% to 3.1%), hospital mortality (11.1% to 6.0%), ICU LOS (3.75 day reduction), and hospital LOS (4.43 day reduction) [212]. Resurrection Health Care diminished mortality by 41% and LOS by 38%, resulting in 1,700 fewer ICU days than prior to tele-ICU implementation [219].

In a large study of more than 10,000 patients across multiple hospitals contracting with Advanced ICU Care, there was a 40% reduction in ICU mortality, 25% reduction in ICU LOS, 17% increase in the number of ICU cases, and continuous process improvement procedures that minimized complications, maximized efficiency, and improved both patient and staff satisfaction [217].

Despite the abundance of healthcare systems reporting significant improvements, not all healthcare systems were able to achieve strong improvements in ICU-related metrics. It is

required that the tele-ICU system be seamlessly integrated with the work streams at the site of care. One review article points out two studies that took place in Texas and Illinois, respectively, that experienced little gain from their newly installed technology as a result of limiting the tele-ICU from intervening in delivery of care to life-threatening emergencies [212].

8.8 *Implementation and Barriers*

8.8.1 Perceptions of Tele-ICU

Despite the positive medical benefits apparently offered by the tele-ICU, this technology has not propagated rapidly throughout the United States. Berenson *et al.* visited 12 different hospital systems throughout the country, five which had installed tele-ICUs and seven which had not, to conduct interviews regarding adoption of this technology [220]. Amongst tele-ICU implementers, the biggest motivation to invest in the technology was the possibility of improving clinical quality, patient safety, and reach of their ICU staff. They were interested in maintaining a reputation for quality and innovation, and tele-ICU implementation was an opportunity to build deeper relationships with smaller, more remote hospitals. This fact highlights the direction of knowledge flow: tertiary care centers tend to be the most open-minded toward adoption of new medical technologies, and by establishing relationships with smaller hospitals through the use of tele-ICU, the larger academic medical centers directly propagate adoption by the remote hospitals. Decision-makers' awareness and visitations to existing successful tele-ICUs systems bolstered their decision to invest in tele-ICU. Expectations of cost savings from reduced complications and LOS were not major factors in the purchase decision, and most did not consider payer or purchaser expectations other than the Leapfrog Group.

Non-implementers (almost all of who were aware of VISICU's product) could not justify the "limited potential benefits" against start-up and operating costs. They felt that their current ICU staffing adequately met their needs and preferred to keep their operations exclusively on-site. Some non-implementers felt that tele-ICU would be most useful in crisis situations, which tended to be uncommon. There was uncertainty whether tele-ICU would

alter clinical decisions, and concern that the technology could create unnecessary overreaction to minor issues. Initial conditions (e.g. mortality rates and average LOS) play a strong role in determining the overall success of a tele-ICU implementation; therefore, tele-ICU oversight may not be as important to top performing ICUs. Finally, the lack of third-party reimbursement for installation and operation was seen as a disincentive, given the challenges over quantifying return on investment. Despite these issues, many non-adopters valued the data management (i.e. presentation and analysis) capabilities of the VISICU system when compared to their currently installed IT systems.

For both implementers and non-implementers, most of the 12 hospitals had undertaken initiatives to improve their ICU performance. This was primarily done through addition of intensivists and adoption of ICU-specific quality improvement initiatives. On average, the 12 hospitals were implementing at least six initiatives to improve best practices and avoid complications. Over two-thirds of these hospitals reported meeting the Leapfrog standard for intensivist staffing. Although the opinions about the necessity of 24/7 intensivist staffing of the ICU were somewhat mixed, the general consensus was that intensivists should be accessible at all times. The major barrier to installing tele-ICU for achieving this end was the capital requirement for implementation, operation, and staffing.

8.8.2 Operation

Patients undergoing critical care can experience clinical conditions that change rapidly—the tele-ICU helps manage care and ensures that patients have access to proper intensivist expertise, when needed. Local clinicians stay focused on delivering bedside care and communicating with families while remote clinicians keeping 24/7 watch over the vital signs and health trends of all patients in the local ICU.

The ICU gives the remote intensivist convenient access to all relevant patient information to help local bedside teams make decisions, as necessary. Remote intensivists view live bedside waveforms on a series of monitors (Figure 8-6). The VISICU software is equipped with automated surveillance tools that employ sophisticated algorithms to analyze and evaluate live patient physiological data, laboratory results, medication lists, and charted

information in the patient's electronic medical records to help provide earlier detection of complications. Patients can exhibit vital signs that do not necessarily trigger standard bedside alarms, but where the tele-ICU software is able to identify a deteriorating trend [220].

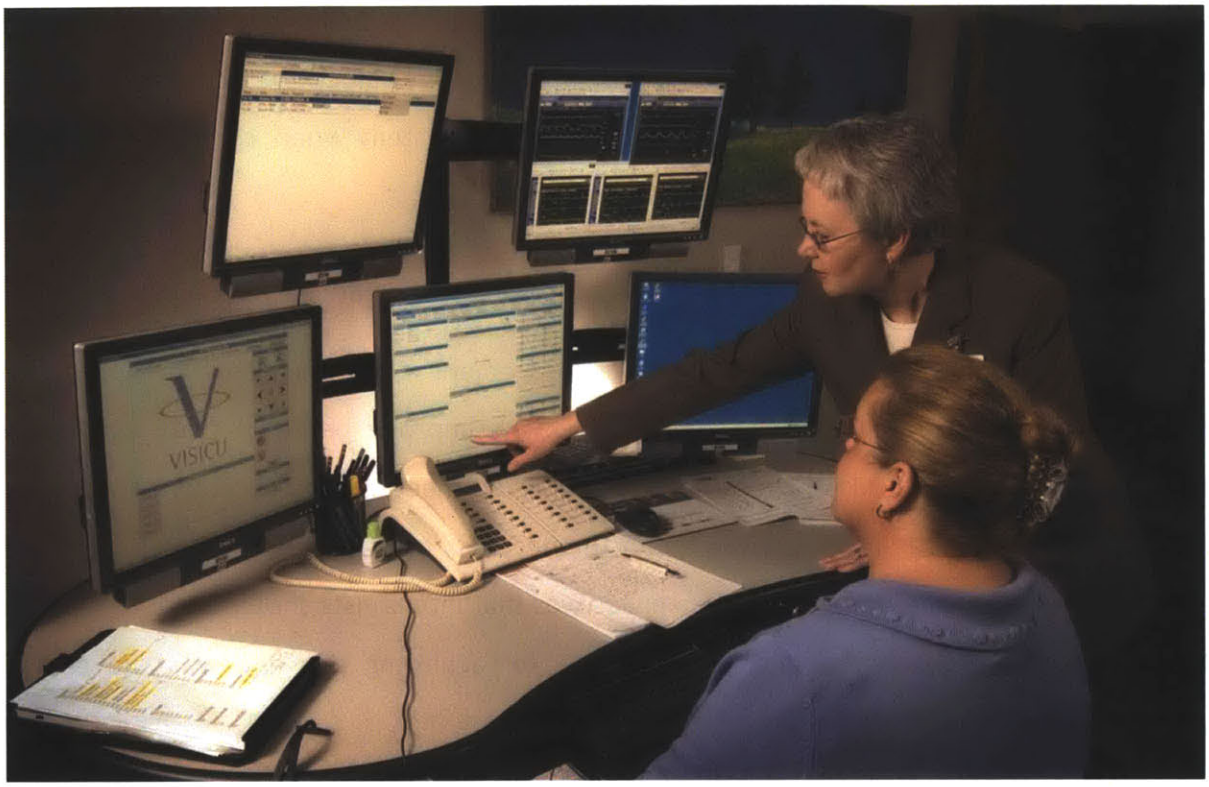

Figure 8-6. VISICU tele-ICU station. Image was extracted from Google Images.

Static-free audio and high-resolution video equipment are installed at the command center and each local ICU bed to allow real-time communication between the two locations. Cameras are able to assess skin color, breathing patterns, pupil size, labels on equipment, and ventilator settings. Although the command center can initiate a communication, the local bedside teams request the immediate presence of the tele-ICU team by pressing a red tele-ICU emergency button located on the wall in the local ICU room. In some healthcare systems, bedside physicians can indicate their preferred level of involvement from the remote-intensivists by selecting a category level ranging from 'monitor and report only' to 'full intervention by remote intensivist' [221].

The intensivist coverage by tele-ICU provides a redundancy that ensures consistent execution of best practices bundles (or checklists), which can sometimes be missed when bedside staff become busy or distracted within the ICU. It is important that tele-ICU programs have a process for systematically reviewing and improving current best practice protocols to ensure compatibility between the remote and local care teams, and that such protocols continue to deliver the most efficient and high-quality care for patients. As an example, Advocate HealthCare System screened every mechanically ventilated patient twice per day to ensure that all five components of its ventilator-associated pneumonia bundle were completed—if missed, the tele-intensivist would write a computerized physician order entry (CPOE) to complete the bundle or call a bedside clinician to resolve the issue. Within three months, Advocate HealthCare was more than 99% compliant [221]. This review process is also a critical opportunity to discuss how new medical technologies can improve existing care regimen, as well as how to incorporate them into existing work streams.

Tele-ICU teams make routine virtual rounds, which include reviewing vital signs and trends over the last few hours, current waveforms, new lab or other diagnostic test results, nursing flow-sheet documentation (including assessments and interventions), physician notes, care plan updates, respiratory therapy flow sheet data, and alerts. Virtual rounds may involve interventions with the local care team, if necessary [206]. Rounds are prioritized in order of patient acuity. The software distinguishes between the most critically ill patients ('red'), moderately ill patients ('yellow'), and the most stable patients ('green') [221]. Virtual rounds do not typically require audio or visual capabilities. They occur immediately after new admission (for initial tele-ICU assessment), during assessments at the beginning of a shift, when requested by local care teams, and in the event that a patient's condition has substantially changed. In the event that an alarm is triggered as data are processed through the decision support software, tele-intensivists critically evaluate its cause (e.g. respiratory distress, impaired oxygenation status, hypotension, tachycardia) and intervene as necessary [209]. Shift lengths for tele-nurses are usually 12 hours, and shift lengths for tele-physicians range from 9 to 12 hours [221].

Tele-ICUs can be staffed with shared and/or dedicated positions. Dedicated positions help maintain team cohesiveness and mitigate scheduling issues; however, lack of intensivist exposure to the bedside ICU can reduce clinical competence over time [206]. Shared positions can improve job satisfaction by balancing the intensity and emotion of the bedside ICU with a more casual environment and provide exposure to many more patient cases; however, shared positions may create loyalty and scheduling challenges since such clinicians report to two separate managers. With respect to propagating a new medical technology, shared positions may offer stronger support toward market penetration; shared positions allow early-adopting intensivists to drive acceptance of the new technology on both ends of the tele-ICU platform. Locally, they work with bedside care teams to help enact behavior change, make purchase decisions, and demonstrate surgical procedures, and then use this experience in the command center to offer better guidance remotely. Tele-ICU command centers should be staffed with medical professionals who are well respected and have strong leadership and communication skills.

8.8.3 Barrier 1: Costs

Costs are the first major potential barrier to implementation of a tele-ICU. For decision-makers, the high costs associated with implementing tele-ICU must be justified. As of 2010, no major third-party payers covered installation or staffing of the tele-ICU command center. Therefore, each healthcare system is responsible for analyzing whether or not the tele-ICU makes economic sense given that it must fund the project internally.

Most existing command centers have capacity for accommodating new ICU beds[††]. The most cost effective way to propagate the tele-ICU technology is to use this capacity rather than build new command centers. The cost to equip a satellite hospital with all necessary hardware and software for communicating with a command center is between $300,000 and $500,000 [207], or about $30,000 to $50,000 per ICU bed. This sum includes software licensing, implementation fees, ICU hardware, build-out of network and infrastructure, and project

[††] The national average is 141 beds per command center out of a maximum of 500.

management efforts. Annual operating costs are about $40,000 per ICU bed per year, 25-50% of which is related to staffing. Staffing models generally allocate 80-125 patients per tele-physician and 30-35 patients per tele-nurse. At the maximum capacity, this equates to 5-7 tele-physicians and 14-17 tele-nurses (or physician assistants) [206, 211].

Command centers cost between $6M and $8M. Two thirds of this investment is related to building out the physical tele-ICU support center and servers, licensing and implementing the tele-ICU technology (e.g. from VISICU), and other equipment costs. The balance consists of network and infrastructure costs, utilities, upgrades to patient monitoring systems, project management fees, and other miscellaneous costs (including travel expenses, marketing, supplies, etc.). The annual operating costs for a command center range between $1M and $3M, with about 90% of this allocated to salaries and benefits. Professional salaries range from $28/h to $50/h for tele-nurses and from $165/h to $200/h for tele-physicians [221].

8.8.4 Barrier 2: Data Integration

Data integration is the second major potential barrier for tele-ICU implementation. The remote care team must be able to access all relevant patient information in a single interface, which requires a standard data format. This is an industry-wide challenge that is being addressed by the not-for-profit firm Health Level Seven International via its HL7 standards for data interoperability. There are many cases where VISICU is not entirely compatible with local data systems. For example, one healthcare system claimed that "half the nurses' time is spent moving data from point A to point B to make it available" [220]. In a second example, remote physicians at both Aurora Health and the University of Pennsylvania Medical Center are required to physically alternate between multiple electronic medical record interfaces (e.g. Allscripts, Epic, eClinicalWorks, etc.), each which corresponds to the choice of the respective local hospital. In even less technically advanced locations, documentation systems may still rely on paper records, requiring the use of fax transmissions and other means of data sharing [212]. Other examples of data that are not traditionally importable are: volume of intravenous fluids administered, ventilator settings, and in some cases, medication lists. Smart alerts on drug interactions or mechanical ventilator problems become useless if the underlying data are

unavailable to the VISICU system. Data that are compatible with HL7 standards can be directly imported into the VISICU software. Data integration issues in healthcare continue to be a primary destination for investment and collaboration with healthcare consulting firms.

Finally, to meet security standards established in the Health Insurance Portability and Accountability Act (HIPPA), all data must be properly encrypted before secure transmission between the local ICUs and the command center.

8.8.5 Barrier 3: Change Management and Relationships

Implementation of tele-ICU technology requires local clinicians to relinquish some of their autonomy to intensivists who support them from the remote unit. MTC and NEHI cite two vivid examples of local physicians who took drastic measures to impede the usefulness of this technology: one who hung clothing over the local camera, and the other who physically removed the camera from the wall. Consequently, change management and relationship issues are widely identified as the third major potential barrier to successful implementation of a tele-ICU system.

For healthcare systems that have implemented tele-ICU, staff acceptance is a daily concern. Prior to adoption, nursing staff tend to present the strongest resistance. On average, they hold neutral views toward the perceived usefulness of the technology. It has been found that in some cases, nurses intentionally avoid the help of tele-nurses while waiting for a tele-physician to become available before seeking advice. Other issues include resentment due to oversight, more frequent interruptions, and increased workload (although such issues were location and participant-specific) [222].

The tele-ICU technology is counterproductive and uneconomical unless clinicians on both sides of the technology—remotely and at the bedside—use it cooperatively. Health care systems must place a focus, and communicate from the beginning, the importance of collaboration amongst all impacted parties. ICU staff should be required to participate early in the planning stages of designing and implementing the tele-ICU. It is important for hospital administrators to generate widespread support for the tele-ICU prior to rollout. Careful thought must be placed on staffing—those with the best communication skills are top

candidates for remote-ICU staffing. Absolute agreement on best-practices for treatment procedures must be established between local and remote teams to avoid conflicting advice during active duty. A team approach can facilitate process improvement initiatives to ensure best practices are up to date and evidence-based medicine is followed throughout the ICU for the benefit of all patients being treated [217]. At Sentara, for example, the protocol for monitoring glucose levels was reworked eight times using VISICU-generated data [223].

These efforts must be coordinated with versatile and supportive IT and clinical engineering departments, who are dedicated to keeping the system online and making improvements to the technology [218]. Tele-ICU consumes a significant amount of bandwidth; Ministry Saint Clare initially dedicated a separate T1 line to support the constant data flow. It is imperative to have detailed disaster plans to mitigate downtime during potential power outages, weather crises, and other complications [224]. Authors Jarrah and Van der Kloot suggest "dedicated, program-focused IT personnel, hospital-based information technology services collaboration, and 24-hour centralized technical support" [212].

The following steps will help develop a strongly supportive environment for hosting a tele-ICU system and maintain a healthy culture. First, installation of a formal orientation program will allow all staff to meet each other and visit the various ICUs and command center. New hires should be given this opportunity, and continuing education programs should be provided annually as refreshers. Second, regular, shared meetings, retreats, and holiday events that include both remote staff and local staff will help build camaraderie. UMMMC holds bi-weekly meetings between tele-ICU leadership and key ICU personnel to discuss critical care activities and financial issues [221]. Third, formal staff liaison positions should be created. These positions act as points of contact for needs that may arise from either party. Fourth, there should be a problem-solving committee and task force with appointments from the remote staff, the local ICU staff, hospital executives, administrators, and the IT and clinical engineering departments. This committee should hold regular leadership meetings and must be given the authority to enact change. Fifth, it is important to identify opportunities for shared research projects related to the tele-ICU technology. News related to these projects

should be communicated broadly. Finally, it is important to maintain clear lines of communication amongst impacted parties. Newsletters, feedback through public dissemination of outcome data related to the tele-ICU, and recognition programs that reward excellence in tele-ICU/ICU behaviors are three examples that can help maintain strong morale [206].

Change management and relationship issues can present a potential barrier to the adoption of any new technology that requires buy-in from humans. Highly successful implementations of the tele-ICU platform correlate well with overcoming these challenges and present a suitable environment for rapid adoption of cutting-edge medical developments.

8.8.6 Lifestyle Improvements Using the Tele-ICU

Tele-ICU increases the options for managers to allocate staff responsibilities. It helps to offset some of the burden of continuously monitoring patients, so that bedside staff can focus more of their time on other important tasks such as meeting with patients' families, collecting patient information, and accomplishing activities related to quality care protocols. The assurance that patients are being vigilantly monitored along with fewer (if any) night and weekend calls offers a better quality of life for intensivists—a fact that has helped the Ministry Saint Clare Hospital recruit intensivists much more effectively post tele-ICU installation [217]. UMMMC added their tele-ICU system, in part, to address the fact that their on-call intensivists would field telephone calls with limited information and to try and offer advice on a patient's proper care. The tele-ICU system provided much more accurate guidance during these off-hours [218]. Also, rather than paging a physician and waiting for a call back, nurses know that they have instantaneous access to an intensivist. As a result of these improvements, one hospital manager at Ministry Saint Clare pointed out that both intensivists and hospitalists have commented that "if the tele-ICU program weren't in [their] hospital, they wouldn't be either" [217].

In the absence of beeping pagers, alarms, distractions, and other interruptions, physicians in the tele-ICU can focus much more carefully as they study the details of the most severely ill patients. Automated problem identification can be more effective than human analysis of a patient in person, especially if the presence of fatigue. According to one intensivist

at Sentara Health—the goal is to have every 'red' patient reviewed by a doctor or nurse at least every hour, but if tele-ICU alerts are firing, such reviews can be much more persistent [223].

The tele-ICU provides welcome job progression for medical professionals who prefer to avoid intense action at the bedside, but would be willing to apply their accumulated ICU experience in the command center. This provides such experienced professionals the opportunity to assist newly trained bedside nurses who "frequently begin their career working the night shift when fewer resources are available" [221]. Young *et al.* found that among residents training in healthcare systems with implemented tele-ICU, two-thirds wanted to do a tele-ICU post-residency [222]. In highly successful implementations of this technology, knowledge sharing is both encouraged and widely accepted as part of the culture making these settings more suitable to initial adoption of new medical developments such as the thesis technology.

8.9 *Financial Impact and Payback*

UMMMC determined that it recovered its initial fixed costs within the first year. On a per-case basis, revenues were slightly reduced due to decreased LOS—payers generally compensated UMMMC on a per diem or pay-per-service model. Costs, however, experienced an approximate 20% reduction. The net effect was a $5,400 savings per case, or $25M annually (4,600 cases) [207]. Sentara Health found that the cost per ICU case fell about $3,000 (25%) mainly due to a dramatic plunge in complications related to nosocomial pneumonia and bloodstream infections—both of which occur much more often in the absence of intensivists who can identify subtle changes in patient condition. More complications equate to more tests, more treatments, and longer stays in the ICU at 3x the cost of an average non-ICU bed. In Sentara's case, the average ICU stay dropped almost a full day from 4.4 to 3.6 allowing it to recover its initial fixed costs of $1.6M within six months [225].

With the support of the tele-ICU, community hospitals treat more severe cases locally rather than transfer them to larger tertiary care centers. In UMMMC's study, the community hospitals improved their ICU retention rate—the fraction of patients who were admitted to the ICU relative to the total number presented—by an average of 23%. This more efficient use of

hospital resources corresponded to an increase in the occupancy rate by 45%. The improved patient throughput and ability to accept more severe cases directly impacted profits: Community Hospital 1 experienced an increase in profits from $3,000 per case and 565 cases per year to $4,000 per case and 791 cases per year ($1.45M annually), and Community Hospital 2 experienced an increase from $5,000 per case and 539 cases per year to $9,000 per case and 806 cases per year ($4.55M annually). In both cases, payback occurred in less than one year.

The cost-savings associated with treating a patient in the tertiary care center as opposed to the local community hospital is estimated using matched pairs. 449 pairs of patients with similar diagnosis, age, and timeframe of hospitalization were matched: one who was treated at a local community hospital and one that was treated at UMMMC. It was found that patients treated at UMMMC cost $10,000 more, on average, than at the community hospitals. Given the post-tele-ICU decline in transfer rates of 23%, payers could save an estimated $2.6M per year just by treating these patients in the community hospital. Scaled to all 33 hospitals in Massachusetts with 10+ beds, the estimated savings reaches about $80M.

The analysis above does not include cost-savings due to:

- Physically transferring patients between medical centers
- Decreased staff turnover
- Increased adherence to evidenced based medicine and best practice guidelines
- Preventable claims settlements
- Rapid identification of patients ready for discharge
- *Not* having to build new ICU beds at $1.5M each to accommodate more patients at tertiary medical centers

In each case, the additional savings favor tele-ICU implementation. For example, Avera Health's tele-ICU contributed to a 37.5% decline in patient transfers to academic medical centers, saving $1.25M including $1M on air transportation for 160 patients that were able to stay in their hometown hospital [206, 212]. Maine Medical Center saved over $1M via a 56% reduction in turnover of registered nurses. Resurrection Health observed a 7% reduction in blood transfusions in 6 months translating to $11,200 in savings and over $5M in preventable claims

settlements [219]. Advocate HealthCare's reduction of ventilator-associated pneumonias saved about $28,000 per case, and paired with a reduction in the annual incidence rate of 87 cases over three years, the total savings amounted to almost $2.5M per year [221]. Via Christi Health System implemented a teaching intervention that allowed avoidance of an estimated $240,000 in non-reimbursible patient care costs under changing Medicare and Medicare reimbursement rules [206]. Baptist Health saved an estimated $3M in streamlining the patient discharge process.

When exclusively considering savings due to reduced LOS, tele-ICU is still a financially sound investment. A sensistivity analysis below (Table 8-2) uses the *UMMMC scenario* of $6M initial capital costs, $5,400 saved per case, and the national average of 141 beds per command center. The *inferior case scenario* uses $8M for the initial capital cost and only 1/5 of the observed $5,400 saved per case. Two highly conservative assumptions are made:

1. *[For inferior case only]* All ICU cases presented to all ICU beds after initial investment are assumed to be 'severe' or 'very severe' (using proportions from 2007 National Trauma Data Bank (NTDB))
2. ICU bed occupancy of 68%, consistent with the 2005 rate [226]

The NTDB has four separate severity rankings: minor, moderate, severe, and very severe. These are associated with average ICU LOS of 0.4, 1.2, 3.6, and 7.6 respectively. Therefore more severe patients require a greater proportion of hospital resources. Assumption 1 over-estimates the average LOS for all patients to be 5.4 days, meaning that patient turnover is slow. Less than 28% of all cases included in the 2007 NTDB report were 'severe' or 'very severe'. The true average LOS across all patients in the NTDB is 2.0 days. Assumption 2 can be interpreted that each ICU bed is only occupied 248 days per calendar year.

Table 8-2. Sensitivity analysis for payback. (Top) Fixed costs. (Bottom) Variable Costs.

		UMMMC	Inferior
Fixed Investment	Command Center (CC) Investment	$6,000,000	$8,000,000
	Net Savings per Case	$5,400	$1,080
	Cases Needed for Payback	1111	7407
	Average Beds per CC (2010)	141	141
	Cases Needed per Bed for Payback	7.9	52.5
	Average Severity-Adjusted LOS (2007)	2.0	5.4
	Days of ICU Use for Payback	16	282
	Average Days per Year Used (2010)	248	248
	Payback (Months)	**1**	**14**

		UMMMC	Inferior
Variable Costs	Annual Operating Cost	$1,000,000	$3,000,000
	Net Savings per Case	$5,400	$1,080
	Cases Needed for Payback	185	2778
	Average Beds per CC (2010)	141	141
	Cases Needed per Bed for Payback	1.3	19.7
	Average Severity-Adjusted LOS (2007)	2.0	5.4
	Days of ICU Use for Payback	3	106
	Average Days per Year Used (2010)	248	248
	Payback (Months)	**0.1**	**5.1**

In the *UMMMC scenario* with 141 beds per CC, all costs are recovered within the first two months. In the *inferior case scenario*, the initial capital costs are recovered slightly over one year and positive return on investment is generated during the third operating year. The profit potential escalates with increasing number of covered ICU beds and occupancy rates. The financial benefit of installing a command center to cover less than 60 beds may not justify the initial costs, and therefore it makes more sense for smaller healthcare systems to partner with existing command centers [221].

The average cost of an ICU per day is $2,400 (2010 Dollars) [227, 228]. Although marginal costs tend to decrease with increasing LOS, in the absence of cost accounting data reduction in ICU LOS is used as a rough proxy to estimate order-of-magnitude annual savings based on patient throughput [221]. In four separate studies, the average estimated annual savings based on ICU LOS reduction alone was substantial (Table 8-3) [215, 225, 229, 230].

Table 8-3. Estimated savings based on reduction in average LOS, total patient throughput, duration of study, and average cost of ICU per day.

Health System	Patients in Study	Average LOS Reduction (Days)	Estimated Savings	Time (mo.)	Annualized Savings (Est.)
Sentara	2,140	0.72	$ 3,700,000	6	$ 7,400,000
Avera	5,146	1.71	$ 21,400,000	30	$ 8,560,000
UPenn	2,811	3.75	$ 25,600,000	36	$ 8,533,333
UMMMC	6,290	1.90	$ 29,000,000	29	$ 12,000,000

Collectively, the measurable improvements that have been widely reported to accompany successful implementation and rollout of a tele-ICU system more than justify the investment, and collateral benefits can be equally magnanimous.

8.10 *National Support and Outlook for Tele-ICU*

This technology has accumulated support from several influential figures in the healthcare space. First, the Leapfrog Group recently adjusted its standard for intensivist care in ICUs. Specifically, intensivist coverage of a distant ICU from a command center facilitated by tele-ICU technology now meets its standard for intensivist staffing [213]. Second, MTC and NEHI have called for all academic medical centers in the state of Massachusetts to implement this technology by 2014 and all hospitals with >10 ICU beds to adopt the technology by 2015 [207]. Third, Kathleen Sebelius, the United States' Secretary of Health and Human Services visited Norfolk, VA last summer (2011) to promote Sentara's innovative move into the tele-ICU space as a major example in her hospital safety initiative whose goal is to cut hospital-caused harms by 40% and hospital readmissions by 20% by 2014 [231]. Finally, in April 2011, the Association of Critical Care Nurses launched their CCRN-E certification, which is an extension of the standard critical care registered nurse (CCRN) certification [209]. The CCRN-E is the first credential specifically for the tele-nurse and a major step toward recognizing the need and importance of remote medicine in critical care.

8.11 *Conclusions*

There is a fundamental and growing imbalance between the supply and demand for critical care medicine. Improving the outreach of existing intensivists through the use of tele-ICU has been demonstrated repetitively in proof-of-principle studies at a multitude of health care systems with often highly encouraging results. This technology benefits all three major parties in the healthcare arena. Patients can more frequently access the resources that they need and receive top-quality care. Payers are the beneficiaries of substantial cost savings as a result of process improvements in the ICU. Providers are able to treat more total patients, and more efficiently manage severe patients. With the adoption of any new technology involving collaboration between humans, there are unique implementation-related challenges that require careful consideration. It is important to achieve sufficient buy-in amongst all impacted parties, develop the necessary technical support to overcome data integration issues, and provide continuous process improvements and updates to the system while facilitating a culture where best-practices are shared, good behaviors are rewarded, and positive outcomes are publicly lauded. The tele-ICU, like implant coatings or any medical technology, is aimed at maximizing healthcare quality while minimizing physical and financial burden to patients and payers. It is an enabling technology that plays a significant role in extending the reach of intensivists, and consequently, a potentially useful tool toward rapidly disseminating new medical technologies and capturing market share.

Appendix: MATLAB Code for Numerical Treatment of Drug Release

```
% Simulate.m
% June 25, 2010
% Joshua Moskowitz
% Input variables: None
% Outputs: this program will simulate the time-space concentration profile
% of the film system and output total release as a function of time.


function Simulate()

% disp('--------------------------')
% disp('Decreasing Drug Diffusivity')
% disp('--------------------------')
% [C1, x1, time1, Qdiffusion1] = Qdiff(20, 4.0*10^(-7), 100, 1);
% [C2, x2, time2, Qdiffusion2] = Qdiff(20, 2.0*10^(-7), 100, 1);
% [C3, x3, time3, Qdiffusion3] = Qdiff(20, 1.0*10^(-7), 100, 1);
% [C4, x4, time4, Qdiffusion4] = Qdiff(20, 5.0*10^(-8), 100, 1);
% [C5, x5, time5, Qdiffusion5] = Qdiff(20, 2.5*10^(-8), 100, 1);
%
% disp('-------------------------')
% disp('Increasing Film Thickness')
% disp('-------------------------')
% [C6, x6, time6, Qdiffusion6] = Qdiff(2.5, 5.0*10^(-7), 100, 1);
% [C7, x7, time7, Qdiffusion7] = Qdiff(5, 5.0*10^(-7), 100, 1);
% [C8, x8, time8, Qdiffusion8] = Qdiff(10, 5.0*10^(-7), 100, 1);
% [C9, x9, time9, Qdiffusion9] = Qdiff(15, 5.0*10^(-7), 100, 1);
% [C10, x10, time10, Qdiffusion10] = Qdiff(20, 5.0*10^(-7), 100, 1);
%
% disp('-----------------------')
% disp('Increasing Drug Content')
% disp('-----------------------')
% [C11, x11, time11, Qdiffusion11] = Qdiff(20, 5.0*10^(-7), 10, 1);
% [C12, x12, time12, Qdiffusion12] = Qdiff(20, 5.0*10^(-7), 20, 1);
% [C13, x13, time13, Qdiffusion13] = Qdiff(20, 5.0*10^(-7), 40, 1);
% [C14, x14, time14, Qdiffusion14] = Qdiff(20, 5.0*10^(-7), 80, 1);
% [C15, x15, time15, Qdiffusion15] = Qdiff(20, 5.0*10^(-7), 160, 1);


% disp('-----------------------')
% disp('Increasing Diffusivity Ratio')
% disp('-----------------------')
% [C16, x16, time16, Qdiffusion16] = Qdiff(20, 5.0*10^(-7), 100, 0.1);
% [C17, x17, time17, Qdiffusion17] = Qdiff(20, 5.0*10^(-7), 100, 0.5);
% [C18, x18, time18, Qdiffusion18] = Qdiff(20, 5.0*10^(-7), 100, 1);
% [C19, x19, time19, Qdiffusion19] = Qdiff(20, 5.0*10^(-7), 100, 5);
% [C20, x20, time20, Qdiffusion20] = Qdiff(20, 5.0*10^(-7), 100, 10);
```

```
%----------------------------------
%----------------------------------
%Plots for changing each parameter as stated above
%Figure 1,3,5,7: Concentration profiles
%Figure 2,4,6,8: Mass released as a function of time
%----------------------------------

% figure(1);
% hold on;
% plot(x1,C1, 'b')
% plot(x2,C2, 'g')
% plot(x3,C3, 'r')
% plot(x4,C4, 'c')
% plot(x5,C5, 'k')
% ylabel('Concentration ug/cm^3');
% xlabel('Distance from Film Surface (um)');
% title('Effect of Decreasing Diffusivity');
% legend('4E(-7)', '2E(-7)', '1E(-7)', '5E(-8)' ,'2.5E(-8)', 'Location',
'Best');
% figure(2);
% hold on;
% plot(time1/60/60,Qdiffusion1, 'b')
% plot(time2/60/60,Qdiffusion2, 'g')
% plot(time3/60/60,Qdiffusion3, 'r')
% plot(time4/60/60,Qdiffusion4, 'c')
% plot(time5/60/60,Qdiffusion5, 'k')
% ylabel('Mass Released ug/cm^2');
% xlabel('Time (Hours)');
% title('Effect of Decreasing Diffusivity');
% legend('4E(-7)', '2E(-7)', '1E(-7)', '5E(-8)' ,'2.5E(-8)', 'Location',
'Best');
%
%
% figure(3);
% hold on;
% plot(x6,C6, 'b')
% plot(x7,C7, 'g')
% plot(x8,C8, 'r')
% plot(x9,C9, 'c')
% plot(x10,C10, 'k')
% ylabel('Concentration ug/cm^3');
% xlabel('Distance from Film Surface (um)');
% title('Effect of Increasing Film Thickness');
% legend('2.5 um', '5', '10', '15' ,'20', 'Location', 'Best');
% figure(4);
% hold on;
% plot(time6/60/60,Qdiffusion6, 'b')
% plot(time7/60/60,Qdiffusion7, 'g')
% plot(time8/60/60,Qdiffusion8, 'r')
% plot(time9/60/60,Qdiffusion9, 'c')
% plot(time10/60/60,Qdiffusion10, 'k')
% ylabel('Mass Released ug/cm^2');
% xlabel('Time (Hours)');
% title('Effect of Increasing Film Thickness');
% legend('2.5 um', '5', '10', '15' ,'20', 'Location', 'Best');
```

```
%
%
%
% figure(5);
% hold on;
% plot(x11,C11, 'b')
% plot(x12,C12, 'g')
% plot(x13,C13, 'r')
% plot(x14,C14, 'c')
% plot(x15,C15, 'k')
% ylabel('Concentration ug/cm^3');
% xlabel('Distance from Film Surface (um)');
% title('Effect of Increasing Drug Concentration');
% legend('10 ug/cm^2', '20', '40', '80' ,'160', 'Location', 'Best');
% axis([0 150 0 20000]);
% figure(6);
% hold on;
% plot(time11/60/60,Qdiffusion11, 'b')
% plot(time12/60/60,Qdiffusion12, 'g')
% plot(time13/60/60,Qdiffusion13, 'r')
% plot(time14/60/60,Qdiffusion14, 'c')
% plot(time15/60/60,Qdiffusion15, 'k')
% ylabel('Mass Released ug/cm^2');
% xlabel('Time (Hours)');
% title('Effect of Increasing Drug Concentration');
% legend('10 ug/cm^2', '20', '40', '80' ,'160', 'Location', 'Best');



%
% figure(7);
% hold on;
% plot(x16,C16, 'b')
% plot(x17,C17, 'g')
% plot(x18,C18, 'r')
% plot(x19,C19, 'c')
% plot(x20,C20, 'k')
% ylabel('Concentration ug/cm^3');
% xlabel('Distance from Film Surface (um)');
% title('Effect of Increasing D/Dfilm');
% legend('0.1', '0.5', '1', '5' ,'10', 'Location', 'Best');
% axis([0 100 0 40000]);
% figure(8);
% hold on;
% plot(time16/60/60,Qdiffusion16, 'b')
% plot(time17/60/60,Qdiffusion17, 'g')
% plot(time18/60/60,Qdiffusion18, 'r')
% plot(time19/60/60,Qdiffusion19, 'c')
% plot(time20/60/60,Qdiffusion20, 'k')
% ylabel('Mass Released ug/cm^2');
% xlabel('Time (Hours)');
% title('Effect of Increasing D/Dfilm');
% % axis([0 300 0 100000]);
% legend('0.1', '0.5', '1', '5' ,'10', 'Location', 'Best');
```

```
%---------------------------------


%---------------------------------
%Use the following for comparison to analytical model
%---------------------------------
[C1, x1, time1, Qdiffusion1] = Qdiff(20, 4.0*10^(-7), 100, 0.1);


%---------------------------------
%CALCULATE LEAST SQUARES FIT TO ANALYTICAL FUNCTION
%Qdiff = a*(1-exp(-B*x^(1/2)))
%---------------------------------
x0_10 = [35 .1];
[EQ_10, FVAL10, EXITFLAG10, OUTPUT10] = fminsearch(@(x)EQUATION_10(x,
Qdiffusion1, time1, length(Qdiffusion1)), x0_10);
disp(['Pre-exponential parameter A = ', num2str(EQ_10(1))]);
disp(['Exponential parameter B = ', num2str(EQ_10(2))]);
for i = 1:length(time1)
    Model10(i) = EQ_10(1)*(1-exp(-EQ_10(2)*time1(i)^0.5));
end
figure(100);
hold on;
plot(time1, Qdiffusion1, 'b');
plot(time1, Model10, 'r');
ylabel('Mass Released ug/cm^2');
xlabel('Time (Seconds)');
legend('Finite Differences', 'Analytical Fit', 'Location', 'Best');
figure(101);
hold on;
plot(x1,C1, 'b')
ylabel('Concentration ug/cm^3');
xlabel('Distance from Film Surface (um)');
%-------------------------------------
%Calculate Pearson's R
%-------------------------------------
%1. Compute X - Xmean and Y - Ymean
%Construct data and model vectors consisting of A) scaled raw data minus the
%mean of the scaled raw data, and B) the model data minus the mean of the
%model data:
FiniteDiffs = Qdiffusion1 - mean(Qdiffusion1);
Model10_Pearson = Model10 - mean(Model10);
%2. Calculate XY
%3. Calculate X^2
%4. Calculate Y^2
for i = 1:length(Qdiffusion1)
    datamodel10(i) = FiniteDiffs(i)*Model10(i);
    datasquare(i) = FiniteDiffs(i)^2;
    model10square(i) = Model10_Pearson(i)^2;
end
R10 = sum(datamodel10)/(sqrt(sum(datasquare))*sqrt(sum(model10square)));
R10square = R10^2
```

```
%---------------------------------------
```

```
%---------------------------%---------------------------
%---------------------------%---------------------------
%---------------------------%---------------------------
%---------------------------%---------------------------
%---------------------------%---------------------------
function [C, x, time, Qdiffusion] = Qdiff(h_in, D_in, Co_in, ratio_in)

%---------------------------
%---------------------------
%Input initial parameters
%---------------------------
h = h_in;                               %um
D = D_in;                               %Aqueous Diffusivity of drug cm^2/s
Dfilm = D/ratio_in;                     %Matrix Diffusivity of drug cm^2/s...
Dfilm <= D
Co = Co_in/(0.0001*h);                  %ug/volume of film in ug/cm^3
Film = 20;                              %number of film elements
Medium = 9*Film;                        %number of medium elements
elemFilm = h/10000/Film;                %element size in film (cm)
timestep = (1/Dfilm)*(elemFilm/2)^2;%time to diffuse 1 element in Film in
seconds... t <= (1/D)*(elementsize/2)^2
elemMedium = 2*sqrt(D*timestep);        %element size in medium (cm)
fulltime = 50;                         %numsteps*timestep, or total duration of
simulation
numsteps = floor(fulltime/timestep);%number of simulation time steps to take
%---------------------------
%---------------------------

%---------------------------
%---------------------------
%Set up initial conditions
%1. Concentration vector C(x,0)
%2. C''(x,0)
%---------------------------
%Initialize C
C = zeros(Film + Medium,1);
% C(x,0) = [Film Film Film|Medium Medium Medium Medium Medium Medium Medium
Medium Medium Medium Medium Medium Medium Medium Medium]
%          [Co  Co   Co   |0     0      0      0      0      0      0      0      0
0     0      0      0      0      0      0      0      0 ]
for i = 1:Film
    C(i) = Co;
end
```

```
%Initialize C''(x,0)

    %Need to take into account the Film/Solution Interface
    %These values are the coefficients that pop out of Taylor expanding
    %with different element sizes
    k1 = elemFilm;
    k2 = (elemFilm + elemMedium) / 2;
    k3 = k1 + k2;
    k4 = k1^2*k2/2 + k1*k2^2/2;
    k5 = elemMedium;
    k6 = (elemFilm + elemMedium) / 2;
    k7 = k5 + k6;
    k8 = k5^2*k6/2 + k5*k6^2/2;


    for i = 2:Film-1
        Cprime2(i) = (C(i+1) - 2*C(i) + C(i-1)) / (elemFilm^2);
    end
    for i = 2:Medium-1
        Cprime2(Film+i) = (C(Film+i+1) - 2*C(Film+i) + C(Film+i-1)) /
(elemMedium^2);
    end
    Cprime2(Film) = (k1*C(Film+1) - k3*C(Film) + k2*C(Film-1)) / k4;
    Cprime2(Film+1) = (k6*C(Film+2) - k7*C(Film+1) + k5*C(Film)) / k8;
    Cprime2(1) = (-C(4) + 4*C(3) - 5*C(2) + 2*C(1)) / (elemFilm^2);
    Cprime2(Film+Medium) = (2*C(Film+Medium) - 5*C(Film+Medium-1) +
4*C(Film+Medium-2) - C(Film+Medium-3)) / (elemMedium^2);
    Cprime2 = Cprime2';


%Keep track of total initial mass
sum1 = 0;
for i = 1:Film+Medium
    sum1 = sum1 + C(i)*elemFilm;
end
disp(['Total initial drug: ', int2str(sum1), ' ug/cm^2']);
%----------------------------
%----------------------------




%----------------------------
%----------------------------
%Iterate the diffusion process
%----------------------------
t = 0;

%Needed to index the total release values and total mass at each iteration
counter = 2;
time = zeros(1,numsteps);
Qdiffusion = zeros(1, numsteps);
```

```
TotalMass = zeros(1, numsteps);
TotalMass(1) = sum1;

while t < fulltime
    %Recalculate C(x,t + timestep)
    for i = 1:Film
        C(i) = C(i) + timestep*Dfilm*Cprime2(i);
    end
    for i = 1:Medium
        C(Film+i) = C(Film+i) + timestep*D*Cprime2(Film+i);
    end
    %--------------
    %DUMP THE ERROR
    %--------------
        CurrentMass = 0;
        for i = 1:Film
            CurrentMass = CurrentMass + C(i)*elemFilm;
        end
        for i = 1:Medium
            CurrentMass = CurrentMass + C(Film+i)*elemMedium;
        end
        for i = 1:Film+Medium
            C(i) = C(i)/CurrentMass*sum1;
        end
    %--------------
    %NO FLUX
    %--------------
    AVG1 = (C(1) + C(2)) / 2;
    AVG2 = (C(length(C)) + C(length(C)-1)) / 2;
    C(1) = AVG1;
    C(2) = AVG1;
    C(length(C)) = AVG2;
    C(length(C)-1) = AVG2;


    %Recalculate C''(x,t + timestep)
    for i = 2:Film-1
         Cprime2(i) = (C(i+1) - 2*C(i) + C(i-1)) / (elemFilm^2);
    end
    for i = 2:Medium-1
         Cprime2(Film+i) = (C(Film+i+1) - 2*C(Film+i) + C(Film+i-1)) /
(elemMedium^2);
    end
    Cprime2(Film) = (k1*C(Film+1) - k3*C(Film) + k2*C(Film-1)) / k4;
    Cprime2(Film+1) = (k6*C(Film+2) - k7*C(Film+1) + k5*C(Film)) / k8;
    Cprime2(1) = (-C(4) + 4*C(3) - 5*C(2) + 2*C(1)) / (elemFilm^2);
    Cprime2(Film+Medium) = (2*C(Film+Medium) - 5*C(Film+Medium-1) +
4*C(Film+Medium-2) - C(Film+Medium-3)) / (elemMedium^2);
    Cprime2 = Cprime2';


    %Keep track of what's in the film and what's been eluted
    %Fill in Qdiffusion(t)
    eluted = 0;
```

```
    for i = 1:Medium
        eluted = eluted + C(Film + i)*elemMedium;
    end
    FilmMass = 0;
    for i = 1:Film
        FilmMass = FilmMass + C(i)*elemFilm;
    end
    time(counter) = t;
    Qdiffusion(counter) = eluted;
    TotalMass(counter) = eluted + FilmMass;

    counter = counter + 1;
    t = t + timestep;
end
%---------------------------------
```

```
%---------------------------------
%---------------------------------
%Keep track of total final mass and report
%---------------------------------
sum2 = 0;
sum3 = 0;
sum4 = 0;
for i = 1:Film
    sum3 = sum3 + C(i)*elemFilm;
end
for i = 1:Medium
    sum4 = sum4 + C(Film + i)*elemMedium;
end
sum2 = sum3 + sum4;
% sum3
% sum4
disp(['Total final drug: ', int2str(sum2), ' ug/cm^2']);
disp(['Total film drug remaining: ', int2str(sum3), ' ug/cm^2']);
disp(['Total eluted drug: ', int2str(sum4), ' ug/cm^2']);
disp(' ');

%Keep track of losses due to error propagation
% figure(10)
% plot(time, TotalMass);
% xlabel('Time (seconds)');
% ylabel('Mass in System (ug)');
%---------------------------------
%---------------------------------
```

```
%---------------------------------
%Set up distace vector for concentration profile
```

```
%---------------------------------
for i = 1:Film
    x(i) = i*elemFilm*10000;
end
for i = 1:Medium
    x(Film + i) = Film*elemFilm*10000 + i*elemMedium*10000;
end
%---------------------------------
return;



%--------------------------------------
%EQUATION 10
%--------------------------------------
%This is the TENTH cost function to be normalized
%EQUATION 10 ==> Scaled Release = a*(1 - exp(-b*time^0.5)) + c*time
%
%INPUTS: x is the variable vector (i.e. the "a", "b", and "c")
%y is the release vector y
%t is the time vector t
%s is the total number of data points to minimize residuals with
%OUTPUTS: a sum of squares difference between the model and data
%--------------------------------------
function sum10 = EQUATION_10(x, y, t, s)
%Create two column vectors of zeros with total number of elements as the
%data set.
f = linspace(0,0,s);
f = f';
g = linspace(0,0,s);
g = g';

%Go through the data set and subtract the model value from the raw data
%value at each time point (this is stored in f.  Square each result and
%store in g.
for i = 1:s
    f(i) = y(i) - (x(1) * (1 - exp(-x(2)*t(i)^0.5)));
    g(i) = f(i)^2;
end

%Start the sum counter at zero
sum10 = 0;

%Add all values in g vector and return
for i = 1:s
    sum10 = sum10 + g(i);
end
return;
%--------------------------------------
```

Bibliography

[1] Kurtz S, Mowat F, Ong K, Chan N, Lau E, Halpern M. Prevalence of primary and revision total hip and knee arthroplasty in the United States from 1990 through 2002. *J Bone Joint Surg Am*. **2005**;87:1487-97.

[2] Moss AJ, Hamburger S, Moore RM, Jr., Jeng LL, Howie LJ. Use of selected medical device implants in the United States, 1988. *Adv Data*. **1991**:1-24.

[3] Parvizi J, Antoci V, Hickok NJ, Shapiro IM. Selfprotective smart orthopedic implants. *Expert Review of Medical Devices*. **2007**;4:55-64.

[4] Ong KL, Mowat FS, Chan N, Lau E, Halpern MT, Kurtz SM. Economic burden of revision hip and knee arthroplasty in Medicare enrollees. *Clin Orthop Relat Res*. **2006**;446:22-8.

[5] Wu P, Grainger DW. Drug/device combinations for local drug therapies and infection prophylaxis. *Biomaterials*. **2006**;27:2450-67.

[6] Liu SJ, Ueng SWN, Lin SS, Chan EC. In vivo release of vancomycin from biodegradable beads. *J Biomed Mater Res*. **2002**;63:807-13.

[7] Khardori N, Yassien M. Biofilms in Device-Related Infections. *Journal of Industrial Microbiology*. **1995**;15:141-7.

[8] Fisman DN, Reilly DT, Karchmer AW, Goldie SJ. Clinical effectiveness and cost-effectiveness of 2 management strategies for infected total hip arthroplasty in the elderly. *Clinical Infectious Diseases*. **2001**;32:419-30.

[9] Lew DP, Waldvogel FA. Osteomyelitis. *Lancet*. **2004**;364:369-79.

[10] Stoodley P, Sauer K, Davies DG, Costerton JW. Biofilms as complex differentiated communities. *Annual Review of Microbiology*. **2002**;56:187-209.

[11] Costerton JW, Stewart PS, Greenberg EP. Bacterial biofilms: A common cause of persistent infections. *Science*. **1999**;284:1318-22.

[12] Barton AJ, Sagers RD, Pitt WG. Bacterial adhesion to orthopedic implant polymers. *J Biomed Mater Res*. **1996**;30:403-10.

[13] Pascual A. Pathogenesis of catheter-related infections: lessons for new designs. *Clin Microbiol Infec*. **2002**;8:256-64.

[14] Tunney MM, Patrick S, Curran MD, Ramage G, Hanna D, Nixon JR, et al. Detection of prosthetic hip infection at revision arthroplasty by immunofluorescence microscopy and PCR amplification of the bacterial 16S rRNA gene. *J Clin Microbiol*. **1999**;37:3281-90.

[15] Gerstenfeld LC, Cullinane DM, Barnes GL, Graves DT, Einhorn TA. Fracture healing as a post-natal developmental process: Molecular, spatial, and temporal aspects of its regulation. *Journal of Cellular Biochemistry*. **2003**;88:873-84.

[16] Soundrapandian C, Datta S, Sa B. Drug-eluting implants for osteomyelitis. *Crit Rev Ther Drug*. **2007**;24:493-545.

[17] Frutos Cabanillas P, Diez Pena E, Barrales-Rienda JM, Frutos G. Validation and in vitro characterization of antibiotic-loaded bone cement release. *Int J Pharm*. **2000**;209:15-26.

[18] Buchholz HW, Elson RA, Heinert K. Antibiotic-Loaded Acrylic Cement - Current Concepts. *Clin Orthop Relat R*. **1984**:96-108.

[19] Trippel SB. Antibiotic-Impregnated Cement in Total Joint Arthroplasty. *J Bone Joint Surg Am*. **1986**;68A:1297-302.

[20] Wininger DA, Fass RJ. Antibiotic-impregnated cement and beads for orthopedic infections. *Antimicrobial Agents and Chemotherapy*. **1996**;40:2675-9.

[21] Winkler H. Rationale for one stage exchange of infected hip replacement using uncemented implants and antibiotic impregnated bone graft. *Int J Med Sci*. **2009**;6:247-52.

[22] Langlais F, Belot N, Ropars M, Thomazeau H, Lambotte JC, Cathelineau G. Antibiotic cements in articular prostheses: current orthopaedic concepts. *Int J Antimicrob Agents*. **2006**;28:84-9.

[23] van de Belt H, Neut D, Uges DRA, Schenk W, van Horn JR, van der Mei HC, et al. Surface roughness, porosity and wettability of gentamicin-loaded bone cements and their antibiotic release. *Biomaterials*. **2000**;21:1981-7.

[24] Masri BA, Duncan CP, Beauchamp CP, Paris NJ, Arntorp J. Effect of Varying Surface Patterns on Antibiotic Elution from Antibiotic-Loaded Bone-Cement. *Journal of Arthroplasty*. **1995**;10:453-9.

[25] Virto MR, Frutos P, Torrado S, Frutos G. Gentamicin release from modified acrylic bone cements with lactose and hydroxypropylmethylcellulose. *Biomaterials*. **2003**;24:79-87.

[26] Bunetel L, Segui A, Cormier M, Percheron E, Langlais F. Release of Gentamicin from Acrylic Bone-Cement. *Clinical Pharmacokinetics*. **1989**;17:291-7.

[27] Hoff SF, Fitzgerald RH, Kelly PJ. The Depot Administration of Penicillin-G and Gentamicin in Acrylic Bone-Cement. *J Bone Joint Surg Am*. **1981**;63:798-804.

[28] Wahlig H, Dingeldein E, Bergmann R, Reuss K. Release of Gentamicin from Polymethylmethacrylate Beads - Experimental and Pharmacokinetic Study. *J Bone Joint Surg Br*. **1978**;60:270-5.

[29] McLaren AC, McLaren SG, Nelson CL, Wassell DL, Olsen KM. The effect of sampling method on the elution of tobramycin from calcium sulfate. *Clin Orthop Relat R*. **2002**:54-7.

[30] Picknell B, Mizen L, Sutherland R. Antibacterial Activity of Antibiotics in Acrylic Bone Cement. *J Bone Joint Surg Br*. **1977**;59:302-7.

[31] Neut D, van de Belt H, Stokroos I, van Horn JR, van der Mei HC, Busscher HJ. Biomaterial-associated infection of gentamicin-loaded PMMA beads in orthopaedic revision surgery. *J Antimicrob Chemother*. **2001**;47:885-91.

[32] Jasty M, Jiranek W, Harris WH. Acrylic Fragmentation in Total Hip Replacements and Its Biological Consequences. *Clin Orthop Relat R*. **1992**:116-28.

[33] Yang JM, You JW, Chen HL, Shih CH. Calorimetric characterization of the formation of acrylic type bone cements. *J Biomed Mater Res*. **1996**;33:83-8.

[34] Leggat PA, Kedjarune U. Toxicity of methyl methacrylate in dentistry. *International Dental Journal*. **2003**;53:126-31.

[35] Jiranek WA, Hanssen AD, Greenwald AS. Antibiotic-loaded bone cement for infection prophylaxis in total joint replacement. *J Bone Joint Surg Am*. **2006**;88A:2487-500.

[36] Hench LL. Bioceramics - from Concept to Clinic. *Journal of the American Ceramic Society*. **1991**;74:1487-510.

[37] Ikada Y, Tsuji H. Biodegradable polyesters for medical and ecological applications. *Macromolecular Rapid Communications*. **2000**;21:117-32.

[38] Anderson JM, Shive MS. Biodegradation and biocompatibility of PLA and PLGA microspheres. *Advanced Drug Delivery Reviews*. **1997**;28:5-24.

[39] Meseguer-Olmo L, Ros-Nicolas MJ, Clavel-Sainz M, Vicente-Ortega V, Alcaraz-Banos M, Lax-Perez A, et al. Biocompatibility and in vivo gentamicin release from bioactive sol-gel glass implants. *J Biomed Mater Res*. **2002**;61:458-65.

[40] Nablo BJ, Rothrock AR, Schoenfisch MH. Nitric oxide-releasing sol-gels as antibacterial coatings for orthopedic implants. *Biomaterials*. **2005**;26:917-24.

[41] Pouton CW, Akhtar S. Biosynthetic polyhydroxyalkanoates and their potential in drug delivery. *Advanced Drug Delivery Reviews*. **1996**;18:133-62.

[42] Iler RK. Multilayers of Colloidal Particles. *J Colloid Interf Sci*. **1966**;21:569-&.

[43] Schlenoff JB. Retrospective on the Future of Polyelectrolyte Multilayers. *Langmuir*. **2009**;25:14007-10.

[44] Decher G. Fuzzy nanoassemblies: Toward layered polymeric multicomposites. *Science*. **1997**;277:1232-7.

[45] Decher G, Hong JD. Buildup of Ultrathin Multilayer Films by a Self-Assembly Process .2. Consecutive Adsorption of Anionic and Cationic Bipolar Amphiphiles and Polyelectrolytes on Charged Surfaces. *Ber Bunsen Phys Chem*. **1991**;95:1430-4.

[46] Decher G, Hong JD, Schmitt J. Buildup of Ultrathin Multilayer Films by a Self-Assembly Process .3. Consecutively Alternating Adsorption of Anionic and Cationic Polyelectrolytes on Charged Surfaces. *Thin Solid Films*. **1992**;210:831-5.

[47] Decher G, Schlenoff JB. Multilayer thin films: sequential assembly of nanocomposite materials. Weinheim: Wiley-VCH; **2003**.

[48] Lynn DM. Layers of opportunity: nanostructured polymer assemblies for the delivery of macromolecular therapeutics. *Soft Matter*. **2006**;2:269-73.

[49] Thierry B, Winnik FM, Merhi Y, Silver J, Tabrizian M. Bioactive coatings of endovascular stents based on polyelectrolyte multilayers. *Biomacromolecules*. **2003**;4:1564-71.

[50] Vautier D, Hemmerle J, Vodouhe C, Koenig G, Richert L, Picart C, et al. 3-D surface charges modulate protrusive and contractile contacts of chondrosarcoma cells. *Cell Motil Cytoskel*. **2003**;56:147-58.

[51] Zhu YB, Gao CY, He T, Liu XY, Shen JC. Layer-by-layer assembly to modify poly(L-lactic acid) surface toward improving its cytocompatibility to human endothelial cells. *Biomacromolecules*. **2003**;4:446-52.

[52] Picart C. Polyelectrolyte multilayer films: From physico-chemical properties to the control of cellular processes. *Curr Med Chem*. **2008**;15:685-97.

[53] Chuang HF, Smith RC, Hammond PT. Polyelectrolyte multilayers for tunable release of antibiotics. *Biomacromolecules*. **2008**;9:1660-8.

[54] Decher G, Hong JD. Buildup of Ultrathin Multilayer Films by a Self-Assembly Process .1. Consecutive Adsorption of Anionic and Cationic Bipolar Amphiphiles on Charged Surfaces. *Makromol Chem-M Symp*. **1991**;46:321-7.

[55] Wood KC, Chuang HF, Batten RD, Lynn DM, Hammond PT. Controlling interlayer diffusion to achieve sustained, multiagent delivery from layer-by-layer thin films. *P Natl Acad Sci USA*. **2006**;103:10207-12.

[56] Jessel N, Atalar F, Lavalle P, Mutterer J, Decher G, Schaaf P, et al. Bioactive coatings based on a polyelectrolyte multilayer architecture functionalized by embedded proteins. *Adv Mater*. **2003**;15:692-5.

[57] Pei RJ, Cui XQ, Yang XR, Wang EK. Assembly of alternating polycation and DNA multilayer films by electrostatic layer-by-layer adsorption. *Biomacromolecules*. **2001**;2:463-8.

[58] Chluba J, Voegel JC, Decher G, Erbacher P, Schaaf P, Ogier J. Peptide hormone covalently bound to polyelectrolytes and embedded into multilayer architectures conserving full biological activity. *Biomacromolecules*. **2001**;2:800-5.

[59] Schultz P, Vautier D, Richert L, Jessel N, Haikel Y, Schaaf P, et al. Polyelectrolyte multilayers functionalized by a synthetic analogue of an anti-inflammatory peptide, alpha-MSH, for coating a tracheal prosthesis. *Biomaterials*. **2005**;26:2621-30.

[60] Chen XJ, Yan XB, Khor KA, Tay BK. Multilayer assembly of positively charged polyelectrolyte and negatively charged glucose oxidase on a 3D Nafion network for detecting glucose. *Biosens Bioelectron*. **2007**;22:3256-60.

[61] Price JS, Tencer AF, Arm DM, Bohach GA. Controlled release of antibiotics from coated orthopedic implants. *J Biomed Mater Res*. **1996**;30:281-6.

[62] Berg MC, Zhai L, Cohen RE, Rubner MF. Controlled drug release from porous polyelectrolyte multilayers. *Biomacromolecules*. **2006**;7:357-64.

[63] Smith RC, Riollano M, Leung A, Hammond PT. Layer-by-Layer Platform Technology for Small-Molecule Delivery. *Angewandte Chemie-International Edition*. **2009**;48:8974-7.

[64] Dierich A, Le Guen E, Messaddeq N, Stoltz JF, Netter P, Schaaf P, et al. Bone formation mediated by synergy-acting growth factors embedded in a polyelectrolyte multilayer film. *Adv Mater*. **2007**;19:693-+.

[65] Macdonald M, Rodriguez NM, Smith R, Hammond PT. Release of a model protein from biodegradable self assembled films for surface delivery applications. *J Control Release*. **2008**;131:228-34.

[66] Muller S, Koenig G, Charpiot A, Debry C, Voegel JC, Lavalle P, et al. VEGF-functionalized polyelectrolyte multilayers as proangiogenic prosthetic coatings. *Adv Funct Mater*. **2008**;18:1767-75.

[67] Etienne O, Schneider A, Taddei C, Richert L, Schaaf P, Voegel JC, et al. Degradability of polysaccharides multilayer films in the oral environment: an in vitro and in vivo study. *Biomacromolecules*. **2005**;6:726-33.

[68] Ren KF, Ji J, Shen JC. Construction and enzymatic degradation of multilayered poly-L-lysine/DNA films. *Biomaterials*. **2006**;27:1152-9.

[69] Serizawa T, Yamaguchi M, Akashi M. Enzymatic hydrolysis of a layer-by-layer assembly prepared from chitosan and dextran sulfate. *Macromolecules*. **2002**;35:8656-8.

[70] Inoue H, Anzai J. Stimuli-sensitive thin films prepared by a layer-by-layer deposition of 2-iminobiotin-labeled poly(ethyleneimine) and avidin. *Langmuir*. **2005**;21:8354-9.

[71] Inoue H, Sato K, Anzai J. Disintegration of layer-by-layer assemblies composed of 2-iminobiotin-labeled poly(ethyleneimine) and avidin. *Biomacromolecules*. **2005**;6:27-9.

[72] Sato K, Imoto Y, Sugama J, Seki S, Inoue H, Odagiri T, et al. Sugar-induced disintegration of layer-by-layer assemblies composed of concanavalin a and glycogen. *Langmuir*. **2005**;21:797-9.

[73] Li BY, Haynie DT. Multilayer biomimetics: Reversible covalent stabilization of a nanostructured biofilm. *Biomacromolecules*. **2004**;5:1667-70.

[74] Schmidt DJ, Moskowitz JS, Hammond PT. Electrically Triggered Release of a Small Molecule Drug from a Polyelectrolyte Multilayer Coating. *Chemistry of Materials*. **2010**;22:6416-25.

[75] Wood KC, Zacharia NS, Schmidt DJ, Wrightman SN, Andaya BJ, Hammond PT. Electroactive controlled release thin films. *Proc Natl Acad Sci U S A*. **2008**;105:2280-5.

[76] Vazquez E, Dewitt DM, Hammond PT, Lynn DM. Construction of hydrolytically-degradable thin films via layer-by-layer deposition of degradable polyelectrolytes. *J Am Chem Soc*. **2002**;124:13992-3.

[77] Lynn DM, Anderson DG, Putnam D, Langer R. Accelerated discovery of synthetic transfection vectors: Parallel synthesis and screening of degradable polymer library. *J Am Chem Soc*. **2001**;123:8155-6.

[78] Lynn DM, Langer R. Degradable poly(beta-amino esters): Synthesis, characterization, and self-assembly with plasmid DNA. *J Am Chem Soc*. **2000**;122:10761-8.

[79] Smith RC, Leung A, Kim BS, Hammond PT. Hydrophobic Effects in the Critical Destabilization and Release Dynamics of Degradable Multilayer Films. *Chemistry of Materials*. **2009**;21:1108-15.

[80] Jewell CM, Zhang J, Fredin NJ, Wolff MR, Hacker TA, Lynn DM. Release of plasmid DNA from intravascular stents coated with ultrathin multilayered polyelectrolyte films. *Biomacromolecules*. **2006**;7:2483-91.

[81] Kim BS, Park SW, Hammond PT. Hydrogen-bonding layer-by-layer assembled biodegradable polymeric micelles as drug delivery vehicles from surfaces. *Acs Nano*. **2008**;2:386-92.

[82] Moskowitz JS, Blaisse MR, Samuel RE, Hsu HP, Harris MB, Martin SD, et al. The effectiveness of the controlled release of gentamicin from polyelectrolyte multilayers in the treatment of Staphylococcus aureus infection in a rabbit bone model. *Biomaterials*. **2010**;31:6019-30.

[83] Shukla A, Fleming KE, Chuang HF, Chau TR, Loose CR, Stephanopoulos CN, et al. Controlling the release of peptide antimicrobial agents from surfaces. *Biomaterials*. **2009**;31:2348-57.

[84] Andrews JM. Determination of minimum inhibitory concentrations. *J Antimicrob Chemoth*. **2001**;48:5-16.

[85] Wood KC, Boedicker JQ, Lynn DM, Hammond PT. Tunable drug release from hydrolytically degradable layer-by-layer thin films. *Langmuir*. **2005**;21:1603-9.

[86] Hsieh YF, Chen TL, Wang YT, Chang JH, Chang HM. Properties of liposomes prepared with various lipids. *Journal of Food Science*. **2002**;67:2808-13.

[87] Kallinteri P, Antimisiaris SG, Karnabatidis D, Kalogeropoulou C, Tsota I, Siablis D. Dexamethasone incorporating liposomes: an in vitro study of their applicability as a slow releasing delivery system of dexamethasone from covered metallic stents. *Biomaterials*. **2002**;23:4819-26.

[88] Jia YM, Joly H, Omri A. Liposomes as a carrier for gentamicin delivery: Development and evaluation of the physicochemical properties. *Int J Pharm*. **2008**;359:254-63.

[89] Abraham AM, Walubo A. The effect of surface charge on the disposition of liposome-encapsulated gentamicin to the rat liver, brain, lungs and kidneys after intraperitoneal administration. *Int J Antimicrob Ag*. **2005**;25:392-7.

[90] Cordeiro C, Wiseman DJ, Lutwyche P, Uh M, Evans JC, Finlay BB, et al. Antibacterial efficacy of gentamicin encapsulated in pH-sensitive liposomes against an in vivo Salmonella enterica serovar typhimurium intracellular infection model. *Antimicrobial Agents and Chemotherapy*. **2000**;44:533-9.

[91] Gamazo C, Blanco-Prieto MJ, Lecároz MC, Vitas AI, Gander B, Irache JM, et al. New Therapeutic Approaches for the Treatment of Brucella Infections: Gentamicin Entrapment into Drug Delivery Systems. *Current Medicinal Chemistry--Anti-Infective Agents*. **2004**;3:43-6.

[92] Lutwyche P, Cordeiro C, Wiseman DJ, St-Louis M, Uh M, Hope MJ, et al. Intracellular delivery and antibacterial activity of gentamicin encapsulated in pH-sensitive liposomes. *Antimicrobial Agents and Chemotherapy*. **1998**;42:2511-20.

[93] Ellington JK, Harris M, Hudson MC, Vishin S, Webb LX, Sherertz R. Intracellular Staphylococcus aureus and antibiotic resistance: Implications for treatment of staphylococcal osteomyelitis. *J Orthop Res*. **2006**;24:87-93.

[94] Ellington JK, Harris M, Webb L, Smith B, Smith T, Tan K, et al. Intracellular Staphylococcus aureus - A mechanism for the indolence of osteomyelitis. *J Bone Joint Surg Br*. **2003**;85B:918-21.

[95] Tang H, Xu YQ, Zheng T, Li G, You YG, Jiang MY, et al. Treatment of osteomyelitis by liposomal gentamicin-impregnated calcium sulfate. *Arch Orthop Traum Su*. **2009**;129:1301-8.

[96] Michel A, Izquierdo A, Decher G, Voegel JC, Schaaf P, Ball V. Layer by layer self-assembled polyelectrolyte multilayers with embedded phospholipid vesicles obtained by spraying: Integrity of the vesicles. *Langmuir*. **2005**;21:7854-9.

[97] Michel M, Arntz Y, Fleith G, Toquant J, Haikel Y, Voegel JC, et al. Layer-by-layer self-assembled polyelectrolyte multilayers with embedded liposomes: Immobilized submicronic reactors for mineralization. *Langmuir*. **2006**;22:2358-64.

[98] Michel M, Vautier D, Voegel JC, Schaaf P, Ball V. Layer by layer self-assembled polyelectrolyte multilayers with embedded phospholipid vesicles. *Langmuir*. **2004**;20:4835-9.

[99] Kim TG, Lee H, Jang Y, Park TG. Controlled Release of Paclitaxel from Heparinized Metal Stent Fabricated by Layer-by-Layer Assembly of Polylysine and Hyaluronic Acid-g-Poly(lactic-co-glycolic acid) Micelles Encapsulating Paclitaxel. *Biomacromolecules*. **2009**;10:1532-9.

[100] Potisatityuenyong A, Tumcharern G, Dubas ST, Sukwattanasinitt M. Layer-by-layer assembly of intact polydiacetylene vesicles with retained chromic properties. *J Colloid Interf Sci*. **2006**;304:45-51.

[101] Yaroslavov AA, Rakhnyanskaya AA, Yaroslavova EG, Efimova AA, Menger FM. Polyelectrolyte-coated liposomes: stabilization of the interfacial complexes. *Adv Colloid Interface Sci*. **2008**;142:43-52.

[102] Volodkin DV, Schaaf P, Mohwald H, Voegel JC, Ball V. Effective embedding of liposomes into polyelectrolyte multilayered films: the relative importance of lipid-polyelectrolyte and interpolyelectrolyte interactions. *Soft Matter*. **2009**;5:1394-405.

[103] Malcher M, Volodkin D, Heurtault B, Andre P, Schaaf P, Mohwald H, et al. Embedded silver ions-containing liposomes in polyelectrolyte multilayers: Cargos films for antibacterial agents. *Langmuir*. **2008**;24:10209-15.

[104] Volodkin D, Arntz Y, Schaaf P, Moehwald H, Voegel JC, Ball V. Composite multilayered biocompatible polyelectrolyte films with intact liposomes: stability and temperature triggered dye release. *Soft Matter*. **2008**;4:122-30.

[105] Oyane A, Kim HM, Furuya T, Kokubo T, Miyazaki T, Nakamura T. Preparation and assessment of revised simulated body fluids. *J Biomed Mater Res A*. **2003**;65:188-95.

[106] Volodkin D, Mohwald H, Voegel JC, Ball V. Coating of negatively charged liposomes by polylysine: drug release study. *J Control Release*. **2007**;117:111-20.

[107] Lichter JA, Rubner MF. Polyelectrolyte Multilayers with Intrinsic Antimicrobial Functionality: The Importance of Mobile Polycations. *Langmuir*. **2009**;25:7686-94.

[108] Wong SY, Li Q, Veselinovic J, Kim BS, Klibanov AM, Hammond PT. Bactericidal and virucidal ultrathin films assembled layer by layer from polycationic N-alkylated polyethylenimines and polyanions. *Biomaterials*. **2010**;31:4079-87.

[109] Salomaki M, Kankare J. Influence of Synthetic Polyelectrolytes on the Growth and Properties of Hyaluronan-Chitosen Multilayers. *Biomacromolecules*. **2009**;10:294-301.

[110] Changez M, Koul V, Dinda AK. Efficacy of antibiotics-loaded interpenetrating network (IPNs) hydrogel based on poly(acrylic acid) and gelatin for treatment of experimental osteomyelitis: in vivo study. *Biomaterials*. **2005**;26:2095-104.

[111] De Giglio E, Cometa S, Cioffi N, Torsi L, Sabbatini L. Analytical investigations of poly(acrylic acid) coatings electrodeposited on titanium-based implants: a versatile approach to biocompatibility enhancement. *Analytical and Bioanalytical Chemistry*. **2007**;389:2055-63.

[112] Dubas ST, Schlenoff JB. Factors controlling the growth of polyelectrolyte multilayers. *Macromolecules*. **1999**;32:8153-60.

[113] Lavalle P, Gergely C, Cuisinier FJG, Decher G, Schaaf P, Voegel JC, et al. Comparison of the structure of polyelectrolyte multilayer films exhibiting a linear and an exponential growth regime: An in situ atomic force microscopy study. *Macromolecules*. **2002**;35:4458-65.

[114] Picart C, Mutterer J, Richert L, Luo Y, Prestwich GD, Schaaf P, et al. Molecular basis for the explanation of the exponential growth of polyelectrolyte multilayers. *P Natl Acad Sci USA*. **2002**;99:12531-5.

[115] Porcel C, Lavalle P, Ball V, Decher G, Senger B, Voegel JC, et al. From exponential to linear growth in polyelectrolyte multilayers. *Langmuir*. **2006**;22:4376-83.

[116] Porcel C, Lavalle P, Decher G, Senger B, Voegel JC, Schaaf P. Influence of the polyelectrolyte molecular weight on exponentially growing multilayer films in the linear regime. *Langmuir*. **2007**;23:1898-904.

[117] Schlenoff JB, Dubas ST. Mechanism of polyelectrolyte multilayer growth: Charge overcompensation and distribution. *Macromolecules*. **2001**;34:592-8.

[118] Choi J, Rubner MF. Influence of the degree of ionization on weak polyelectrolyte multilayer assembly. *Macromolecules*. **2005**;38:116-24.

[119] Darouiche RO, Mansouri MD, Zakarevicz D, AlSharif A, Landon GC. In vivo efficacy of antimicrobial-coated devices. *J Bone Joint Surg Am*. **2007**;89A:792-7.

[120] Isefuku S, Joyner CJ, Simpson AHRW. Gentamicin may have an adverse effect on osteogenesis. *Journal of Orthopaedic Trauma*. **2003**;17:212-6.

[121] Eisenber.A, Yokoyama T, Sambalid.E. Dehydration Kinetics and Glass Transition of Poly(Acrylic Acid). *Journal of Polymer Science Part a-1-Polymer Chemistry*. **1969**;7:1717-&.

[122] Maurer JJ, Eustace DJ, Ratcliffe CT. Thermal Characterization of Poly(Acrylic Acid). *Macromolecules*. **1987**;20:196-202.

[123] Shao L, Lutkenhaus JL. Thermochemical properties of free-standing electrostatic layer-by-layer assemblies containing poly(allylamine hydrochloride) and poly(acrylic acid). *Soft Matter*. **2010**;6:3363-9.

[124] Yang SY, Rubner MF. Micropatterning of polymer thin films with pH-sensitive and cross-linkable hydrogen-bonded polyelectrolyte multilayers. *J Am Chem Soc*. **2002**;124:2100-1.

[125] Rothstein SN, Federspiel WJ, Little SR. A unified mathematical model for the prediction of controlled release from surface and bulk eroding polymer matrices. *Biomaterials*. **2009**;30:1657-64.

[126] Siepmann J, Kranz H, Peppas NA, Bodmeier R. Calculation of the required size and shape of hydroxypropyl methylcellulose matrices to achieve desired drug release profiles. *Int J Pharm*. **2000**;201:151-64.

[127] Harland RS, Gazzaniga A, Sangalli ME, Colombo P, Peppas NA. Drug Polymer Matrix Swelling and Dissolution. *Pharmaceutical Research*. **1988**;5:488-94.

[128] Kharlampieva E, Ankner JF, Rubinstein M, Sukhishvili SA. pH-induced release of polyanions from multilayer films. *Physical Review Letters*. **2008**;100:-.

[129] Kharlampieva E, Ankner JF, Rubinstein M, Sukhishvili SA. pH-induced release of polyanions from multilayer films. *Phys Rev Lett*. **2008**;100:128303.

[130] Deen WM. Analysis of transport phenomena. New York: Oxford University Press; **1998**.

[131] Schwartz JB, Simonell.Ap, Higuchi WI. Drug Release from Wax Matrices .I. Analysis of Data with First-Order Kinetics and with Diffusion-Controlled Model. *Journal of Pharmaceutical Sciences*. **1968**;57:274-&.

[132] Stewart PS. Theoretical aspects of antibiotic diffusion into microbial biofilms. *Antimicrobial Agents and Chemotherapy*. **1996**;40:2517-22.

[133] Veyries ML, Couarraze G, Geiger S, Agnely F, Massias L, Kunzli B, et al. Controlled release of vancomycin from Poloxamer 407 gels. *Int J Pharm*. **1999**;192:183-93.

[134] He JT, Zhong CL, Mi JG. Modeling of drug release from bioerodible polymer matrices. *Drug Delivery*. **2005**;12:251-9.

[135] Hoffman AS. Hydrogels for biomedical applications. *Ann N Y Acad Sci*. **2001**;944:62-73.

[136] Antheunis H, van der Meer JC, de Geus M, Heise A, Koning CE. Autocatalytic Equation Describing the Change in Molecular Weight during Hydrolytic Degradation of Aliphatic Polyesters. *Biomacromolecules*. **2010**;11:1118-24.

[137] Lindqvist R. Estimation of Staphylococcus aureus growth parameters from turbidity data: characterization of strain variation and comparison of methods. *Appl Environ Microbiol*. **2006**;72:4862-70.

[138] Cui L, Iwamoto A, Lian JQ, Neoh HM, Maruyama T, Horikawa Y, et al. Novel mechanism of antibiotic resistance originating in vancomycin-intermediate Staphylococcus aureus. *Antimicrob Agents Chemother*. **2006**;50:428-38.

[139] Ray PS, Simonis RB. Management of acute and chronic osteomyelitis. *Hosp Med*. **2002**;63:401-7.

[140] Darouiche RO. Device-associated infections: A macroproblem that starts with microadherence. *Clinical Infectious Diseases*. **2001**;33:1567-72.

[141] Walls RJ, Roche SJ, O'Rourke A, McCabe JP. Surgical site infection with methicillin-resistant Staphylococcus aureus after primary total hip replacement. *J Bone Joint Surg Br*. **2008**;90B:292-8.

[142] Faber C, Hoogendoorn RJW, Stallmann HP, Lyaruu DM, Amerongen AV, Wuisman PIJM, et al. In vivo comparison of Dhvar-5 and gentamicin in an MRSA osteomyelitis prevention model. *J Antimicrob Chemoth*. **2004**;54:1078-84.

[143] Tiwari HK, Sen MR. Emergence of vancomycin resistant Staphylococcus aureus (VRSA) from a tertiary care hospital from northern part of India. *Bmc Infect Dis*. **2006**;6:-.

[144] Rushton N. Applications of local antibiotic therapy. *European Journal of Surgery*. **1997**;163:27-30.

[145] Yoshizawa S, Fourmy D, Puglisi JD. Structural origins of gentamicin antibiotic action. *Embo Journal*. **1998**;17:6437-48.

[146] Schafer JA, Hovde LB, Rotschafer JC. Consistent rates of kill of Staphylococcus aureus by gentamicin over a 6-fold clinical concentration range in an in vitro pharmacodynamic model (IVPDM). *J Antimicrob Chemoth*. **2006**;58:108-11.

[147] Jacqueline C, Asseray N, Batard E, Le Mabecque V, Kergueris MF, Dube L, et al. In vivo efficacy of linezolid in combination with gentamicin for the treatment of experimental endocarditis due to methicillin-resistant Staphylococcus aureus. *Int J Antimicrob Ag*. **2004**;24:393-6.

[148] Falco FG, Smith HM, Arcieri GM. Nephrotoxicity of Aminoglycosides and Gentamicin. *Journal of Infectious Diseases*. **1969**;119:406-&.

[149] Yoshii T, Magara S, Miyai D, Nishimura H, Kuroki E, Furudoi S, et al. Local levels of interleukin-1 beta,-4,-6, and tumor necrosis factor alpha in an experimental model of murine osteomyelitis due to Staphylococcus aureus. *Cytokine*. **2002**;19:59-65.

[150] Lucke M, Schmidmaier G, Sadoni S, Wildemann B, Schiller R, Haas NP, et al. Gentamicin coating of metallic implants reduces implant-related osteomyelitis in rats. *Bone*. **2003**;32:521-31.

[151] Lucke M, Wildemann B, Sadoni S, Surke C, Schiller R, Stemberger A, et al. Systemic versus local application of gentamicin in prophylaxis of implant-related osteomyelitis in a rat model. *Bone*. **2005**;36:770-8.

[152] Passl R, Muller C, Zielinski CC, Eibl MM. A Model of Experimental Post-Traumatic Osteomyelitis in Guinea-Pigs. *J Trauma*. **1984**;24:323-6.

[153] Emslie KR, Nade S. Acute Hematogenous Staphylococcal Osteomyelitis - Evaluation of Cloxacillin Therapy in an Animal-Model. *Pathology*. **1984**;16:441-6.

[154] Rodeheaver GT, Rukstalis D, Bono M, Bellamy W. A New Model of Bone Infection Used to Evaluate the Efficacy of Antibiotic-Impregnated Polymethylmethacrylate Cement. *Clin Orthop Relat R*. **1983**:303-11.

[155] Varshney AC, Singh H, Gupta RS, Singh SP. Experimental-Model of Staphylococcal Osteomyelitis in Dogs. *Indian Journal of Experimental Biology*. **1989**;27:816-9.

[156] Patterson AL, Galloway RH, Baumgartner JC, Barsoum IS. Development of Chronic Mandibular Osteomyelitis in a Miniswine Model. *Journal of Oral and Maxillofacial Surgery*. **1993**;51:1358-62.

[157] Curtis MJ, Brown PR, Dick JD, Jinnah RH. Contaminated Fractures of the Tibia - a Comparison of Treatment Modalities in an Animal-Model. *J Orthop Res*. **1995**;13:286-95.

[158] An YH, Kang QK, Arciola CR. Animal models of osteomyelitis. *Int J Artif Organs*. **2006**;29:407-20.

[159] Anwar H, Dasgupta MK, Costerton JW. Testing the Susceptibility of Bacteria in Biofilms to Antibacterial Agents. *Antimicrobial Agents and Chemotherapy*. **1990**;34:2043-6.

[160] Marrie TJ, Costerton JW. Mode of Growth of Bacterial Pathogens in Chronic Polymicrobial Human Osteomyelitis. *J Clin Microbiol*. **1985**;22:924-33.

[161] Gillaspy AF, Hickmon SG, Skinner RA, Thomas JR, Nelson CL, Smeltzer MS. Role of the Accessory Gene Regulator (Agr) in Pathogenesis of Staphylococcal Osteomyelitis. *Infect Immun*. **1995**;63:3373-80.

[162] Erdfelder E, Faul F, Buchner A. GPOWER: A general power analysis program. *Behavior Research Methods Instruments & Computers*. **1996**;28:1-11.

[163] An YHH, Friedman RJ. Animal models of orthopedic implant infection. *J Invest Surg*. **1998**;11:139-46.

[164] Alvarez H, Castro C, Moujir L, Perera A, Delgado A, Soriano I, et al. Efficacy of ciprofloxacin implants in treating experimental osteomyelitis. *J Biomed Mater Res B*. **2008**;85B:93-104.

[165] Kanellakopoulou K, Galanakis N, Giamarellos-Bourboulis EJ, Rifiotis C, Papakostas K, Andreopoulos A, et al. Treatment of experimental osteomyelitis caused by methicillin-resistant Staphylococcus aureus with a biodegradable system of lactic acid polymer releasing pefloxacin. *J Antimicrob Chemoth*. **2000**;46:311-4.

[166] Gursel I, Korkusuz F, Turesin F, Alaeddinoglu NG, Hasirci V. In vivo application of biodegradable controlled antibiotic release systems for the treatment of implant-related osteomyelitis. *Biomaterials*. **2001**;22:73-80.

[167] Koo KH, Yang JW, Cho SH, Song HR, Park HB, Ha YC, et al. Impregnation of vancomycin, gentamicin, and cefotaxime in a cement spacer for two-stage cementless reconstruction in infected total hip arthroplasty. *Journal of Arthroplasty*. **2001**;16:882-92.

[168] Krasko MY, Golenser J, Nyska A, Nyska M, Brin YS, Domb AJ. Gentamicin extended release from an injectable polymeric implant. *J Control Release*. **2007**;117:90-6.

[169] Nelson CL, McLaren SG, Skinner RA, Smeltzer MS, Thomas JR, Olsen KM. The treatment of experimental osteomyelitis by surgical debridement and the implantation of calcium sulfate tobramycin pellets. *J Orthop Res*. **2002**;20:643-7.

[170] Walenkamp GHIM, Kleijn LLA, de Leeuw M. Osteomyelitis treated with gentamicin-PMMA beads - 100 patients followed for 1-12 years. *Acta Orthop Scand*. **1998**;69:518-22.

[171] Jackson WO, Schmalzried TP. Limited role of direct exchange arthroplasty in the treatment of infected total hip replacements. *Clin Orthop Relat R*. **2000**:101-5.

[172] Lewis G, Janna S. Estimation of the optimum loading of an antibiotic powder in an acrylic bone cement - Gentamicin sulfate in SmartSet HV. *Acta Orthopaedica*. **2006**;77:622-7.

[173] Klemm K. The use of antibiotic-containing bead chains in the treatment of chronic bone infections. *Clin Microbiol Infec*. **2001**;7:28-31.

[174] Li BY, Jiang BB, Boyce BM, Lindsey BA. Multilayer polypeptide nanoscale coatings incorporating IL-12 for the prevention of biomedical device-associated infections. *Biomaterials*. **2009**;30:2552-8.

[175] Sikiric MD, Gergely C, Elkaim R, Wachtel E, Cuisinier FJG, Furedi-Milhofer H. Biomimetic organic-inorganic nanocomposite coatings for titanium implants. *Journal of Biomedical Materials Research Part A*. **2009**;89A:759-71.

[176] Aviv M, Berdicevsky I, Zilberman M. Gentamicin-loaded bioresorbable films for prevention of bacterial infections associated with orthopedic implants. *Journal of Biomedical Materials Research Part A*. **2007**;83A:10-9.

[177] Anglen JO. Comparison of soap and antibiotic solutions for irrigation of lower-limb openfracture wounds - A prospective, randomized study. *J Bone Joint Surg Am*. **2005**;87A:1415-22.

[178] Josepovitz C, Pastorizamunoz E, Timmerman D, Scott M, Feldman S, Kaloyanides GJ. Inhibition of Gentamicin Uptake in Rat Renal Cortex Invivo by Aminoglycosides and Organic Polycations. *Journal of Pharmacology and Experimental Therapeutics*. **1982**;223:314-21.

[179] Singh MP, Stefko J, Lumpkin JA, Rosenblatt J. The Effect of Electrostatic Charge Interactions on Release Rates of Gentamicin from Collagen Matrices. *Pharmaceutical Research*. **1995**;12:1205-10.

[180] Jabbari E, Nozari S. Swelling behavior of acrylic acid hydrogels prepared by gamma-radiation crosslinking of polyacrylic acid in aqueous solution. *European Polymer Journal*. **2000**;36:2685-92.

[181] Merkli A, Heller J, Tabatabay C, Gurny R. Gamma-Sterilization of a Semisolid Poly(Ortho Ester) Designed for Controlled Drug-Delivery - Validation and Radiation Effects. *Pharmaceutical Research*. **1994**;11:1485-91.

[182] Mohr D, Wolff M, Kissel T. Gamma irradiation for terminal sterilization of 17 beta-estradiol loaded poly-(D,L-lactide-co-glycolide) microparticles. *J Control Release*. **1999**;61:203-17.

[183] Volland C, Wolff M, Kissel T. The Influence of Terminal Gamma-Sterilization on Captopril Containing Poly(D,L-Lactide-Co-Glycolide) Microspheres. *J Control Release*. **1994**;31:293-305.

[184] Cavanaugh DL, Berry J, Yarboro SR, Dahners LE. Better prophylaxis against surgical site infection with local as well as systemic antibiotics. An in vivo study. *J Bone Joint Surg Am*. **2009**;91:1907-12.

[185] Moriarty TF, Schlegel U, Perren S, Richards RG. Infection in fracture fixation: Can we influence infection rates through implant design? *J Mater Sci Mater Med*. **2009**.

[186] Leslie LF, Faulkner BC, Woods JA, Hill RA, Thacker JG, Rodeheaver GT, et al. Wound cleansing by irrigation for implant surgery. *Journal of Long-Term Effects of Medical Implants*. **1995**;5:111-28.

[187] Morais JM, Papadimitrakopoulos F, Burgess DJ. Biomaterials/Tissue Interactions: Possible Solutions to Overcome Foreign Body Response. *Aaps Journal*. **2010**;12:188-96.

[188] Scheller B, Hehrlein C, Bocksch W, Rutsch W, Haghi D, Dietz U, et al. Treatment of coronary in-stent restenosis with a paclitaxel-coated balloon catheter. *New England Journal of Medicine*. **2006**;355:2113-24.

[189] Yang CM, Burt HA. Drug-eluting stents: Factors governing local pharmacokinetics. *Advanced Drug Delivery Reviews*. **2006**;58:402-11.

[190] Koschwanez HE, Reichert WM. In vitro, in vivo and post explantation testing of glucose-detecting biosensors: Current methods and recommendations. *Biomaterials*. **2007**;28:3687-703.

[191] Polikov VS, Tresco PA, Reichert WM. Response of brain tissue to chronically implanted neural electrodes. *Journal of Neuroscience Methods*. **2005**;148:1-18.

[192] Darouiche RO. Treatment of infections associated with surgical implants. *N Engl J Med*. **2004**;350:1422-9.

[193] Johnson JR, Kuskowski MA, Wilt TJ. Systematic review: antimicrobial urinary catheters to prevent catheter-associated urinary tract infection in hospitalized patients. *Ann Intern Med*. **2006**;144:116-26.

[194] Ratner BD. Biomaterials science: an introduction to materials in medicine. 2nd ed. Amsterdam ; Boston: Elsevier Academic Press; **2004**.

[195] Nelson JL, Roeder BL, Carmen JC, Roloff F, Pitt WG. Ultrasonically activated chemotherapeutic drug delivery in a rat model. *Cancer Res*. **2002**;62:7280-3.

[196] Costerton JW, Ellis B, Lam K, Johnson F, Khoury AE. Mechanism of electrical enhancement of efficacy of antibiotics in killing biofilm bacteria. *Antimicrob Agents Chemother*. **1994**;38:2803-9.

[197] Moskowitz JS, Blaisse MR, Samuel RE, Hsu HP, Harris MB, Martin SD, et al. The effectiveness of the controlled release of gentamicin from polyelectrolyte multilayers in the treatment of Staphylococcus aureus infection in a rabbit bone model. *Biomaterials*.

[198] Argun AA, Ashcraft JN, Hammond PT. Highly conductive, methanol resistant polyelectrolyte multilayers. *Adv Mater*. **2008**;20:1539-+.

[199] Farhat TR, Hammond PT. Designing a new generation of proton-exchange membranes using layer-by-layer deposition of polyelectrolytes. *Adv Funct Mater*. **2005**;15:945-54.

[200] Lyles BF, Terrot MS, Hammond PT, Gast AP. Directed patterned adsorption of magnetic beads on polyelectrolyte multilayers on glass. *Langmuir*. **2004**;20:3028-31.

[201] Schmidt DJ, Cebeci FC, Kalcioglu ZI, Wyman SG, Ortiz C, Van Vliet KJ, et al. Electrochemically Controlled Swelling and Mechanical Properties of a Polymer Nanocomposite. *Acs Nano*. **2009**;3:2207-16.

[202] Haldar J, An DQ, de Cienfuegos LA, Chen JZ, Klibanov AM. Polymeric coatings that inactivate both influenza virus and pathogenic bacteria. *P Natl Acad Sci USA*. **2006**;103:17667-71.

[203] Thomas M, Lu JJ, Ge Q, Zhang C, Chen J, Klibanov AM. Full deacylation of polyethylenimine dramatically boosts its gene delivery efficiency and specificity to mouse lung. *Proc Natl Acad Sci U S A*. **2005**;102:5679-84.

[204] Shah NJ, Hong J, Hyder MN, Hammond PT. Osteophilic Multilayer Coatings for Accelerated Bone Tissue Growth. *Adv Mater*. **2012**;24:1445-50.

[205] Singer N. Johnson & Johnson Recalls Hip Implants. *The New York Times*. **2010**:http://www.nytimes.com/2010/08/27/business/27hip.html.

[206] Goran SF. A second set of eyes: An introduction to Tele-ICU. *Crit Care Nurse*. **2010**;30:46-55.

[207] Fifer S, Everett W, Adams M, Vincequere J. Critical Care, Critical Choices: The Case for Tele-ICUs in Intensive Care. *Massachusetts Technology Collaborative and New England Healthcare Institute*. **2010**.

[208] Angus DC, Kelley MA, Schmitz RJ, White A, Popovich J, Jr. Caring for the critically ill patient. Current and projected workforce requirements for care of the critically ill and patients with pulmonary disease: can we meet the requirements of an aging population? *JAMA*. **2000**;284:2762-70.

[209] Rufo R. Using the Tele-ICU care delivery model to build organizational performance, part 1. *Crit Care Nurs Q*. **2011**;34:177-81.

[210] Ewart GW, Marcus L, Gaba MM, Bradner RH, Medina JL, Chandler EB. The critical care medicine crisis: a call for federal action: a white paper from the critical care professional societies. *Chest*. **2004**;125:1518-21.

[211] Berkmeyer J, Berkmeyyer C, Wennbury D. Leapfrog Patient Safety Standards. **2000**:20-6.

[212] Jarrah S, Van der Kloot TE. Tele-ICU: Remote Critical Care Telemedicine. *American College of Chest Physicians*. **2010**:http://www.chestnet.org/accp/pccsu/tele-icu-remote-critical-care-telemedicine?page=0,3.

[213] Pronovost P, Rainey T. Factsheet: ICU Physician Staffing (IPS). *The Leapfrog Group*. **2011**.

[214] Dara SI, Afessa B. Intensivist-to-bed ratio: association with outcomes in the medical ICU. *Chest*. **2005**;128:567-72.

[215] Lilly CM, Cody S, Zhao H, Landry K, Baker SP, McIlwaine J, et al. Hospital mortality, length of stay, and preventable complications among critically ill patients before and after tele-ICU reengineering of critical care processes. *JAMA*. **2011**;305:2175-83.

[216] Simon L, Everett W. Planning for Tele- ICU in California. **2011**:http://www.intouchhealth.com/2011%20NEHI-Tele%20ICU%20Report.pdf.

[217] Gorman MJ. Tele-ICU comes of age: studies, hospital five-year results validate effectiveness of the technology. *Health Manag Technol*. **2011**;32:8, 10-1.

[218] Dmyterko K. Tele-ICU: Intensive Care Anywhere. *Healthcare Technology Management*. **2011**:http://www.healthcaretechnologymanagement.com/index.php?option=com_articles&view=article&id=30564:tele-icu-intensive-care-anywhere.

[219] Rufo B. Tele-ICU: Positive return on investment. *Health Affairs*. **2009**;28:1859-60.

[220] Berenson RA, Grossman JM, November EA. Does telemonitoring of patients--the eICU--improve intensive care? *Health Affairs*. **2009**;28:937-47.

[221] Ries M. Tele-ICU: a new paradigm in critical care. *Int Anesthesiol Clin*. **2009**;47:153-70.

[222] Young LB, Chan PS, Cram P. Staff acceptance of tele-ICU coverage: a systematic review. *Chest*. **2011**;139:279-88.

[223] Mullaney TJ. The Doctor Is (Plugged) In *BusinessWeek*. **2006**:http://www.businessweek.com/magazine/content/06_26/b3990076.htm.

[224] Jackson S. Tele-ICU helps to reduce patient readmissions, length of stay. *FierceMobileHealthcare*. **2012**:http://www.fiercemobilehealthcare.com/story/tele-icu-helps-reduce-patient-readmissions-length-stay/2012-01-02.

[225] Breslow MJ, Rosenfeld BA, Doerfler M, Burke G, Yates G, Stone DJ, et al. Effect of a multiple-site intensive care unit telemedicine program on clinical and economic outcomes: an alternative paradigm for intensivist staffing. *Crit Care Med*. **2004**;32:31-8.

[226] Halpern NA, Pastores SM. Critical care medicine in the United States 2000-2005: an analysis of bed numbers, occupancy rates, payer mix, and costs. *Crit Care Med*. **2010**;38:65-71.

[227] Dasta JF, McLaughlin TP, Mody SH, Piech CT. Daily cost of an intensive care unit day: the contribution of mechanical ventilation. *Crit Care Med*. **2005**;33:1266-71.

[228] Noseworthy TW, Konopad E, Shustack A, Johnston R, Grace M. Cost accounting of adult intensive care: methods and human and capital inputs. *Crit Care Med*. **1996**;24:1168-72.

[229] Kohl BA, Gutsche JT, Kim P, Sites FD, Ochroch EA. Effect of telemedicine on mortality and length of stay in a university ICU. *Crit Care Med*. **2007**;35:A22-A.

[230] Zawada ET, Jr., Herr P, Larson D, Fromm R, Kapaska D, Erickson D. Impact of an intensive care unit telemedicine program on a rural health care system. *Postgrad Med*. **2009**;121:160-70.

[231] Vergakis B. Sebelius pushes hospital safety in Va. *KXAN*. **2011**:http://www.kxan.com/dpps/health/healthy_living/sebelius-pushes-hospital-safety-in-va_3840116.